

A MULTIDIMENSIONAL ANALYSIS OF CLIMATE PROJECTIONS ON THE GREAT BARRIER REEF

Submitted by

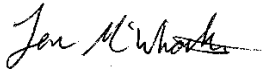
Jennifer McWhorter

to the University of Exeter as a thesis for the degree of Doctor of Philosophy in Physical
Geography, December 2021.

DECLARATION OF AUTHORSHIP

This thesis is available for Library use on the understanding that it is copyright material and that no quotation from the thesis may be published without proper acknowledgement.

I certify that all material in this thesis which is not my own work has been identified and that any material that has previously been submitted and approved for the award of a degree by this or any other University has been acknowledged.

A handwritten signature in black ink, appearing to read "Jennifer McWhorter". The signature is written in a cursive style with a horizontal line extending to the right.

Jennifer McWhorter

CULTURAL RECOGNITION

I would like to recognize the Aboriginal and Torres Strait Islander Peoples throughout the expanse of the Great Barrier Reef past, present and future. The many languages, knowledge and cultural practices throughout this unique location have my utmost respect and I thank the Traditional Custodians for their care and value of such an incredible wonder of the world.

Supervisors

Prof Paul Halloran, University of Exeter (lead supervisor)

Prof Peter Mumby, University of Queensland

Dr George Roff, CSIRO, University of Queensland

Prof Chris Perry, University of Exeter

Jury

Prof Gareth Williams, Bangor University external examiner

Prof Jamie Shutler, University of Exeter internal examiner

Funding

This PhD was funded by the QUEx Institute, a partnership between the University of Queensland and the University of Exeter.

ABSTRACT

Tropical coral reefs are increasingly threatened due to global warming. Corals live within a narrow thermal threshold making them one of the most sensitive species to changes in temperature. Recent warming events on the Great Barrier Reef (GBR) (2016, 2017, 2020) have caused mass coral mortality on approximately 30% of the reef (Bozec et al., 2020; Hughes, Kerry et al., 2018). This research focuses on the development and implementation of a 1-D semi-dynamic downscaling method to improve climate projections on the GBR. Coral stress metrics are used to provide detailed projections on the magnitude and frequency of warming for four socio-economic pathways (SSP) under the 6th phase of the Climate Model Intercomparison Project. Following a chapter on methods and model validation, the results in chapter 3 reveal the importance of adhering to the lowest possible emissions trajectory which limits warming to 1.5°C by the end of the century. This scenario keeps projected warming to slightly above current conditions. Under the higher emissions trajectories (~4°C and ~5°C of global average warming) coral stress metrics quadruple present-day warming conditions which would result in annual mass coral mortality events by 2080. In chapter 4, climate refugia have been identified from present-day conditions based on downscaled surface temperature outputs in agreement with observations. The lower emissions trajectories maintain these locations as refugia while the higher emissions trajectories reveal the loss of these increasingly valuable locations. Areas of climate refugia can be attributed to tidal and wind energy fluctuations providing relief from warming. However, this advantage does not persist after global warming exceeds ~3°C. Refugia are more likely to persist in the northern GBR under increased warming even though recent evidence suggests there are fewer refugia in this region. Atmospheric spatial patterns on the GBR under warming above ~3° C reveal a change in wind and shortwave radiation patterns driving a loss in the identified climate refugia locations. Lastly, stratification was tested in chapter 5 to determine if increases in stratification could provide thermal relief to bottom temperature waters from 0-50 m under increased warming into the future using downscaled bottom temperature projections. Chapter 5 results demonstrate that warming influences bottom temperatures of stratified locations, showing little support

for deeper reefs to act as a climate refuge. The temporal, spatial, and bottom temperature analysis of downscaled climate projections provides insight into the consequences of a warming planet for the GBR and can be used to inform management and policy decisions to protect coral reefs.

CONTENTS

DECLARATION OF AUTHORSHIP	2
CULTURAL RECOGNITION.....	3
ABSTRACT	5
LIST OF FIGURES	13
LIST OF TABLES	15
LIST OF ACRONYMS.....	16
CHAPTER 1	17
1.1 INTRODUCTION	17
1.2 GREAT BARRIER REEF	17
1.3 PHYSICAL OCEANOGRAPHY OF THE GREAT BARRIER REEF	18
1.3.1 BATHYMETRY	18
1.3.2 THERMAL STRATIFICATION AND MIXING	19
1.3.3 TIDES.....	20
1.3.4 WIND DRIVEN CURRENTS.....	20
1.3.5 SOUTHERN EQUATORIAL CURRENT AND WESTERN BOUNDARY CURRENTS	22
1.3.6 EDDIES.....	24
1.3.7 UPWELLING	25
1.3.8 ROSSBY WAVES.....	26
1.3.9 CONTINENTAL SHELF WAVES	27
1.3.10 RIVER PLUMES.....	27
1.4 ATMOSPHERIC COMPONENTS OF VARIABILITY ON THE GREAT BARRIER REEF	27
1.4.1 WINDS	28
1.4.2 AIR AND SEA SURFACE TEMPERATURE	28
1.4.3 RAINFALL	28
1.4.4 SUMMER MONSOON.....	29
1.4.5 TROPICAL CYCLONES	29
1.4.6 EL NIÑO SOUTHERN OSCILLATION.....	29
1.4.7 HADLEY CIRCULATION	30
1.4.8 WALKER CIRCULATION	30
1.4.9 SOUTHERN ANNULAR MODE	30
1.4.10 SUBTROPICAL HIGH	31
1.4.11 MADDEN-JULIAN OSCILLATION	31

1.4.12 INDIAN OCEAN DIPOLE.....	31
1.4.13 INTERDECADAL PACIFIC DECADEAL OSCILLATION	32
1.5 BIOGEOGRAPHY	32
1.5.1 LAGOON FLOOR.....	32
1.5.2 SEAGRASS.....	33
1.5.3 ISLANDS	33
1.5.4 CORAL REEFS	33
1.5.5 SHOALS.....	34
1.5.6 WATER COLUMN	35
1.5.7 CONTINENTAL SHELF	35
1.6 GLOBAL WARMING.....	36
1.6.1 FOSSIL FUELS AND GREENHOUSE GASES	36
1.6.2 OCEAN WARMING	37
1.6.3 GREAT BARRIER REEF AND CLIMATE CHANGE	38
1.7 CORAL BLEACHING.....	40
1.7.1 OBSERVED GLOBAL CORAL BLEACHING.....	40
1.7.2 LABORATORY BASED CORAL BLEACHING STUDIES	41
1.7.3 GREAT BARRIER REEF CORAL BLEACHING	42
1.7.4 CORAL STRESS METRIC: DEGREE HEATING WEEKS	42
1.7.5 MAXIMUM MONTHLY MEAN CALCULATION	44
1.7.6 DEGREE HEATING WEEKS CALCULATION	45
1.7.7 DEGREE HEATING WEEKS VERSES DEGREE HEATING MONTH	46
1.7.8 SATELLITE PRODUCTS FOR CORAL BLEACHING.....	47
1.8 CLIMATE PROJECTIONS.....	48
1.8.1 CLIMATE MODEL INTERCOMPARISON PROJECT (CMIP), CURRENTLY ON THE 6TH PHASE	48
1.8.2 SHARED SOCIOECONOMIC PATHWAY (SSP).....	49
1.8.3 EVOLUTION OF CLIMATE PROJECTIONS OVER CORAL REEFS.....	50
1.8.4 DOWNSCALING CLIMATE MODELS	51
1.8.5 DYNAMIC DOWNSCALING	51
1.8.6 STATISTICAL DOWNSCALING	52
1.8.7 DOWNSCALING OVER CORAL REEF ENVIRONMENTS	53
1.9 3-D MODELS FOR CORAL BLEACHING.....	56
1.10 CLIMATE PROJECTIONS OF ATMOSPHERIC DRIVERS OF WARMING ON THE GREAT BARRIER REEF.....	57

1.10.1 PROJECTIONS OF THE HADLEY AND WALKER CIRCULATION PROJECTIONS.....	59
1.10.2 EL NIÑO SOUTHERN OSCILLATION PROJECTIONS.....	60
1.10.3 SUBTROPICAL HIGH PROJECTIONS	60
1.10.4 SOUTHERN ANNULAR MODE PROJECTIONS.....	61
1.11 THESIS PLAN	61
CHAPTER 2	63
METHODS AND MODEL UNDERSTANDING:.....	63
DOWNSCALING CLIMATE MODELS USING S2P3-R V2.0 ON THE GREAT BARRIER REEF.....	63
PART A	63
2.1 INTRODUCTION	64
2.2 OVERVIEW OF S2P3-R V2.0.....	64
2.3 IMPROVEMENTS TO S2P3-R	67
2.4 S2P3-R V2.0 FRAMEWORK	68
2.4.1 TIDAL INPUTS.....	74
2.4.2 METEOROLOGICAL INPUTS.....	74
2.4.3 NUTRIENT INPUT.....	75
2.5 GLOBAL EVALUATION OF S2P3-R V2.0	75
2.6 GREAT BARRIER REEF PHYSICAL EVALUATION	76
PART B	80
2.7 MODELING UNDERSTANDING: S2P3-R V2.0 DEGREE HEATING WEEKS METRICS.....	80
2.7.1 RECENT BLEACHING EVENTS.....	81
2.7.2 ATMOSPHERIC CONDITIONS DURING RECENT BLEACHING EVENTS	82
2.7.3 ATMOSPHERIC VARIABLES; CLOUD COVER, PRESSURE, AND HUMIDITY .	83
2.7.4 ATMOSPHERIC VARIABLES; LONGWAVE AND SHORTWAVE RADIATION...	86
2.7.5 ATMOSPHERIC VARIABLE; AIR SURFACE TEMPERATURE.....	88
2.7.6 ATMOSPHERIC VARIABLE; WIND SPEED.....	89
2.7.7 ATMOSPHERIC DRIVERS OF MASS CORAL BLEACHING EVENT, 2002.....	90
2.7.8 ATMOSPHERIC DRIVERS OF MASS CORAL BLEACHING EVENT, 2016.....	91
2.7.9 ATMOSPHERIC DRIVERS OF MASS CORAL BLEACHING EVENT, 2017.....	91
2.8 VALIDATION OF DEGREE HEATING WEEKS: NOAA CORAL REEF WATCH PRODUCT AND S2P3-R V2.0 DOWNSCALED ERA5 COMPARISON.....	92
CHAPTER 3	97
THE IMPORTANCE OF 1.5°C WARMING FOR THE GREAT BARRIER REEF	97

3.1 ABSTRACT	98
3.2 INTRODUCTION	98
3.2.1 PREVIOUS STUDIES; CLIMATE PROJECTION METHODOLOGY FOR CORAL STRESS METRICS.....	100
3.2.2 STUDY DESIGN.....	103
3.3 MATERIALS AND METHODS	104
3.3.1 DOWNSCALING MODEL DATA	104
3.3.2 CORAL STRESS METRICS.....	104
3.4 RESULTS.....	105
3.4.1 MAGNITUDE OF THERMAL STRESS	105
3.4.2 FREQUENCY OF THERMAL STRESS	108
3.4.3 GREAT BARRIER REEF-WIDE STATISTICAL ANALYSIS.....	111
3.4.4 REGIONAL MAGNITUDE OF THERMAL STRESS UNDER LOW EMISSIONS	113
3.4.5 REGIONAL FREQUENCY OF THERMAL STRESS UNDER LOW EMISSIONS	116
3.4.6 REGIONAL STATISTICAL ANALYSIS	117
3.4.7 RESULTS PER MODEL, NUMBER OF SEVERE BLEACHING EVENTS AND DEGREE HEATING WEEKS	121
3.5 DISCUSSION	125
CHAPTER 4	129
CLIMATE REFUGIA ON THE GREAT BARRIER REEF FAIL WHEN GLOBAL WARMING EXCEEDS 3°C	129
4.1 ABSTRACT	129
4.2 INTRODUCTION	130
4.2.1 STUDY DESIGN.....	133
4.3 METHODS.....	134
4.3.1 DOWNSCALING MODEL DATA	134
4.3.2 SHARED SOCIOECONOMIC PATHWAYS (SSP)	135
4.3.2 CORAL STRESS METRICS.....	136
4.3.3 REFUGIA CALCULATION.....	137
4.3.4 GLOBAL WARMING METRICS.....	138
4.3.5 POTENTIAL ENERGY ANOMALIES; WIND AND TIDAL ENERGY FLUX METRICS.....	138
4.3.6 RATE OF WARMING CALCULATIONS	139
4.3.7 BLEACHING CONDITIONS	140
4.3.8 WIND SPEED AND SHORTWAVE RADIATION DURING BLEACHING CONDITIONS	140
4.3.9 STATISTICAL TESTS FOR WIND SPEED AND SHORTWAVE RADIATION ...	141

4.4 RESULTS.....	141
4.4.1 CLIMATE REFUGIA	141
4.4.2 VALIDATION OF THE CLIMATE REFUGIA LOCATIONS USING ERA5	142
4.4.3 TIDAL AND WIND ENERGY FLUX OVER CLIMATE REFUGIA LOCATIONS ..	143
4.4.4 LOSS OF CLIMATE REFUGIA.....	145
4.4.5 RATE OF DEGREE HEATING WEEKS WARMING	147
4.4.6 RATE OF RELATIVE SURFACE AIR TEMPERATURE WARMING	150
4.4.7 PROJECTED CHANGES IN WIND	152
4.4.8 PROJECTED CHANGES IN SHORTWAVE RADIATION.....	157
4.5 DISCUSSION	161
4.5.1 ATMOSPHERIC CIRCULATION DRIVING CHANGES TO WIND AND SHORTWAVE RADIATION.....	162
4.5.2 CLIMATE MODEL VARIABILITY	162
4.5.3 DOWNSCALING LIMITATIONS	163
4.5.4 CLIMATE TRAJECTORY UNCERTAINTY FOR CORALS	163
4.5.5 CORAL ADAPTATION AND RECOVERY	164
CHAPTER 5	166
UNDER PRESSURE; CLIMATE CHANGE AT DEPTH.....	166
5.1 ABSTRACT	166
5.2 INTRODUCTION	166
5.3 METHODS.....	169
5.3.1 DOWNSCALING	170
5.3.2 SUMMER METRICS APPLIED TO SURFACE AND BOTTOM TEMPERATURE OUTPUTS.....	170
5.3.4 DOWNSCALED ERA5 VALIDATION.....	172
5.3.5 DOWNSCALED ERA5 BASED WIND AND TIDAL ENERGY FLUX CALCULATIONS.....	172
5.4 RESULTS.....	173
5.4.1 LOCATIONS OF STRATIFICATION DURING AUSTRAL SUMMER	173
5.4.2 DOWNSCALED ERA5 TIDAL AND WIND MECHANISMS.....	175
5.4.3 FURTHER VALIDATION OF STRATIFICATION CONDITIONS	176
5.4.4 FUTURE STRATIFICATION.....	178
5.4.5 PROJECTIONS OF THE AUSTRAL SUMMER STRATIFICATION	179
5.4.6 BOTTOM TEMPERATURE PROJECTIONS	180
5.5 DISCUSSION	183
5.5.1 CAVEATS FROM THE S2P3-R V2.0 DOWNSCALING	183

5.5.2 SEASONAL PROPERTIES, THERMAL REGIME OF WINTER MIXING	184
5.5.3 WIND PROJECTIONS	185
5.5.4 SEA LEVEL RISE.....	185
5.6 CONCLUSION.....	186
CHAPTER 6	187
CONCLUSION AND FUTURE RESEARCH DIRECTIONS.....	187
6.1 CONCLUSION.....	187
6.1.1 THESIS OVERVIEW	187
6.1.2 SUMMARY FOR THE BROADER CORAL REEF COMMUNITY	189
6.1.3 CLIMATE ACTION	189
6.1.4 CORAL REEF MANAGEMENT STRATEGIES.....	190
6.2 FUTURE RESEARCH DIRECTIONS.....	191
6.2.1 REGIONAL PROJECTIONS USING 3-D MODELLING	192
6.2.2 EXPLORATION OF LARGER ATMOSPHERIC CHANGES UNDER WARMING	193
6.2.3 IMPORTANCE OF DOWNSCALING CLIMATE PROJECTIONS.....	193
ACKNOWLEDGEMENTS	195
REFERENCES	198

LIST OF FIGURES

- 1.1 Great Barrier Reef grid for this study
- 1.2 Australia atmospheric patterns
- 1.3 Great Barrier Reef bathymetry and currents
- 1.4 Capricorn Eddy
- 1.5 CO₂ concentrations from Mauna Loa, Hawaii
- 1.6 Ocean acidification
- 1.7 Degree Heating Weeks and bleaching correlation
- 1.8 Monthly reef heat stress
- 1.9 Degree Heating Week and Degree Heating Month
- 1.10 Sea surface temperature interpolation
- 1.11 Annual severe bleaching downscaling
- 2.1 S2P3-R v2.0 downscaling diagram
- 2.2 Great Barrier Reef sea surface temperature validation
- 2.3 Sea surface temperature validation by region
- 2.4 Surface and bottom temperature mooring validation
- 2.5 NOAA Degree Heating Weeks, 2002, 2016, 2017, 2020
- 2.6 ERA5 cloud coverage, bleaching and non-bleaching conditions
- 2.7 ERA5 pressure, bleaching and non-bleaching conditions
- 2.8 ERA5 humidity, bleaching and non-bleaching conditions
- 2.9 ERA5 longwave radiation, bleaching and non-bleaching conditions
- 2.10 ERA5 shortwave radiation, bleaching and non-bleaching conditions
- 2.11 ERA5 air surface temperature, bleaching and non-bleaching conditions
- 2.12 ERA5 wind speed, bleaching and non-bleaching conditions
- 2.13 Downscaled ERA5 Degree Heating Weeks validation
- 2.14 Downscaled ERA5 regional Degree Heating Weeks validation
- 2.15 Downscaled ERA5 spatial validation
- 3.1 Frequency of severe bleaching events by global average temperature
- 3.2 Magnitude and frequency of projected coral stress

- 3.3 Difference in magnitude and frequency of coral stress for low scenarios
- 3.4 Regional differences in projected coral stress
- 3.5 Histogram of Degree Heating Weeks data
- 3.6 Histogram of severe bleaching events per decade data
- 3.7 Projections of Degree Heating Weeks by model
- 3.8 Projections of the number of severe bleaching events by model
- 3.9 Difference in magnitude of coral stress for low scenarios by model
- 3.10 Difference in the number of severe bleaching events for low scenarios by model
- 4.1 Climate refugia locations
- 4.2 Downscaled ERA5 climate refugia locations, wind and tidal energy flux
- 4.3 Difference in projections, refugia and non-refugia
- 4.4 Degree Heating Weeks projections refugia and non-refugia
- 4.5 Per model Degree Heating Weeks refugia and non-refugia comparison
- 4.6 Per model rate of air surface temperature warming per model
- 4.7 Per model Degree Heating Weeks projections refugia and non-refugia
- 4.8 Wind speed and shortwave radiation change under SSP5-8.5
- 4.9 Projected wind speed comparison
- 4.10 Per model wind speed, present, future, and the percent change
- 4.11 Projected shortwave radiation comparison
- 4.12 Per model shortwave radiation, present, future, and the percent change
- 5.1 Stratified anomaly locations for ERA5 and climate models, depth histogram
- 5.2 Downscaled ERA5 wind and tidal energy flux, stratified and unstratified locations
- 5.3 Stratified anomaly locations for each summer month
- 5.4 Stratified anomaly locations for each model
- 5.5 Surface and bottom temperature difference, stratified and Great Barrier Reef wide locations
- 5.6 Annual anomalously stratified locations per climate change scenario
- 5.7 Bottom temperature projections for anomalously stratified locations

LIST OF TABLES

- 1.1 Strengths and weaknesses of statistical downscaling
- 1.2 Large-scale drivers of rainfall over Australia
- 2.1 Atmospheric variable inputs to S2P3-R v2.0
- 3.1 Average Degree Heating Weeks for recent events, satellite-based
- 3.2 Main effects and pairwise comparison of coral stress metrics for year 2060
- 3.3 Regional coral stress metrics for year 2060
- 4.1 Wind speed comparison per model, refugia and non-refugia locations
- 4.2 Shortwave radiation comparison per model, refugia and non-refugia locations

LIST OF ACRONYMS

CMIP: Climate Model Intercomparison Project
CRW: Coral Reef Watch
DHM: Degree Heating Month
DHW: Degree Heating Week
ENSO: El Niño-Southern Oscillation
GAM: Generalised Additive Model
GBR: Great Barrier Reef
GBRMPA: Great Barrier Reef Marine Park Authority
IPCC: Intergovernmental Panel on Climate Change
NOAA: National Oceanic and Atmospheric Administration
OTPS: Oregon State University Tidal Prediction Software
PAR: Photosynthetically Active Radiation
RCP: Representative Concentration Pathways
SLR: Sea Level Rise
SST: Sea Surface Temperature
SSP: Shared Socioeconomic Pathways
S2P3-R v2.0: Shelf Seas Physics and Primary Production model
TKE: Turbulent Kinetic Energy

CHAPTER 1

1.1 INTRODUCTION

Tropical coral reefs extend from approximately 30°N to 30°S of the equator and are among the most biodiverse ecosystems in the world, often referred to as the rainforests of the sea. Approximately 25% of the world's small-scale fisheries depend on coral reefs (Teh et al., 2013). The structure of a reef not only supports a wide range of organisms and fisheries, but also provides an important buffer from storms to vulnerable coastal communities (van Zanten et al., 2014). Coral reefs attract a range of tourism activities from diving, fishing, surfing, snorkelling, and more, providing revenue to many businesses. Increasing anthropogenic threats to coral reefs reduce these services and therefore create a need for quantitative information to guide management.

1.2 GREAT BARRIER REEF

On the western margin of the Coral Sea, the Great Barrier Reef (GBR) sits on the continental shelf and slope of the Australian continent. The GBR is the largest continuous reef system in the world containing over 3,500 coral reefs. There are currently believed to be over 450 species of hard, stony, or Scleractinia corals found here (Veron, 2000). However, many species remain undescribed, and this number is expected to increase soon with recent advances in phylogenomic sequencing technology (Kitahara et al., 2016).

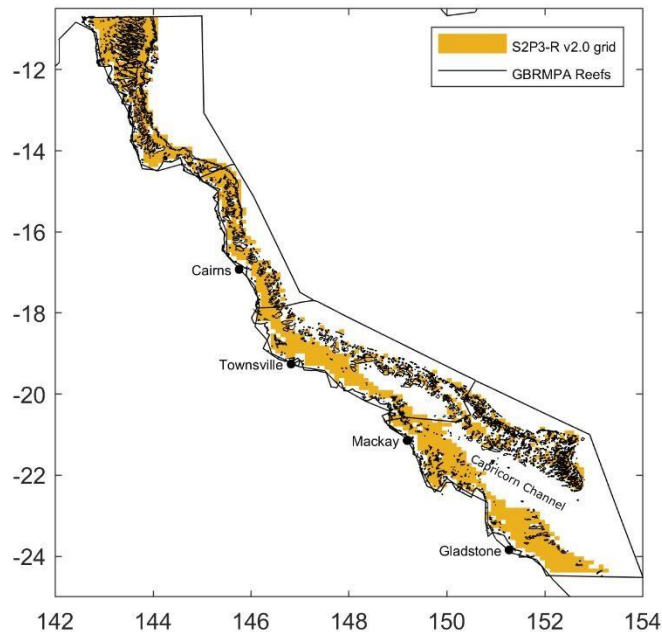


Figure 1.1: The Great Barrier Reef is in the southwestern Pacific Ocean offshore Queensland, Australia. Outlined are the reefs on top of the spatial grid used in this study (labelled as S2P3-R v2.0 for the spatial grid and Great Barrier Reef Marine Park Authority (GBRMPA) Reefs as the reefs). Depths range from 4-50 m over 10 km pixels. Referred to in this study are four geographic regions that have been established by GBRMPA, the far north, north, central, and south.

1.3 PHYSICAL OCEANOGRAPHY OF THE GREAT BARRIER REEF

1.3.1 BATHYMETRY

The GBR extends roughly 2,600 km from 25°S to 9.2°S (Wolanski & Pickard, 2018). The reef matrix on Australia's continental shelf varies in width, depth, and size. The continental shelf of the far north and northern GBR is relatively narrow in comparison to the central and southern GBR (Figure 1.1). The widest component of the continental shelf is ~250 km located around 21°S and the narrowest components are ~60 km

located in the far north and northern GBR as well as the furthest region south. The Capricorn channel separates the inner and outer shelf between 20°S to 24°S reaching depths of 90 meters. The narrow shelf components gradually deepen to a relatively shallow 40-60 meters while the wider components of the central region slope to depths near 100 meters. (Figure 1.1)

The outer shelf contains over 90% reef cover (Steinberg, 2007). The orientation, density, and complexity of the reefs control water flow of oceanic waters and tides passing over the shelf. For example, the central region has a more open matrix of reefs, and the orientation allows more water flow into the lagoon around 17°S and 18°S (Brinkman et al., 2002) (Figure 1.1). Barrier and ribbon reefs funnel water through their narrow channels (Steinberg, 2007).

1.3.2 THERMAL STRATIFICATION AND MIXING

The top five meters of the ocean absorbs 75% of total shortwave radiation (Mann & Lazier, 2013) and as a result, most of the warming in the ocean occurs at the surface. Shortwave radiation refers to the visible, infrared, and ultraviolet radiation from the sun. The amount of radiation coming into the ocean is determined by atmospheric conditions such as cloud cover, aerosols, water vapor as well as the angle of incidence, depth, reflection, and scattering. The warming of the ocean causes thermal expansion (Church et al., 1991) and reduces the density of the water. Thermal layers in the water column can develop from a lack of mixing and increases in heat at the ocean surface. These thermal layers can then change due to mixing forces such as wind from the surface through Ekman transport (Ekman, 1905), tidal forces from the bottom of the seafloor, and other advection processes. The thermocline refers to a significant drop in temperature as depth increases, and it is impacted by wind driver turbulence in the water column. In shallower regions the wind and tidal mixing can overlap causing mixing from the surface to the bottom of the water column. This is commonly seen near the coast, between reefs in channels and in macro-tidal regions of the GBR (Steinberg,

2007). Salinity gradients can also drive stratification as the higher the salinity, the denser the water.

1.3.3 TIDES

Tides are a dominant form of mixing on the GBR with significant topographic amplification (Steinberg, 2007). Tides draw a frictional force from the seafloor becoming more amplified over the wide and shallow continental shelves (Steinberg, 2007), therefore accounting for complexities in depth is important when modelling reef locations. Tidal ranges vary latitudinally across the GBR with the largest tidal ranges exceeding six meters in the southern region and approximately three meters in the northern and central GBR (Pickard et al., 1977; Steinberg, 2007; Wolanski & Spagnol, 2000). Tidal driven mixing from the bottom to the surface of the ocean can occur in shallow waters and/or in macrotidal areas (Steinberg, 2007) such as the southern GBR.

1.3.4 WIND DRIVEN CURRENTS

Southeasterly trades dominate wind patterns south of 15°S (Pickard et al., 1977), a significant driver of regional mixing (Figure 1.2). The southeast trades strengthen currents that flow in a complementary direction, such as the northward flowing Hiri current (Figure 1.3). In contrast, the dominant trades oppose the southward flowing Eastern Australian current (Figure 1.3). Southeasterly trades generally dominate mixing along the inner shelf resulting in a northward current. The trades also cause a suppression of upwelling and drive surface waters onshore (Steinberg, 2007).

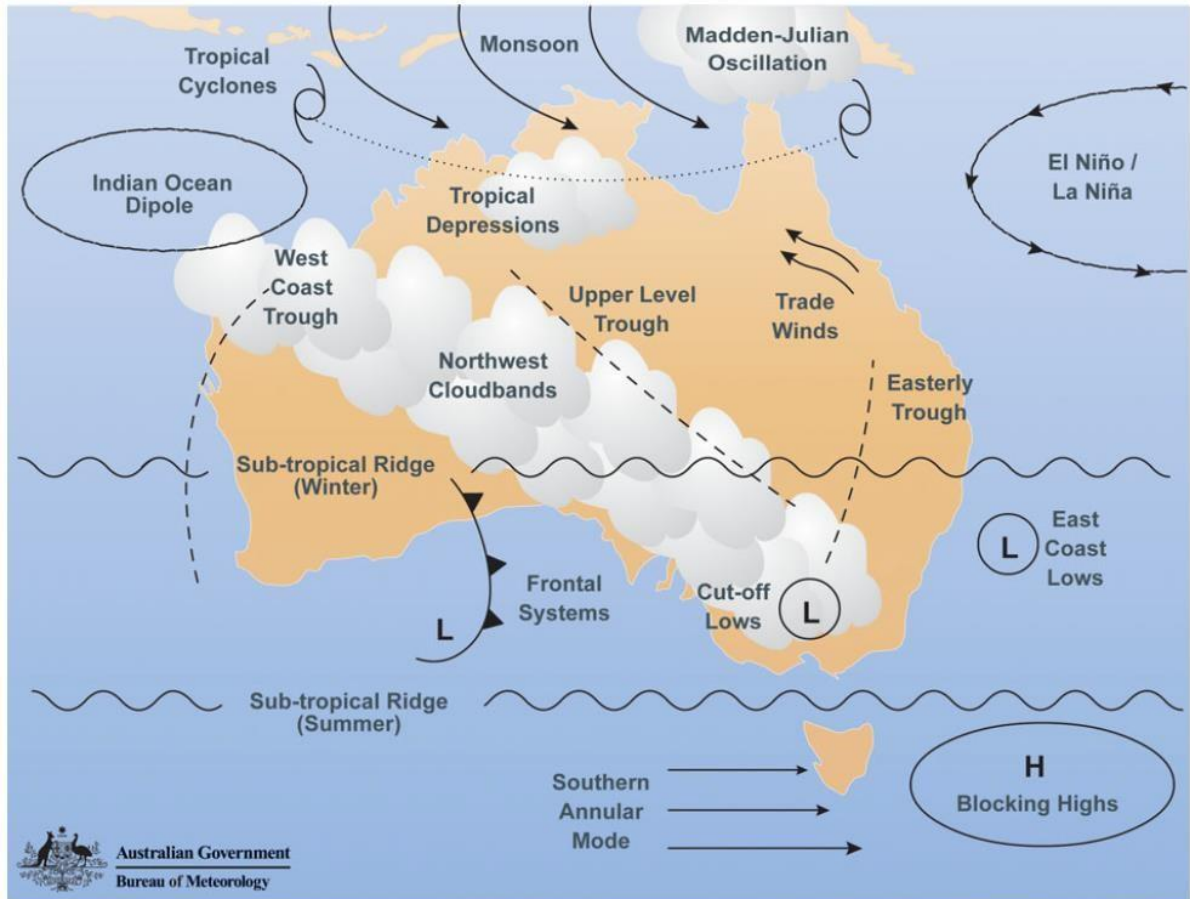


Figure 1.2: Rainfall drivers over Australia. Source: Bureau of Meteorology Copyright 1018 commonwealth of Australia, Dey et al (2019)

North of 15°S, the summer monsoon dominates the region with strong winds and increased rainfall in December, January, and February (Pickard et al., 1977) (Figure 1.2). Generally, winds north of the summer monsoon trough will flow southward and winds south of the trough will flow northward (Wolanski & Spagnol, 2000). Within the GBR lagoon, the most influential forcing mechanism on currents is wind (Burrage, 1993; Wolanski & Pickard, 2018; Wolanski & Thomson, 1984). Wind strength changes seasonally, with the prevailing wind in the winter being stronger from the southeasterly trades and reducing in the austral summer. Wind strength can also change due to the summer monsoon as well as other atmospheric patterns.

1.3.5 SOUTHERN EQUATORIAL CURRENT AND WESTERN BOUNDARY CURRENTS

The South Equatorial Current is the northern part of the South Pacific Subtropical gyre responsible for driving most of the circulation in the Coral Sea (Wolanski & Pickard, 2018). As the South Pacific Subtropical gyre reaches the equator, the cool bottom water that is upwelled warms as it traverses the equatorial Pacific (Wolanski & Pickard, 2018). The South Equatorial Current surface waters are well-mixed to approximately 150 m (Cane, 1983). The South Equatorial Current reaches the Australian continent between latitude 14°S and 18°S (Andrews & Clegg, 1989; Burrage, 1993; Church, 1987) from which the East Australian Current then flows southward and the Hiri Current flows northward (Figure 1.3). The location of bifurcation varies seasonally and interannually and these currents mostly influence waters on the outer shelf (Burrage et al., 1991; Wolanski & Spagnol, 2000) (Figure 1.3). This location of bifurcation marks the division of the warm tropical and cool subtropical gyres (Ridgway et al., 2018).

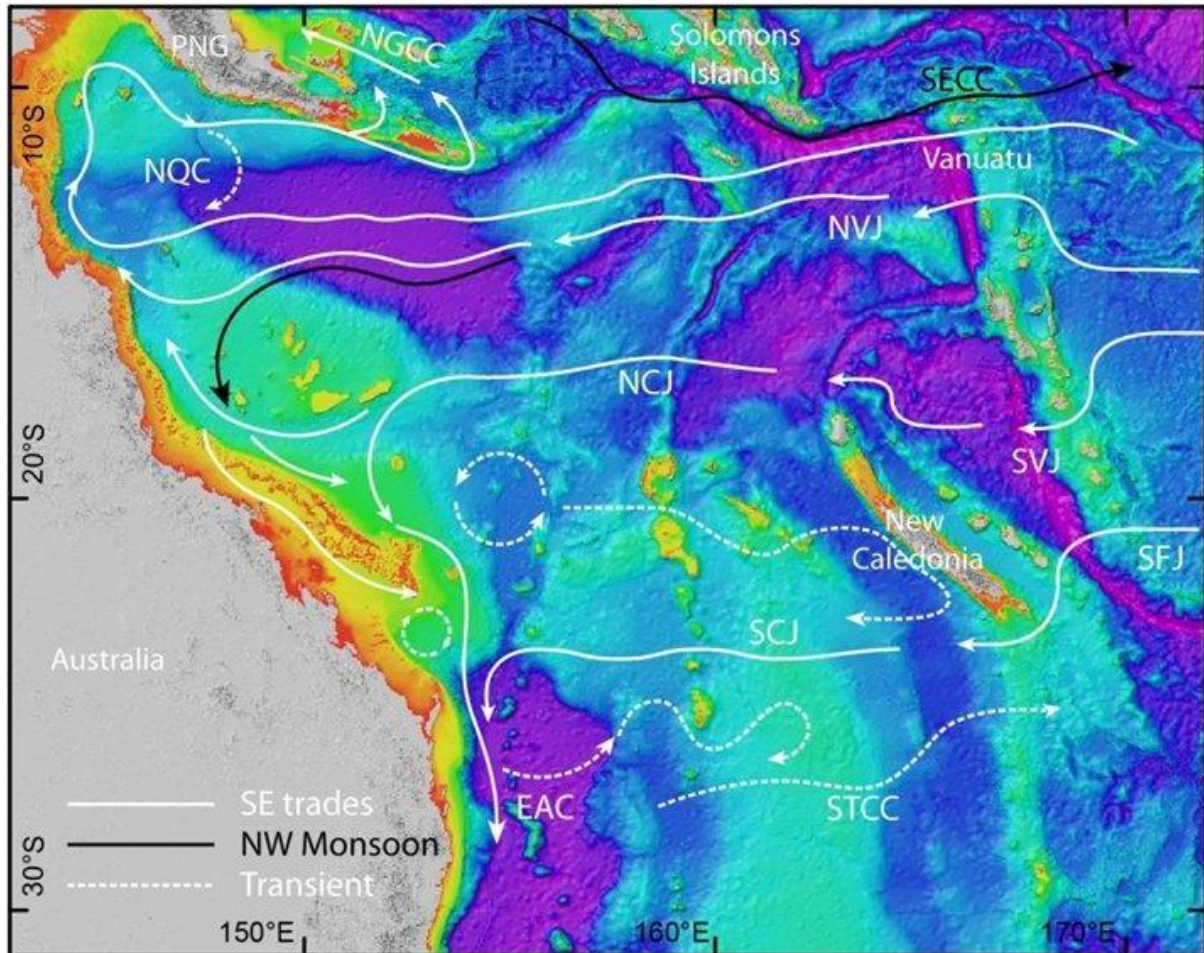


Figure 1.3: Great Barrier Reef bathymetry and important currents. “NGCC: New Guinea Coastal Current, mirroring the deeper New Guinea Coastal Undercurrent; GPC: Gulf of Papua Current, including the North Queensland Current and Hiri Gyre; SECC: South Equatorial Countercurrent; Jets of the South Equatorial Current (SEC): NVJ: North Vanuatu Jet; NCJ: North Caledonia Jet; SVJ: South Vanuatu Jet; SFJ: South Fiji Jet; SCJ: South Caledonia Jet; EAC: East Australian Current; STCC: Subtropical Countercurrent” Source: Commonwealth Scientific and Industrial Research Organization (CSIRO) eReefs

The East Australian Current is at minimum strength during April – May when the opposing southeasterly trade winds are strongest (Burrage et al., 1991). In contrast, the current is strongest during November – December when the trades are typically weaker (Burrage et al., 1991). The East Australian Current gains more energy when it meets

other southward flowing currents that branch off the South Equatorial current around 26°S such as the South Caledonia Jet (Steinberg, 2007) (Figure 1.3).

1.3.6 EDDIES

Eddies are a circular current of water found throughout the ocean. In the GBR region, there is a highly observed eddy using satellite and mooring observations known as the Capricorn Eddy. This stable cyclonic eddy can be found at the mouth of the Capricorn Channel on the continental shelf and contributes to northwest-ward flow into the region as well as upwelling (Burrage et al., 1996; Griffin et al., 1987; Kleypas & Burrage, 1994; Middleton et al., 1994; Weeks et al., 2010; Woodhead, 1970). The East Australian Current flows on the outer edge of the GBR and as it passes the Swains Reefs a “lee” is created due to the cape-like feature where the current encounters a land boundary and shallowing sea floor. The conditions produce a frontal zone with strong velocity shear tracking the deeper continental slope. A lateral stress is then formed with the lee zone and the swiftly flowing south-eastward water mass. The cyclonic torque creates the Capricorn Eddy in the lee zone. Centrifugal and Coriolis forces act to transport surface water outwards producing upwelling. In the summer and during times of anomalous warming, this eddy system feeds cooler, more dense, nutrient rich waters to nearby reefs. (Weeks et al., 2010)

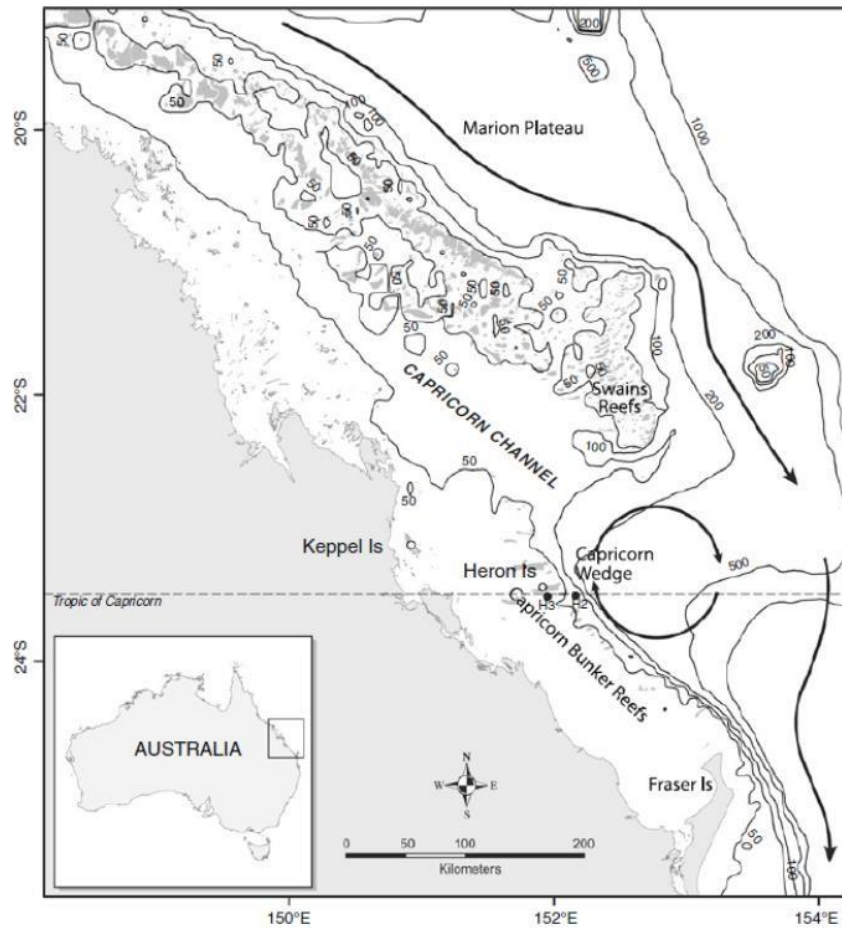


Figure 1.4: The features of the Capricorn Eddy are included in this map, bathymetry, coral reefs, and islands. The East Australian Current is the dark solid line with an arrow showing the flow direction. The eddy is located over a 200 m isobath known as the Capricorn Wedge, represented with dark circular arrows. Land and coral reefs are light gray. Source: Weeks et al (2010)

1.3.7 UPWELLING

Upwelling refers to cold water being uplifted to the surface layer of the ocean and typically restricted to certain depths on tropical coral reefs (Williams et al., 2018). The most intense upwelling, known as eastern boundary currents, occurs on the western boundaries of continents. There, wind-driven coastal upwelling processes bring cold, nutrient rich water driving primary production and further support most global fisheries (Mann & Lazier, 2013). Western boundary currents alternatively have less intense

upwelling than the eastern boundary currents resulting in a smaller impact on ecosystems. Although, upwelling can still influence tropical reef environments. Upwelling in the northern GBR has formed banks of calcareous algae known as *Halimeda* banks (Wolanski et al., 1988). These banks are formed where upwelling passes through the outer reef forming nutrient rich eddies on the lee of the ribbon reefs offshore Cooktown (Marshall & Davies, 1988).

The East Australian Current moving southward along the GBR shallow continental shelf edge leads to subgeostrophic flow due to the imbalance of onshore and offshore pressure gradients (Bakun, 2006). Upwelling in this region occurs with tidal energy, cyclonic eddies, and internal wave disturbances on the thermocline in combination with subthermocline waters from the bottom Ekman layer moving towards the shore and to the surface (Berkelmans et al., 2010; Griffin & Middleton, 1986; Wolanski, 1993). Shelf-break upwelling occurs dominantly in the central GBR due to the orientation of the reef between 18°S and 19°S (Bakun, 2006). Deep channels of the reef such as the Palm and Magnetic Passages, near 18°S and 19°S are ingress points of upwelling allowing the coral sea waters to enter the GBR lagoon.

The Eastern Australian Current moves north to south, and the dominant trades move in an opposing direction. Therefore, when winds are suppressed, upwelling is enhanced. These conditions are known as doldrums and are also associated with local warming events and stratification of the water column. Upwelling is strongest during summer months (December – February). The faster flowing Eastern Australian Current during doldrum conditions lifts the thermocline closer to the surface allowing for cooler water to reach the shelf. The Eastern Australian Current upwelling is restricted to the subsurface, is intermittent, and restricted to the central GBR providing limited relief to warming events of coral reefs. (Berkelmans et al., 2010)

1.3.8 ROSSBY WAVES

Rossby waves can be atmospheric or oceanic and are also known as planetary waves largely occurring due to the rotation of the Earth. Oceanic Rossby waves at lower latitudes can move across the ocean at a horizontal wave speed of months to a year at high-latitudes, or at mid-latitudes 10 to 20 years (Chelton & Schlax, 1996). Oceanic Rossby waves can influence the mixing processes at the shelf edge of the GBR due to the deep displacement of the thermocline by over 50 m (Steinberg, 2007).

1.3.9 CONTINENTAL SHELF WAVES

Continental shelf waves on the GBR can form from distant metrological forcings or locally from atmospheric pressure and wind forcings. As a result of continental shelf waves, changes in currents can break the thermocline leading to intrusions of cold water moving through the complex reef matrix.

1.3.10 RIVER PLUMES

Two major rivers feed into the GBR region, the Burdekin River in the central GBR and the Fitzroy River in the southern GBR. Rain feeds into the local rivers which eventually flow out to the ocean. Freshwater plumes move northward in the Southern Hemisphere along the coastline until they are mixed with wind and tidal forcings. Rainfall is most dominant during the summer monsoon and cyclone season. (Steinberg, 2007) Coral reefs can be harmed by excess nutrients from river plumes causing disease and overabundance of algae (Nugues & Roberts, 2003). River plumes can also cause excess sedimentation which can smother corals (Nugues & Roberts, 2003).

1.4 ATMOSPHERIC COMPONENTS OF VARIABILITY ON THE GREAT BARRIER REEF

Atmospheric conditions over the GBR drive important physical processes that can influence heat budgets over coral reefs. This research uses atmospheric input variables

to improve the projected coastal resolution of anomalous warming events into the water column, therefore a thorough explanation of various influences over the GBR is needed for context. Warming events also occur at time scales of weeks to months likely associated with the influence of local meteorology and reef-scale hydrodynamics on water temperatures.

1.4.1 WINDS

Winds over the GBR are described in the Physical Oceanography section regarding wind driven currents (Section 1.3.4). The wind patterns on the GBR are dominantly seasonal and are driven by larger atmospheric circulation patterns.

1.4.2 AIR AND SEA SURFACE TEMPERATURE

Air and sea surface temperature (SST) tends to peak in January/February and reach a minimum in October. The monthly mean SST ranges from 29°C in the far north during the summer and 22°C in the south during the winter. SST differences between the minimum and maximum generally range between 2 and 3°C. Compared to offshore waters, SSTs tend to be warmer over inshore, shallow reefs in the summer and cooler in the winter. (Lough, 2007)

1.4.3 RAINFALL

Northeastern Australia and parts of the coastal region of southeastern Australia typically have higher rainfall than the continent with an annual average of 475 mm yr⁻¹ (Dey et al., 2019). The highly variable summer monsoon brings rainfall to the far north and north GBR. Larger circulation patterns are correlated to seasonal and annual rainfall, such as the 30 to 60 day progression of Madden Julian Oscillation bringing bursts of rainfall during the summer monsoon (Lough, 2007; Madden & Julian, 1994) and La Niña years that typically drive higher than average annual rain (Dey et al., 2019) (Figure 1.2).

1.4.4 SUMMER MONSOON

The summer monsoon season occurs when northwesterly winds bring moist air and convective clouds which drive substantial increases in rainfall (Dey et al., 2019). These conditions are observed in austral summer from December February over 120°E to 150°E and 10°S to 20°S (Brown et al., 2016).

1.4.5 TROPICAL CYCLONES

Tropical cyclones are characterized by low atmospheric pressure, strong winds, waves, and heavy rainfall that use warm, moist air to gain energy. Tropical cyclones occur at the highest frequency during January and February between 16°S and 18°S on the GBR (Lough, 2007).

1.4.6 EL NIÑO SOUTHERN OSCILLATION

The El Niño-Southern Oscillation (ENSO) cycle is driven by swings in atmospheric pressure between the tropical Indo-Pacific and the eastern Pacific, strongly correlated to the strength of the Pacific trade winds (McPhaden, 2004). ENSO cycles between warm El Niño events and cold La Niña events result in the most prominent year-to-year mode of global climate variability (McPhaden, 2004). The warm El Niño refers to anomalous warming of generally 0.5°C offshore of Peru in the eastern equatorial Pacific and extending towards 180° W that lasts for at least 6 months (Trenberth, 1997). The atmospheric driver of El Niño is a weakening of the Pacific trades. An El Niño typically occurs every few years and can last for 1-2 years (Trenberth, 1997). The magnitude and duration of the warming is variable. El Niño is the primary source of interannual climate variability on the GBR causing a two-phase shift from anomalously cooler and wetter conditions (La Niña) to anomalously warmer and drier conditions (El Niño) (Dey et al., 2019). The summer monsoon typically weakens during an El Niño resulting in less rainfall and tropical cyclone activity (Risbey et al., 2009; Wolanski & Pickard, 2018).

1.4.7 HADLEY CIRCULATION

The Hadley circulation refers to a north-south movement of air with a low-level convergence at the equator causing the air to rise, move poleward and sink around 30°S and move back towards the equator (Lu et al., 2007). Latitudinal heating gradients cause this large-scale atmospheric overturning. The rising air along the equator has been named the Intertropical Convergence Zone. The large atmospheric circulation pattern of the Hadley circulation drives the generally westward trade winds. This circulation spans half of the globe and greatly influences Earth's energy budget. (Diaz & Bradley, 2004)

1.4.8 WALKER CIRCULATION

Located in the lower troposphere of the tropics, the Walker circulation refers to the east-west overturning (Julian & Chervin, 1978). Warm temperatures in the western Pacific cause air to rise and then cool and sink in the eastern Pacific (Vallis, 2011). During an El Niño, there are noticeable changes to the Walker circulation causing anomalously warm SSTs in the eastern Pacific (Baker et al., 2008). Comparable in certain respects, both the Hadley and Walker circulations are driven by horizontal temperature gradients at the surface (Julian & Chervin, 1978). The physical properties of both the Hadley and Walker circulation (atmospheric components of El Niño) can strongly dictate warming on the GBR (Dey et al., 2019).

1.4.9 SOUTHERN ANNULAR MODE

Southern Annular Mode refers to the north-south movement of the westerly belt of winds circulating Antarctica (Wang & Cai, 2013) (Figure 1.2). The negative phase of Southern Annular Mode has been associated with El Niño resulting in less rainfall over Australian mid-latitudes (Dey et al., 2019), or the southern portion of the GBR. There is a strong interannual signal correlated between El Niño and Southern Annular Mode (Wang &

Cai, 2013). The positive phase of Southern Annular Mode refers to strong westerly winds contracting toward Antarctica which limits fronts to southern Australia during austral summer and has been increasing since the 1960s due to ozone depletion (Marshall, 2003; World Meteorological Organization, 2007).

1.4.10 SUBTROPICAL HIGH

The Subtropical High is the area of high mean sea level pressure over the midlatitudes of Australia (Figure 1.2) (Dey et al., 2019; Timbal & Drosowsky, 2013). The Subtropical High is formed by the descending branch of the Hadley circulation (Timbal & Drosowsky, 2013). The location of the Subtropical High is important on the GBR because this is the boundary of fronts and storm which provide clouds over the southern portion of the reef.

1.4.11 MADDEN-JULIAN OSCILLATION

Madden-Julian Oscillation is a burst of tropical cloud and rainfall which develops over the Indian Ocean and propagates eastwards over to the Pacific Ocean and sometimes around the entire global equator (Madden & Julian, 1971, 1972, 1994) (Figure 1.2). Madden-Julian Oscillation occurs on time scales of 60-90 days and can influence intra-seasonal rainfall variability such as the timing of the summer monsoon on the GBR (Wheeler et al., 2009).

1.4.12 INDIAN OCEAN DIPOLE

Indian Ocean Dipole patterns show anomalous SST conditions in the tropical western and eastern Indian Ocean from June-November (Dey et al., 2019) (Figure 1.2). A positive Indian Ocean Dipole event is often associated with below-average rainfall in central and south-eastern Australia in spring (Risbey et al., 2009) and is more likely to occur alongside an El Niño (Dey et al., 2019).

1.4.13 INTERDECADAL PACIFIC DECADAL OSCILLATION

Pacific Decadal Oscillation is a recurring decadal pattern of mid-latitude anomalous SSTs that can exacerbate warming events in Australia as seen in the 1997-1998 mass coral mortality event (Steinberg, 2007; Wolanski & Spagnol, 2000).

1.5 BIOGEOGRAPHY

The GBR supports a range of habitats, species, and processes. While corals are the focus of this study, other ecosystems are indirectly included, and the impacts of climate change will be felt across the entire range of biogeography described in following sections. Anomalous heat stress over a prolonged period from weeks to months and projected to lengthen into the future can impact all living organisms from benthic to open ocean species. For example, while variable across species, stress from increased warming can influence aspects of fish reproduction at all stages of life (Pankhurst & Munday, 2011). Additionally, the lack of habitat that results from coral mortality will influence many organisms. Without habitat or food directly from corals, damage to the food web, observable in a loss of microorganisms and eventually larger predators, can occur. Coral habitat also provides protection from predators. The biogeography provides additional context for the GBR region.

1.5.1 LAGOON FLOOR

The lagoon floor is the area within a barrier reef, for example the area often seen within a coral cay or sand island. The lagoon floor is commonly between 20-40 meters depth (GBRMPA, 2012) and can be comprised of structures ranging from mud and sand bottoms to reefs formed by algae, sponges, corals, ascidians, gorgonians, and other organisms. The lagoon floor accounts for 61% of the GBR region and contains over 5,000 species (GBRMPA, 2013; Pitcher et al., 2007). The species within the lagoon each serve unique functions to support the larger ecosystem. For example, the

structures made by sessile organisms provide shelter and nurseries for many species of fish, sharks, turtles, and rays (Ponder et al., 2002; Veron, 2000).

1.5.2 SEAGRASS

The seagrass meadows on the GBR provide a buffer from storm erosion and are also extremely important for nutrient cycling and carbon sequestration (Lamb et al., 2017; McKenzie et al., 2017; York et al., 2015, 2018). These habitats are extremely productive environments for fish, invertebrates, and algae (McKenzie et al., 2017) and provide food for dugongs and green sea turtles (Coles et al., 2015; Marsh et al., 2012; Read & Limpus, 2002).

1.5.3 ISLANDS

The ~1,050 islands on the GBR consist of coral cays, continental islands, and mangrove islands. The islands support many bird and plant species which play a critical role in providing nutrients to the reef ecosystem (Graham et al., 2018). The islands also provide an important buffer from storms to the more populated coastline and contribute to soil and sand formation (Mather & Bennett, 1984; Read et al., 2018).

1.5.4 CORAL REEFS

Coral reefs support the largest known diversity of plant and animal species (Luckhurst & Luckhurst, 1978; Messmer et al., 2011; Stella et al., 2011) among the world's habitats. The GBR is the world's largest continuous reef ecosystem spanning over 2,300 km. Coral reefs can range in depth distribution from shallow estuaries to deeper waters off the continental shelf. The coral reefs discussed in this thesis are light dependent, tropical corals as opposed to the deep, cold-water corals.

Corals are classified into hard and soft corals. Hard corals are habitat forming and can be thought of as part animal and part plant. Hard corals contain a calcareous skeleton

underneath the fleshy tissue. Tabular and branching hard corals (i.e. *Acroporids* and *Pocilloporids*) form complex structures that provide critical habitats to a range of fish and invertebrate species (Kerry & Bellwood, 2015; Pratchett et al., 2008; Stella et al., 2011). Faster growing corals are branching corals that grow at ~10-30 cm per year (Veron, 2011) and slower growing corals are boulder shaped species that grow around 1.3 cm per year (Lough & Barnes, 2000). Within the fleshy tissue of coral are microscopic algae known as 'zooxanthellae' which photosynthesize to provide the coral with a source of food. Corals can also eat by catching zooplankton in their stinging tentacles. The zooxanthellae are light dependent, so many tropical corals are found in less than 30 meters depth. Mesophotic coral reefs are defined as light dependent reefs that exist beyond recreational SCUBA limitations and are typically within 30-150 m. Mesophotic coral reefs are therefore also limited by light with an upper range of 150 m (Loya et al., 2016).

Reef function has previously been described in the context of habitat structure and the production of biomass. Coral reefs are biogenic structures formed by calcifying organisms that further provide habitat for many other species. The complex carbonate structure of a coral reef supports many trophic levels as they interact through predator-prey relationship. Bioerosion of the reef structure is another function of the reef, as certain organisms erode the calcium carbonate structure. Algal growth can compete with coral growth, driving parrotfish grazing, and placing the reef in a negative state of growth (Harborne et al., 2016; Lange et al., 2020).

1.5.5 SHOALS

Shoals are defined as submerged ridges or bank locations that are separated from the lagoon and barrier reef complexes with depth ranging from 10–130 m (Beaman, 2010; Harris et al., 2013). Shoals can vary in shape and size and be comprised of corals, sponges, algae and/or seagrass (Cappo et al., 2010; Speare & Stowar, 2007). Coral dominated shoals are often called submerged reefs which can grow into emergent reefs

(Buddemeier & Hopley, 1988). Another type of shoal commonly seen on the GBR is a *Halimeda* bank formed by the skeletons of *Halimeda* (genus), a calcareous green macroalgae (Hopley et al., 2007). Most *Halimeda* banks are in the far north and northern GBR in areas with cold, nutrient rich upwelling (Wolanski et al., 1988).

1.5.6 WATER COLUMN

The water column is the obvious medium between species for energy, nutrients, and larvae. The planktonic communities in the water column are the basis of marine food webs (Pomeroy, 1974). Certain species primarily live in the water column, or open ocean, such as marine mammals, pelagic fish species, invertebrates, and microbes.

1.5.7 CONTINENTAL SHELF

The edge of the Australian continent is the continental slope where depth increases rapidly from the shallow shelf to deep ocean basins and submarine canyons (Beaman, 2010; Webster et al., 2008). The shelf edge is generally defined as the boundary of the continental slope to approximately 100 m depth (GBRMPA, 2009). Mesophotic reef communities are often associated with the shelf edge habitat. These deeper, light dependent coral reefs, known as, 'mesophotic coral ecosystems', typically range from 30–150 m depth (Bongaerts et al., 2010; Kahng et al., 2010), and have not been well studied due to difficulties in collecting data at these depths (Bridge et al., 2012). They are defined as reef communities in the mid to lower photic zone that contain phototrophic taxa (Kahng et al., 2010), and in comparison, to shallow reef communities, these reefs have received little attention due to certain depth limitations of SCUBA (Bridge et al., 2012). Recent technologies have allowed for further studies among mesophotic coral ecosystems using autonomous underwater vehicles and remotely operated vehicles (Bridge et al., 2012).

1.6 GLOBAL WARMING

Global warming refers to the increase in the average temperature of the Earth's surface and atmosphere relative to the late nineteenth century and the continued projection (IPCC, 2021). Temperature records through observations date as far back as 140 years ago but, proxies from tree rings and isotopic records from ice cores, corals, and stalactites are used to generate further reconstructions of temperature (Jones & Mann, 2004; Vallis, 2011). These multi-record proxies are combined and calibrated over the past 100 years between instrumental records and the proxy measurements to extend the temperature record. Global average temperatures have increased by approximately 1°C since the 1880s (IPCC, 2021; Stocker, 2014).

1.6.1 FOSSIL FUELS AND GREENHOUSE GASES

Most solar radiation that passes through the atmosphere is absorbed by the Earth's surface causing warming. The warm surface of the planet emits longwave radiation. Greenhouse gases in the atmosphere absorb, then re-emit much of the longwave radiation coming from the Earth's surface. Some of this re-emitted radiation warms that Earth's surface and the lower atmosphere. The most dominant greenhouse gas is water vapor which is controlled by evaporation and precipitation and largely determined by atmospheric temperature. The second most dominant greenhouse gas is CO₂, a product of fossil fuel burning and other sources.

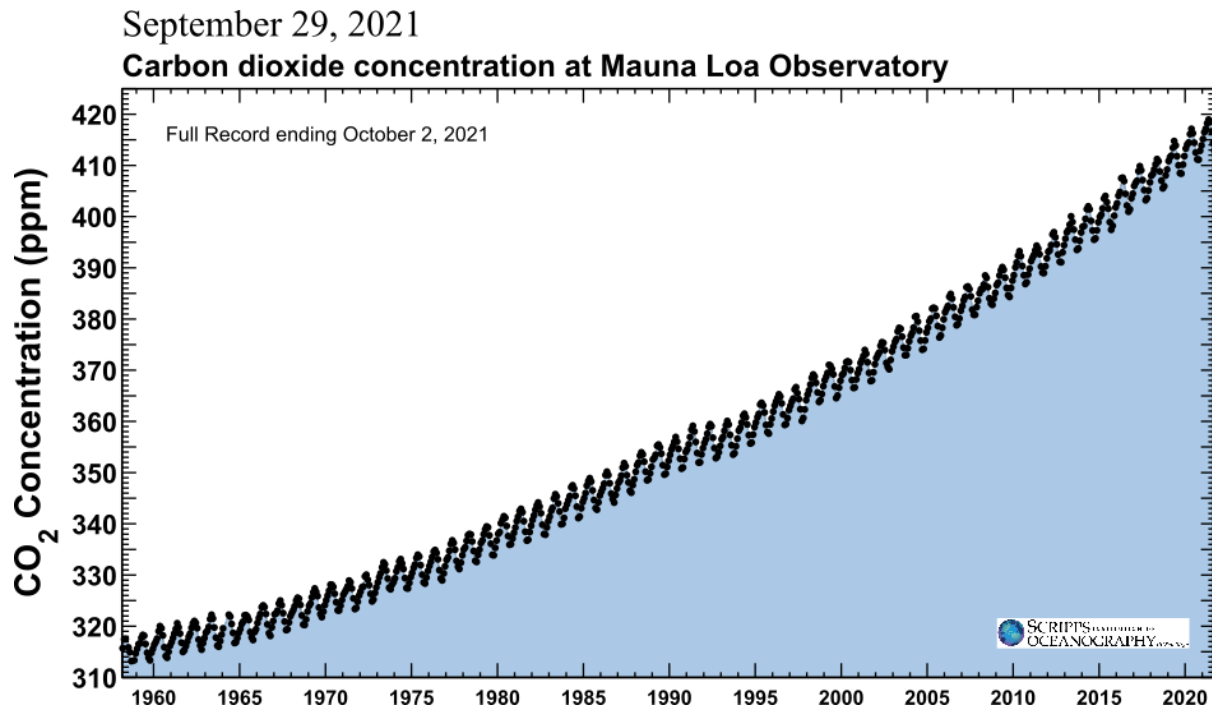


Figure 1.5: The full record of CO₂ concentrations from Mauna Loa, Hawaii from 1958-2021 in parts per million. Source: Keeling Lab, Scripps Institution of Oceanography, University of California, San Diego

There has been a steady increase in CO₂ concentration over the past 5 decades rising from ~310 ppm to exceeding 410 ppm in 2021 (Figure 1.5). This rate of increase is faster than any increase of CO₂ in the past 10,000 years (Fischer et al., 1999).

Radiative forcing, which warms the Earth, increases approximately 4 Wm⁻² with each doubling of CO₂ (Solomon et al., 2007). Methane, another important greenhouse gas, has also been increasing in recent years.

1.6.2 OCEAN WARMING

The ocean surface has warmed by ~0.11°C per decade [CI 0.09 to 0.13] since the 1970s (IPCC, 2021; Stocker, 2014). Sea level is expected to rise 25-123 cm over the next century due to thermal expansion of sea water and melting of land-ice sheets. This rise in sea level will cause annual flooding for 0.2%-4.6% of the global population

(IPCC, 2021). The circulation of the ocean is largely maintained by differences in density gradients from high to low latitudes (Marshall, 1995). The South Equatorial Current bifurcation is expected to move poleward which would result in a deepening of the thermocline of the northward flowing Hiri current. The deepening of this thermocline will further result in a reduction in nutrients and warmer waters to the central and southern reefs (Steinberg, 2007). The East Australian Current is expected to strengthen under climate change due to change in the prevailing wind conditions (Cai et al., 2005).

1.6.3 GREAT BARRIER REEF AND CLIMATE CHANGE

The increases in average temperatures over the period 1871-2017 for the northern, central and southern GBR were 0.71°C, 0.85°C and 0.86°C respectively (Lough et al., 2018). Heat waves have increased in frequency and duration in Australia since 1910 (Oliver et al., 2018). Marine heatwaves are the most imminent and threatening climate driven events in terms of impact on coral reef ecosystems. Tropical cyclones can provide relief from marine heatwaves and bring rain to the region but, cyclones can also cause severe damage to the reef. The breakage of corals can lead to regrowth but can also lead to destruction if repetitive high energy continues to move the broken fragments (Kenyon et al., 2020). Tropical cyclones are expected to decrease by 30% in frequency but increase in intensity into the future, although there is not great certainty behind this projection due to the coarse resolution of climate models (Lavender & Walsh, 2011). While mean rainfall over the southern portion of the GBR is expected to decrease under global warming (Grose et al., 2015; Grose et al., 2017; Whetton et al., 2016), short and intense storm events are expected to increase in frequency (Dey et al., 2019).

The carbonate accretion of corals will likely be compromised by global warming and ocean acidification resulting in a lack of diversity amongst coral communities and eventual failure of coral reef structures (Hoegh-Guldberg et al., 2007). Since the industrial revolution, the pH of the ocean has increased by 0.1 pH unit (Solomon et al., 2007). Approximately 25% of emitted anthropogenic CO₂ is absorbed by the ocean.

When CO_2 is absorbed into the seawater, it forms carbonic acid, lowering the pH, making the seawater more acidic and causing the deterioration of calcium carbonate structures (Figure 1.6). It is estimated that ocean acidification will reduce calcification rates of corals and calcifying macroalgae to 10-50% less than pre-industrial rates by mid-century (Kleypas & Yates, 2009).

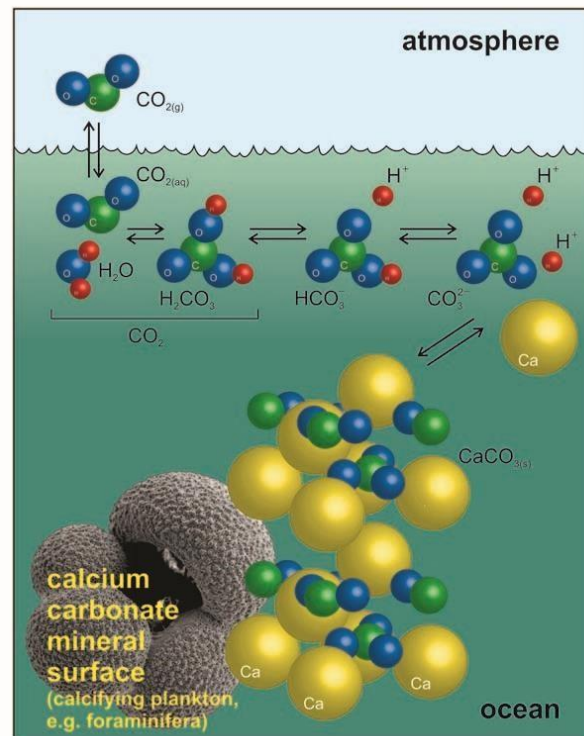


Figure 1.6: Carbonic acid is formed because of CO_2 absorption in seawater which causes the further deterioration of calcium carbonate structures. Source: Barker & Ridgwell (2012)

Corals can also be threatened by invasive species, fishing, and run-off. Crown-of-thorns, while native to Australian water, predate on coral tissue and are known for having large outbreaks of the population. Crown-of-thorns control programs are currently in effect on the GBR but, the success of the program is still highly contested due to a lack of understanding of the cause of the outbreak (Hughes et al., 2014). One obvious negative impact from fishing is the removal of herbivorous fish that help manage algal growth on the reef. Algae can cover and smother corals (McCook et al.,

2001) if herbivorous fishes are removed (Kelly et al., 2017). Algal growth can increase significantly due to excess nutrients from storm run-off in combination with a lack of herbivorous fishes (Kelly et al., 2017). During storms increased rainfall causes increased nutrient run-off from rivers and land-based sources, especially from fertilized land. Excess nutrients can also lead to coral diseases (Green & Bruckner, 2000). Coral diseases can cause tissue loss and often lead to mortality of the entire colony (Willis et al., 2004). The stress to corals caused by disease, invasive species, and other threats is only exacerbated when facing additional pressure from climate change.

1.7 CORAL BLEACHING

Within the tropical oceans, periods of anomalously warm sea temperatures have increased in frequency (Eakin et al., 2010; Hughes, Anderson, et al., 2018; Hughes, Kerry, et al., 2018) and severity, resulting in the deterioration of global coral ecosystems (Wilkinson & Souter, 2008). Recent mass coral bleaching events on the GBR (1998, 2002, 2016, 2017, 2020) occurred as a result of thermal stress (GBRMPA, 2019; Bozec et al., 2020; Eakin et al., 2010; Hughes et al., 2017; Hughes, Kerry, et al., 2018), often after several weeks of temperatures exceeding their usual summer temperature by 1°C to 2°C (Berkelmans & Willis, 1999; Glynn & D'croz, 1990; Reaser et al., 2000). Light absorption by zooxanthellae is heavily influenced by pigment and light scattering properties due to skeletal characteristics allowing corals to regulate their internal light field (Enríquez et al., 2005). During coral bleaching caused by prolonged warmer than usual temperatures, high light conditions cause increases in the respiration rate which further accelerates bleaching (Jokiel & Coles, 1990). The release of their zooxanthellae leaves their tissue transparent appearing white or bleached (Berkelmans & Willis, 1999; Glynn & D'croz, 1990; Reaser et al., 2000). Bleaching can result in mass coral mortality if stress is sufficiently prolonged or intense (Eakin et al., 2010; Hughes, Anderson, et al., 2018).

1.7.1 OBSERVED GLOBAL CORAL BLEACHING

Global coral bleaching and mortality were initially correlated to warming sea temperatures in the 1982-83 El Niño-Southern Oscillation event (Glynn, 1984, 1988; Robinson, 1982). Coral bleaching events commonly coincide with El Niño events (Baker et al., 2008; Glynn et al., 2001; Kleypas et al., 2015) but this is not always the case (Hughes, Anderson, et al., 2018). Bleaching conditions over individual coral reefs can be linked to weather patterns during El Niño events driving reduced cloud cover, higher than normal air temperature, and higher than normal pressure conditions (McGowan & Theobald, 2017). In the early 1980s, global severe coral bleaching was occurring once every 25-30 years. The frequency of severe bleaching has since increased to approximately once every 6 years in 2016 (Hughes, Anderson, et al., 2018) with more recurring events happening most recently in 2016, 2017 and 2020. As our climate continues to warm, bleaching is a significant threat to the future of coral reefs (Hoegh-Guldberg, 1999; Hoegh-Guldberg et al., 1997; IPCC, 2018; IPCC, 2021).

1.7.2 LABORATORY BASED CORAL BLEACHING STUDIES

In the tropical eastern Pacific, experimental evidence determined the upper thermal tolerance limits of corals correlated to the 1982-1983 El Niño related mass bleaching event (Glynn & D'croz, 1990). A laboratory study mimicking field conditions from the 1982-1983 warming event demonstrated thermal tolerance of the coral *Pocillopora damicornis* declined throughout the 10-week period with temperatures of 30-32°C, compared to normal temperatures of 26-28°C (Glynn & D'croz, 1990). Further research determined the upper thermal tolerances for a range of species, *Pocillopora damicornis*, *Acropora elseyi*, and *Acorpora formosa* at Orpheus Island Research Station on the GBR. The study concluded that these coral populations can survive in conditions only slightly above ambient mean summer temperatures (Berkelmans & Willis, 1999). The summer bleaching threshold for *A. formosa* was 2-3°C higher than the local mean summer temperature. *P. damicornis* and *A. elseyi* appeared to show a seasonal acclimatization with 3-4°C higher (Berkelmans & Willis, 1999). In 1997-1998, another El Niño event triggered the most geographically extensive and severe mass coral bleaching to date impacting tropical coral reefs globally in the Pacific Ocean, Indian

Ocean, Red Sea, Arabian Gulf, and the Caribbean (Reaser et al., 2000). In 2005, record warm temperatures caused thermal stress on coral reefs in the Caribbean (Eakin et al., 2010). Quantifying warm temperatures using satellite data while observing bleaching and mortality of coral's enabled the calibration of the sensitive relationship between warming waters and coral bleaching (Eakin et al., 2010).

1.7.3 GREAT BARRIER REEF CORAL BLEACHING

The thermal induced, widespread mass coral bleaching events that occurred on the GBR during the austral summer of 2016, 2017 and 2020 have been the most tightly clustered events to date. Coral cover was impacted throughout the entire GBR by the 2017 and 2020 events while the 2016 event was mainly concentrated in the far north and northern GBR (Bozec et al., 2020). Hughes et al (2017) estimated that as much as 50% of shallow water corals on the GBR were lost due to thermal stress from the 2016 event. Another estimate from Bozec et al (2020), claims that these three-events reduced coral cover by one third across the entire GBR (Bozec et al., 2020).

During previous warming events, while large areas on the GBR were bleaching, there were areas that did not bleach due to mesoscale mixing processes providing a cooling effect, shading from clouds, and/or turbid waters (Baird et al., 2018; McGowan & Theobald, 2017). It has been well established that coral bleaching occurs in the absence of mixing (Wolanski & Pickard, 2018). Glynn (Glynn, 1996) hypothesized that certain areas exposed to vigorous circulation (upwelling centres, oceanic banks, island shores), as well as high latitudes, and moderate depths may provide corals with a refuge from warming ocean temperatures (Glynn, 1996; Madin et al., 2018).

1.7.4 CORAL STRESS METRIC: DEGREE HEATING WEEKS

In 1995, Gleeson and Strong applied a cumulative heat stress algorithm referred to as Degree Heating Weeks (DHW) to demonstrate that the duration and intensity of increased water temperatures can predict the strength of coral bleaching. Initially,

satellite temperature from 1982-1992 was compared with moored buoy temperatures to validate the satellite data. The satellite SST data was then applied to bleaching events in Tahiti (1984, 1987), Bermuda (1988, 1991), and Jamaica (1987, 1989, 1990). The temperature data coincided with the bleaching events in the initial onset and duration. (Gleeson & Strong, 1995)

The DHW algorithm was then applied using SST data for thousands of reefs from 1985-2002 and this study tested the method of accumulating SST anomalies over a 12-week time period (Donner et al., 2005). It has been well established through independent coral bleaching reports that some bleaching occurs at four DHW and coral mortality tends to occur around eight DHW (Bozec et al., 2020; Donner et al., 2005; Eakin et al., 2010; Hughes, Kerry, et al., 2018; Hughes et al., 2017) (Figure 1.7).

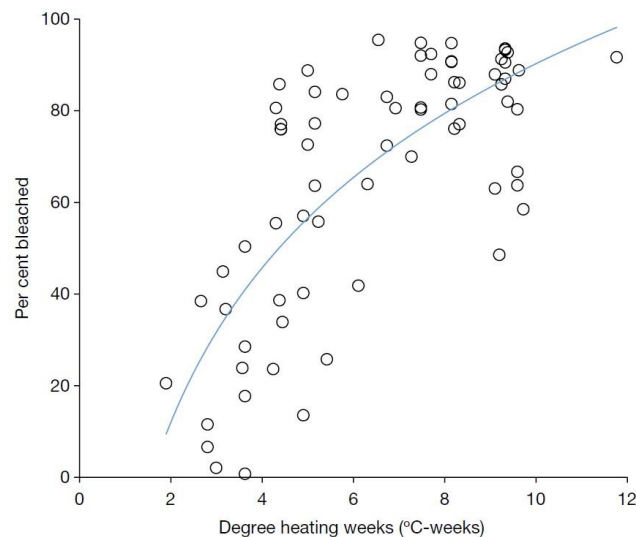


Figure 1.7: Satellite-based Degree Heating Weeks during the 2016 event and the percent of corals bleached in March and April are shown as data points representing an individual reef ($n=69$). The fit is $y=48.6\ln(x)-21.6$, $R^2 = 0.545$. Source: Hughes et al (2017).

The DHW algorithm continues to be tested and improved throughout the coral community at large. The DHW values are a potential trigger for coral bleaching and have been strongly correlated to bleaching events in the past (Bozec et al., 2020;

Donner et al., 2005; Hughes, Kerry, et al., 2018; Hughes et al., 2017) (Figure 1.7) but do not necessarily provide evidence of coral bleaching. Importantly, the National Oceanic and Atmospheric Administration (NOAA) Coral Reef Watch (CRW) organization has developed standardized products to provide a range of coral stress metrics. The DHW metric is dependent on anomalies which are created based on the difference from a climatological period. Therefore, the creation of a consistent and correct climatology is a very important aspect of the DHW algorithm. The difficulties in creating a useful climatology have been, 1.) having a long enough time series, and 2.) linking the climatology dataset to the near-real time datasets (Skirving et al., 2020). One difficulty in creating a long-term time series for a climatology was the eruption of Mt. Pinatubo which caused aerosol contamination to the satellite derived SST data. The data from 1991-1992 was then removed and to account for the missing data, an average of the existing years from 1985-1993 (without 1991 and 1992) was centred on 1988.2857. This method continues to be used in the NOAA CRW climatology. As satellite data continued to improve in resolution and quality, a large bias occurred between the old dataset and the new dataset. In 2017 the CRW group created a single product suite to provide high resolution, continuous SST products for coral stress metrics. These products and the methods behind their creation are used throughout this thesis for consistency in practice and are described below. (Heron et al., 2014; Skirving et al., 2020).

1.7.5 MAXIMUM MONTHLY MEAN CALCULATION

For each grid point, the monthly mean climatology was calculated. The monthly mean is a set of 12 temperature values that represent the average temperature for each month at each point. The monthly mean is calculated over the period 1985 to 2012 (inclusive). The climatology is then linearly adjusted to the value which would be expected in the year 1988.2857. This adjustment accounts for missing satellite derived data due to air contamination from the eruption of Mt. Pinatubo (1991-1992) (used in the original NOAA CRW maximum monthly mean climatology (Skirving et al., 2020)). The data from 1991-1992 was removed and to account for the missing data, an average of the existing

years from 1985-1993 (without 1991 and 1992) was centred on 1988.2857. The maximum monthly mean climatology is the maximum of the 12 monthly mean values for each grid point.

1.7.6 DEGREE HEATING WEEKS CALCULATION

Using the maximum monthly mean, a warm SST anomaly was created called a 'HotSpot'. The 'HotSpot' (Skirving et al., 2020) is calculated by subtracting the maximum monthly mean from daily SST values. The DHW product is a daily summation of 'HotSpot' values over an 84-day running window which represents the summer duration. Since thermal stress is considered to begin at maximum monthly mean + 1, the 'HotSpot' values are isolated to be greater than or equal to one, therefore all values less than one are set to zero. The daily 'Hotspot' values over the 84-day running window are then divided by seven to produce weeks, or DHW (Skirving et al., 2020).

Following the DHW calculations and prior to the calculation of annual maximum DHW values, calendar years were modified to be centred on the austral summer (i.e., August 1, 2014 – July 31, 2015) to avoid double counting maximum DHW that cross from one calendar year to the next (Skirving et al., 2019) (Figure 1.8). In Australia, coral bleaching typically occurs during the months of December, January, February, March, and sometimes November and April as well (Figure 1.8).

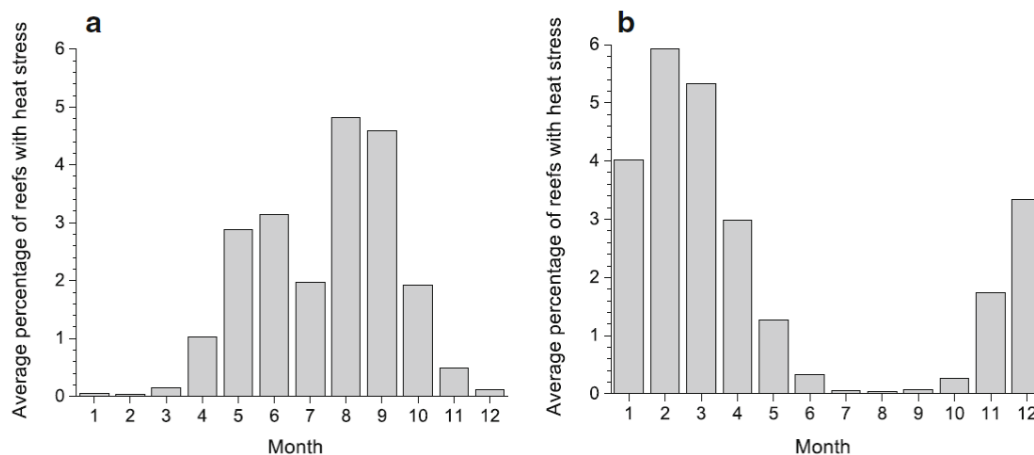


Figure 1.8: Histogram for the average percentage of reef pixels with heat stress for each month from 1986-2017 in a.) the Northern Hemisphere and b.) the Southern Hemisphere. Source: Skirving et al (2019)

Hypothetically, if an analysis were to extract the maximum DHW from the months in the calendar year January-December of 2020, and the bleaching event spanned December 2019 to March 2020, the December 2019 DHW values would be counted in the year 2019 and the rest of the event would be counted in 2020 (Figure 1.8). This is an example of double counting severe bleaching years. By placing the austral summer in the middle of a year calculation, the problem of double counting can be avoided.

1.7.7 DEGREE HEATING WEEKS VERSES DEGREE HEATING MONTH

Donner et al (2005) used Degree Heating Month (DHM) because previous studies used monthly averages to project the frequency of bleaching events (Hoegh-Guldberg, 1999; Sheppard, 2003). These studies assumed that monthly average temperatures 1°C above the maximum monthly mean led to bleaching (Hoegh-Guldberg, 1999; Sheppard, 2003). DHM yields different results to DHW (Figure 1.8). When calculating DHM, the maximum monthly mean does not detrend values towards 1988.2857 as in the DHW climatology (Donner et al., 2005). The maximum monthly mean is simply an average of each month from 1985 to 2012 (inclusive). The anomalies or 'HotSpots' in the monthly data are then accumulated over a four-month window, not a three-month window as in the DHW calculations (Donner et al., 2005).

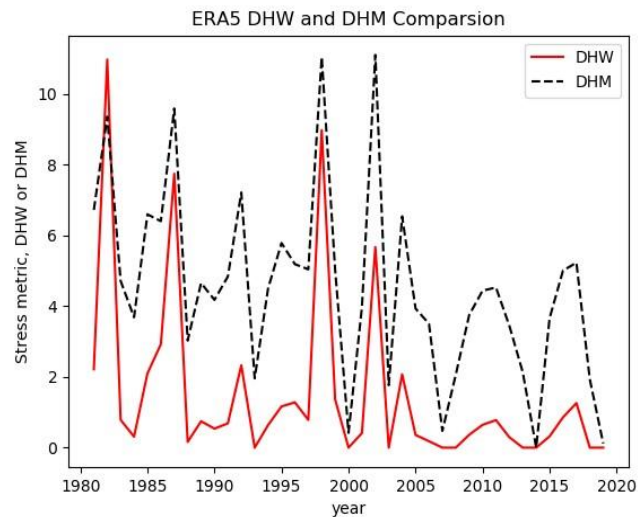


Figure 1.9: Downscaled ERA5 data were used to show the difference between the Degree Heating Month and the Degree Heating Week methods. These results are representative of the area across the entire spatial grid surrounding the Great Barrier Reef, not just within the Great Barrier Reef Marine Park Authority boundary. These data do not account for austral summer years verses calendar years.

As a result of the different methodology, 1 DHM = 4 DHW, therefore DHM has a higher coral stress metric (Figure 1.9). Numerous studies have used DHM and they have been the basis for major climate policy decisions. In the literature severe bleaching leading to mortality is generally defined at 2 DHM or 8 DHW (Donner et al., 2005; Frieler et al., 2013; Schleussner et al., 2016; Skirving et al., 2019). Figure 1.9 highlights an understanding and inconsistency in the literature and methodology surrounding coral stress metrics.

1.7.8 SATELLITE PRODUCTS FOR CORAL BLEACHING

Satellite observations provide near real-time monitoring of coral reef locations. The NOAA CRW program has developed and implemented early warning products from satellite observations. These operational products vary in terms of ways to measure coral stress from SST anomalies, Hotspots, and DHW. The CRW monitoring products continue to evolve in sophistication and implementation. For example, higher spatial

resolutions and other environmental parameters are now included as well as more refined numerical models and further development of bleaching algorithms. (Liu et al., 2006) Importantly, satellite observations are taken at the surface of the ocean and do not have predictive capabilities.

1.8 CLIMATE PROJECTIONS

1.8.1 CLIMATE MODEL INTERCOMPARISON PROJECT (CMIP), CURRENTLY ON THE 6TH PHASE

Climate scenarios were first used by the Intergovernmental Panel on Climate Change (IPCC) Special Report (Morita et al., 2000) to investigate future outcomes of anthropogenic drivers of climate change, such as greenhouse gases, aerosols, and land use change. The climate scenarios then formed the basis for the climate model projections. Climate model projections continue to be used to help inform the changes to the climate system, impacts on the community and environment, as well as the effects of mitigation and adaptation measures.

The development of Representative Concentration Pathways (RCPs; Van Vuuren et al., 2011) followed an expert meeting in 2007 with the intent to create a process for developing new community scenarios. RCPs are a set of four pathways that describe emissions of air pollutants and greenhouse gases, in addition to land-use. The RCPs span a wide range of outcomes through the end of the 21st century. The climate modelling phase that applied RCPs was phase 5 of the Coupled Model Intercomparison Project (CMIP5). Since the RCPs in CMIP5, the Scenario Model Intercomparison Project has been designed to account for societal concerns on the changes of climate adaptation, mitigation and impacts using multi-model climate projections. New emissions and land use scenarios (Riahi et al., 2017) have been produced with integrated assessment models based on projections of societal development. Further, Shared Socioeconomic Pathways (SSP) provide a new basis for climate projections

accounting for new projections on societal developmental pathways. Related to RCPs, SSPs are now the basis for the 6th phase of the Coupled Model Intercomparison Project (CMIP6) along with updates to a wide range of climate models. (O'Neill et al., 2016)

1.8.2 SHARED SOCIOECONOMIC PATHWAY (SSP)

The IPCC recently discussed the putative benefits of achieving the most optimistic warming scenario of 1.5°C above pre-industrial global temperatures (cf. the original target of 2°C warming) (IPCC, 2018). A formal analysis of the potential benefits that might accrue from adopting the 1.5°C vs 2.0°C warming scenario is now feasible given the newly released CMIP6, which distinguishes the 1.5°C focused SSP1-1.9 (Riahi et al., 2017) from alternatives (O'Neill et al., 2016).

There are five SSPs for various possible socio-economic developments. The pathways include sustainable development, inequality, regional conflict, fossil fuel-based development, and middle-of-the-road development. While consistent with the literature, there is a wide range of uncertainty surrounding economic and demographic projections. Within this study, the focus will be on three SSP trajectories (SSP1, SSP3, SSP5) (Riahi et al., 2017) and four emissions trajectories (SSP1-1.9, SSP1-2.6, SSP3-7.0, SSP5-8.5) (Riahi et al., 2017). The last numbers (1.9, 2.6, 7.0, and 8.5) refer to the peak radiative forcing (W/m^2). SSP1 refers to the most sustainable future, involving low material growth and lower resource and energy intensity. As a result of development goals being more focused on the global commons investing in education, health and economic growth emphasizing human well-being, inequality is reduced across countries. SSP3 focuses on 'regional rivalry', a rise in nationalism, a scenario where regional competitiveness and conflict drives countries to focus on their own energy and food security goals. Additionally, investments in education and technology decline, inequalities worsen, and economic development is slow.

Population growth in this scenario is high in developing countries and low in industrialized countries. Also, the international community does not prioritize

environmental issues in SSP3. SSP5 is a world based on fossil fuel development, energy intensive lifestyles which grow the global economy and population. Competitive markets drive technology, innovation, and human capital towards sustainable development. Population peaks and then declines; local environmental problems are successfully managed and solutions such as geo-engineering may be included to manage social and ecological systems (Riahi et al., 2017). While SSP1-1.9 and SSP1-2.6 are within the same SSP category (SSP1), they contain different radiative forcing pathways. SSP1-1.9 was designed to limit warming to 1.5°C by the end of the century. This scenario uniquely contains the application of technology which extracts large amounts of CO₂ out of the atmosphere resulting in net negative emissions in the second half of the 21st century. (O'Neill et al., 2016)

1.8.3 EVOLUTION OF CLIMATE PROJECTIONS OVER CORAL REEFS

Climate models are used to inform global and regional policy decisions on the impacts of climate change (Lemos & Rood, 2010). Hoegh-Guldberg (1999) was the first to predict the global thermal stress impacts from warming temperatures on coral reefs. This study used climate models and knowledge of existing information on the relationship between elevated SSTs and mass coral bleaching to project the frequency and intensity of bleaching events in the next 100 years (Hoegh-Guldberg, 1999). The 1998 severe bleaching event was the worst on record at the time of this study and the projections indicated that the 1998 event would become more common in the proceeding 20 years with coral thermal tolerances likely being exceeded nearly every year in the next few decades (Hoegh-Guldberg, 1999). The results correctly predicted that the frequency and strength of the 1998 event would become more common in the 20 years following the study. Since this study, Donner et al (2005) continued the development of the DHM heat stress algorithm and applied a frequency analysis of DHM thresholds to global climate models. These results indicated that global bleaching events would occur annually or biannually over the next 20-30 years (Donner et al., 2005).

Climate models typically have a coarse horizontal resolution from 1 to 2 degrees and are unable to resolve mesoscale features such as ocean boundary currents, eddies, tidal mixing, continental shelf, and detailed biogeochemical processes (Van Hooidek et al., 2016; Zhang et al., 2016). Due to this coarse resolution, climate models lack the ability to demonstrate detailed hydrodynamics influencing the spatial variability of individual coral reefs (Donner et al., 2005; Kwiatkowski et al., 2013). In Kwiatkowski et al. (2014), spatial patterns of SSTs from CMIP5 models were assessed in five different coral regions. The models performed best at scales greater than 4-degree resolution (Kwiatkowski et al., 2014). The models also failed to capture warming anomalies between 1960-1980 and 1985-2005 (Kwiatkowski et al., 2014). Also, the differences between climate models are demonstrated in the IPCC reports as models are used as an ensemble to best inform climate projections (IPCC, 2018; IPCC, 2019; IPCC, 2021; Solomon et al., 2007).

1.8.4 DOWNSCALING CLIMATE MODELS

Management of coral reef environments, often restricting human influences, requires climate projections at local scales, around 3-10 km (Hoegh-Guldberg et al., 2007; Hughes et al., 2003; McLeod et al., 2009; Palumbi, 2004; Van Hooidek et al., 2015). To provide more detail in the coastal environment, methods of downscaling are often used, which involve linking a variable on a global scale to a variable at a regional or local scale (Deliang & Inger, 2008). Two methods for downscaling exist and can be implemented separately or together; 1.) dynamical downscaling and 2.) statistical downscaling. The quality of the information driving the downscaling is one of the most limiting factors (IPCC, 2021).

1.8.5 DYNAMIC DOWNSCALING

Dynamic downscaling uses high-resolution regional and local scale details of system processes to extrapolate from climate models (Knutson et al., 2008) enabling the simulation of more regional to local scale features but requires expensive computing

and considerable time spent setting up and testing models (Van Hooidonk et al., 2015; Van Hooidonk et al., 2016). While the dynamic downscaling allows for recovery of regional to local scale features, it is still associated with the biases in the parent climate models used to drive the downscaling. A further improvement upon dynamic downscaling is to correct for the biases on the climate model forcing (Bruyère et al., 2014; Drenkard et al., 2021; Machu et al., 2015; Pozo Buil et al., 2021; Xu et al., 2019). The cost of running dynamic downscaling and applying corrections to the climate model biases comes at the cost of running more models, exploring more scenarios, or undertaking longer simulations. These studies tend to be limited to individual models rather than the full ensemble typically shown in climate reports (IPCC, 2021).

1.8.6 STATISTICAL DOWNSCALING

Statistical downscaling applies a suite of various statistical methods to determine the relationship between climate patterns in large-scale climate models and local observations. Statistical downscaling is a more cost-effective method than dynamic downscaling but can often lead to highly interpolated, unphysically realistic, products (Wilby et al., 2004) especially in the coastal zone. For example, the grid spacing of the observation field and the climate model often require interpolation of the climate model to the grid resolution of the predictor field (Wilby et al., 2004). (Table 1.1)

Table 1.1 Strengths and weaknesses are summarized of main statistical downscaling methods.
Source: Wilby et al (2004)

Method	Strengths	Weaknesses
Weather typing (e.g. analogue method, hybrid approaches, fuzzy classification, self-organizing maps, Monte Carlo methods).	<ul style="list-style-type: none"> • Yields physically interpretable linkages to surface climate • Versatile (e.g., can be applied to surface climate, air quality, flooding, erosion, etc.) • Compositing for analysis of extreme events 	<ul style="list-style-type: none"> • Requires additional task of weather classification • Circulation-based schemes can be insensitive to future climate forcing • May not capture intra-type variations in surface climate
Weather generators (e.g. Markov chains, stochastic models, spell length methods, storm arrival times, mixture modelling).	<ul style="list-style-type: none"> • Production of large ensembles for uncertainty analysis or long simulations for extremes • Spatial interpolation of model parameters using landscape • Can generate subdaily information 	<ul style="list-style-type: none"> • Arbitrary adjustment of parameters for future climate • Unanticipated effects to secondary variables of changing precipitation parameters
Regression methods (e.g. linear regression, neural networks, canonical correlation analysis, kriging).	<ul style="list-style-type: none"> • Relatively straightforward to apply • Employs full range of available predictor variables • 'Off-the-shelf' solutions and software available 	<ul style="list-style-type: none"> • Poor representation of observed variance • May assume linearity and/or normality of data • Poor representation of extreme events

Importantly, certain statistical downscaling methods, such as using regression, can suppress extreme events and coral bleaching events occur during anomalously warm events.

1.8.7 DOWNSCALING OVER CORAL REEF ENVIRONMENTS

The van Hooijdonk et al (2015) study compares spatial patterns in the Caribbean from three different approaches to evaluate downscaling over coral reef environments; 1.) CMIP5 climate models (1x1 degree resolution), and 2.) statistical, and 3.) dynamic downscaling. SST values are used from the climate models, which means there are a large amount of missing data in the nearshore due to grid size and the land mask. This

statistical downscaling method applied a Poisson zonal interpolation landward to replace missing cells. The actual SST values are boundary conditions, left unchanged and then the values are interpolated landward to fill in missing values. The value assumed over land greatly determines how different the missing values are from the boundary condition, or the actual SST data (Figure 1.10). The land value in this study is given the value of zero and could be improved by using the latitudinal mean SST. The Poisson interpolation method is dependent on the resolution of the variable interpolated and the land value.

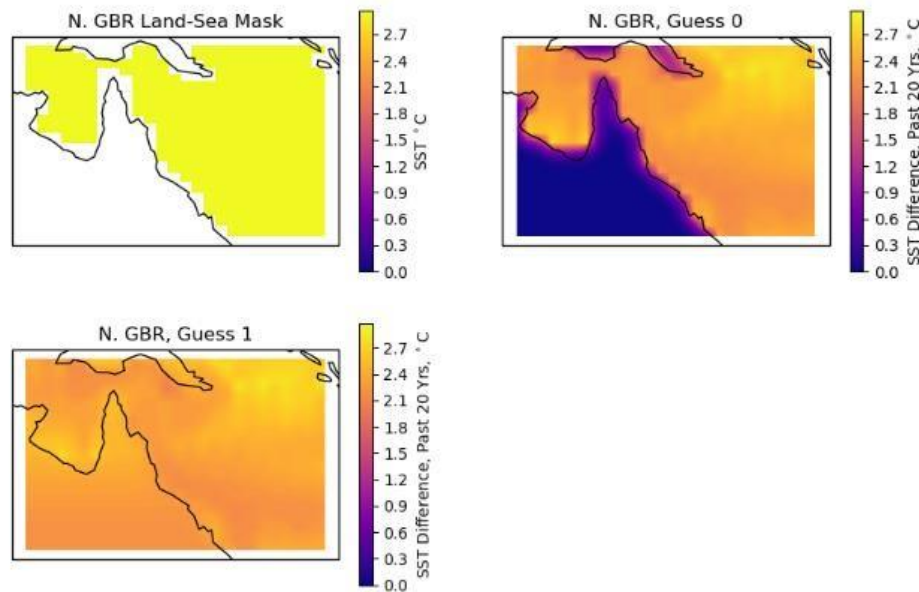


Figure 1.10: Sea surface temperature data was used to demonstrate the interpolation method used in van Hooijdonk et al. (2016) and (2015). (Top left) The plot is displaying the land-sea mask surrounding the Northern Great Barrier Reef (GBR) showing the coastal infilling that would be required. (Top right) The plot displays a guess of 0 for the Poisson grid filling method. (Bottom left) The plot displays a guess of 1 which assumes the zonal mean or latitudinal mean for the Poisson grid filling method.

The larger the difference in the land value from the SST values offshore, the more the data is “stretched” in the landward direction. Also, if the land was given the latitudinal mean, the mean is therefore generated using data from other ocean basins to inform

this initial guess and would begin to stand out when using data from earlier in the century to later in the century (Figure 1.10).

The dynamic downscaling in the Van Hooidonk et al (2015) study applied a high-resolution, eddy-resolving model called, Modular Ocean Model version 4.1 (Griffies et al., 2004) by the Geophysical Fluid Dynamics Laboratory. The Modular Ocean Model version 4.1 model has a resolution of approximately 11 km and was forced with bias-corrected temperature and salinity from the climate models. Only reef cells were used for the analysis and DHW were calculated to determine the onset of annual severe bleaching at >6 DHW and >8 DHW between a 10–15-year window. The results in this study show general similarities between all three downscaling approaches with more detail on high local-scale variation of annual severe bleaching. (Van Hooidonk et al., 2015). The differences in the dynamic and statistical downscaling approaches are most apparent in the areas known to have strong currents within the Caribbean. The dynamic downscaling resolved regional currents and projects an earlier onset of annual severe bleaching, than the statistical downscaling and the straight 1x1 degree climate model approach.

The Van Hooidonk et al (2016) paper expands the statistical downscaling method globally showing the effect of the landward interpolation towards the latitudinal zonal mean (Figure 1.10, Figure 1.11). These projections clearly show lower values closer to the coast due to the landward interpolation method (Figure 1.11). A large and significant part of this analysis is identifying areas of temporary refugia, or locations that will be impacted by bleaching later than others. This spatial analysis of temporary refugia is problematic as the landward interpolation resulting in a nearshore-offshore gradient proves problematic and is not representative of coastal warming patterns (Figure 1.11). Shallower water is generally quicker to warm due to having less of an offshore influence. The interpolation mechanism also does not show change into the future as warming increases in certain nearshore locations.

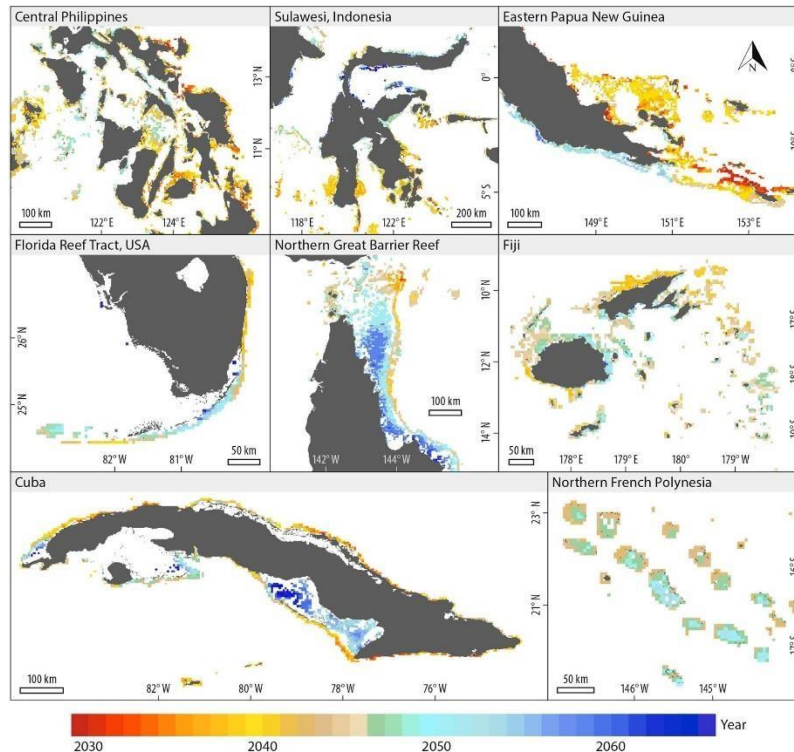


Figure 1.11: “Statistically downscaled projections of the timing of the onset of annual severe bleaching conditions under RCP8.5 for selected coral reef regions. These exemplify the high local-scale (10’s of km) variation seen in projected ASB timing in most locations and, though atypical, the low variation seen in Northern French Polynesia. This figure was created with NCL (NCAR Command Language Version 6.3.0, <http://www.ncl.ucar.edu/>.” Source: Van Hooijdonk et al (2016)

The methods used in Van Hooijdonk et al (2015) are used in the later study described and shown in Figure 1.10, Van Hooijdonk et al (2016). These results are the focus of a recent United Nations Environment Programme report and referenced in multiple IPCC reports (IPCC, 2019; IPCC, 2021.).

1.9 3-D MODELS FOR CORAL BLEACHING

In Australia, an advanced, biogeochemical, hydrodynamic 3-D model exists, called eReefs which was developed by a scientific research agency in Australia, the

Commonwealth Scientific and Industrial Research Organisation (CSIRO). They are interested in using eReefs to downscale climate projections on the GBR. The eReefs 3-D model is currently forced with weather predictions from ACCESS-R, and inputs include wind, atmospheric pressure, surface heat fluxes, and rainfall. The open ocean information is supplied to the model from the Bureau of Meteorology's Ocean Modelling Analysis Prediction System (OceanMAPS). eReefs outputs provide information on sea level, currents, temperature, salinity, and mixing properties. eReefs is currently run as a hindcast modelling tool but has the potential to improve the level of detail of climate projections.

Coastal 3-D biogeochemical-hydrodynamic models, such as eReefs on the GBR, tend to account for more oceanographic processes such as high resolution temperatures at depth. Although, more detailed models are computationally expensive to run, so it is typically not feasible to run longer hindcasts or projections for climate change. In addition, 3-D models are typically designed for certain regions lacking global coverage. eReefs has been successful in providing water quality information on the GBR. Sediment, nutrients, and pesticides have been modelled from the catchment to the complex hydrodynamics on the reef. As a result, policy decisions have been made to manage run-off from excess nutrient sources.

1.10 CLIMATE PROJECTIONS OF ATMOSPHERIC DRIVERS OF WARMING ON THE GREAT BARRIER REEF

Robust patterns of ocean-atmosphere climate variability such as ENSO, Madden-Julian Oscillation, Indian Ocean Dipole and Pacific Decadal Oscillation can enhance or suppress severe bleaching conditions on the GBR (Table 1.2). These large climatic patterns can influence wind and convective properties resulting in changes to the heat budget in the water column. The projections of these larger atmospheric patterns are critical to the understanding of spatial patterns of warming on the reef.

Table 1.2: Large-scale drivers of rainfall characteristics over Australia, past and future changes. (El Niño Southern Oscillation (ENSO), Indian Ocean Dipole (IOD), Subtropical Ridge (STR), Madden-Julian Oscillation (MJO), Tropical Cyclones (TC), and Southern Annular Mode (SAM))
Source: Dey et al (2019)

Drivers	Past changes	Projected future changes
ENSO	The weakening of Walker circulation since the beginning of 20th century (Deser et al., 2010), strengthening over the period 1980-2012 however, the mechanism of the strengthening of the Walker circulation is not clear (Luo et al., 2012).	A further weakening of Walker circulation is projected (low confidence) (Collins et al., 2010) along with frequent and intensified El Niño and La Niña events (Cai et al., 2015). The occurrence of El Niño events is projected to almost double due to climate change (Santoso et al., 2013).
IOD	The IOD events have increased while negative events have decreased since 1950 with more frequent IOD events. The mechanism is not clear and needs to be studied further. Although, global warming could be one possible reason (Cai, Sullivan, & Cowan, 2009).	Increased IOD events with an increase in frequency (Abram, Gagan, Cole, Hantoro, & Mudelsee, 2008; Cai et al., 2013).
STR	Increase in the STR intensity since 1970 (Timbal & Drosowsky, 2013). The reason is not clear as the trend in the intensity of Hadley Circulation needs to be studied further (Timbal & Drosowsky, 2013).	Increase in the STR intensity and a poleward shift in CMIP3 (Kent et al., 2013) and CMIP5 (Grose et al., 2015) models.
MJO	Increase in MJO amplitude (Lee & Seo, 2011) and frequency (Jones & Carvalho, 2006).	MJO amplitude is projected to increase by 30% (Chang et al., 2015).
Fronts	A small increase in frequency in fronts over the period 1989-2009. (Figure 2 of Berry et al. (2011)).	The southward shift in location. A small increase in front frequency and strength in RCP8.5 in southern Australia (see Figure 3b & d of Catto et al. (2014)).

Australian monsoon	The historical trend is not clear. Some monsoon indices show a clear reduction post-1980. (Christensen, Kanikicharla, Marshall, & Turner, 2013), however, Kajikawa, Wang, and Yang (2009) index shows an increase in monsoonal winds (Dey et al., 2018). The changes in Australian Monsoon in response to greenhouse emissions need to be studied further.	There is a little consensus among models. Although, CMIP5 models show an increase of 0.4% K-1 in monsoon rainfall in RCP8.5 simulations (Brown et al., 2016).
TC	There is a significant decline in total number of cyclones since 1969/1970. Also, there has been a decline in moderate and weak cyclones, but there is a weak, insignificant positive trend in the intense cyclone (Nicholls et al., 1998).	The downscaled GCMs show that the number of cyclones is projected to decrease by the end of the 21st century. A decrease in TC occurrence by 50% and 30% are projected by Abbs (2012) and Lavender and Walsh (2011) respectively by the end of the 21st century relative to the current climate.
SAM	The significant positive trend since observational records began in the 1960s (Marshall, 2003), and possibly since the 1940s based on paleoclimate evidence (Abram et al., 2014). Ozone depletion over the Antarctic and increasing GHG in the atmosphere are the possible mechanisms (Thompson et al., 2011).	In future, ozone is projected to restore, however, the continuous rising levels of GHG will have opposing impacts on the SAM trend (Thompson et al., 2011). A positive trend is projected in CMIP5 models by the end of the 21st century under RCP4.5 and RCP8.5 (Gillett & Fyfe, 2013).
East Coast Low (ECL)	No significant change (Ji et al., 2015).	Fewer ECLs with weaker intensity (Ji et al., 2015). The most intense ECLs are projected a small decrease in winter but an increase in summer (Pepler et al., 2016).

1.10.1 PROJECTIONS OF THE HADLEY AND WALKER CIRCULATION PROJECTIONS

As the planet warms, climate models project an expansion of the Hadley circulation poleward (Frierson et al., 2007; Lu et al., 2007) and a weakening of the Walker circulation (DiNezio et al., 2009; Vecchi et al., 2006; Vecchi & Soden, 2007). Although, the speculation on the weakening of the Walker circulation has been recently counterbalanced with evidence demonstrating a strengthening in the Pacific Trade since the early 1900s (Merrifield & Maltrud, 2011). Changes to the Hadley circulation drive changes to the Subtropical Ridge which is the descending branch of this circulation pattern (Dey et al., 2019).

1.10.2 EL NIÑO SOUTHERN OSCILLATION PROJECTIONS

With additional background warming, more historically hot summers are expected to occur regardless of the El Niño phase (King et al., 2017). El Niño's are expected to double in frequency with global warming (Cai et al., 2015) and El Niño and La Niña phases are expected to intensify (Santoso et al., 2013) (Table 1.2). The atmospheric variables associated with El Niño conditions prove to be important associations with wide-spread, mass coral bleaching conditions such as a reduction in clouds and increases in shortwave radiation (McGowan & Theobald, 2017). Generally, patterns of rainfall can help describe these atmospheric patterns as projections of future rainfall are intently studied for agriculture. (Table 1.2) Patterns of rainfall can be indicators of mixing or shading which can provide thermal relief to corals during warm spells. Since El Niño events are highly correlated to coral bleaching events, future projections of ENSO are critical for understanding the changes expected to occur on the GBR and global coral reefs.

1.10.3 SUBTROPICAL HIGH PROJECTIONS

There is an expected increase in the Subtropical High, sometimes referred to as the Subtropical Ridge, or the descending branch of the Hadley cell. This means that the Subtropical High is expected to intensify pushing storms poleward and driving a reduction in rainfall over Southeast Queensland. This change is well simulated in two

phases of climate modelling projections (CMIP3 and CMIP5). (Dey et al., 2019; Grose et al., 2015; Kent et al., 2013) (Table 1.2)

1.10.4 SOUTHERN ANNULAR MODE PROJECTIONS

The Wang & Cai (2013) study demonstrates that although El Niño and a negative Southern Annular Mode are strongly correlated, which would reduce rainfall and clouds over the southern GBR, the increases in global mean temperatures are driving a positive Southern Annular Mode into the 21st century. A positive phase strengthens and pushes this belt of westerly winds towards Antarctica. The projected positive phase of Southern Annular Mode is commonly seen in the literature and noted as 'high confidence' in the IPCC reports. (Dey et al., 2019; Gillett & Fyfe, 2013; Wang & Cai, 2013) (Table 1.2)

1.11 THESIS PLAN

The introduction, Chapter 1, has broadly provided an overview of climate exposure on the GBR for coral reef ecologists. The literature review focuses on GBR physical oceanographic and climate dynamics, reef habitats, the threats of climate change to the reef system, and recent studies on downscaling climate projections for coral reefs. The methods and model validation for the study are then described in Chapter 2 as two components (a, b); a.) to describe the downscaling processes used in this study as it pertains to the GBR and, b.) to understand the downscaling input variables as well as the derived output variable for calculating prolonged, anomalous heat stress to corals, DHW. The validation of the downscaling method has been published (Halloran, **McWhorter**, et al., 2021). Then in Chapter 3, the importance of limiting future ocean warming to the Paris Agreement target of 1.5°C of global average warming by 2100 is discussed as the temporal component of the downscaled GBR climate projections. This chapter was published in *Global Change Biology* (**McWhorter et al., 2021**). Chapter 4 continues to analyse and describe the downscaled climate projections using more of a

spatial context. Additionally, this chapter describes the oceanographic and atmospheric variables driving the ability of certain areas of the reef to persist as a climate refugia, or areas less exposed to extreme and prolonged heat stress than other areas of the GBR. This chapter was recently published in *Global Change Biology* (**McWhorter et al., 2022**). Chapter 5 then explores the bottom temperature output of GBR climate projections using a stratification metric to classify cool anomalies at depth (0-50 m). The final chapter, Chapter 6, provides an overview of the main conclusions, caveats of the work, and discusses ideas for future research building upon these findings.

CHAPTER 2

METHODS AND MODEL UNDERSTANDING: DOWNSCALING CLIMATE MODELS USING S2P3-R V2.0 ON THE GREAT BARRIER REEF

This chapter has been divided into two parts: a.) downscaling methods using S2P3-R v2.0 and, b.) understanding the model inputs and Degree Heating Weeks calculation outputs in the context of coral bleaching.

PART A

Halloran, P. R., **McWhorter, J. K.**, Arellano Nava, B., Marsh, R., & Skirving, W. (2021). S2P3-R v2. 0: computationally efficient modelling of shelf seas on regional to global scales. *Geoscientific Model Development Discussions*, 1-30.

Author contributions:

Conceptualization: PRH, JKM, RM

Methodology: PRH, JKM, BAN, RM, WS

Investigation: PRH, JKM, BAN

Visualization: PRH, JKM, BAN

Supervision: PRH

Writing—original draft: PRH, JKM (Upgrade report)

Writing—review & editing: PRH, JKM

My main contributions to Halloran et al (2021) are listed below.

- Conceptualization began with wanting to look at bottom temperature for coral reef climate projections which led Paul to suggest the application of S2P3, based on the work of Bob Marsh
- Conceptualization of incorporating local bathymetry to better represent water column mixing process
- Detection of the hotspot error led to changing the input cloud variable to long and shortwave radiation, which also led to further developing an understanding for the heat trapping effect that was causing the hotspot
- Gathered data and initially validated Great Barrier Reef surface and bottom temperature outputs using the Integrated Marine Observing System mooring data
- Investigation and visualization of initial regional sea surface temperature plots of the Great Barrier Reef
- Drafts and notes on the development of the manuscript came from my upgrade report document
- Created the first diagram describing the model updates
- Ran numerous iterations of global and Great Barrier Reef model runs to investigate errors and understanding for S2P3

2.1 INTRODUCTION

This chapter describes the S2P3-R v2.0 downscaling process in detail and the validation of the surface and bottom temperature outputs as it applies to the Great Barrier Reef (GBR). The analysis contains some figures from Halloran et al (2021) but is not limited to this paper.

2.2 OVERVIEW OF S2P3-R V2.0

The 1-D biogeochemical-physical Shelf Seas Physics and Primary Production (S2P3-R v2.0) model now enables more detailed climate projections in the coastal seas without requiring expensive computing (Halloran et al., 2021). Originally the S2P3 model

(Sharples, 1999) was used as a teaching tool to demonstrate primary production, linking theory and observations. Marsh et al (2015) further expanded and applied the model regionally (S2P3-R) on the Northwest European Shelf, Western English Channel, and the East and Yellow China Seas (Marsh et al., 2015). Since the model is 1-D, it demonstrates biological and physical processes that are largely controlled by vertical processes, more specifically vertical heat fluxes (Marsh et al., 2015).

Seasonal heating and cooling rates modify seawater density, stratifying or causing convection in the water column. Surface heat primarily enters the ocean through short wavelength radiation from the sun. Surface heat can also be transferred into the ocean through conduction from the air. The heat that is returned to the atmosphere is in the form of long wavelength radiation, latent heat, and conduction. Heat exchange at the surface of the ocean greatly impacts density properties in the water column (Simpson & Sharples, 2012). The salinity content in the ocean also has an important influence on the buoyancy. In the S2P3-R model, salinity is a constant value of 35 (Marsh et al., 2015) so buoyancy is not altered by the salinity content in these simulations.

The main physical processes in the S2P3 1-D simulation influencing the vertical heat fluxes are tidal and wind mixing processes. These energy forces are simulated in a turbulent kinetic energy scheme. Depending on the location, tidal energy can inject large amounts of energy into the coastal zone. Tidal energy is dissipated in the shallower waters when the energy interacts with friction forces such as a coral reef on the bottom of the ocean. Frictional forces also interact with wind on the surface of the ocean followed by the transfer of energy downwards.

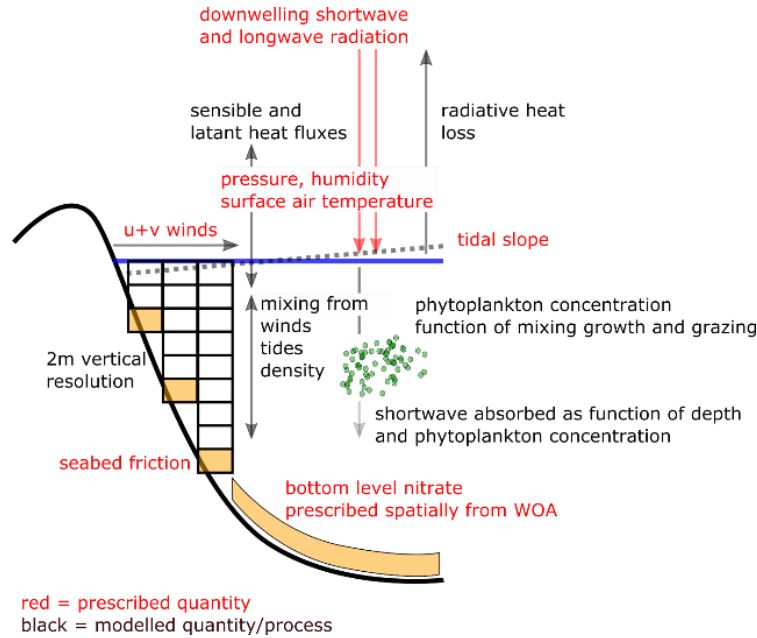


Figure 2.1: Schematic description of the processes accounted in S2P3-R v2.0 and prescribed quantities, both forcing's and constants (World Ocean Atlas). Source: Halloran et al (2021)

In the biological component of the S2P3-R model, an output variable of considerable interest to research on photosynthesizing corals is Photosynthetically Active Radiation (PAR) or, the proportion of light in the ocean that is used by photosynthesis and generally taken to be light waves of 400 to 700 nm (Pierson et al., 2008). PAR accounts for roughly 50% of the total incident radiation at the ocean surface (Riley, 1957).

Phytoplankton blooms can significantly influence PAR measurements. The supply of light, nutrients, and mixing commonly drives a phytoplankton bloom (Riley, 1957). The movement of the thermocline often determines whether and when nutrients from near the seabed are driven up to the surface of the ocean (Riley, 1957). Nutrients can also come from river run-off, land-based sources (Bricker et al., 2008), and submarine groundwater in some cases (Gove et al., 2016). Internal waves breaking from tidal stratification flow on and off-banks generating mixing processes (Moum & Nash, 2000) and the effects of wind on a bloom could either increase the supply of nutrients and increase growth or deepen the base of the thermocline disrupting light properties (Simpson & Sharples, 2012). The biologically driven outputs were not directly explored in this thesis, although they do impact light penetration within the model.

2.3 IMPROVEMENTS TO S2P3-R

The meteorological data used within the S2P3-R model has been expanded from one location in each of the regions in Marsh et al (2015) to spatially and temporally varying input grids in Halloran et al (2021). The S2P3-R v2.0 model can now be run at any specified resolution around the globe with minimal model setup requirements. After suggesting the use of local bathymetry to set the depth parameter of the model, I decided to focus my research on the GBR versus global coral reefs as the GBR has a 100 m resolution bathymetry dataset (Beaman, 2010). The previous bathymetry dataset, ETOP01 Global Relief Model, is a 1 arc-minute bathymetry dataset and the high-resolution dataset proved to dramatically improve the downscaling when comparing the model to mooring observations in the initial stages of validation. Depth is one of the most important variables for simulating vertical mixing as the vertical energy and density of water interact with the near-bottom stress (Polzin et al., 1997). Mixing from winds and tides as they interact with various depth gradients can provide relief from warming events, especially in shallow locations (Baird et al., 2018; Glynn, 1996; Skirving et al., 2006; Wolanski & Pickard, 2018). There is a balance between prescribing a detailed resolution and a reasonable computing time. We decided to use 10 km horizontal resolution and 2 m vertical spacing spanning 4-50 m water depth. On our computing system, it takes approximately a week to downscale five climate models for four scenarios over the GBR grid at 10 km resolution. Simulations were run on an AMD 2990WX 32-core 3 Ghz processor using multi-threading. It is also important to note that even though the downscaling simulations use depths 4-50 m, within each 10 km seabed depths from the bathymetry dataset are averaged.

The S2P3-R v2.0 downscaling process not only uses local bathymetry, but it also prescribes net long and shortwave radiation instead of using clouds as an input as previously done in S2P3. The cloud input proved problematic, potentially because the clouds were not evaporating properly causing temperatures to increase. As a solution, long and shortwave radiation were prescribed instead of being calculated with the cloud

variable. Previous iterations calculated longwave radiation based on the cloud fraction and clear sky irradiance at a given latitude.

2.4 S2P3-R V2.0 FRAMEWORK

Our semi-dynamic downscaling method applies the S2P3-R v2.0 model (Halloran et al., 2021), driven by surface air temperature, winds, air pressure, humidity, and net longwave and shortwave radiation, as simulated by the fully coupled global climate models or reanalysis. The atmospheric forcing's are used in conjunction with high resolution bathymetry (Beaman, 2010) and tidal forcing (Egbert & Erofeeva, 2002) to simulate water column properties in the vertical dimension. The S2P3-R v2.0 model has been applied over the domain 142.0°W, 157.0°E, 30.0°S, 10.0°S from 4-50 m water depth, at a 10 km horizontal resolution and 2 m vertical resolution. In later chapters the S2P3 model is driven by surface level atmospheric data from the CMIP6 models, MRI-ESM2-0 (Adachi et al., 2013), EC-Earth3-Veg (Döscher et al., 2021), UKESM1-0-LL (Sellar et al., 2019), CNRM-ESM2-1 (Séférian et al., 2019), and IPSLESM2-0 (Boucher et al., 2019). Variables were output daily from 1950-2100 (inclusive) and masked to contain values just within the Great Barrier Reef Marine Park Authority Boundary (GBRMPA, 2004).

The S2P3-R v2.0 physical component is driven by tides and winds to simulate vertical profiles of temperature, turbulence, and currents. A tidal slope is calculated from M2, S2, N2, O1, and K1 ellipses to then calculate the water's velocity 1 m above the seabed. The bottom stress is calculated as a function of this velocity and a prescribed bottom drag coefficient (Sharples et al., 2006). Wind stress is calculated as a function of the surface drag coefficient, air pressure, and wind speed and direction with respect to tides (Smith & Banke, 1975). Mixing profiles are then calculated from these in a turbulence closure scheme as a function of vertical density (Canuto et al., 2001). Temperature is considered the only factor in the density calculation, with the salinity variability being second order in terms of variability and therefore ignored. This model is expected to be of less value in areas where; 1.) the horizontal controls, i.e. advection,

exceed vertical controls, i.e. atmospheric or tidal forcing, and 2.) where density variations are strongly dependent on salinity (Halloran et al., 2021; Marsh et al., 2015; Sharples et al., 2006).

Energy movement in the water depends on the eddy viscosity and eddy diffusivity. Eddy viscosity describes the transfer of fluid momentum through turbulent eddies propagating down momentum gradients in the water. Eddy diffusivity describes the vertical mixing of water either from turbulent kinetic energy or other scalar properties such as temperature. The vertical eddy viscosity is used with the surface and bottom stress calculation. Temperature is calculated as it transfers from the top layer to the bottom of each depth level using the vertical energy diffusivity. (Halloran et al., 2021; Marsh et al., 2015; Sharples et al., 2006)

Physical Components (Marsh et al., 2015)

Tendency of turbulent kinetic energy (TKE) for tidal currents:

Eddy diffusivity describes the vertical mixing of either TKE or other scalar properties such as temperature. The equation below describes this process.

$$\frac{\partial}{\partial t} \left(\frac{q^2}{2} \right) = \frac{\partial}{\partial z} \left(K_q \frac{\partial}{\partial z} \left(\frac{q^2}{2} \right) \right) + N_z \left[\left(\frac{\partial u}{\partial z} \right)^2 + \left(\frac{\partial v}{\partial z} \right)^2 \right] + K_z \left(\frac{g}{\rho} \frac{\partial \rho}{\partial z} \right) - \frac{q^3}{B_1 l}$$

TKE = $q^2 / 2$

ρ = density, quadratic in temperature T ($1028.11 - 6.24956 \times 10^{-2} - 5.294 \times 10^{-3} T^2$, assuming a constant salinity of 35.00)

t = time (daily)

q = turbulent intensity, or velocity scale ($m s^{-1}$)

z = depth (m)

K_q = vertical eddy diffusivity for TKE ($m^2 s^{-1}$)

K_z = vertical eddy diffusivity for other scalar properties ($m^2 s^{-1}$)

N_z = vertical eddy viscosity ($m^2 s^{-1}$)

B_1 = constant for closure scheme

l = eddy length scale ($l = \kappa z(1 - z/h)^{0.5}$ at depth z , given total depth h and von kare'n's constant $K = 0.41$)

u = tidal current x ($m\ s^{-1}$)

v = tidal current y ($m\ s^{-1}$)

Δt = time steps, constrained by $\Delta t < \Delta z^2 / 2N_z$

Δz = depth intervals (m)

Tides and winds force the TKE profile for given boundary conditions: The equations below account for the forces influencing TKE at the surface due to winds and tidal currents at the near-bottom layer of the water column.

$$q_{z=h}^2 = B_1^{2/3} \frac{\tau_s}{\rho_{z=0}}$$

$$q_{z=0}^2 = B_1^{2/3} \frac{\tau_b}{\rho_{z=0}}$$

τ_s = surface stress ($z = h$) due to the wind

h = height above the seabed, depth of the water column

τ_b = near-bottom stress ($z = 0$) due to tidal currents

Surface wind stress:

At the surface of the water column, wind stress needs to account for drag at the surface, air density, and the surface wind velocities in the North-South and East-West directions.

$$\tau_{sx} = -c_d \rho_a v_w \sqrt{(u_w^2 + v_w^2)}$$

$$\tau_{sy} = -c_d \rho_a v_w \sqrt{(u_w^2 + v_w^2)}$$

w = wind speed ($m\ s^{-1}$)

c_d = drag coefficient ($c_d = 0.75 + 0.067w$) $\times 10^{-3}$)

ρ_a = air density ($= 1.3\ kg\ m^{-3}$)

u_w = x winds ($m\ s^{-1}$)

$v_w = y$ winds ($m\ s^{-1}$)

Near-bottom stress:

Near-bottom stress is calculating the drag 1 m above the seabed accounting for the density of water and currents above the seabed.

$$\tau_{bx} = -k_b \rho_0 u_1 \sqrt{(u_l^2 + v_l^2)}$$

$$\tau_{by} = -k_b \rho_0 v_1 \sqrt{(u_l^2 + v_l^2)}$$

k_b = drag coefficient (=0.003)

ρ_0 = representative density for seawater (=1025 $kg\ m^{-3}$)

u_1 = x current 1 m above the seabed ($m\ s^{-1}$)

v_1 = y current 1 m above the seabed ($m\ s^{-1}$)

Local heating and cooling of the water column at each depth level: Temperature is being calculated as it transfers to each depth level in the equation below. The vertical energy diffusivity of scalar properties is being accounted for through K_z .

$$\frac{\partial T}{\partial t} = \frac{\partial}{\partial z} \left(K_z \frac{\partial T}{\partial z} \right) + Q_h(z)$$

T = tendency of temperature ($^{\circ}C$)

Q_h = net heating at z

z = height above the seabed

Surface net heat flux:

Shortwave radiation enters the ocean, some radiation is absorbed, and some is returned to the atmosphere through longwave radiation. In addition, heat changes state through the process of latent and sensible heat. Latent heat refers to the change in

state such as evaporation and sensible heat referring to heat that causes changes in temperature. This net heat flux is calculated using the equation below.

$$Q_{net} = Q_{SW} - (Q_{LW} + Q_{sens} + Q_{lat})$$

Q_{sw} = shortwave radiation ($W\ m^{-2}$)

Q_{lw} = long-wave back radiation ($W\ m^{-2}$)

Q_{sens} = sensible heat exchange with the atmosphere ($W\ m^{-2}$)

Q_{lat} = latent heat exchange with the atmosphere ($W\ m^{-2}$)

Sensible heat flux:

Described in the net heat flux equation, sensible heat flux refers to the capacity of heat to cause changes in temperature. The meteorological data inputs surface winds and surface air temperature used in this equation. There are also two constants, the specific heat capacity of air and the transfer coefficient. Sea surface temperature (SST) is derived from the model. These variables calculate sensible heat flux from the water column in the model.

$$Q_{sens} = \rho_a c_p C_h U (T_s - T_a)$$

c_p = specific heat capacity of air ($c_p=1004\ J\ kg^{-1}K^{-1}$)

C_h = transfer coefficient ($C_h = 1.45 \times 10^{-3}$)

U = surface wind speed ($m\ s^{-1}$)

T_s = sea surface temperature ($^{\circ}C$)

T_a = surface air temperature ($^{\circ}C$)

Latent heat flux:

Also described above, latent heat refers to the energy that is fluctuating based on changing form from a liquid to a gas through evaporation. Given properties of relative humidity and atmospheric pressure from the meteorological observations, the specific heat capacity of air and transfer coefficient can be used to calculate latent heat flux back into the atmosphere.

$$Q_{lat} = \rho_a L_v C_e U (q_s - q)$$

L_v = specific heat capacity of air ($L_v = 2.5 \times 10^6 - 2.3 \times 10^3 T_s$)

C_e = transfer coefficient ($C_e = 1.5 \times 10^{-3}$)

55% of shortwave radiation is absorbed at the top depth level (red end of the spectrum):

Surface net heat flux into the top depth level in the water column is calculated by multiplying 0.55 with the shortwave radiation coming into the system and then subtracting the longwave radiation, sensible heat and latent heat that is lost.

$$Q_{h,0} = 0.55 Q_{SW} - (Q_{LW} + Q_{sens} + Q_{lat})$$

45% remaining is distributed exponentially throughout the water column as heating rate

$Q_{h(z)}$:

Using properties from the equation above, the light is attenuated throughout the water column exponentially. Pigment is absorption calculated downwards with a standard coefficient. Local shading from chlorophyll a is accounted for using the biological component of the model described further in Marsh et al (2015). Also further described in Marsh et al (2015) is the carbon concentration.

$$\frac{\partial Q_h}{\partial z} = -Q_h(z)(\lambda_0 + \epsilon X_T(z))$$

λ_0 = attenuation coefficient ($\lambda_0 = 0.1 \text{ m}^{-1}$)

ϵ = pigment absorption cross section ($\epsilon = 0.012 \text{ m}^2(\text{mg chl}^{-1})$)

$X_T(z)$ = shading from local chlorophyll a (chl a) concentration (mg chl m^{-3}) (X_T

$(z) = q^{\text{chl}} P_c$)

q^{chl} = chl a: carbon ratio ($q^{\text{chl}}(0.03 \text{ mg chl}(\text{mg C})^{-1})$) (assumed constant)

2.4.1 TIDAL INPUTS

Tides are an important process in driving vertical mixing in the S2P3-R v2.0 model. The first step in creating a tidal input file is to specify a spatial grid (decimal degrees) and a resolution (degrees) to generate tidal constituents through the Oregon State University Tidal Prediction Software (OTPS) (Egbert et al., 1994; Egbert & Erofeeva, 2002) based off a 100 m resolution gridded bathymetry dataset covering approximately 3,000,000 km² of the GBR and the Coral Sea (Beaman, 2010). This bathymetry grid can be swapped for global or other local/regional datasets depending on the location. The OTPS model extracts harmonic constants, or cosine curves, from elevations, transports, or currents (barotropic tidal solutions) to predict tides at specified times and locations. Global and/or regional barotropic inverse tidal solutions are obtained with OTIS (OSU Tidal Inverse software) which processes TOPEX/POSEIDON altimeter data. The tidal output file contains each point of the model grid at the specified resolution, 5 tidal variables (O1, K1, (diurnal constituents), S2, M2, N2 (semidiurnal constituents), and depth.

2.4.2 METEOROLOGICAL INPUTS

Daily meteorological forcing data inputs were surface relative humidity, surface sea level pressure, 2 m air temperature, north-south, and east-west wind speed, and short and longwave radiation (Table 2.1). ERA5 atmospheric reanalysis product and the CMIP6 models have the same atmospheric input variables used in S2P3-R v2.0 downscaling (Table 2.1).

Table 2.1: Atmospheric input variables to the S2P3-R v2.0 downscaling used for the ERA5 hindcast product and climate models.

Atmospheric variable	Unit	Location	Description
Relative Humidity (hur)	%	surface	The amount of water vapor in the air generally calculated in relation to saturated water vapor density
Air pressure at sea level (psl)	Pa	surface	Density of air, indicator of weather systems
Air temperature (tas)	K	2 m	The measure of hot or cold air, or heat energy, that describes the kinetic energy or movement of gas molecules in the air
Northward wind (vas)	m s ⁻¹	10 m	The horizontal movement of air in the north-south direction
Eastward wind (uas)	m s ⁻¹	10 m	The horizontal movement of air in the east-west direction
Surface downwelling shortwave flux in air (rsds)	W m ⁻²	2 m	Visible light
Surface downwelling longwave flux in air (rls)	W m ⁻²	2 m	Radiation emitted back towards the atmosphere from Earth that is not absorbed from the shortwave radiation

2.4.3 NUTRIENT INPUT

The nutrient input is a key driver of the biological component of the S2P3-R v2.0 model. Nutrient data is obtained from the World Ocean Atlas climatology which contains a global one-degree mean field of nitrate at standard depth levels. These data are collected through scientifically quality-controlled ocean casts. More information on this process is provided in the biological component breakdown of the model in Halloran et al (2021) and Marsh et al (2015).

Tidal, meteorological, and nutrient forcing files are then used to drive the S2P3R v2.0 model producing outputs in the form of NetCDFs. The outputs used in this study are surface temperature, bottom temperature, tidal energy, and wind energy.

2.5 GLOBAL EVALUATION OF S2P3-R V2.0

A global evaluation in Halloran et al (2021) demonstrated that more than half of the shelf-seas grid cells globally are capturing ~60% of the interannual SST variability and 20% of grid cells are capturing >80% of the interannual variability (Halloran et al., 2021). The global evaluation excluded high latitudes (<65°N/S) and used SSTs from the downscaling for comparison against satellite SSTs (Merchant et al., 2019). The smallest bias appears to generally be in regions of the subtropics and subpolar regions. Areas with higher tidal mixing can contribute to better simulations although weak tidal mixing still demonstrates efficient seasonal skill. There is little bias in the mid-latitudes from winter to summer mixing conditions (Halloran et al., 2021).

Regional bias is expected as the model does not include lateral advection. The GBR and the Northwest European Shelf seas were used as a low and mid-latitude regional evaluation. Low latitudes reflected larger SST biases than mid-latitudes (Halloran et al., 2021).

2.6 GREAT BARRIER REEF PHYSICAL EVALUATION

In Halloran et al (2021), the S2P3-R v2.0 method uses the vertical 1-D physical biogeochemical model at each grid box to capture the temperature response resulting from the interaction of ERA5 hindcast meteorology with local tides and local bathymetry (Beaman, 2010). The model's GBR domain spans 142.0°W, 157.0°E, 30.0°S, 10.0°S from 4-50 m water depth, at a 10 km horizontal resolution and 2 m vertical resolution.

The S2P3-R v2.0 SST averaged output from 1986-2006 in the GBR revealed a latitudinal bias (Figure 2.2). The downscaled SST output relative to satellite SST showed a warm bias in the north and a cool bias in the south (Figure 2.2). As the S2P3-R v2.0 downscaling does not account for boundary currents, one explanation could be the lack of lateral advection being transported to the south from the East Australian Current (Halloran et al., 2021) and similarly the Hiri Current could have improved the northern bias. The East Australian Current would bring warm waters to the central and

southern portions of the GBR. Clouds could also be impacting the ability to collect satellite data near the coast causing a possible discontinuity.

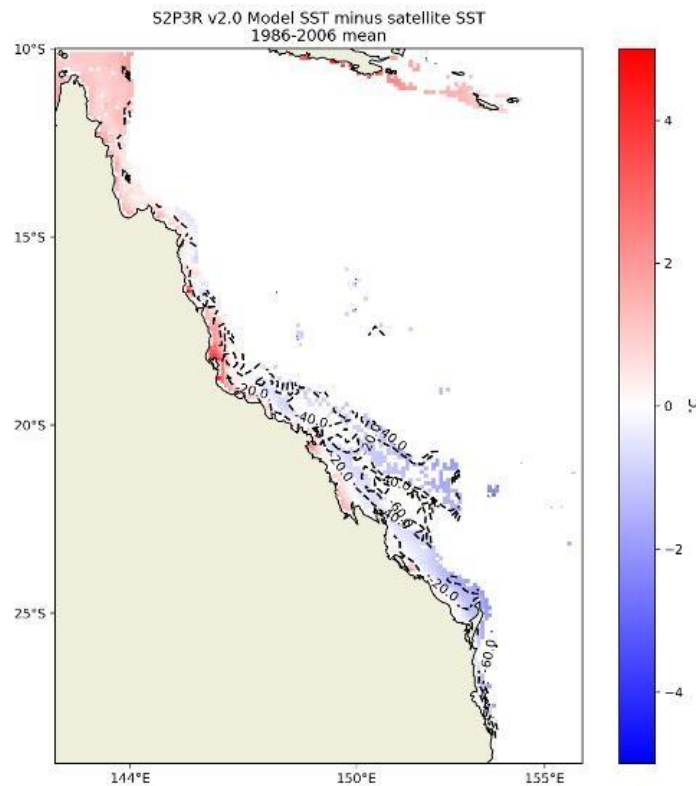


Figure 2.2: Great Barrier Reef regional bias is demonstrated using the time interval 1986-2006 (inclusive) to subtract averaged satellite sea surface temperatures (SSTs) from S2P3-R v2.0 SSTs. Bathymetry is shown in meters using labelled dashed lines. Source: Halloran et al (2021)

Following year 2000, a cooling in the downscaled ERA5 SST data occurs potentially due to a change in the assimilation of the observations in the ERA5 reanalysis product (Figure 2.3). This pattern is consistent in all three sectors of the GBR seen in Figure 2.3. The central sector appears to show the greatest temperature agreement with the satellite-based data. The latitudinal bias, likely driven by a lack of lateral advection, is even more apparent by region in the agreement plots shown in Figure 2.3.

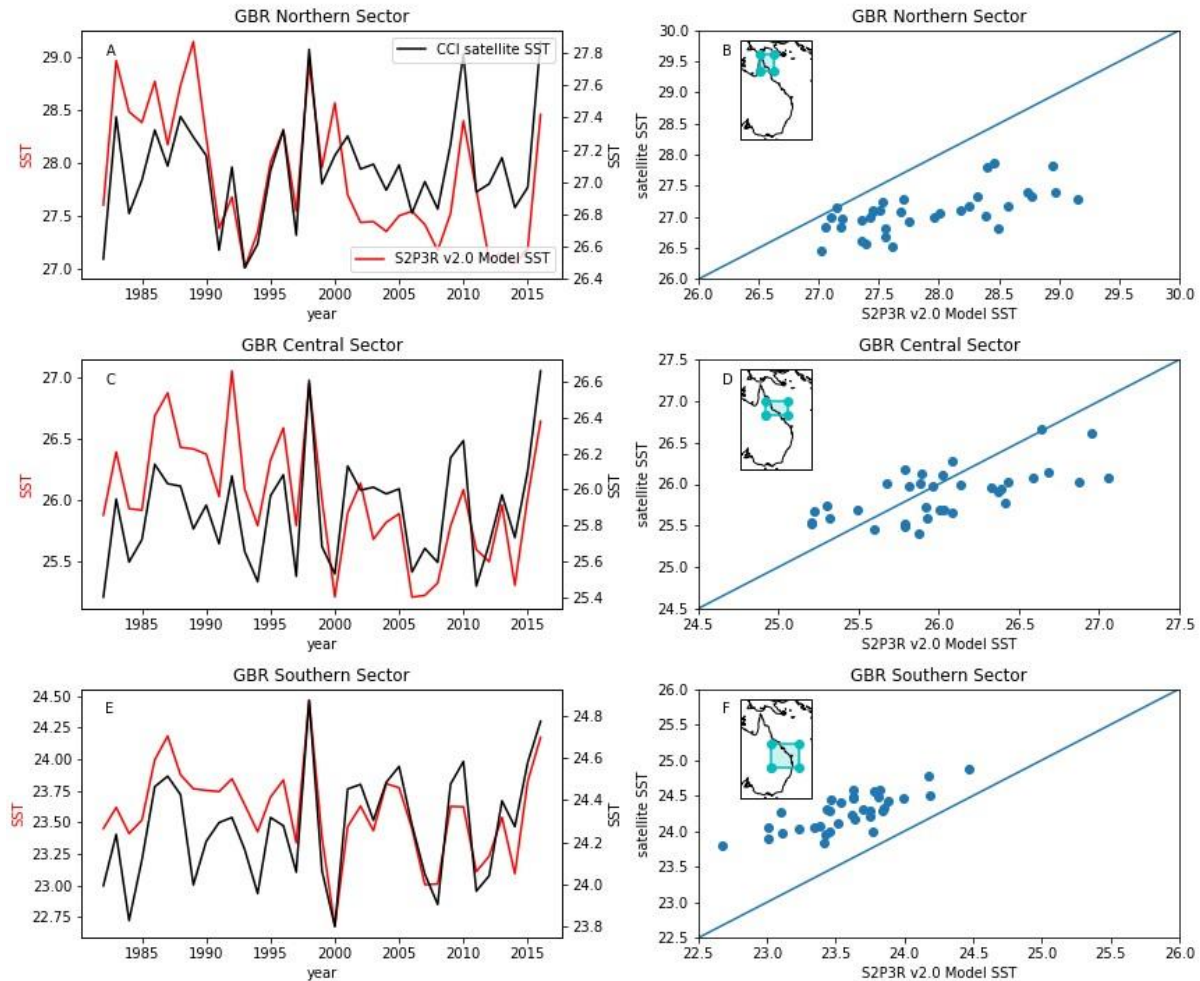


Figure 2.3: Interannual sea surface temperature (SST) variability is compared regionally between the S2P3-R v2.0 downscaled SST output and satellite SST data over the Great Barrier Reef. The three regions were subdivided by latitude and are further identified through inset maps. Source: Halloran et al (2021)

Mooring observation-based validation indicates a bias in surface and bottom temperatures outputs of $\sim 0.5 - 1^{\circ}\text{C}$. The mooring observations indicate a cool bias during winter months in the modelled SSTs (Figure 2.4c). In the lower latitude of the southern and central GBR, the modelled bottom temperature shows a slight cool bias. The cool bias could reflect the average across a 10 km spatial grid in the model output, not reflecting the exact depth in which the mooring observations were taken. (Figure 2.4d)

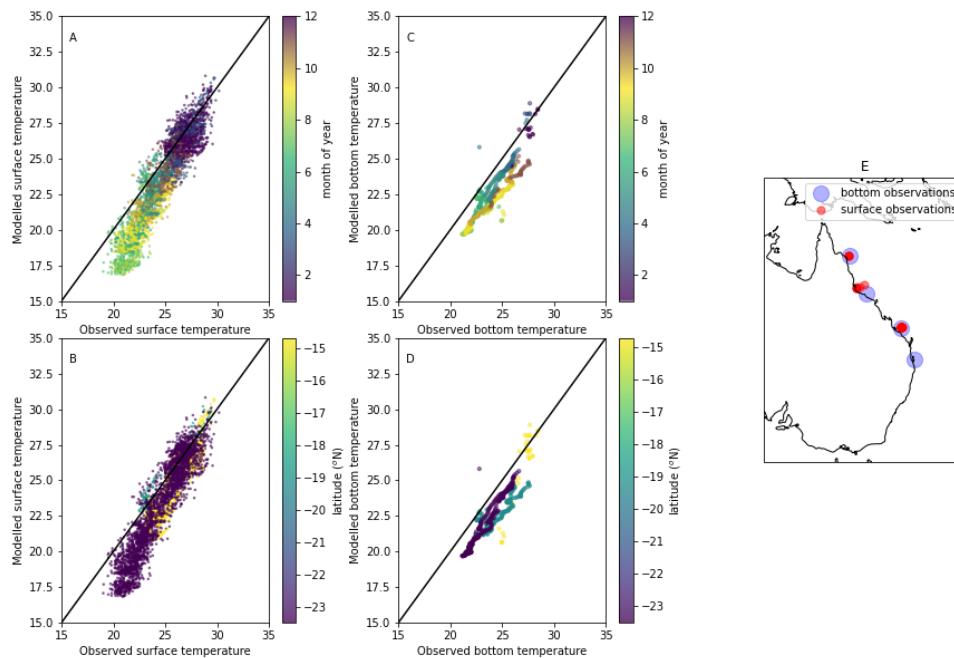


Figure 2.4: Downscaled S2P3-R v2.0 surface and bottom temperature outputs were compared to mooring observations from the Integrated Marine Observing System and Facility for the Automated Intelligent Monitoring of Marine Systems. The data in the plots show continuity on the x and y axis, therefore if the values were the same, they would fall on the black line. Colours describe either temporal or geographical locations in the data. The downscaled bottom temperature is limited to within 5 m of the site depth for each mooring location for comparison. Mooring locations are shown in the map indicating red for the surface and blue for the bottom temperature observations. (GBRHIS: Heron Island South Shelf mooring component of the GBR mooring array; GBRLSH: Lizard Island Shelf mooring component of the GBR mooring array; GBRPPS: Palm Passage Shelf mooring component of the GBR mooring array; Northern Australia Automated Marine Weather and Oceanographic Stations, sites: Yongala mooring (NRSYON); GBROTE: One Tree Island Shelf mooring component of the GBR mooring array; IMOS – ANMN National Reference Station (NRS) Ningaloo mooring (NRSNIN)) Source: Halloran et al (2021)

The moorings used for this analysis are in deeper waters, not always over coral reefs, which means they may not be capturing the same data used in the satellite data-based validation. Given more bottom temperature observations, this validation could be greatly improved. Overall, there is enough general agreement to provide confidence in the S2P3-R v2.0 downscaling method. The GBR extensive mooring network through Integrated Marine Observing System, Facility for Automated Intelligent Monitoring of Marine Systems (IMOS FAIMMS) Sensor Network (2009a, 2009b, 2009d, 2009e, 2009c, 2015, 2017) was used in this evaluation of modelled surface and bottom temperature outputs. (Figure 2.4)

PART B

2.7 MODELING UNDERSTANDING: S2P3-R V2.0 DEGREE HEATING WEEKS METRICS

The application of downscaling climate models with S2P3-R v2.0 for coral stress metrics needs to be validated using Degree Heating Weeks (DHW). The ability for S2P3-R v2.0 to capture extreme conditions is important since coral bleaching occurs during anomalously warm periods. Therefore, SST values that have been averaged annually in Halloran et al (2021) are not representative of the ability of the downscaling to capture extreme temperatures. First, I will discuss the recent widespread bleaching events using the well-established NOAA Coral Reef Watch DHW product. Second, I will qualitatively compare the spatial patterns of the bleaching events to the spatial patterns of ERA5 atmospheric variables that are used as inputs to the S2P3-R v2.0 downscaling. McGown et al (2017) attributes El Niño associated bleaching events on the GBR to atmospheric conditions causing anomalously warm temperatures. The main drivers of bleaching in the McGowan et al (2017) study were reduced cloud fraction, higher than average temperatures, and higher than average pressure gradients. Since S2P3-R v2.0 uses atmospheric input variables to simulate warming into the water column, an understanding for atmospheric conditions from each variable during bleaching events

was informative when understanding changes to the DHW metric in subsequent chapters. The general spatial patterns of the atmospheric components and how they correspond to the areas that have bleached in the past provides a visual representation of the warming mechanisms.

2.7.1 RECENT BLEACHING EVENTS

More frequent and severe coral bleaching events have been seen in recent years on the GBR: 2002, 2016, 2017, and 2020 (Hughes et al., 2017; Hughes, Kerry, et al., 2018). The 2002 event was widespread, affecting offshore reefs in the central and southern GBR (Figure 2.5). The strong latitudinal gradient in the 2016 event relieving warming in the south and central GBR was an effect of the passing of tropical cyclone Winston (Hughes et al., 2017) (Figure 2.5). The cyclone brought high wind, rain, and clouds causing partial relief from the warming event (Hughes et al., 2017) (Figure 2.5). The 2017 event was more focused in the central region. The 2020 event was the most widespread, extending further into the southern GBR than has been previously recorded (Bozec et al., 2020) (Figure 2.5). The recent warming events are shown in Figure 2.5 as annual maximum DHW values during austral summer years from the National Oceanic and Atmospheric Administration (NOAA) Coral Reef Watch (CRW) DHW product (i.e., bleaching year 2002 is July 31, 2001 – August 1, 2002) (Figure 2.5).

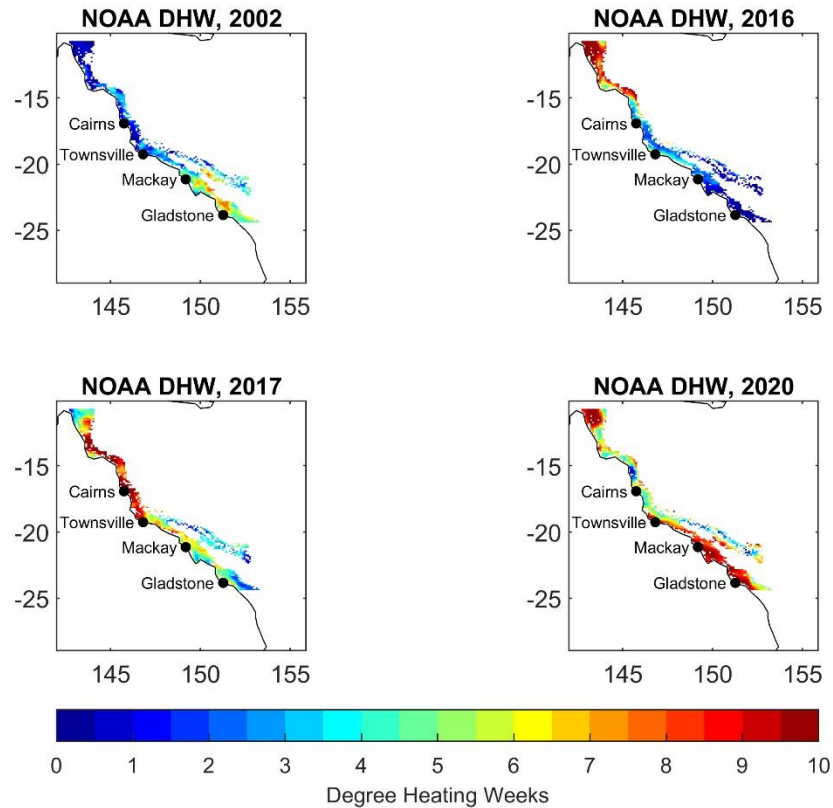


Figure 2.5: NOAA Degree Heating Weeks (DHW) are shown as the annual maximum DHW for bleaching years 2002, 2016, 2017, 2020 using austral calendar years (i.e., July 31, 2001 – August 1, 2002) during summer months (December, January, February, March).

During all four bleaching events most of the bleaching occurred in the northern GBR (Figure 2.5) but, the spatial extent was not very consistent. According to Bozec et al (2020) three recent events (2016, 2017, 2020) resulted in net coral cover declining by ~33% across the entire GBR (Bozec et al., 2020).

2.7.2 ATMOSPHERIC CONDITIONS DURING RECENT BLEACHING EVENTS

ERA5 2020 atmospheric data was not yet available, so the following qualitative atmospheric analysis is for 2002, 2016, and 2017 bleaching events. Warming during the

recent bleaching events on the GBR cannot necessarily be ascribed to one atmospheric variable but there are generally low and high-pressure systems that help build an understanding for bleaching and non-bleaching conditions (Figure 2.6-2.12). What is consistent spatially and temporally between each event is that areas that experienced high DHW tend to have; 1.) a rise in surface air temperature (Figure 2.11), 2.) reduced cloud cover (Figure 2.6), and 3.) higher than normal shortwave radiation (Figure 2.10). While the spatial extent between bleaching events varied, there was consistently more recurring bleaching in the far north and northern GBR (Bozec et al., 2020; Hughes et al., 2017) (Figure 2.5) and the ERA5 atmospheric analysis complements this pattern agreeing with the results in McGowan et al (2017). Some other general atmospheric patterns, not limited to bleaching conditions, are latitudinal low to high-pressure gradients from the far north to southern GBR as well as stronger wind speeds in the southern and central regions relative to the far north and northern regions (Figure 2.7, Figure 2.12). These latitudinal atmospheric patterns are complementary to our understanding of the larger atmospheric system referring to the summer monsoon and the prevailing trade winds (Section's 1.4.1, 1.4.4).

2.7.3 ATMOSPHERIC VARIABLES; CLOUD COVER, PRESSURE, AND HUMIDITY

In the far north and northern GBR during bleaching conditions, there were consistently less clouds, and higher than normal pressure conditions and yet, no relative change in humidity (Figure 2.6, Figure 2.7, Figure 2.8). Cloud cover shows relative consistency to bleaching locations, where reduced cloud cover reflects higher DHW values (Figure 2.6), especially in the southern GBR for 2002 and the far north for 2016 (Figure 2.6). Although, the 2017 warming conditions do not show an obvious reduction in cloud cover over areas of high DHW (Figure 2.6), Frade et al (2018) suggests that the warming from 2016 lasted into 2017 with winter temperatures not showing much relief from warming. Cloud cover is no longer an input to the downscaling method, but it is still useful to see the average cloud conditions between severe bleaching and non-severe bleaching conditions as they are telling of general weather systems. The presence or absence of

clouds is also generally captured in the shortwave radiation variable for climate projections. The ERA5 input variable, surface air pressure, shows a strong latitudinal gradient with higher pressure in the far north and northern GBR and lower pressure in the south during bleaching conditions during years 2002, 2016, and 2017 (Figure 2.7). In high-pressure locations, the air is descending vertically and left towards low-pressure locations, resulting in a reduction in clouds and therefore light winds and calm conditions (Figure 2.6, Figure 2.7). This latitudinal gradient reflects what has been seen in the 2016 bleaching event, the high-pressure in the north and low pressure in the south (Figure 2.6, Figure 2.7). (Hughes, Kerry, et al., 2018)

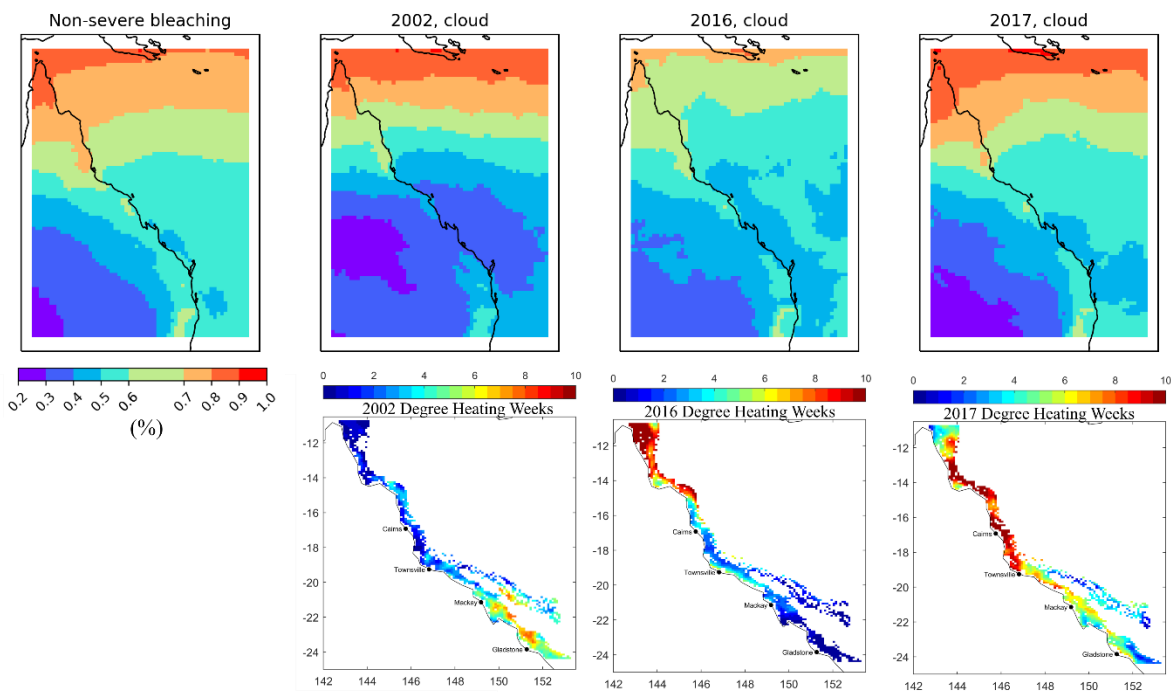


Figure 2.6: The ERA5 atmospheric variable cloud coverage (clt) is shown as non-bleaching conditions and for summer months in bleaching years, 2002, 2016, and 2017. Cloud was removed as an input variable to S2P3-R v2.0. It is used here for general understanding. The colour bar for the atmospheric plots was scaled to reflect the conditions over the ocean. Degree Heating Weeks from NOAA are shown to reference spatial patterns of warming.

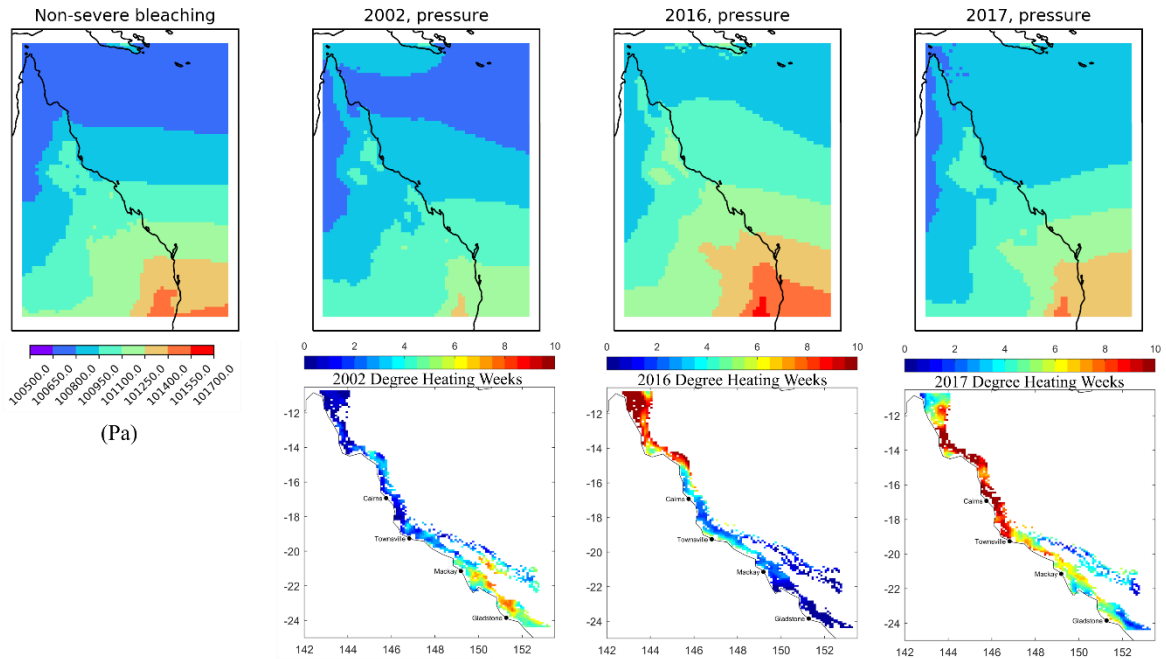


Figure 2.7: The ERA5 atmospheric input variable, surface air pressure (psl), used for the downscaling process, is shown as non-bleaching conditions and for summer months in bleaching years, 2002, 2016, and 2017. The colour bar for the atmospheric plots was scaled to reflect the conditions over the ocean. Degree Heating Weeks from NOAA are shown to reference spatial patterns of warming.

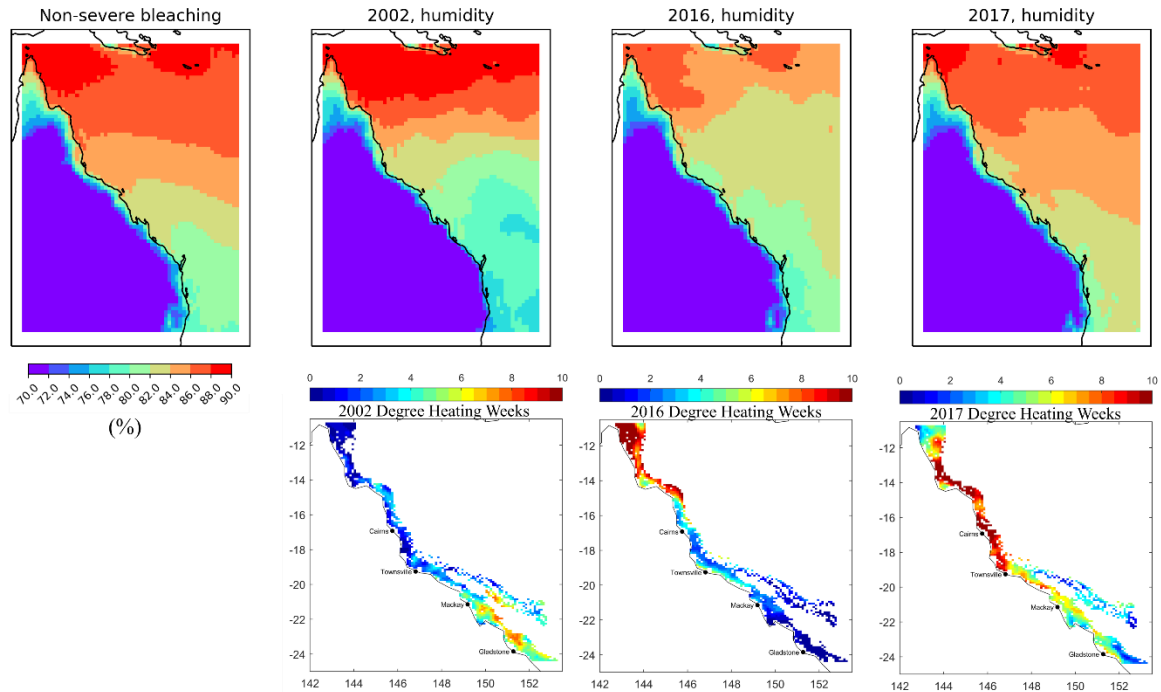


Figure 2.8: The ERA5 atmospheric input variable, humidity (hurs), used for the downscaling process is shown as non-bleaching conditions and for summer months in bleaching years, 2002, 2016, and 2017. The colour bar for the atmospheric plots was scaled to reflect the conditions over the ocean. Degree Heating Weeks from NOAA are shown to reference spatial patterns of warming.

The humidity variable shows no clear distinction from non-severe bleaching years to severe bleaching years (Figure 2.8). The spatial patterns are also not reflective of the DHW patterns (Figure 2.8).

2.7.4 ATMOSPHERIC VARIABLES; LONGWAVE AND SHORTWAVE RADIATION

Longwave radiation does not show an obvious spatial patterns relating to DHW values, in contrast, there is an obvious signal from shortwave radiation (Figure 2.9, Figure 2.10). There is a strong shortwave radiation signal over locations of high DHW values during the 2002, 2016, and 2017 events (Figure 2.10). The highest shortwave radiation

for the 2002 event is mainly over the central and southern GBR, while the highest DHW values were seen dominantly in the southern GBR (Figure 2.10). The 2016 event had the strongest shortwave radiation in the far north as well as a region in the north and central GBR, but as mentioned the warming was relieved in the central region by tropical cyclone Winston (Hughes, Kerry, et al., 2018) (Figure 2.10). In 2017 during bleaching conditions, the shortwave radiation signal was higher than normal along the entire GBR, with no obvious spatial cluster. This is sensible as the 2017 event was widespread and warming likely remained in the water from the 2016 event (Frade et al., 2018). The shortwave signal appears to be one of the most apparent atmospheric variables indicative of DHW values in this preliminary analysis and complementary to the finds in McGowan et al (2017).

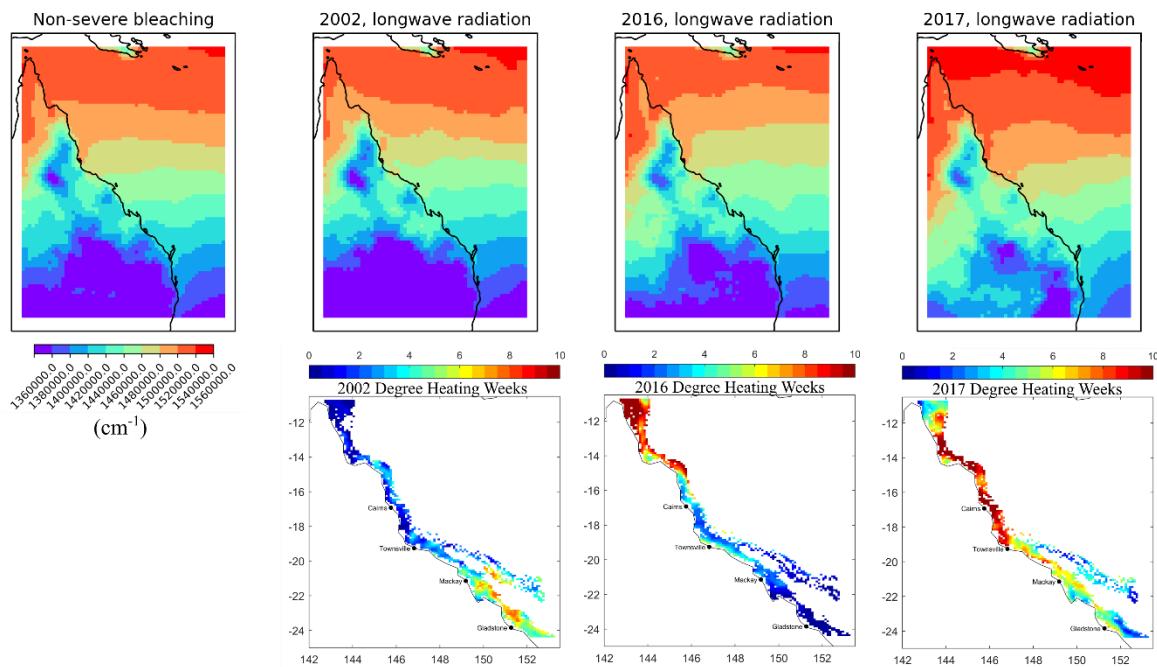


Figure 2.9: The ERA5 atmospheric input variable, longwave radiation (rlds), used for the downscaling process is shown as non-bleaching conditions and for summer months in bleaching years, 2002, 2016, and 2017. The colour bar for the atmospheric plots was scaled to reflect the conditions over the ocean. Degree Heating Weeks from NOAA are shown to reference spatial patterns of warming.

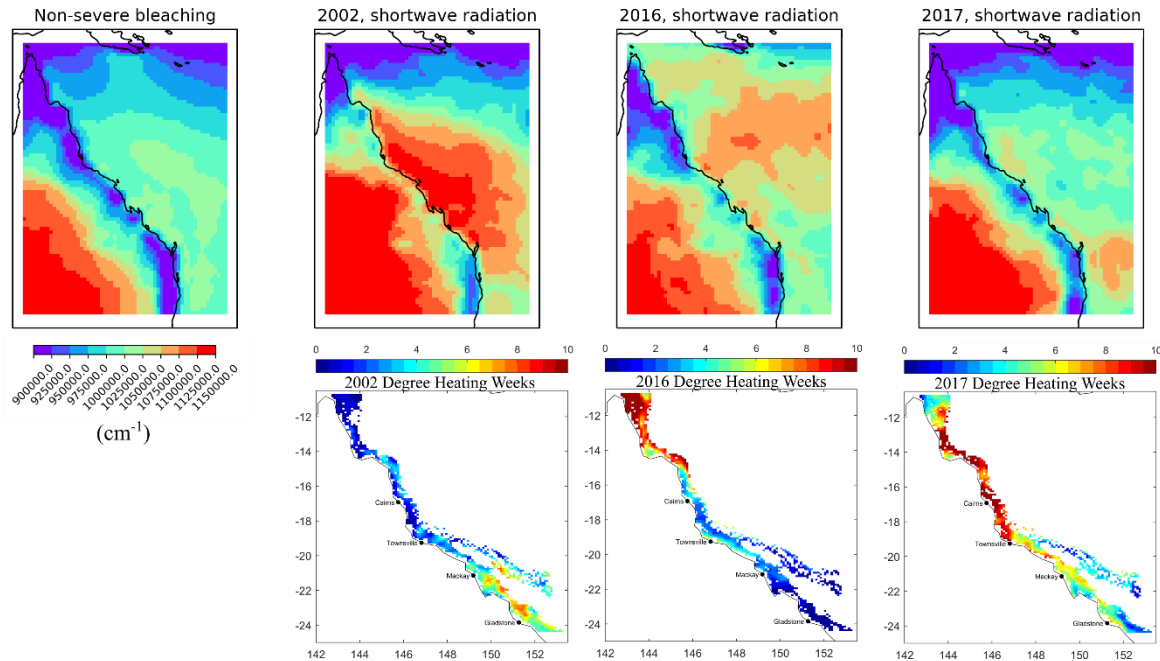


Figure 2.10: The ERA5 atmospheric input variable, shortwave radiation (rsds), used for the downscaling process is shown as non-bleaching conditions and for summer months in bleaching years, 2002, 2016, and 2017. The colour bar for the atmospheric plots was scaled to reflect the conditions over the ocean. Degree Heating Weeks from NOAA are shown to reference spatial patterns of warming.

2.7.5 ATMOSPHERIC VARIABLE; AIR SURFACE TEMPERATURE

Air surface temperature is consistently slightly higher during bleaching conditions than non-bleaching conditions (Figure 2.11), but air surface temperature alone does not show an obvious spatial pattern in relation to high DHW values (Figure 2.11). There is a latitudinal gradient showing air temperatures reducing by approximately 1°C from north to south, but this occurs during non-bleaching conditions as well. The land-based air temperature is clearly warmer in bleaching years than non-bleaching years (Figure 2.11). Downscaled DHW values provide a more detailed analysis of the duration and intensity of coral stress relative to surface air temperature.

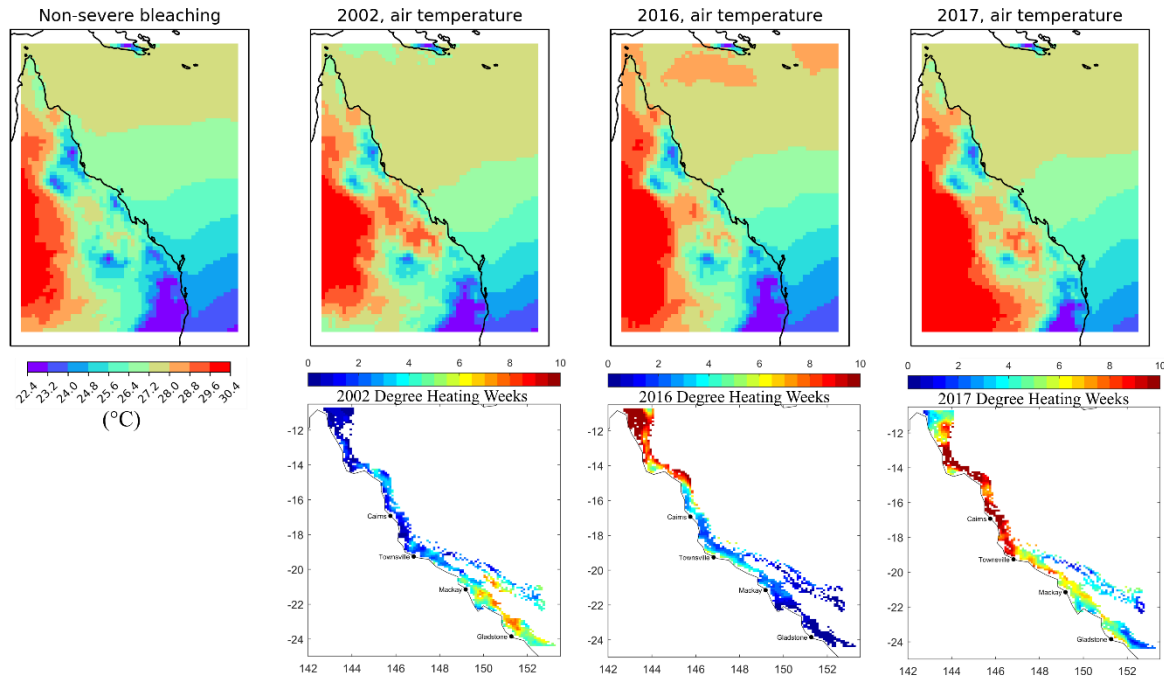


Figure 2.11: The ERA5 atmospheric input variable, air surface temperature (tas), used for the downscaling process is shown as non-bleaching conditions and for summer months in bleaching years, 2002, 2016, and 2017. The colour bar for the atmospheric plots was scaled to reflect the conditions over the ocean. Degree Heating Weeks from NOAA are shown to reference spatial patterns of warming.

2.7.6 ATMOSPHERIC VARIABLE; WIND SPEED

Wind speed generally weakens throughout the entire GBR during bleaching conditions (Figure 2.12), but the prevailing trades remain relatively high over the southern GBR and parts of the central GBR (Figure 2.12). As wind is an important mechanism of relief from warming for corals (Glynn, 1996), the reduction of wind speed seen in the far north, northern, and parts of the central GBR reflect the DHW patterns seen in 2016 but, not necessarily the patterns seen in 2002 and 2017 (Figure 2.12).

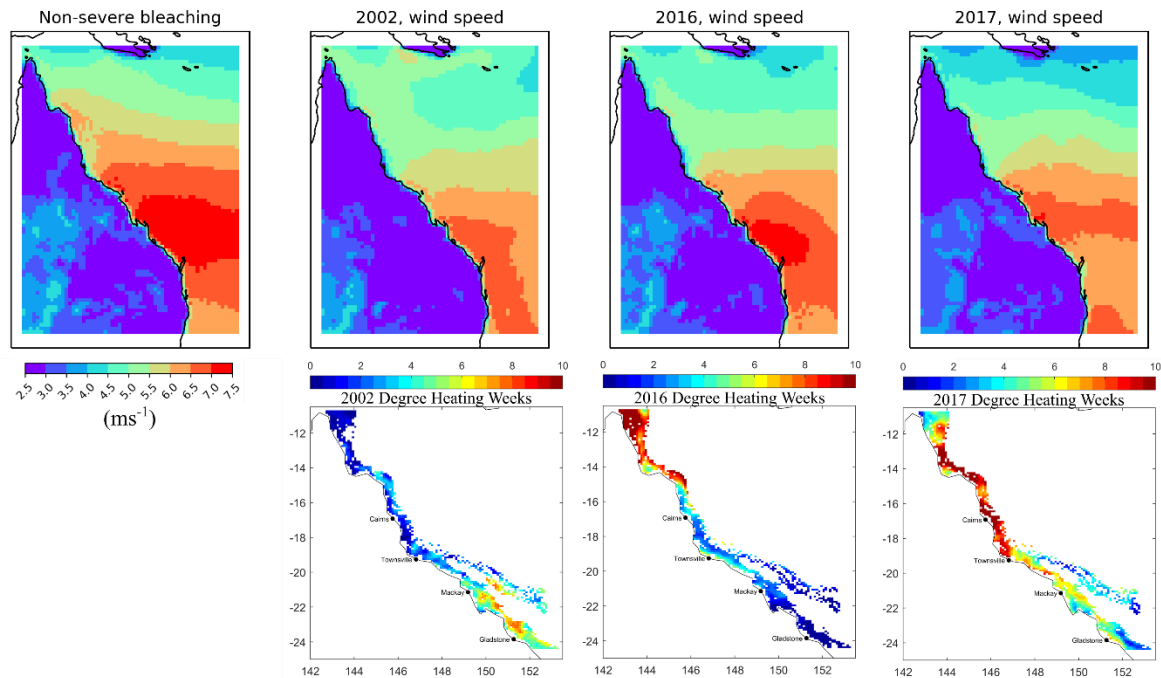


Figure 2.12: The ERA5 atmospheric input variable, wind speed (uas , vas), used for the downscaling process is shown as non-bleaching conditions and for summer months in bleaching years, 2002, 2016, and 2017. The colour bar for the atmospheric plots was scaled to reflect the conditions over the ocean. Degree Heating Weeks from NOAA are shown to reference spatial patterns of warming.

2.7.7 ATMOSPHERIC DRIVERS OF MASS CORAL BLEACHING EVENT, 2002

The 2002 bleaching event had the highest DHW values in the southern GBR where there is a reduction in clouds (Figure 2.6). While the reduction in cloud is clear in the southern GBR, the warming around $15^{\circ}S$ could reflect a patch of warm surface air temperature and therefore warm water (Figure 2.11). The high shortwave radiation over the high DHW region reflects a consistent spatial pattern yet, most likely in combination with the reduced cloud and warm surface temperatures (Figure 2.6, Figure 2.10, Figure 2.11). The winds seem to remain stronger over the southern extent which could have

reduced the DHW from getting even higher in some areas although, the wind pattern is not trivial (Figure 2.12).

2.7.8 ATMOSPHERIC DRIVERS OF MASS CORAL BLEACHING EVENT, 2016

The high latitudinal air surface temperature gradient is the strongest atmospheric spatial pattern informing the DHW in the 2016 event (Figure 2.11). The high shortwave radiation throughout the GBR is also useful, revealing that without the cyclone that passed through during the time of the event, this event could have been much worse (Figure 2.10). The clouds are not extremely informative of the cyclone or the DHW pattern in 2016 (Figure 2.6). Interestingly, the pressure gradients becoming closer together towards the southern extent of the GBR and the wind speed in a circular concentration could be telling of the cyclonic conditions (Figure 2.7, Figure 2.12). One would not expect this level of detail in future projections of the climate models, clouds and cyclones are meteorological conditions that are continuously being improved (IPCC, 2021).

2.7.9 ATMOSPHERIC DRIVERS OF MASS CORAL BLEACHING EVENT, 2017

The 2017 warming was extremely widespread (Figure 2.5) making it difficult to attribute atmospheric conditions to this event. There is not a concentration of a specific atmospheric signal over the northern GBR where the highest DHW were seen. The high air surface temperature, reduction in winds, and high shortwave radiation was throughout the entire GBR (Figure 2.10, Figure 2.11, Figure 2.12) while high cloud cover was just in the far north GBR (Figure 2.6). The warming seen in 2017 likely remained from 2016 (Frade et al., 2018). Additionally, the boundary currents (not simulated in the downscaling) could have been providing warm waters from two anomalously warm years of equatorial temperatures.

2.8 VALIDATION OF DEGREE HEATING WEEKS: NOAA CORAL REEF WATCH PRODUCT AND S2P3-R V2.0 DOWNSCALED ERA5 COMPARISON

Across the entire GBR, there was reasonable agreement between downscaled ERA5 outputs and the NOAA product, except in some locations during bleaching event years 2002 and 2016 (Figure 2.13, Figure 2.14, Figure 2.15). Further exploring these differences, the areas that show higher DHW values in the downscaled ERA5 outputs from 2002 were in the north and central regions of the GBR (Figure 2.14) and most of the high DHW values were concentrated in the southern GBR during this event (Figure 2.5). To further evaluate the S2P3-R v2.0 downscaling process for the application of this study, DHW values were calculated using downscaled ERA5 SST outputs and compared to satellite-based observations from NOAA's CRW DHW product. The DHW scripts were validated by the NOAA CRW programmer.

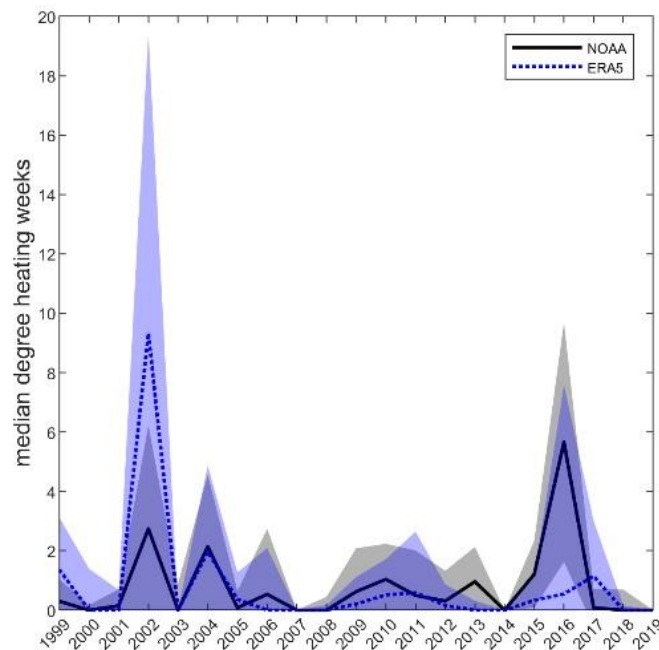


Figure 2.13: Downscaled ERA5 atmospheric reanalysis and NOAA Coral Reef Watch

Degree Heating Weeks data are shown as the median value across the Great Barrier Reef. These values are based on the annual maximum Degree Heating Weeks per austral summer year. Austral summer years were used to avoid double counting during calendar years. Shaded areas denote the interquartile range across the spatial grid.

The northern and central regions of the GBR under predicted DHW values in 2016 (Figure 2.14), but most of the bleaching occurred in the far north where the DHW values align well between the NOAA CRW product and the downscaled ERA5 output (Figure 2.5, Figure 2.14). The 2017 DHW values are not as easily demonstrated in the timeseries plot as this event was right after the 2016 event and the highest DHW values were also in the far north and northern GBR (Figure 2.5).

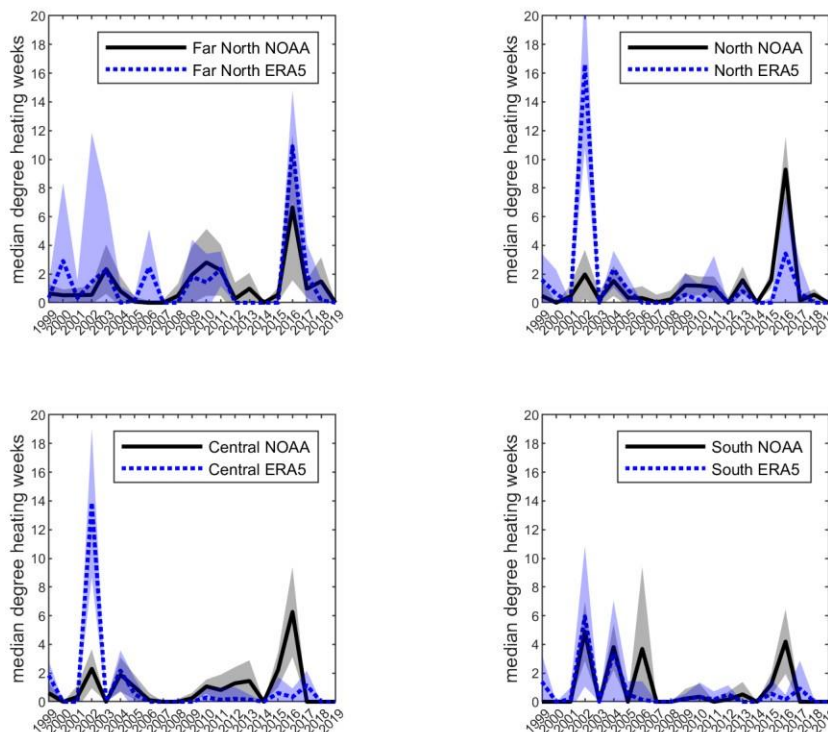


Figure 2.14: Downscaled ERA5 atmospheric reanalysis and NOAA Coral Reef Watch Degree Heating Weeks data are shown as the median value across four regions of the Great Barrier Reef as defined by the Great Barrier Reef Marine Park Authority. These values are based on the annual maximum Degree Heating Weeks per austral summer year. Austral summer years were used to avoid double counting during calendar years.

The shaded areas denoted the interquartile range across the spatial grid.

The regional disagreement between the downscaled ERA5 outputs and the NOAA CRW product are further demonstrated spatially for 2002 and 2016, reflecting the largest disparities in the central and some portions of the northern GBR (Figure 2.14, Figure 2.15). These locations are the areas of the bifurcation discussed in the Physical Oceanography section 1.3. This disparity could be due to the large influx of advection from boundary currents in the central and northern GBR, where the downscaling mechanism could be failing (Halloran et al., 2021). Alternatively, during the 2017 event, DHW values show general regional agreement between the two DHW products throughout the GBR (Figure 2.15). These maps were created using the spatial grid from the downscaled ERA5 simulation, which is the same grid used in the climate model simulations, ERA5 DHW values were subtracted from NOAA DHW values for bleaching event years, 2002, 2016, and 2017 (Figure 2.15).

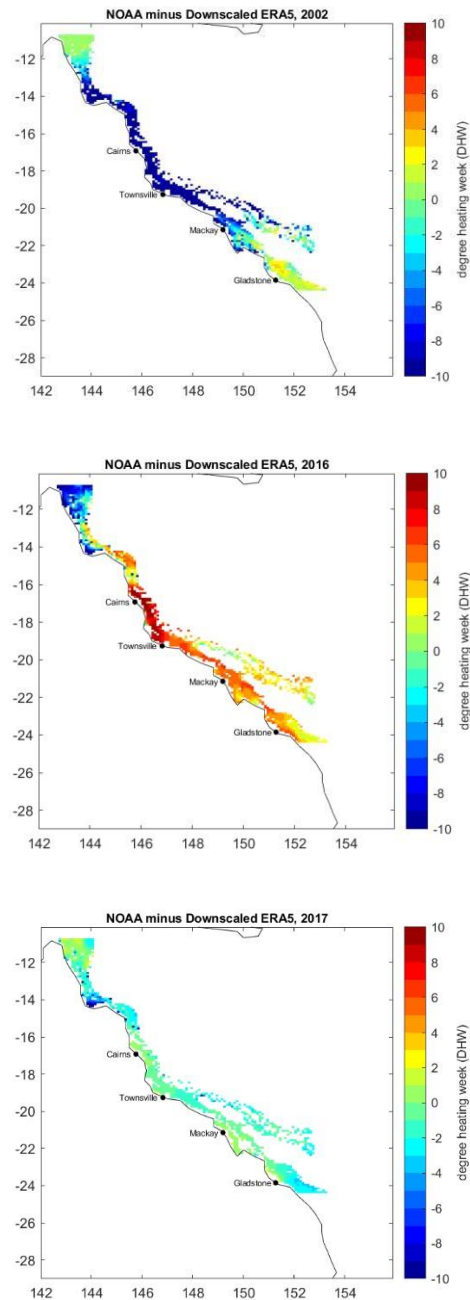


Figure 2.15: The difference between the NOAA Coral Reef Watch Annual Maximum Degree Heating Weeks product compared to the downscaled ERA5 Annual Maximum Degree Heating Weeks values for bleaching event years, 2002, 2016 and 2017, using the austral summer years to avoid double counting in calendar years.

The main difference between the satellite output and the downscaled output is likely due to the 1-D nature of the S2P3-R v2.0 downscaling. This infers that it does not account

for the horizontal energy in the ocean driven by eddies and boundaries currents, and importantly the area of bifurcation of the Southern Equatorial Current. Also, there could be a large disparity between the two datasets due to the way satellite imagery is collected, data with clouds are simply thrown out, potentially influencing the measurement. The NOAA satellite data is in fact a product, interpolated when clouds are in the picture, and interpolated towards the coast and between swaths. Regardless of the way the NOAA product is produced, the indifference between the NOAA product and the downscaled ERA5 output is more reflective of a lack of 3-D processes in the S2P3-R v2.0 downscaling. Also, there was an update to the ERA5 data in 2000, possibly causing some errors that are seen in this validation (Halloran et al., 2021). Another consideration is that these are anomalies of events that are driven by weather conditions, not averages of seasonal or yearly patterns, therefore, we would expect a certain level of uncertainty between the two products. The downscaled ERA5 reanalysis product is used to drive the S2P3-R v2.0 with the same atmospheric inputs used in the CMIP6 models that will be further explored in subsequent chapters as a metric of validation to address the issue of capturing anomalies. The satellite data validation was demonstrated as a metric of validation to measure the uncertainties in both, measuring anomalous events and accounting for 3-D processes that are shown on the surface of the ocean.

The implications for the S2P3-R v2.0 downscaling not capturing 3-D processes and potentially missing some anomalous conditions are relatively minor as this downscaling method is a vast improvement from previous downscaling methods. The caveats are clearly discussed per chapter in each discussion and the areas that may not be performing as well as other areas have been thoroughly outlined. Models do not completely represent Earth's physics but are constantly being improved and then compared.

CHAPTER 3

THE IMPORTANCE OF 1.5°C WARMING FOR THE GREAT BARRIER REEF

McWhorter, J. K., Halloran, P. R., Roff, G., Skirving, W. J., Perry, C. T., & Mumby, P. J. (2021). The importance of 1.5° C warming for the Great Barrier Reef. *Global change biology*.

This chapter is an expanded version of the publication including a more extensive literature review, an expanded description of the statistical methods, as well as additional figures that were in the supplementary material or not included in the publication itself.

Author contributions:

Conceptualization: JKM, PJM, PRH, CTP

Methodology: JKM, PRH, PJM, GR, WJS

Investigation: JKM, PRH, PJM, GR

Visualization: JKM, PJM, GR

Supervision: PJM, PRH, GR

Writing—original draft: JKM, PJM

Writing—review & editing: JKM, PJM, PRH, GR

3.1 ABSTRACT

Tropical coral reefs are among the most sensitive ecosystems to climate change and will benefit from the more ambitious aims of the United Nations Framework Convention on Climate Change's Paris Agreement, which proposed to limit global warming to 1.5° rather than 2°C above preindustrial levels. Only in the latest IPCC focused assessment, the Coupled Model Intercomparison Project phase 6 (CMIP6), have climate models been used to investigate the 1.5° warming scenario directly. Here, we combine the most recent model updates from CMIP6 with a semi-dynamic downscaling to evaluate the difference between the 1.5°C and 2°C global warming targets on coral thermal stress metrics for the Great Barrier Reef. By ~2080, severe bleaching events are expected to occur annually under intensifying emissions (Shared Socioeconomic Pathway SSP5-8.5). Adherence to 2° warming (SSP1-2.6) halves this frequency but the main benefit of confining warming to 1.5° (SSP1-1.9) is that bleaching events are reduced further to 3 events per decade. Attaining low emissions of 1.5° is also paramount to prevent the mean magnitude of thermal stress from stabilizing close to a critical thermal threshold (8 DHW). Thermal stress under the more pessimistic pathways SSP3-7.0 and SSP5-8.5 is 3- to 4-fold higher than present-day, with grave implications for future reef ecosystem health. As global warming continues, our projections also indicate more regional warming in the central and southern Great Barrier Reef than the far north and northern Great Barrier Reef.

3.2 INTRODUCTION

The frequency of severe bleaching events on the Great Barrier Reef (GBR) has increased as an effect of climate change (Hughes, Kerry, et al., 2018b). Hughes, Anderson, et al (2018) correlates measurements of sea surface temperature (SST) anomalies to recurring bleaching of 100 global reef locations from 1980 to 2016, finding that the time between events has been diminishing since 1980. Based on this study, the median return time between events in 2016 was only 6 years apart. By contrast, in the

early 1980s severe bleaching was occurring once every 25-30 years. Globally, there have been positive associations in the literature between El Niño years and coral bleaching events (1983, 1987, 1992, 1993, 1998, 2010, 2016) (McGowan & Theobald, 2017). However, SSTs have increased most notably during La Niña and neutral years (neither El Niño or La Niña), increasing the likelihood of annual bleaching (Hughes, Anderson, et al., 2018).

The widespread mass coral bleaching events that occurred on the GBR during the austral summer of 2016, 2017 and 2020 have been the most severe events to date in the region. Corals were impacted throughout the entire GBR by the 2017 and 2020 events while the 2016 event was mainly concentrated in the far north and northern GBR (Hughes et al., 2017). The impact of these recent events on corals has been unprecedented with estimated losses of live coral cover ranging from 30% across the entire GBR (Bozec et al., 2020) to 50% in shallow waters after the 2016 event alone (Hughes, Kerry, et al., 2018). Moreover, Cheung et al (2021) estimated that the average supply of coral larvae to reefs could have declined by 70% due to a loss of breeding adults (Cheung et al., 2021, Hughes et al., 2019).

The implications of global warming for coral reefs (Donner et al., 2005; Frieler et al., 2013; Hoegh-Guldberg, 1999; Hoegh-Guldberg et al., 2014) have contributed to the rallying call for more ambitious emissions reductions as part of the Paris Agreement under the 2016 Convention of Parties on Climate Change (Gattuso et al., 2015; Hoegh-Guldberg et al., 2018; IPCC, 2018; IPCC, 2019; IPCC, 2021). Indeed, the Intergovernmental Panel on Climate Change (IPCC), recently discussed the putative benefits of achieving the most optimistic warming scenario of 1.5° above pre-industrial (cf. the original target of 2° warming) (Hoegh-Guldberg et al., 2018; IPCC, 2018; IPCC, 2019; IPCC, 2021). Previous studies suggest that 70-90% of global coral reefs will be lost under the 1.5° target and 99% of reefs lost under the 2° target (Frieler et al., 2013; Hoegh-Guldberg et al., 2018; Schleussner et al., 2016). Specific to the GBR, King et al (2017) estimates that events like the 2016 bleaching event would be ~25% less likely to occur under the 1.5° target than the 2° target. A formal analysis of the potential benefits

that might accrue from adopting the 1.5° vs 2.0° warming scenarios is now feasible given the newly released 6th phase of the Coupled Model Intercomparison Project (CMIP6), which distinguishes the 1.5° focused Shared Socioeconomic Pathway (SSP1-1.9) (Riahi et al., 2017) from alternatives (O'Neill et al., 2016). Additionally, we allow for a more focused study of the GBR which provides a more detailed account of climate projections due to the availability of the 1.5° scenario and our downscaling process.

3.2.1 PREVIOUS STUDIES; CLIMATE PROJECTION METHODOLOGY FOR CORAL STRESS METRICS

In an earlier assessment of the difference between 1.5°C and 2°C of warming relative to preindustrial levels, Schleussner et al. (2016) followed Frieler et al (2013) in setting a global reef degradation threshold of >2 bleaching events per decade. Applying these criteria to reef cells globally, they found that virtually all cells risk degradation after 2050 under 2°C of global warming while the 1.5°C scenario reduces this to 90% of cells in 2050 and 70% in 2100 (Schleussner et al., 2016). Schleussner et al (2016) uses the existing projections and coral bleaching model from Frieler et al (2013). The bleaching threshold algorithm uses Degree Heating Month (DHM) based on Donner et al (2009), a monthly metric of prolonged, anomalously warm SSTs. The DHMs were calculated from 19 CMIP3 climate models across seven different emissions scenarios. The DHMs were then based on 2160 global reef locations by means of interpolation from the four closest climate model's grid points. The outputs were calculated as fractions of long-term degradation or when a reef cell exceeded 2 DHM twice in a decade counting for a mass severe bleaching event when this contained over 20% of reef cells. The long-term degradation assumption was based off Baker et al (2008) and Donner et al (2009), assuming that reef recovery is limited within the first 5 years (Baker et al., 2008; Donner, 2009). Schleussner et al (2016) considers this study conservative as it does not account for additional threats to coral reef ecosystems. Additional threats can be disease, invasive species (Maynard et al., 2016), increases in the magnitude of El Niño events (Power et al., 2013), the uncertainty behind tropical cyclones (Knutson et al., 2010), as well as sea level rise. A caveat in this study is the method for extracting the

1.5° and 2° information, the 1.5° scenario had yet to be developed in CMIP3, or CMIP5, so this method combines all scenarios and extracts information on long-term degradation solely on when 1.5°C was reached and similarly when 2°C was reached. When grouping all scenarios together and extracting information at a given time of global warming, it results in an uneven distribution of data across the models (Figure 3.1). To disprove the concept behind creating a ‘constant scenario’ in which large quantities of climate data are lumped together, we tested the differences between each scenario against global surface temperature. The main issue when doing this comparison is extracting all the data at 2°C for example, shown with the solid black line in Figure 3.1, is not evenly distributed among all models (Figure 3.1). From the interpolation of the climate models to reef cells, the use of DHM over Degree Heating Weeks (DHW) (a weekly metric of warming used by NOAA, Section’s 1.7.5, 1.7.6, 1.7.7), and the lack of scenario-independence in this previous study, means that the research in this chapter is a dramatic improvement.

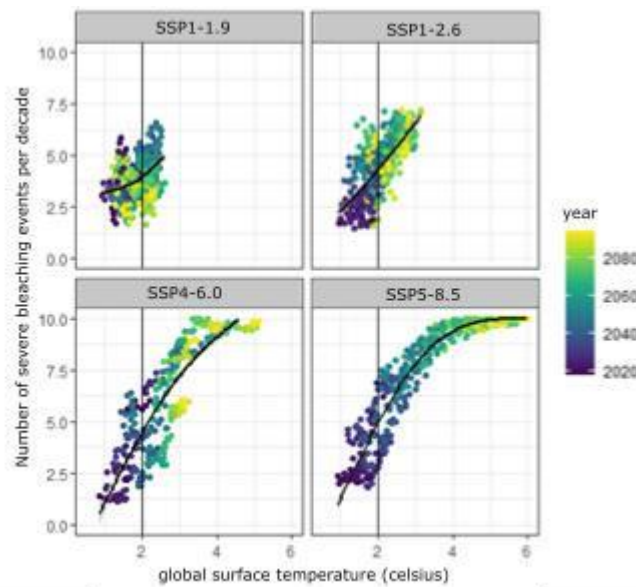


Figure 3.1: The frequency of severe bleaching, or when a grid cell exceeds >8 Degree Heating Weeks each year over a decadal period was plotted from 5 downscaled CMIP6 models grouped by each climate scenario (SSP1-1.9, SSP1-2.6, SSP3-7.0, and SSP5-8.5). The solid black line is global warming at 2°C.

Complementary to the work in Frieler et al (2013) and Schleussner et al (2016), King et al (2017) concludes that the probability of extreme warming events is 22% more likely to occur in a 2°C world than a 1.5°C world on the GBR. King et al (2017) also found that under 1.5°C or 2°C, there is a significant warming of SSTs compared with present-day temperatures and there is a clear anthropogenic contribution to warming. Unlike Schleussner et al (2016), the King et al (2017) study specifically focused on the GBR. The King et al (2017) study creates 4 'worlds' for analysis, 1.) the natural world, or a world that has no anthropogenic influence, 2.) the modern world centred on 2016, 3.) a 1.5°C world, and 4.) a 2°C world. The natural world scenario demonstrates a lack of interannual variability showing no anomalous warming near the 2016 warming event on the GBR revealing the anthropogenic influence on extreme warming events. The likelihood of Coral Sea heat from January, February, March in year 2016 occurring again was found to be 31% under the modern conditions, 64% under the 1.5°C scenario and 87% under the 2°C scenario. Grid cells were interpolated to a 2-degree resolution. A calibration test was used to select models with strong agreement when compared to observations (ERSSTv4). With the use of 4 Representative Concentration Pathways (RCP) (RCP2.6, RCP4.5, RCP6.0, RCP8.5) from 16 CMIP5 models, model years were extracted during January, February, and March. Then, the selection of 1.5°C and 2°C scenarios were based on decadal averages temperatures between 1.3-1.7°C for the 1.5°C scenario and 1.8-2.2°C for the 2°C scenario. There were years falling into both scenarios. The validation of the historical data from the models compared to an observational dataset demonstrates a useful technique, but the extraction of the climate scenarios based on decadal averages of temperature extremes could be improved upon given that the specific scenarios are available in the CMIP6 models.

The King et al (2017) study utilized a simple relationship between global average temperature and the fraction of reefs at risk of long-term degradation. Like Schuessler et al (2016), there was no downscaling of climate models and DHMs were used instead of DHW due to CMIP5 being limited to mainly monthly data for sea surface temperatures. We update this analysis for the GBR by; 1.) examining climate model

simulations which explicitly examine the more ambitious socio-economic pathways, 2.) utilize the latest generation of climate models, 3.) downscale the climate models to account for the influence of local bathymetry, tides, and other physical properties, and 4.) consider the magnitudes as well as frequency of stress derived from coral stress metrics. Importantly, the downscaling process works to resolve basic coastal mixing processes that may influence heating and cooling processes on the reef during a warming event.

3.2.2 STUDY DESIGN

Given that global ocean warming and the associated meteorological changes interact with local-scale oceanographic processes, we downscaled five CMIP6 models to a resolution of 10 km using semi-dynamic mechanistic approach (Halloran et al., 2021). These scales are closer to the scales at which local management decisions are made. This method uses a vertical 1-D physical-biogeochemical model at each grid box to capture the temperature response resulting from the interaction of the CMIP6 models' meteorology with local tides and bathymetry. The five selected models were chosen based on the availability of their atmospheric variables at the time of analysis.

Downscaled SSTs were used to derive standard metrics of coral thermal stress using DHW, a measure of accumulated anomalous warm SSTs (Donner et al., 2005; Skirving et al., 2020). We calculate two elements of stress upon corals. First, the magnitude of stress, measured by the absolute maximum DHW value in each year. Second, the number of bleaching events within a decade where such events occur once $DHW \geq 8$ (Donner et al., 2005). It has been well established through independent coral bleaching reports that some bleaching occurs at 4 DHW and widespread severe coral mortality tends to occur around 8 DHW (Bozec et al., 2020; Dietzel et al., 2020; Donner et al., 2005; Eakin et al., 2010; Hughes et al., 2017; Hughes, Kerry, et al., 2018). Therefore, in this study, widespread severe bleaching/mortality events are assumed to occur once 8 DHW is reached each year. These updated climate projections of coral stress help illuminate the consequences of various emissions trajectories and any benefits from achieving the 1.5°C target.

3.3 MATERIALS AND METHODS

3.3.1 DOWNSCALING MODEL DATA

Our semi-dynamic downscaling method applies the S2P3-R v2.0 model (Halloran et al., 2021), driven by surface air temperature, winds, air pressure, humidity, and net longwave and shortwave radiation, as simulated by the fully coupled global climate models. The atmospheric forcings are used in conjunction with high resolution bathymetry (Beaman, 2010) and tidal forcing (Egbert & Erofeeva, 2002) to simulate water column properties in the vertical dimension. The S2P3-R v2.0 model has been run for this study over the domain 142.0°W, 157.0°E, 30.0°S, 10.0°S from 4-50 m water depth, at a 10 km horizontal resolution and 2 m vertical resolution. We drive the model with surface level atmospheric data from the CMIP6 models, MRI-ESM2-0 (Adachi et al., 2013), EC-Earth3-Veg (Döscher et al., 2021), UKESM1-0-LL (Sellar et al., 2019), CNRM-ESM2-1 (Séférian et al., 2019), IPSL-ESM2-0 (Boucher et al., 2019). SST data were outputted daily from 1950-2100 (inclusive) and masked to contain values just within the Great Barrier Reef Marine Park Authority Boundary (GBRMPA, 2004).

3.3.2 CORAL STRESS METRICS

To calculate coral stress, two metrics were applied to the SST output: DHW, and the frequency of severe bleaching years. The DHW values are a potential trigger for coral bleaching and have been strongly correlated to bleaching events in the past (Bozec et al., 2020; Hughes et al., 2018a; Hughes et al., 2017; Skirving et al., 2020), but do not necessarily provide evidence of coral bleaching. The DHW values were calculated using the National Oceanic and Atmospheric Administration (NOAA) Coral Reef Watch methodology (Section's 1.7.4, 1.7.5, 1.7.6) (Heron et al., 2014; Skirving et al., 2020). Importantly, prior to the calculation of annual maximum DHW, calendar years were modified to be centred on the austral summer (e.g., August 1, 2014 – July 31, 2015) to

avoid double counting severe bleaching events that cross from one calendar year to the next (Skirving et al., 2019).

Maximum Monthly Mean Climatology

(Section 1.7.5)

Degree Heating Weeks Calculation

(Section's 1.7.4, 1.7.6)

Frequency of Severe Bleaching per Decade Calculation

The maximum DHW was extracted for each reef cell, from each year of the 2014-2100 time series (exclusive) for each model and each scenario. For each reef cell, the frequency of severe bleaching (≥ 8 DHW) was determined over an 11-year moving average giving a near decadal projection. The median frequency value was then taken annually across the spatial domain for all models and scenarios. The timeseries was then averaged using all models within each scenario resulting in an ensemble mean per scenario and scaled to a decade.

3.4 RESULTS

3.4.1 MAGNITUDE OF THERMAL STRESS

The magnitude of thermal stress upon GBR corals intensifies dramatically over time, particularly in the absence of strong international efforts to tackle climate change (SSP3-7.0) (Riahi et al., 2017) or an energy intensive fossil-based economy (SSP5-8.5) (Figure 3.2a) (O'Neill et al., 2016; Riahi et al., 2017). These scenarios lead to a 3- to 4-fold increase in the magnitude of thermal stress upon corals (Figure 3.2a) compared to the worst of recent bleaching events, which have already caused mass mortality on

many GBR reefs (Bozec et al., 2020; Hughes, Kerry, et al., 2018b). By the end of the century the model ensembles project DHW values of 50 under SSP5-8.5 and DHW values of 35 under SSP3-7.0 (Figure 3.2a). The worst of recent mass bleaching events had a median value of ~6 DHW by comparison across the entire GBR (Table 3.1).

In contrast, long-term projections under global collaboration on climate policy targeting a mean warming above preindustrial levels of 2° (SSP1-2.6) (Riahi et al., 2017), or accepting the need for negative emissions to limit warming to 1.5° (SSP1-1.9) (O'Neill et al., 2016; Riahi et al., 2017), lead to far smaller increases in absolute stress. Long-term bleaching projections under these scenarios have a similar mean magnitude to that experienced already but with higher variability (Figure 3.2a, Table 3.1, Table 3.2). Adopting the SSP1-1.9 pathway results in mean thermal stress remaining below the 8 DHW threshold by ~1.5 DHW in 2060 (Table 3.3), with thermal stress returning to present-day levels by 2100 (Figure 3.2c), whereas the SSP1-2.6 pathway stabilizes after 2050 and remains close to the 8 DHW threshold until 2100 (Figure 3.2c). Note that a DHW of 8 has been reached, and even exceeded, in some recent bleaching events, but the GBR-wide median DHW in the worst event to date (2020) was 6.40, which is consistent with ensemble model predictions (Table 3.1; Figure 3.2c).

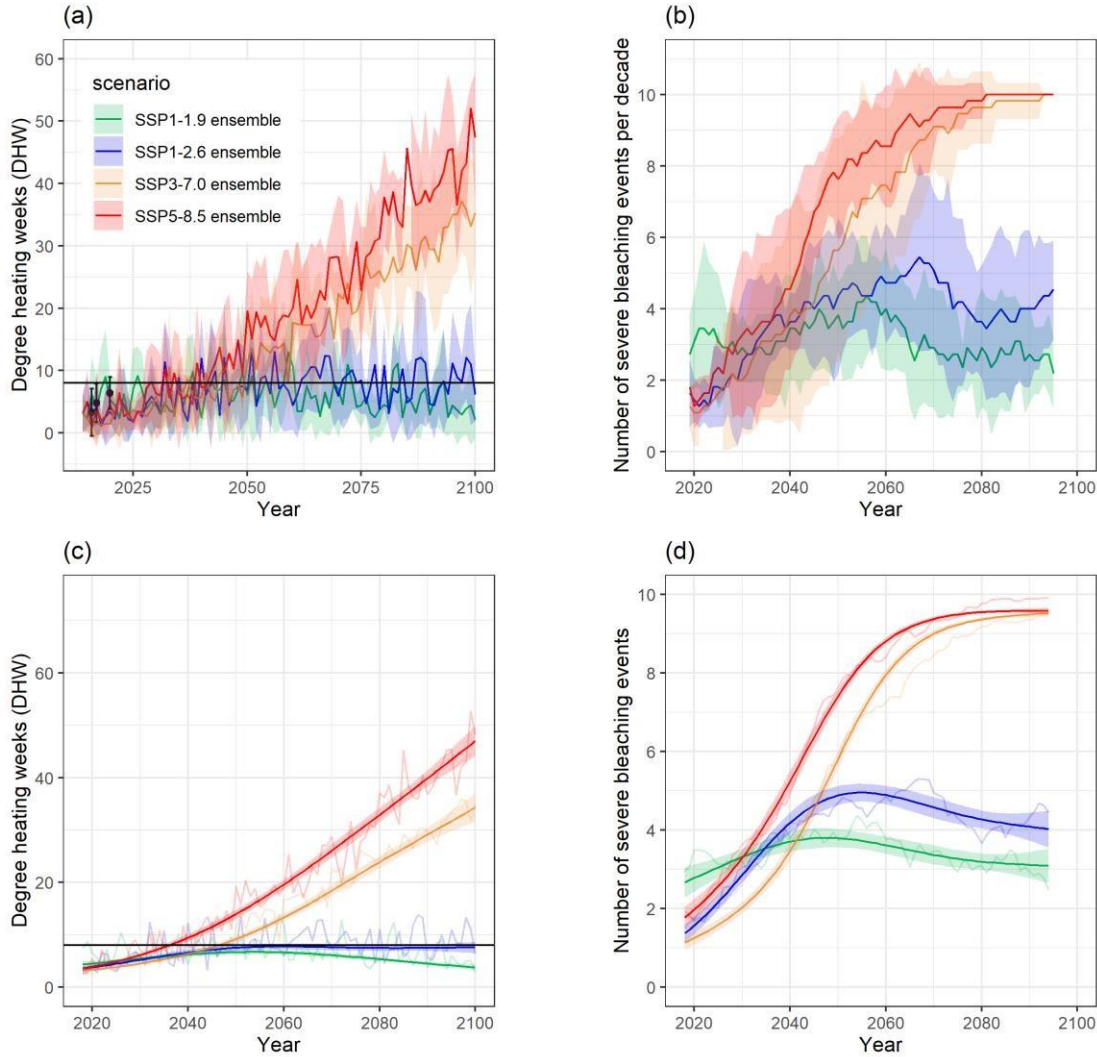


Figure 3.2: Metrics of coral stress averaged across the Great Barrier Reef for four socioeconomic pathways and an ensemble of five climate models. Coral stress metrics disaggregate magnitude as Degree Heating Weeks (DHW) (a,c), and frequency as the number of severe bleaching years per decade (b,d). Top row presents the multi-model ensemble mean (a, b) whereas the bottom row is the smoothed Generalised Additive Model fitted to the data, which helps visualise underlying trends. The multi-model ensemble is made up of MRI-ESM2-0, EC-Earth3-Veg, UKESM1-0-LL, CNRM-ESM21, and IPSL-ESM2-0. Shaded areas denote the standard deviation for each scenario averaged across models (a,b,c,d). The points and error bars (a) show the median and standard deviation DHW from recent bleaching events, 2016, 2017, 2020, satellite observations of reef pixels. The horizontal black line in (a) and (c) marks 8 DHW, a metric of coral stress that often leads to mortality.

Table 3.1: Present-day average intensities of coral bleaching stress on reefs of the Great Barrier Reef expressed in units of Degree Heating Weeks (DHW) as determined from satellite surface temperature. Std denotes standard deviation.

Year	Mean DHW	Median DHW	Std of DHW
2016	4.57	3.31	3.80
2017	5.50	4.78	3.07
2020	6.23	6.40	2.59

3.4.2 FREQUENCY OF THERMAL STRESS

Pathways SSP1-1.9 and SSP1-2.6 differ markedly in the frequency at which severe bleaching stress would occur (Figure 3.2b, Figure 3.2d, Table 3.2). The frequency metric speaks to the interannual variability as the number of severe bleaching events is derived from values exceeding >8 DHW within a near decadal rolling window (11 year rolling window to allow the year to be placed in the middle, avoiding decimals). From 2060 major bleaching events are expected approximately every other year under SSP1-2.6 (i.e., 5 events per decade) whereas the rate of bleaching is eventually lower at three events per decade under SSP1-1.9 (Figure 3.2b, Figure 3.2c). In marked contrast, bleaching eventually becomes an annual event (10 events / decade) under the higher emissions pathways (Figure 3.2b). Table 3.2 allows for a comparison of the trends between scenarios in 2060 as the main effects and pairwise comparisons show significant differences ($p < .0001$).

Our results highlight the effects of a committed warming even under SSP1-1.9 where bleaching frequency peaks around 2050 with 4.4 ± 1.4 events per decade (Figure 3.2b) of average magnitude 7.4 DHW ± 2.1 (Figure 3.2a, from 2051-2061 inclusive). Based on this outcome, we would expect a temporary worsening of present-day conditions even under the best-case scenario. We define present-day conditions as

1.9 events/decade ± 0.2 (Figure 3.2b) and 3.5 DHW ± 0.9 (Figure 3.2a), or the average of our initial conditions across all scenarios from 2014-2025 (inclusive).

Table 3.2: Complementary to Figure 3.2c, and Figure 3.2d, this table shows main effects and pairwise comparisons from generalized additive mixed effects models for Degree Heating Weeks and mean frequency of severe bleaching years per decade for 2060.

Degree Heating Weeks				
Factor	df	F-value	P	
s(Year):SSP1-1.9	3	5662	<.0001	
s(Year):SSP1-2.6	3	11865	<.0001	
s(Year):SSP3-7.0	3	174428	<.0001	
s(Year):SSP3-7.0	3	217810	<.0001	
s(model)	4	41633	<.0001	
s(long,lat)	1	39763	<.0001	
Pairwise comparisons	odds ratio	SE	T ratio	P
SSP1-1.9 - SSP1-2.6	0.843	0.00262	-55.22	< .0001
SSP1-1.9 - SSP3-7.0	0.461	0.00135	-263.91	< .0001
SSP1-1.9 - SSP5-8.5	0.290	0.00083	-431.57	< .0001
SSP1-2.6 - SSP3-7.0	0.548	0.0016	-205.61	< .0001
SSP1-2.6 - SSP5-8.5	0.345	0.00099	-371.76	< .0001
SSP3-7.0 - SSP5-8.5	0.629	0.00168	-172.99	< .0001
Mean frequency of severe bleaching years per decade				
Factor	df	F-value	P	
s(Year):SSP1-1.9	3	1908	<.0001	
s(Year):SSP1-2.6	3	25402	<.0001	
s(Year):SSP3-7.0	3	365717	<.0001	
s(Year):SSP3-7.0	3	298768	<.0001	
s(model)	4	60799	<.0001	

s(long,lat)	1	18591	<.0001	
Pairwise comparisons	odds ratio	SE	T ratio	P
SSP1-1.9 - SSP1-2.6	0.592	0.00237	-131.02	< .0001
SSP1-1.9 - SSP3-7.0	0.146	0.00057	-496.37	< .0001
SSP1-1.9 - SSP5-8.5	0.077	0.0003	-658.17	< .0001
SSP1-2.6 - SSP3-7.0	0.247	0.00096	-361.3	< .0001
SSP1-2.6 - SSP5-8.5	0.130	0.00051	-524.36	< .0001
SSP3-7.0 - SSP5-8.5	0.526	0.00197	-171.59	< .0001

The two low emissions scenarios demonstrate differences in coral stress metrics particularly in the second half of the 21st century, most notably shown in the reduction of the number of severe bleaching events (Figure 3.3b). The difference in magnitude following 2050 is ~5 DHW and ~2 severe bleaching events less per decade at most (Figure 3.3 (a, b)). These GBR wide values reflect median value of all cells across the spatial grid from 4-50 m, 10km resolution within the GBRMPA boundary. The shaded area reflecting the standard deviation is helpful when understanding the range of outcomes in each scenario. The standard deviations are demonstrating the spatial variability of the DHW values. The spatial context is further discussed in the next chapter/paper.

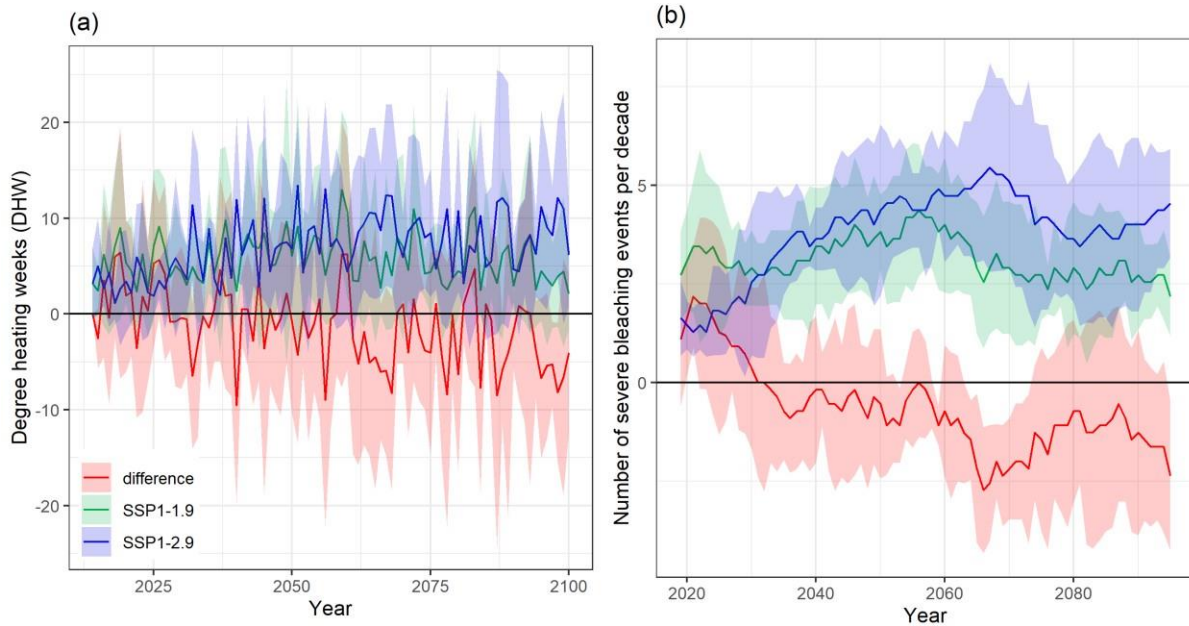


Figure 3.3: The trends for SSP1-1.9 and SSP1-2.6 as well as the differences between these two climate-change scenarios are shown for (a) mean Degree Heating Weeks and (b) mean frequency of severe bleaching per decade relative to the Maximum Monthly Mean from 1985-2012 (inclusive). The shaded areas represent the standard deviation.

3.4.3 GREAT BARRIER REEF-WIDE STATISTICAL ANALYSIS

Statistical analysis was required to quantify the differences between climate-change scenario trends, most importantly the two lower climate-change scenarios, 1.5°C (SSP1-1.9), and 2°C (SSP1-2.6) in terms of heat stress. Generalised additive random effects models (GAM) were used to test for differences in magnitude and frequency of

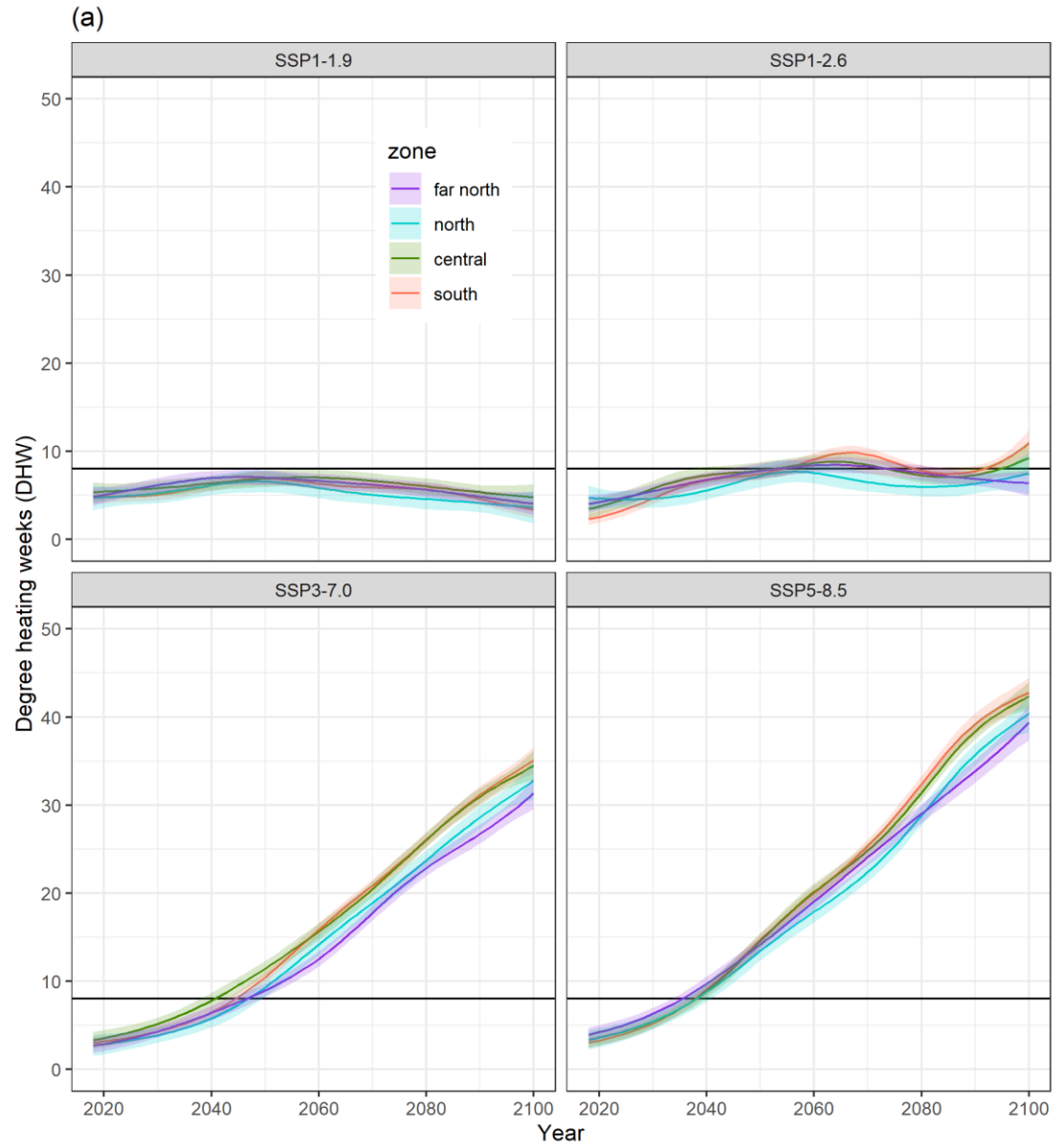
severe bleaching among climate-change scenarios (Wood, 2011) (Figure 3.2c, Figure 3.2d). A GAM is essentially a generalized linear model in which the response variable depends linearly on smooth functions of predictor variables. In this case, our predictor variables, model, and climate-change scenario, were used as random effects to account for variance between models and climate change scenarios. Penalized regression splines of 4 knots ($k=4$) were fit across years and allowed to vary across climate-change scenarios. The reasoning for using a penalized regression spline of $k=4$ was to reduce overfitting in the model, allowing smoothing every 20 years. The latitude and longitude of each grid cell ($n = 1100$ cells) were included as a smoothed interaction term in the model to account for spatial autocorrelation (Wood, 2017).

The *bam* function in the 'mgcv' package (Wood, 2017) in R proved useful as the *gam* function did not allow enough memory within the R software to run all the data. Using a representative subset of the data, the *bam* function initially sets up the characteristics for the smoothing curves. The data are then split into necessary blocks using the function *predict.gam* and information from each block such as factor R, the sum of squares of y , and $Q'y$ is updated for the whole matrix. The fitting can then be done at the end following the blocking process, without needing the entire model matrix (Wood, 2011, 2017, 2018).

Significant differences between climate-change scenarios were tested using tukey adjusted pairwise comparisons using the 'emmeans' package (Lenth et al., 2018). The 'emmeans' package refers to estimated marginal means, also known as least-squares means (Lenth et al., 2018). The tukey's multiple comparison test determined significant differences between each climate change scenario. The standard deviation was also calculated per year across the spatial grid within each climate-change scenario. For example, values from the far north to the southern GBR could range from five to zero DHW and the standard deviation gives a metric of how variable the DHW are across the entire spatial grid in a given warming year.

3.4.4 REGIONAL MAGNITUDE OF THERMAL STRESS UNDER LOW EMISSIONS

As warming continues in the 21st century, the magnitude of DHW increases more in the southern and central GBR relative to the far north and northern GBR (Figure 3.4a). However, the scenario with the least warming, SSP1-1.9, shows no discernible regional separation in the magnitude of warming while regions remain under 8 DHW on average (Figure 3.4a). Meanwhile, even in SSP1-2.6 there is an increase in warming in the southern GBR by ~1 DHW in 2060 relative to other regions (Figure 3.4a, Table 3.3b). The magnitude of stress in the far north and north uniquely remains closer to 8 DHW in SSP1-2.6, while the southern and central GBR rise above 8 DHW just after mid-century (Table 3.3b) and again at the end of the century (Figure 3.4a). Under the most intense warming scenarios, SSP3-7.0 and SSP5-8.5, the central and southern GBR are generally warming more than the far north and northern GBR and by ~1-3 DHW in 2060 (Figure 3.4a, Table 3.3c, Table 3.3d).



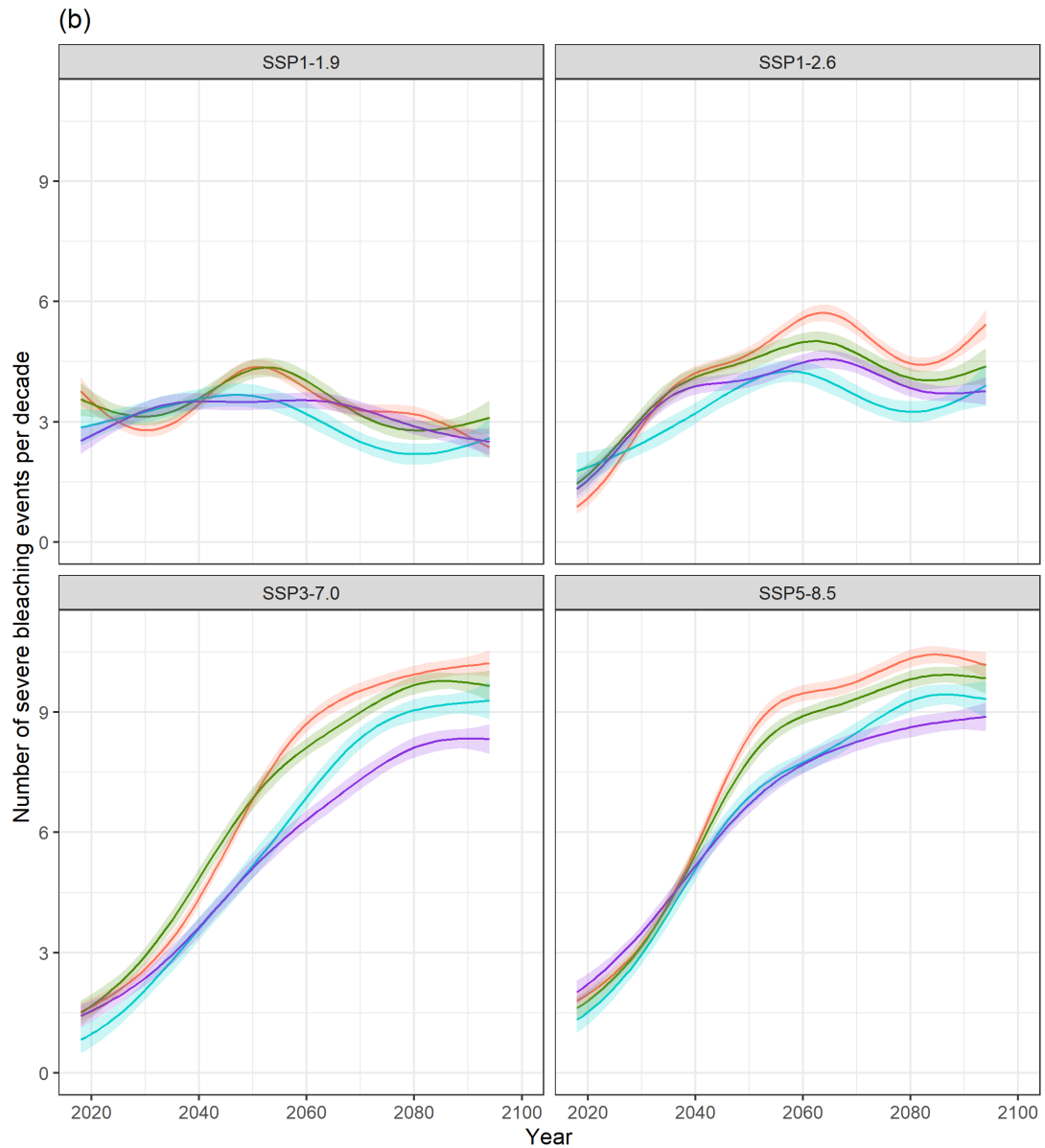


Figure 3.4: Metrics of coral stress averaged regionally across the Great Barrier Reef for low emissions socioeconomic pathways and an ensemble of five climate models. Coral stress metrics disaggregate magnitude as Degree Heating Weeks (a), and frequency as the number of severe bleaching years per decade (b). A smoothed Generalised Additive Model was fitted to the data, which helps visualise underlying regional trends. The multi-model ensemble is made up of MRI-ESM2-0, EC-Earth3-Veg, UKESM1-0-LL, CNRM-ESM2-1, and IPSL-ESM2-0. Shaded areas denote the standard deviation for each zone averaged across models (a, b). The horizontal black line in (a) marks the 8 DHW, a metric of coral stress that often leads to mortality.

3.4.5 REGIONAL FREQUENCY OF THERMAL STRESS UNDER LOW EMISSIONS

As warming continues, our results indicate an increase in the number of severe bleaching years in the southern and central GBR under all emissions scenarios (SSP1-1.9, SSP1-2.6, SSP3-7.0, SSP5-8.5) (Figure 3.4b). The regional separation becomes most apparent in higher emissions scenarios such that the drastic increase in warming causes approximately two more severe bleaching years/decade in the southern and central GBR relative to the far north and northern GBR (Figure 3.4b, Table 3.3c, Table 3.3d). SSP1-1.9 only exhibits this regional separation around mid-century before the expected extraction of CO₂ from the atmosphere in the latter half of the century. In year 2060 under SSP11.9 the far north/northern regions can expect ~0.50 severe bleaching events/decade less than central/southern regions (Figure 3.4b, Table 3.3a). While SSP1-2.6 also shows the same latitudinal separation, the far north/northern regions project ~1 severe bleaching year/decade less than central/southern regions in 2060 (Figure 3.4b, Table 3.3b).

Table 3.3: The values for each region, far north, north, central, and south GBR, for year 2060 were extracted for Degree Heating Weeks (DHW) and the frequency as the number of severe bleaching years per decade. The scenarios are separated as; a) SSP1-1.9, b) SSP1-2.6, c) SSP3-7.0, and d) SSP5-8.5.

(a)

SSP1-1.9, Year 2060		
Region	DHW ± SE	Frequency ± SE
Far North	6.6 ± 0.05	3.5 ± 0.01
North	5.9 ± 0.07	3.2 ± 0.02
Central	7.0 ± 0.05	4.0 ± 0.01
South	6.3 ± 0.04	3.8 ± 0.01

(b)

SSP1-2.6, Year 2060		
Region	DHW \pm SE	Frequency \pm SE
Far North	8.4 \pm 0.05	4.3 \pm 0.01
North	7.5 \pm 0.07	4.2 \pm 0.02
Central	8.7 \pm 0.05	5.0 \pm 0.01
South	9.1 \pm 0.04	5.6 \pm 0.01

(c)

SSP3-7.0, Year 2060		
Region	DHW \pm SE	Frequency \pm SE
Far North	12.5 \pm 0.05	6.3 \pm 0.01
North	14.2 \pm 0.07	6.9 \pm 0.02
Central	15.6 \pm 0.05	8.1 \pm 0.01
South	15.9 \pm 0.04	8.7 \pm 0.01

(d)

SSP5-8.5, Year 2060		
Region	DHW \pm SE	Frequency \pm SE
Far North	19.0 \pm 0.05	7.7 \pm 0.01
North	17.9 \pm 0.07	7.8 \pm 0.02
Central	20.1 \pm 0.06	8.9 \pm 0.01
South	20.1 \pm 0.04	9.5 \pm 0.01

3.4.6 REGIONAL STATISTICAL ANALYSIS

The regional analysis assessed how the predicted magnitude and frequency of bleaching events varied across regions of the GBR. The Great Barrier Reef Marine Park Authority (GBRMPA) regions, far north, north, central, and south were used to

classify the four regions of the GBR to account for spatial trends (GBRMPA, 2004). As for the GBR-wide analysis, the regional analysis utilized GAM using the *bam* function, but included a three-way interaction between the predictor variables of climate-change scenario, model, and GBR region. In the GBR-wide analysis, only a two-way interaction was included (climate-change scenario and model). For the regional analysis, the penalized regression splines were assigned $k=6$, which allows optimal model fitting with knots approximately every 15 years. Given the regional analysis used a smaller dataset (per region) than the GBR-wide analysis, a higher number of knots was chosen to improve the fits needed to improve with a smaller dataset per region versus four splines were used in the GBR wide analysis. Model was also included as a random effect. Smoothing terms were allowed to vary across both region and climate change scenario (four climate-change scenarios) for both magnitude and frequency of severe bleaching events, to allow scenarios within zones to follow independent trajectories.

Model fits were implemented using a *family* in the *bam* function and compared using the Akaike information criterion (AIC). Based on the lowest AIC scores, the scaled t family (implemented for heavily tailed data) was used with a logarithmic scale (function *scat*, *link = "log"*) for the frequency of severe bleaching events and an inverse fit for DHWs (*link = "inverse"*).

After applying these methods, the models for the regional analysis had poorer fits than those for the GBR-wide analysis. Ultimately, this was due to the reduced number of datapoints (per region) and a wider range of values in the higher climate-change scenarios (i.e., annual bleaching events by the end of the century). The lower climate-change scenarios had better model fits due to the values having a smaller range. In the process of improving the model fitting, the data were explored at length and various methods were tested. The data type and distribution were ascertained for the frequency of severe bleaching events and DHW. DHW is a complex metric to apply a model fit to, as it is not measured by weeks in a year but rather as values that roll over a 3-month window counting an anomaly. It comprises continuous data and non-integer values, with a zero-inflated distribution (Figure 3.5).

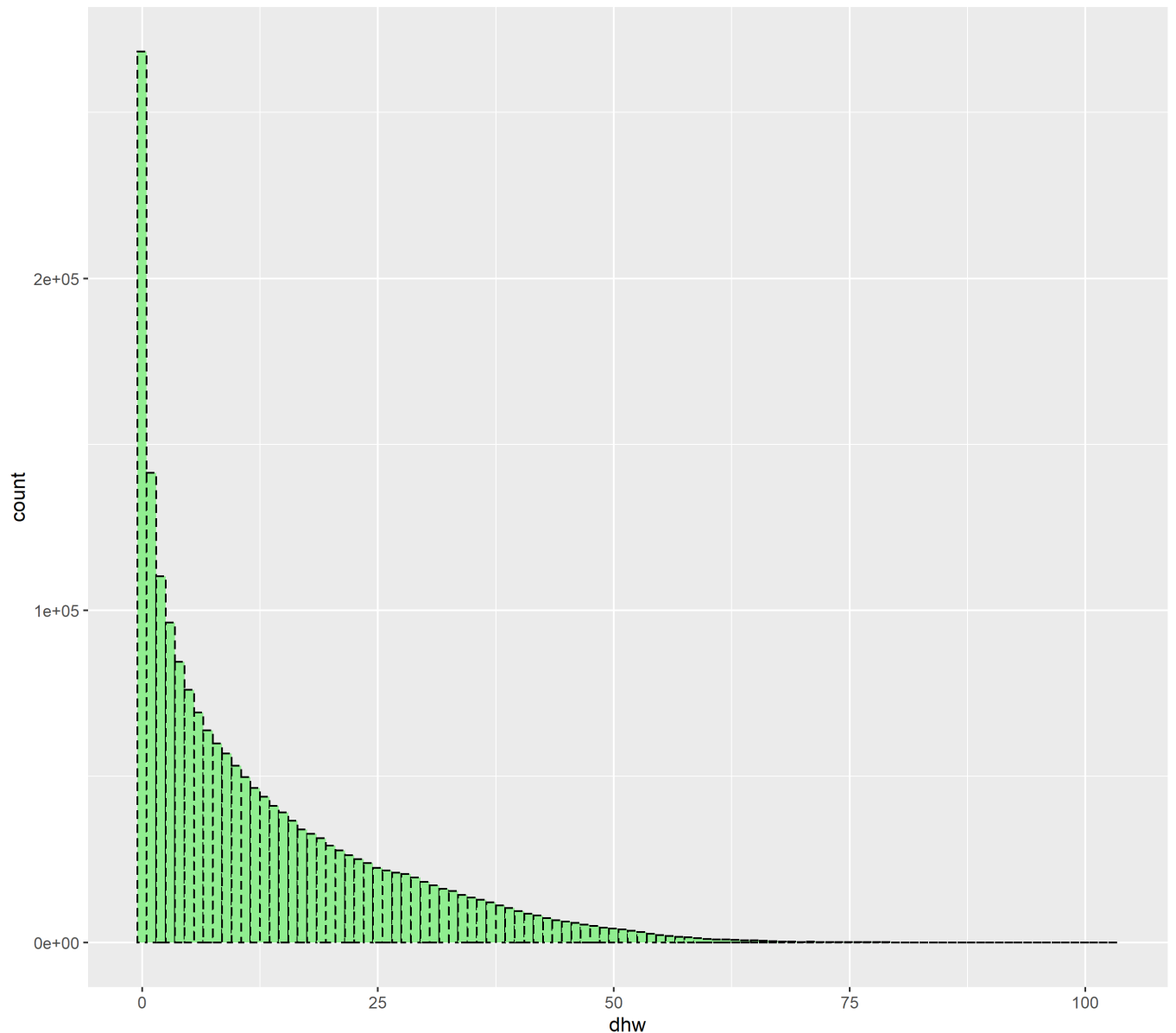


Figure 3.5: The histogram of Degree Heating Weeks (DHW) values for the downscaled S2P3-R v2.0 dataset on the Great Barrier Reef for four climate change scenarios.

The number of severe bleaching events, defined as when a value exceeds 8 DHW in an 11-year rolling mean produces a ratio of the number of years in a decade that will have a severe bleaching event per cell on the GBR, where one represents annual bleaching or 11/11 years. The distribution of these values among the entire dataset is bimodally

distributed due to an increase in annual events under high emissions scenarios and spike in warming just after mid-century in the lower emissions scenarios (Figure 3.6).

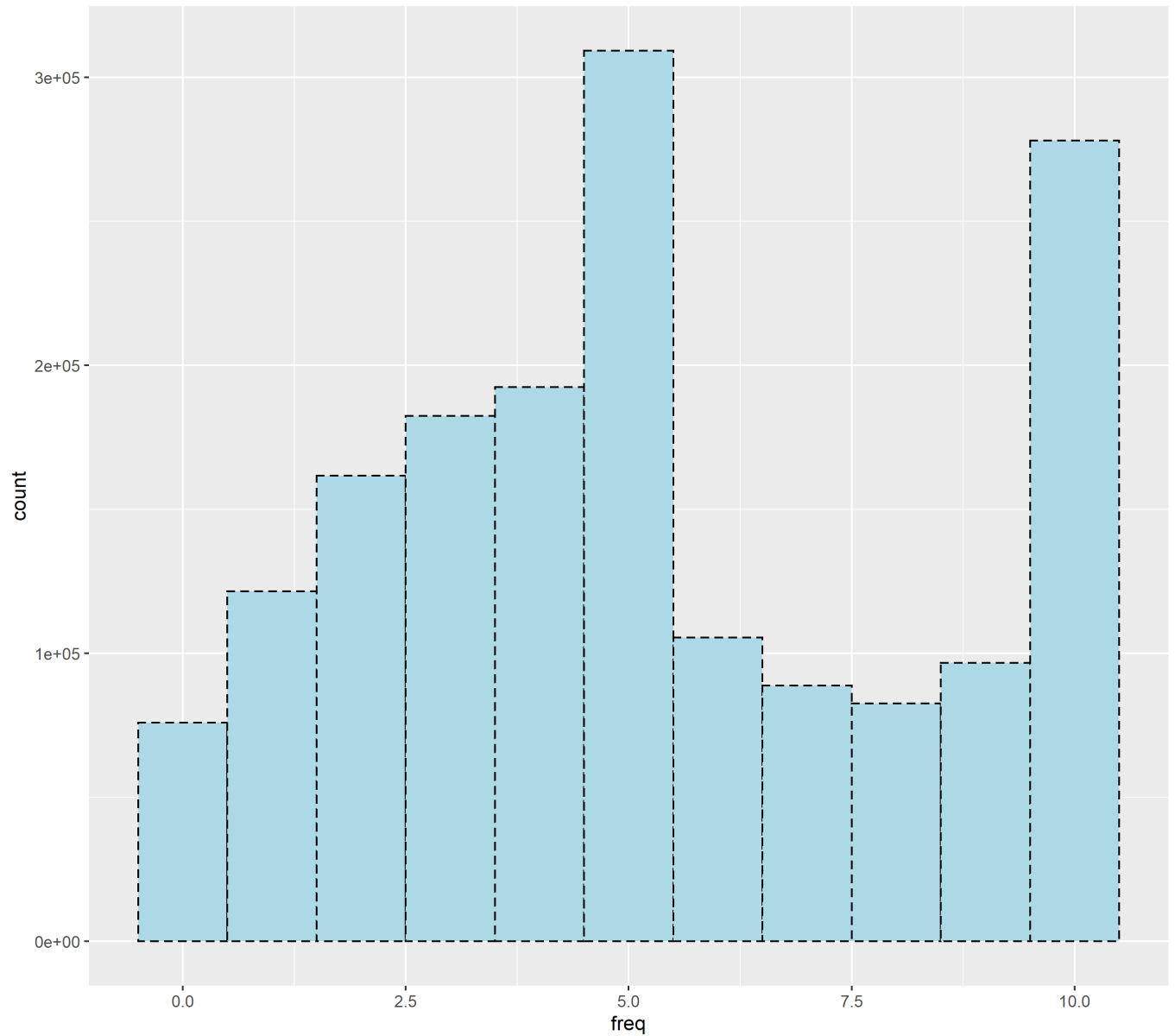


Figure 3.6: The histogram of the number of severe bleaching events per decade (freq) for the entire dataset.

Link functions convert the data from a linear predictor to different scales, exponential or logistic. These functions facilitate the application of a linear model form, but model

coefficients cannot then be interpreted without back transforming the data to the original scale. Link functions are specified in combination with the model distribution type, which is implemented using the *family* argument within the *bam* function. Based on the best residual values under various model fits, *scat*, a scaled t family distribution with a logarithmic scale link function (*link = "log"*) was used for the frequency of severe bleaching events, and an inverse fit link function was used for DHW (*link = "inverse"*). The *scat* family is used for heavily tailed data, where $y - \mu/\text{sig} \sim t_{nu}$, and *mu* is determined by a linear predictor, while *sig* and *nu* are parameters to be estimated alongside the smoothing parameters (Wood, 2017).

The inverse logit was better suited to the DHW data verses the frequency data because it allows values that are not bound between 0-1, unlike the logit function. The inverse logit runs along the y-axis instead of the x-axis. The linear combination of the independent variables (climate-change scenario, model, zone) and their coefficients are returned in a probability of 0 or 1.

3.4.7 RESULTS PER MODEL, NUMBER OF SEVERE BLEACHING EVENTS AND DEGREE HEATING WEEKS

The individual models have different interannual variability trends and are all slightly different in their projections (Figure 3.7-3.10). MRI-ESM2-0 does not distinguish between the two low scenarios, SSP1-1.9 and SSP1-2.6, as much as the other models for the number of severe bleaching events per decade (Figure 3.10). The DHW values do not exceed 8 DHW in MRI-ESM2-0 and there is less interannual variability in this model (Figure 3.7, Figure 3.8). The greatest difference in the number of severe bleaching events between the two low scenarios in the second half of the century is most apparent in EC-Earth3-Veg and UKESM1-0-LL (Figure 3.10). The model variability clearly ranges and is best used as an ensemble (IPCC, 2021).

Model variability can influence projections. Variability between models was accounted for in our statistical methods using a GAM and further shown in subsequent plots (Figures 3.7-3.10). The interannual variability makes the difference between scenarios and models hard to distinguish for DHW (Figure 3.7, Figure 3.9). In contrast, the number of severe bleaching events per decade metric uses a rolling mean, so the data are smoother compared to the DHW (Figure 3.8, Figure 3.10) allowing for a more visual analysis of the differences between models.

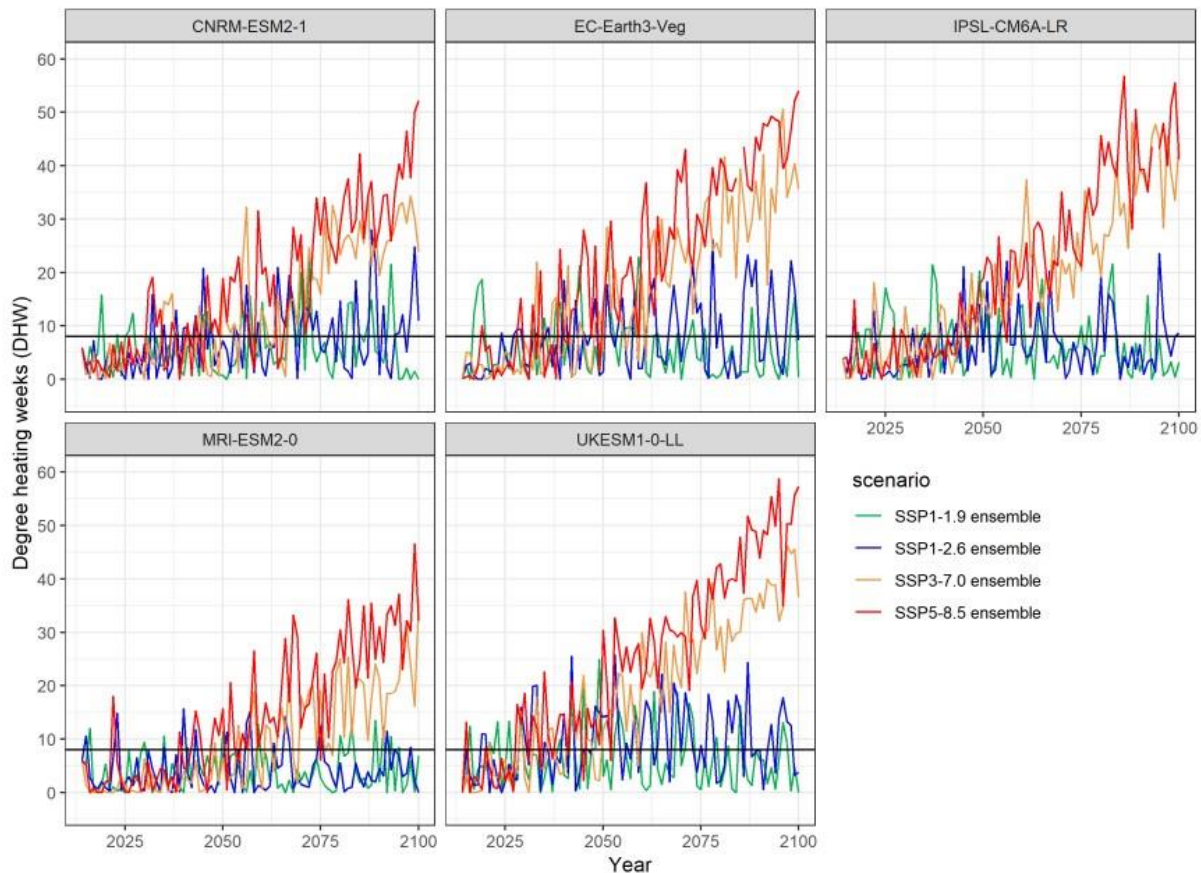


Figure 3.7: Metrics of the median value of coral stress across the Great Barrier Reef for four Shared Socioeconomic Pathways per model show magnitude as Degree Heating Weeks (DHW). The horizontal black line in 1a marks 8 DHW, a metric of coral stress that often leads to coral mortality.

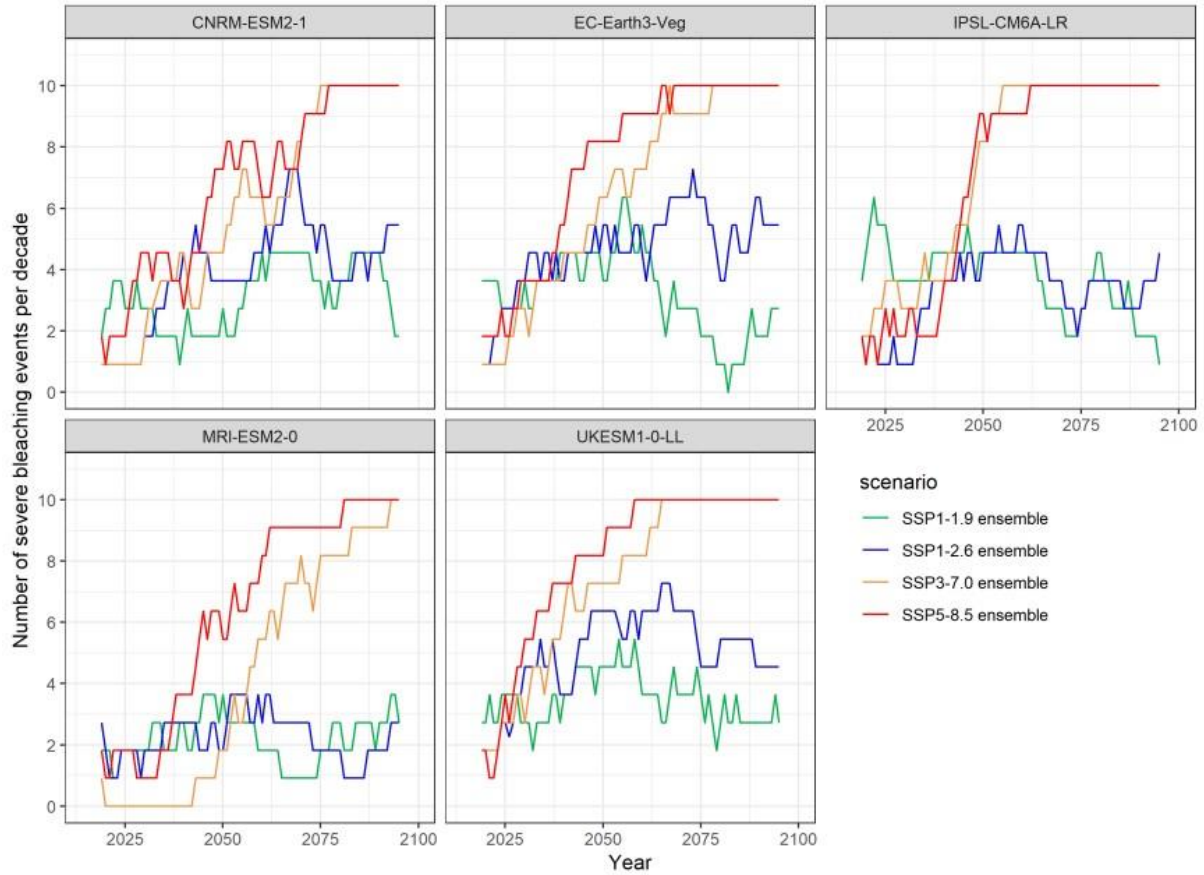


Figure 3.8: Metrics of the median value of coral stress across the Great Barrier Reef for four Shared Socioeconomic Pathways per model show the frequency of severe bleaching years per decade.

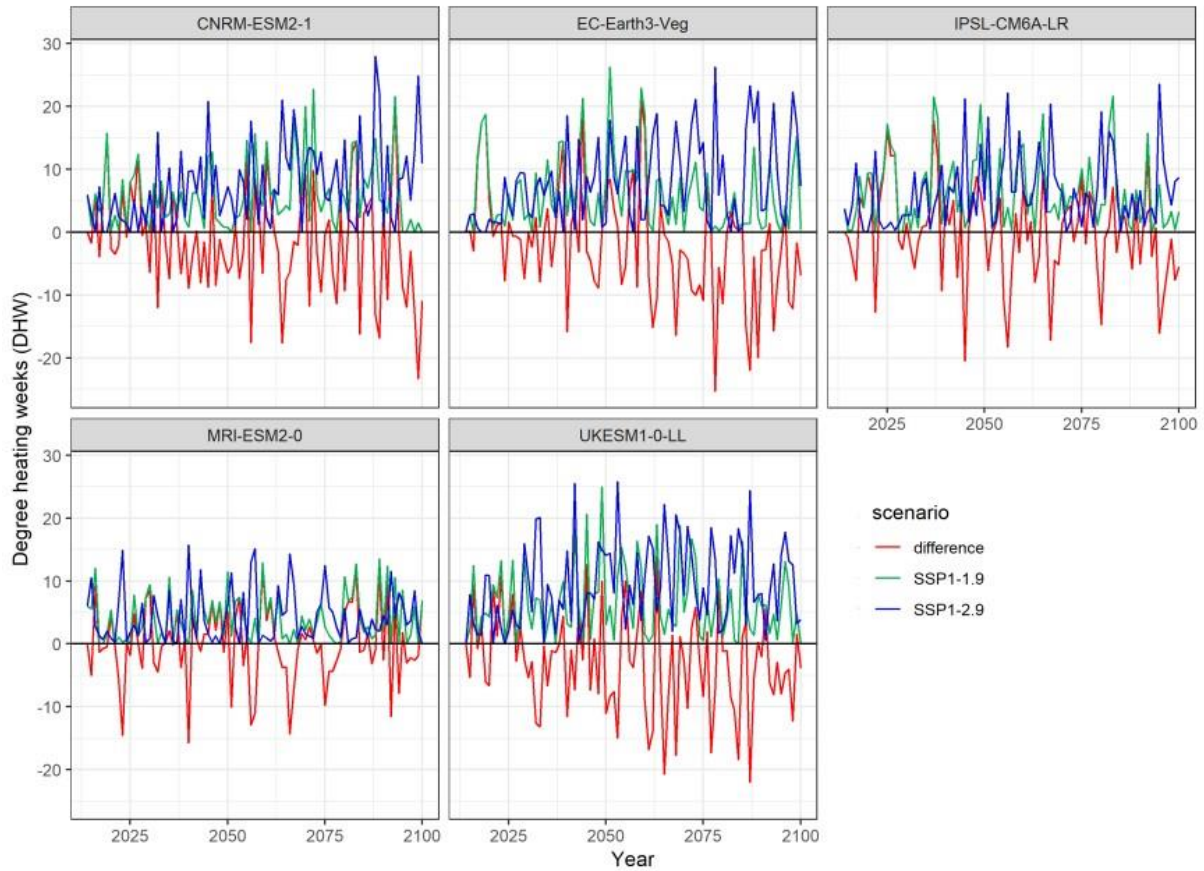


Figure 3.9: The trends for SSP1-1.9 and SSP1-2.6 as well as the differences between these two scenarios are shown per model for mean Degree Heating Weeks relative to the Maximum Monthly Mean from 1985-2012 (inclusive).

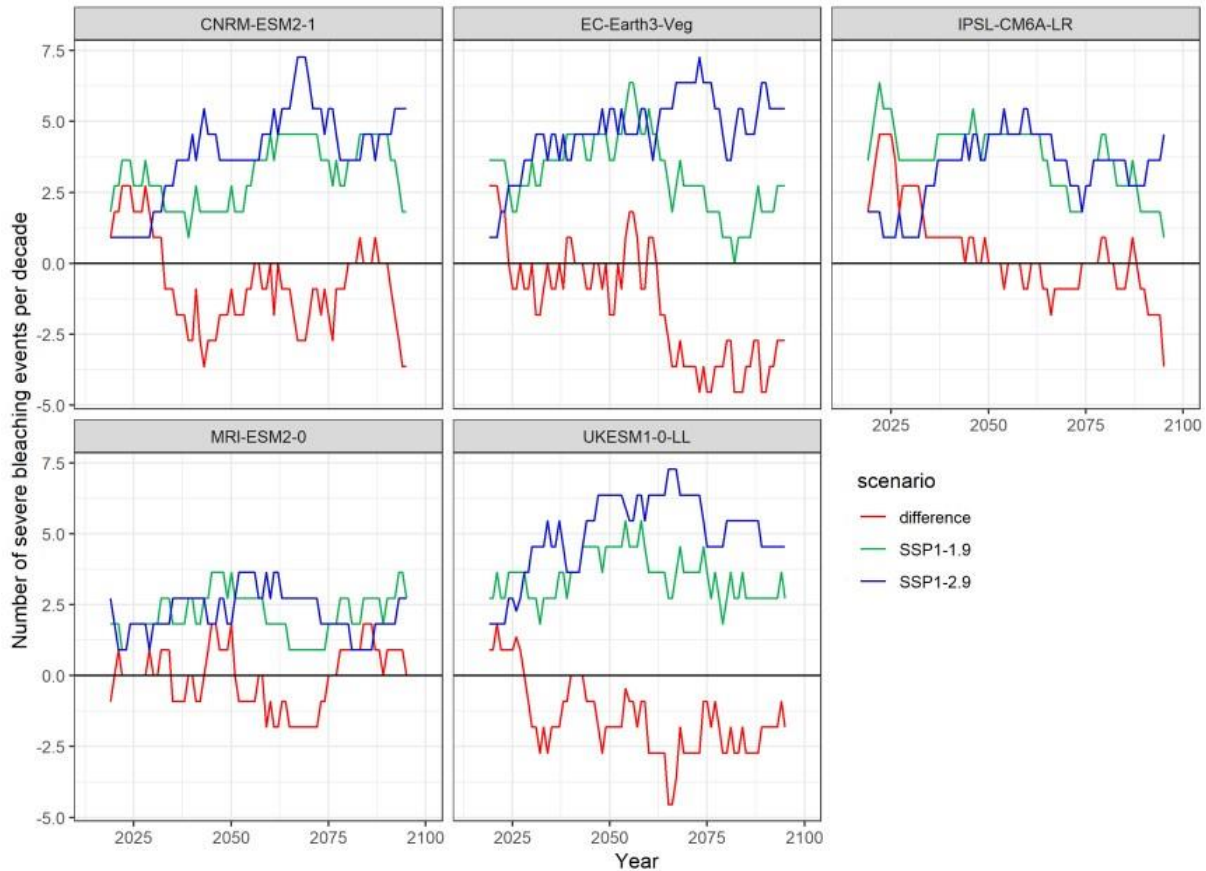


Figure 3.10: The trends for SSP1-1.9, SSP1-2.6, and the differences between these two scenarios are shown per model for mean frequency of severe bleaching per decade relative to the Maximum Monthly Mean from 1985-2012 (inclusive).

3.5 DISCUSSION

An earlier global assessment of the difference between 1.5° and 2° of warming (Schleussner et al., 2016), followed Frieler et al (2013) and their analysis used a simple relationship between global average temperature and the fraction of reefs at risk of long-term degradation. We update this analysis for the GBR by examining climate model simulations which explicitly examine the updated climate scenarios (SSPs), utilize the latest generation of climate models, downscale the results to account for the interaction of tides and winds with local bathymetry, and to consider the magnitudes as

well as the frequency of stress on relevant scales for managers and decision-makers. None of the updated SSPs were able to secure a bleaching frequency of two per decade for the GBR. Yet, like Schleussner et al (2016), moving from 2° to 1.5° of warming does reduce the incidence of bleaching. Specifically, it reduces the occurrence of bleaching by up to 2 events per decade and keeps the magnitude approximately below 8 DHW towards the end of the century.

Less intense and less frequent warming in the far north and northern GBR are likely attributed to projected changes in large-scale atmospheric processes influencing the summer monsoon in the far north and northern GBR and the location of the Subtropical Ridge in the central and southern GBR. McGowan and Theobald (2017) found that reduced cloud coverage and anomalously high pressures and temperatures were positively correlated with bleaching conditions. An intensification and poleward shift of the Subtropical Ridge has been shown in model ensemble projections for both, CMIP3 (Dey et al., 2019; Kent et al., 2013) and CMIP5 (Dey et al., 2019; Grose et al., 2015) which would reduce cloud cover over the southern GBR. Projected increases in the summer monsoon based on CMIP5 (Brown et al., 2016; Dey et al., 2019) could contribute to reduced warming in the far north and northern GBR region in comparison to the central and southern GBR.

The S2P3-R v2.0 downscaling of CMIP6 models is not without limitations. First is the uncertainty within the underlying CMIP6 model projections. Typically, the more models used, the more rigorous the projection of the ensemble mean projection (IPCC, 2018). Second, is the downscaling process, S2P3-R v2.0 does not resolve horizontal advection or salinity (Halloran et al., 2021). Therefore, not simulated are the effects of the South Equatorial currents, the Hiri Current and the Eastern Australian Current as well as eddies, internal waves, and the impacts of freshwater on stratification and mixing in areas of river runoff. These processes would affect the location of the mixed layer, which is expected to deepen with increased surface temperature warming (IPCC, 2021). We would expect the largest error in the downscaling process to be in the location of bifurcation from the South Equatorial current due to the large input of horizontal

advection. Third is the inclusion of a variety of socioeconomic pathways and the implicit assumption that they represent the range of possible futures. Although limiting climate change to 1.5°C will be extremely difficult, it is recognized as an achievable, albeit highly ambitious, target (Rogelj et al., 2015). Arguably the technology exists to meet this target, though this can involve high risk methods of geoengineering (MacMartin et al., 2018; Sanderson et al., 2016). Some underlying themes exist within all the SSPs to reduce the impacts of climate change, such as investing in technology to extract CO₂ from the air and ocean, as well as focusing on global human well-being to move away from competitive, capitalistic markets (Riahi et al., 2017).

Even under SSP1-1.9, a bleaching frequency of once every 3-4 years will be challenging for coral ecosystems as corals are slow growing and the expected recovery time between disturbances is generally estimated to be 5-10 years (Donner et al., 2009; Frieler et al., 2013). Yet, if the average magnitude of events is constrained below 8 DHW, which is still possible under low emissions, then we can hope that genetic adaptation will help maintain functioning ecosystems. At this stage, our empirical understanding of genetic adaptation is only beginning to emerge, in part because of the complexity of the holobiont which includes corals, their endosymbionts, and microbiome (Logan et al., 2021; Van Oppen & Medina, 2020). Logan et al (2021) applies a global ecological and evolutionary model to determine the effectiveness of various adaptation strategies for corals, 1.) symbiont shuffling, 2.) symbiont evolution, as well as 3.) both symbiont shuffling and evolution. Branching and mounding corals were considered in this study across 4 climate scenarios. The adaptation strategy of symbiont shuffling towards heat tolerant taxa was more effective than symbiont evolution (Logan et al., 2021). Warming outpaced adaptation processes in warmer scenarios. Warming also outpaced the effects of ocean acidification (Logan et al., 2021). In a laboratory setting, 10 strains of coral microalgal endosymbionts were exposed to warm conditions over four years. When these 10 strains were reintroduction to their coral host, 3 of 10 strains had evolved improving the holobionts' tolerance to bleaching. (Van Oppen & Medina, 2020) The field of adaptation will only improve as climate change continues to impact corals. These studies are critical to understanding the impacts of the most optimistic to

the most pessimistic warming pathways on coral reefs. Moreover, any reduction on the frequency of bleaching events is likely to be beneficial, particularly if their magnitude remains under 8 DHW. Thus, although the average benefit of moving to 1.5° warming rather than 2°, is a reduction of two bleaching events per decade, the existence of substantial spatial and temporal variation means that some reefs will experience longer recovery periods between events (Bozec et al., 2020; Cheung et al., 2021). This is because not all reefs and not all corals bleach during a given event (Hughes, Anderson, et al., 2018; Hughes, Kerry, et al., 2018; Mumby et al., 2011) and many acute disturbances are temporally clustered giving longer recovery periods (Mumby et al., 2011). What is clear, however, is that failure to achieve either of the low emissions scenarios will be devastating for future reefs. The functioning of coral reefs, or their ability to provide structure and support various trophic levels (Harborne et al., 2016), requires ambitious emissions targets and well targeted management of local stressors, in part to facilitate natural processes of adaptation (Walsworth et al., 2019).

CHAPTER 4

CLIMATE REFUGIA ON THE GREAT BARRIER REEF FAIL WHEN GLOBAL WARMING EXCEEDS 3°C

Published 02 August 2022 in *Global Change Biology*

McWhorter, J. K., Halloran, P. R., Roff, G., Skirving, W. J., & Mumby, P.

J. (2022). Climate refugia on the Great Barrier Reef fail when global warming exceeds 3°C. *Global Change Biology*, 00, 1– 13. <https://doi.org/10.1111/gcb.16323>

This chapter is an expanded version of the publication including an expanded description of the statistical methods, as well as additional figures that were in the supplementary material or, not included in the publication itself.

Author contributions:

Conceptualization: JKM, PRH, PJM

Methodology: JKM, PRH, PJM, GR, WJS

Investigation: JKM, PRH, PJM, GR

Visualization: JKM, PRH, PJM, GR

Supervision: PRH, PJM, GR

Writing—original draft: JKM, PRH, PJM

Writing—review & editing: JKM, PRH, PJM, GR, WJS

4.1 ABSTRACT

Increases in the magnitude, frequency, and duration of warm seawater temperatures are causing mass coral mortality events across the globe. Although, even during the

most extensive bleaching events, some reefs escape exposure to severe stress, constituting potential refugia. Here, we identify present-day climate refugia on the Great Barrier Reef (GBR) and project their persistence into the future. To do this, we apply semi-dynamic downscaling to an ensemble of climate projections released for the IPCC's recent 6th Assessment Report. We find that GBR locations experiencing the least thermal stress over the past 20 years have done so because of their oceanographic circumstance, which implies that longer-term persistence of climate refugia is feasible. Specifically, tidal and wind mixing of warm water away from the sea surface appears to provide relief from warming. However, on average this relative advantage only persists until global warming exceeds $\sim 3^{\circ}\text{C}$.

4.2 INTRODUCTION

Tropical corals are one of the most vulnerable groups of organisms to warming temperatures because they live within a narrow thermal threshold (Berkelmans & Willis, 1999; Glynn & D'croz, 1990; Reaser et al., 2000). When anomalously warm temperatures are prolonged and intensified, coral bleaching, a loss of photosynthetic endosymbiotic dinoflagellates (*Symbiodinium spp.*) in the tissue (Berkelmans & Willis, 1999; Glynn & D'croz, 1990; Reaser et al., 2000), can lead to coral mortality (Eakin et al., 2010; Hughes, Anderson, et al., 2018). Global coral bleaching and mortality were initially correlated to warming sea temperatures in the 1982-83 El Niño-Southern Oscillation (ENSO) event (Glynn, 1984; Robinson, 1982). While historically associated with ENSO events (Baker et al., 2008; Glynn et al., 2001; Kleypas et al., 2015), global-warming driven increases in sea surface temperatures (Bindoff et al., 2013) are decreasing the time between marine heatwaves, escalating the frequency of mass coral mortality events (Hughes, Anderson, et al., 2018; Hughes, Kerry, et al., 2018). These events will continue to become more frequent – reducing recovery time – as greenhouse gas emissions continue (McWhorter et al., 2021).

The large-scale geographical pattern of global warming is defined by more rapid warming at the poles than at lower latitudes (Holland & Bitz, 2003), particularly in the

Northern Hemisphere (Cohen et al., 2014) and amplification of warming over land in contrast with the oceans (Byrne & O’gorman, 2013). Warm air moving off the land can warm shallow coastal seas, which have been warming faster than deeper waters (Heron et al., 2016) owing to their lower heat capacity. However, tropical coastal oceans experience a more complex pattern of change (Liao et al., 2015), with the superposition of natural variability associated with climate modes such as ENSO on top of these global trends. Despite the significance of ENSO, the relative stability of low-latitude climates means their temperatures are emerging from the variability they have historically experienced faster than elsewhere on the planet (Hawkins et al., 2020), a factor critical to coral bleaching (Safaie et al., 2018). From 1985-2012 tropical ocean warming was most rapid in the Indian Ocean and slowest in the Atlantic Ocean, a pattern seen also in bleaching season temperatures (Heron et al., 2016). More recently the Pacific appears to be experiencing the most extreme and frequent heating events (Skirving et al., 2019), leading to high coral mortality (Eakin et al., 2019).

Regional-scale mass coral bleaching events have increased in frequency and severity since the early 1980s (Beyer et al., 2018; Darling et al., 2019; Hughes, Anderson, et al., 2018; Skirving et al., 2019). In a global study of bleaching intensity between 1980-2016, Hughes, Anderson, et al (2018) found that the most recurrent and highest intensity bleaching occurred in the Western Atlantic affecting >50% of locations prior to 2010. This was followed by the Pacific Ocean where warming events increased after 2010 (Hughes, Anderson, et al., 2018). Record oceanic and atmospheric temperatures then drove the largest global-scale coral bleaching event that lasted from 2014-2017 (Eakin et al., 2019; Skirving et al., 2019). This event resulted in a rapid decline of coral reefs worldwide (Eakin et al., 2019; Skirving et al., 2019). However, even during the most extensive bleaching events, areas have been observed that have consistently not bleached (Baird et al., 2018; Eakin et al., 2019).

‘Climate refugia’ in the context of exposure to climate stress have been defined as areas where low frequency or severity of bleaching conditions are expected to persist longer into the future than surrounding areas (Chollett & Mumby, 2013; Dixon et al., 2022;

Glynn, 1996; Kavousi & Keppel, 2018; Morelli et al., 2016; Riegl & Piller, 2003; Van Hooidek et al., 2013, 2016). Numerous studies have developed methods for quantifying refugia in terms of ecosystem vulnerability. In these studies, ecosystem vulnerability is considered a response to thermal exposure, species-specific resistance, and capacity for recovery. (Beyer et al., 2018; Bozec et al., 2020; Cheung et al., 2021; Hock et al., 2017; Kavousi & Keppel, 2018; Morelli et al., 2016)

Small scale ecological differences on the reef can determine the heterogeneous impacts of thermal exposure. Coral morphology and physiology influence the responses of endosymbionts and the animal to bleaching (Dunn et al., 2012; Fitt et al., 2009; Grottoli et al., 2006, 2014; Loya et al., 2001; Rodrigues & Grottoli, 2007; Wilkinson & Hodgson, 1999) with changes in coral assemblage and function often following a warming event (Hughes, Anderson, et al., 2018; Loya et al., 2001; Marshall & Baird, 2000; Stimson et al., 2002).

Bleaching conditions over individual coral reefs can be linked to weather conditions such as reduced cloud cover, higher than normal air temperature, and higher than normal atmospheric pressure conditions (Gonzalez-Espinosa & Donner, 2021; McGowan & Theobald, 2017). Clouds have been shown to provide shading during warming events by limiting the amount of shortwave radiation and reducing coral heat stress (Gonzalez-Espinosa & Donner, 2021; McGowan & Theobald, 2017; Mumby et al., 2001). In fact, the changing light conditions from winter to summer has been shown to provide a cumulative effect on light stress experienced by corals, and therefore modulating the effect of temperature (Skirving et al., 2017). Low wind speeds and neap tides, observed during the 1998 Great Barrier Reef bleaching event (Skirving & Guinotte, 2000) result in reduced mixing of heat away from the surface water and lower turbidity. Increased suspended particulate load, associated with turbidity, can reduce the penetration of shortwave radiation into the water column, providing shading and short-term relief from bleaching as identified by Cacciapaglia & van Woesik (2016). In addition to wind and tidal mixing, mesoscale processes such as boundary currents and

eddies can provide thermal relief (Chollett & Mumby, 2013; Glynn, 1996), while also supplying the reef with larvae (Hock et al., 2017) and food (Grottoli et al., 2006).

The conditions through which refugia arise are highly localised. This presents a challenge when trying to explore their behaviour or project their future state using models. Global climate models (GCMs) typically have a coarse horizontal resolution of around 1 degree and are unable to resolve important mesoscale features in the coastal zone (Van Hoodonk et al., 2016; Zhang et al., 2016). The coarse resolution means that shallow coastal waters are rarely accounted for in models, and consequently processes such as tidal mixing are not simulated. Without representing the hydrodynamics occurring in shelf seas, GCMs are unable to simulate the heat stress experienced by tropical coral reefs adequately (Donner et al., 2005; Kwiatkowski et al., 2013). Here, we use an ensemble of semi-dynamic downscaled climate models to examine the locations of refugia in the context of thermal exposure and their persistence under a range of climate projections on the GBR as a case study for identifying refugia worldwide.

4.2.1 STUDY DESIGN

To improve the resolution of climate projections in the coastal environment one can use dynamic or statistical downscaling (Halloran et al., 2021; Van Hoodonk et al., 2013; Van Hoodonk et al., 2015; Van Hoodonk et al., 2016). Here we apply a semi-dynamical downscaling approach (see Materials and Methods for detailed information), utilising the S2P3-R v2.0 model (Halloran et al., 2021), to projections from the newly released 6th phase of Coupled Model Intercomparison Project (CMIP6) (O'Neill et al., 2016). We consider three Shared Socioeconomic Pathways (SSPs), SSP1, SSP3, and SSP5 (Riahi et al., 2017) and four emission trajectories (SSP1-1.9, SSP1-2.6, SSP3-7.0, SSP5-8.5) (Riahi et al., 2017) explored across five climate models, MRI-ESM2-0 (Adachi et al., 2013), EC-Earth3-Veg (Döscher et al., 2021), UKESM1-0-LL (Sellar et al., 2019), CNRM-ESM2-1 (Séférian et al., 2019), IPSL-ESM2-0 (Boucher et al., 2020). These models were selected based on the availability of atmospheric variables: surface atmosphere air temperature, winds, air pressure, humidity, and net longwave and

shortwave radiation, at the initial release of CMIP6 data (April 2021). Our downscaling approach simulates the detailed temperature response resulting from the interaction of the CMIP6 models' meteorology with local tides and bathymetry. The model domain spans 142.0° W, 157.0° E, 30.0° S, 10.0° S from 4-50 m water depth, at a 10 km horizontal resolution and 2 m vertical resolution.

Downscaled sea surface temperature (SST) was used to derive standard metrics of coral thermal stress; The National Oceanic and Atmospheric Administration (NOAA) Coral Reef Watch's Degree Heating Weeks (DHW) (Donner et al., 2005; Skirving et al., 2020). DHW refers to a measurement of anomalous warm temperatures accumulating over a summer, or three-month period. DHW correlates strongly with coral bleaching/mortality, even though the nature of such relationships change as more susceptible corals are lost through bleaching (Hughes et al., 2017; Hughes, Kerry, et al., 2018). To find present-day locations of less impacted reefs in the context of climate exposure (refugia), we identified the locations with the lowest 20% of averaged DHW values from 1999-2019 from climate model simulations, in line with previous approaches (Cheung et al., 2021; Hock et al., 2017). These locations are used throughout the study to determine spatial patterns of global warming on the GBR.

4.3 METHODS

4.3.1 DOWNSCALING MODEL DATA

The S2P3-R v2.0 semi-dynamic (Halloran et al., 2021) downscaling method is driven by fully coupled global climate model variables of surface atmosphere air temperature, winds, air pressure, humidity, and net longwave and shortwave radiation with high resolution bathymetry (Beaman, 2010) and tidal components to calculate water column properties. The domain of the model spans 142.0° W, 157.0° E, 30.0° S, 10.0° S with a 10 km horizontal resolution and 2 m vertical resolution. The model was run in water depths from 4-50 m. The S2P3-R v2.0 model is driven with surface level atmospheric

data from CMIP6 models, GCMs, MRI-ESM2-0, EC-Earth3-Veg, UKESM1-0-LL, CNRM-ESM2-1, and IPSL-ESM2-0.

Initially, a tidal slope is calculated from M2, S2, N2, O1, and K1 tidal ellipses to then calculate the water's velocity 1 m above the seabed. Water velocity interacts with a prescribed standard bottom drag coefficient (Sharples et al., 2006). Wind velocity is calculated with respect to tides and air pressure, as it interacts with a surface drag coefficient (Smith & Banke, 1975). Profiles of vertical eddy viscosity and diffusivity are calculated in a turbulence closure scheme as functions of current shear and vertical density (Canuto et al., 2001) then used with the surface and bottom stress calculations. Density is described in the model only as a function of temperature. SST data from 1950-2100 were output daily. Further information on validation and physical components of the model are in Halloran et al (2021) or in Chapter 2.

4.3.2 SHARED SOCIOECONOMIC PATHWAYS (SSP)

There are five SSPs for various possible socioeconomic developments. The pathways include sustainable development, inequality, regional conflict, fossil fuel-based development, and middle-of-the-road development. While consistent with the literature, there is a wide range of uncertainty surrounding economic and demographic projections. Within this study, we focused on three SSP trajectories (SSP1, SSP3, SSP5) (Riahi et al., 2017) and four emissions trajectories (SSP1-1.9, SSP1-2.6, SSP3-7.0, SSP5-8.5) (Riahi et al., 2017). The last numbers (1.9, 2.6, 7.0, and 8.5) refer to the peak radiative forcing (W/m^2). SSP1 refers to the most sustainable future, involving low material growth and lower resource and energy intensity. As a result of development goals being more focused on the global commons investing in education, health and economic growth emphasizing human well-being, inequality is reduced across countries. SSP3 focuses on 'regional rivalry', a rise in nationalism, a scenario where regional competitiveness and conflict drives countries to focus on their own energy and food security goals. Additionally, investments in education and technology decline, inequalities worsen, and economic development is slow. Population growth in this

scenario is high in developing countries and low in industrialized countries. Also, the international community does not prioritize environmental issues in SSP3. SSP5 is a world based on fossil fuel development, energy intensive lifestyles which grow the global economy and population. Competitive markets drive technology, innovation, and human capital towards sustainable development. Population peaks and then declines; local environmental problems are successfully managed and solutions such as geo-engineering maybe be included to manage social and ecological systems (Riahi et al., 2017). While SSP1-1.9 and SSP1-2.6 are within the same SSP category (SSP1), they contain different radiative forcing pathways. SSP1-1.9 was designed to limit warming to 1.5°C by the end of the century. This scenario uniquely contains the application of technology which extracts large amounts of CO₂ out of the atmosphere resulting in net negative emissions in the second half of the 21st century. (O'Neill et al., 2016)

4.3.2 CORAL STRESS METRICS

NOAA Coral Reef Watch's operational suite of coral heat stress products have been used by the global coral reef community for more than two decades (www.coralreefwatch.noaa.gov). The DHW product is by far the most used metric used by reef managers and scientists to monitor coral bleaching related heat stress. This study uses the exact methodology used by NOAA Coral Reef Watch and described in Skirving et al. (2020) to derive coral stress metrics. Following is a brief description of the methodology. More detail and the rational for the methodology can be found in Skirving et al (2020).

A monthly mean climatology was initially created for each grid point. For each grid point, monthly mean values (12) were calculated from 1985 to 2012 and linearly adjusted to 1988.2857 to be consistent with the original NOAA Coral Reef Watch MMM climatology. The original NOAA Coral Reef Watch climatology, i.e., 1985–1990 and 1993 was adjusted to account for missing years due to aerosol contamination from the Mt.

Pinatubo eruption. Although modern satellite data now account for the missing years, the climatology remains adjusted to match the original seven-year climatology.

Daily SST values in each month were averaged to produce 12 mean SST values for each of the 28 climatology years (1985-2012). Then a least squares linear regression was applied to each month corresponding to the temperature value in 1988.2857. For example, to derive the January value, the 28 January averages (Y-values) were regressed against the years (X-values), and the temperature value when $X = 1988.2857$ was assigned as the monthly mean value. This was repeated for each of the 12 months and at each pixel location until each pixel had a set of 12 monthly mean values which represents the monthly mean climatology for 1988.2857. The maximum of these 12 monthly means is the Maximum Monthly Mean, called MMM. (Skirving et al., 2020)

The next step is to use the MMM to create values for a warm SST anomaly, called a 'HotSpot' (Skirving et al., 2020). Daily SST values are first subtracted from the MMM climatology. Then, all negative values are set to zero to select only warm anomalies, therefore, 'HotSpot' ≥ 0 . The DHW calculation is then a daily summation over an 84-day running window of the 'HotSpot' values. Additionally, the DHW calculation only selects 'HotSpot' values greater than or equal to 1. Thermal stress amongst corals has been considered to begin at $MMM + 1^{\circ}\text{C}$. (Skirving et al., 2020)

Further, the maximum DHW was used per grid cell per year. For time series calculations, the median DHW value was then taken annually across the spatial domain for each model in each scenario. Then, the median DHW values were further averaged using all models within each scenario resulting in an ensemble median per scenario.

4.3.3 REFUGIA CALCULATION

Austral summer years (i.e., July 31, 1999 - August 1, 2000) were used to calculate the annual maximum DHW, avoiding double counting when using calendar years (Skirving

et al., 2019). Refugia locations were found by calculating the average DHW per cell from 1999-2019, then, calculating the 20th percentile value across the GBR grid from the downscaled output (142.0° W, 157.0° E, 30.0° S, 10.0° S with a 10 km horizontal resolution from 4-50 m depths, within the Great Barrier Reef Marine Park Authority boundary (GBRMPA, 2009)). All cells that were less than or equal to the 20th percentile value were kept as 'refugia' locations. 'Non-refugia' locations were the remaining cells. This method is consistent with the literature (Cheung et al., 2021; Hock et al., 2017).

4.3.4 GLOBAL WARMING METRICS

Global average temperatures were extracted per climate model using the historical data surface air temperature, the 'tas' variable. Global average temperatures were calculated relative to pre-industrial time (1860-1880).

The relationship between global warming and the magnitude of the DHW difference, non-refugia - refugia was modelled using a generalised additive model with a scaled t-distribution and with a spline with 3 knots. Models were fit using the bam function in the 'mgcv' package in R and using the scaled to family with a logarithmic scale (link = "scat"). Significant differences were tested using Tukey adjusted pairwise comparisons using the emmeans function in the 'emmeans' package (Lenth et al., 2018).

4.3.5 POTENTIAL ENERGY ANOMALIES; WIND AND TIDAL ENERGY FLUX METRICS

Atmospheric reanalysis product ERA5 was downscaled using S2P3-R v2.0 to provide a link between observational outputs and climate model outputs. Energy flux from winds and tides within the water column are outputs of the S2P3-R v2.0 downscaling process. The turbulent power generated by tides is calculated using the bottom drag coefficient, $k_b=0.003$, the density of seawater, ρ , and the amplitude of the tidal current, u_0 .

$$P_{\text{tide}} = \frac{4k_b r u_0^3}{3\rho}$$

Wind mixing at the sea surface is derived from δ as wind mixing. Further, k_s represents 6.4×10^{-5} of the drag coefficient multiplied by the slippage factor. w represents wind speed, h represents total depth, and ρ_a represents air density.

$$\frac{\partial f_{\text{wind}}}{\partial t} = -dk_s r_a \frac{w^3}{h}$$

The wind and tidal energy flux were calculated using the average conditions during austral summer months, December, January, February, March, over refugia and non-refugia locations. For the wind energy flux analysis, only mass coral bleaching years were used from 1999-2019 (2002, 2016, 2017) (Hughes et al., 2017; Hughes, Kerry, et al., 2018). Refugia locations for this analysis are defined as locations where the lowest 20th percentile DHW values from the downscaled ERA5 dataset are observed and locations where 2-5 models agree with ERA5 refugia location. Non-refugia locations are all other locations, or where 0-1 models agree.

Additive mixed effect models were used to explore differences between refugia and non-refugia locations using the 'bam' function (Wood, 2004) in R version 4.1.1 (Pinheiro et al., 2021) where longitude and latitude were included as a random effect to account for the spatial correlation of the data. Pairwise comparisons were determined using the 'pairs' function (Lenth, 2021) in R version 4.1.1 (Pinheiro et al., 2021).

4.3.6 RATE OF WARMING CALCULATIONS

Rates of warming were calculated for two variables, 1.) the air surface temperature variable from all models under SSP5-8.5 and 2.) the annual maximum DHW under

SSP5-8.5 over refugia locations per model. The surface air temperature rate of warming was calculated by initially masking the data within the GBRMPA boundary and calculating the median value per year. The median value was then subtracted from each grid cell per year. The values in each grid cell were then used in a linear regression resulting in a slope value, this is the value referred to as the rate of warming. For the DHW rate of warming, the non-refugia GBR median was calculated per year and then subtracted from each refugia grid cell in that year. Following this step, a linear regression was fitted to the timeseries of each cell, resulting in a metric of relative warming to the non-refugia locations, or slope. The SSP5-8.5 scenario was used to draw out the most dramatic spatial signal and is assumed to be representative of similar spatial warming trends in SSP3-7.0.

4.3.7 BLEACHING CONDITIONS

Bleaching conditions were defined by isolating austral summer months December, January, February, and March, and then selecting the years where the median DHW value across the GBR was ≥ 2 . It was common for most years following 2050 among all models to fall under 'bleaching conditions' in the highest scenario, SSP5-8.5.

4.3.8 WIND SPEED AND SHORTWAVE RADIATION DURING BLEACHING CONDITIONS

The five models used in the downscaling from the highest emission scenario (SSP5-8.5) were used to analyse the wind speed and shortwave radiation conditions during present-day and future bleaching conditions. Present day years were isolated to 1999-2019 and future years were 2020-2100. It was common that most years following 2050 among all models fall under bleaching conditions in the highest scenario SSP5-8.5.

4.3.9 STATISTICAL TESTS FOR WIND SPEED AND SHORTWAVE RADIATION

Additive mixed effect models were used to explore differences between refugia and non-refugia locations using the 'bam' function (Wood, 2004) in R version 4.1.1 (Pinheiro et al., 2021), where climate model was included as a random effect, and longitude and latitude were included as a smoothed function to account for the spatial correlation of the data. Pairwise comparisons were determined using the 'pairs' function (Lenth, 2021) in R version 4.1.1 (Pinheiro et al., 2021) This analysis was also used to compare differences between refugia and non-refugia locations within and between models.

4.4 RESULTS

4.4.1 CLIMATE REFUGIA

Using satellite-derived observations of DHW (Donner et al., 2005; Skirving et al., 2020), we found evidence of refugia around the Swains (near 21° S, the widest component of the GBR, onshore to offshore) as well as offshore Mackay and offshore Gladstone and the east coast of the Cape York Peninsula (Figure 4.1a). We define refugia locations as being the lowest 20% of climatological DHWs (see methods). We then confirmed that such observations were broadly consistent with the downscaled climate model output, based on the atmospheric conditions experienced over the same 20-year interval (1999-2019) as used for the refugia calculation (Figure 4.1b). Despite climate model simulations being only a plausible realisation of the weather, our CMIP6 driven results identified a consistent geographical pattern to the refugia locations across models and with observations (Figure 4.1c). Such agreement between mechanistic models and observations strongly implies that these refugia occur because of fundamental local oceanographic or meteorological attributes, rather than by chance.

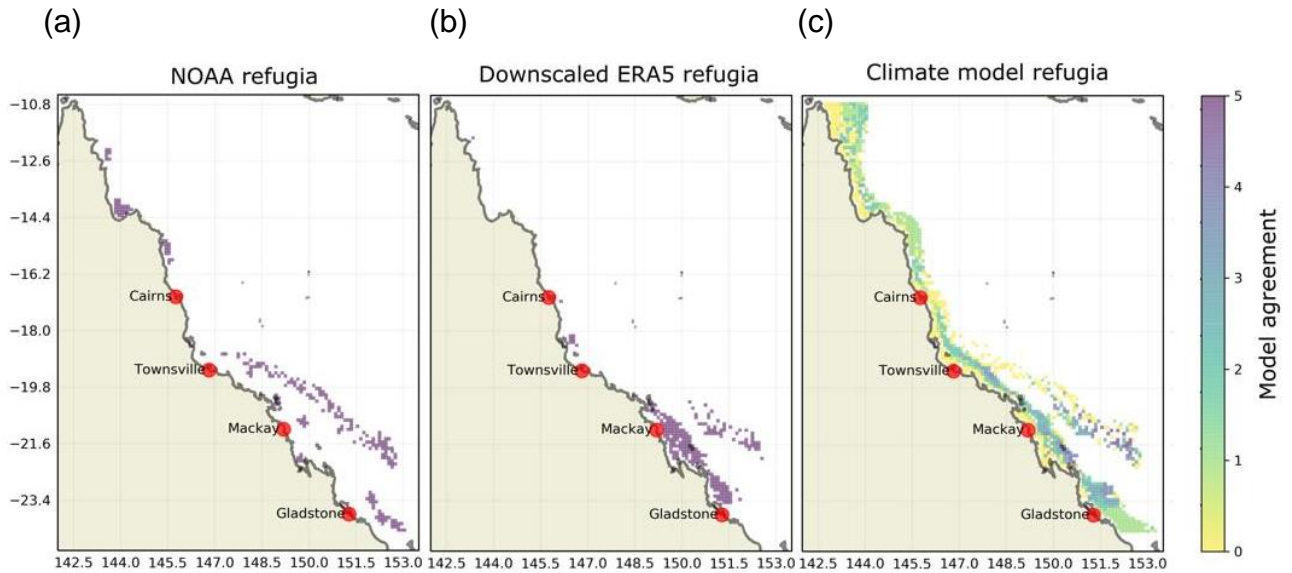


Figure 4.1: Spatial agreement is shown through observation-based products and model outputs. (a) Refugia locations derived from the NOAA Coral Reef Watch Degree Heating Weeks product, 1999-2019. (b) Refugia locations from the downscaled ERA5 atmospheric product. (c) Climate model agreement on refugia locations from five downscaled CMIP6 models, MRI-ESM2-0, EC-Earth3-Veg, UKESM1-0-LL, CNRMESM2-1, IPSL-CM6A-LR. The 0 value, or yellow, represents areas of no agreement from any models. The 5 value, or dark purple, represents the most agreement, from all 5 models.

4.4.2 VALIDATION OF THE CLIMATE REFUGIA LOCATIONS USING ERA5

Downscaled observational product ERA5 shows spatial agreement to identified climate model refugia locations around the Swains (central branch off the GBR) and offshore Mackay and Gladstone (southern GBR) (Figure 4.2a). The areas where 2-5 downscaled climate models agree with the ERA5 downscaled refugia locations provides confidence in the climate models spatial patterns (Figure 4.2a). Additionally, regarding non-refugia locations, there is large spatial agreement between the downscaled ERA5 output and the downscaled climate models (Figure 4.2a). Atmospheric reanalysis product ERA5 was downscaled using S2P3-R v2.0 to link the spatial patterns in the observations to

the climate models, these data were also used for validation in the methods chapter (Section 2.8). The downscaled outputs from ERA5 use the same methods seen in Figure 4.1 for the spatial analysis.

4.4.3 TIDAL AND WIND ENERGY FLUX OVER CLIMATE REFUGIA LOCATIONS

Exploring the mechanisms leading to refugia using the downscaled ERA5 observational product for the last 20 years, we find that climate refugia have stronger wind energy by 0.02 W/m^2 SE 0.004 (<0.0001 p-value) and stronger tidal energy by 0.64 W/m^2 SE 0.08 (<0.0001 p-value) than the rest of the GBR (Figure 4.2b and c). The relief from warming provided by tidal energy will persist into the future, but the locations and strength of wind energy are vulnerable to climate change.

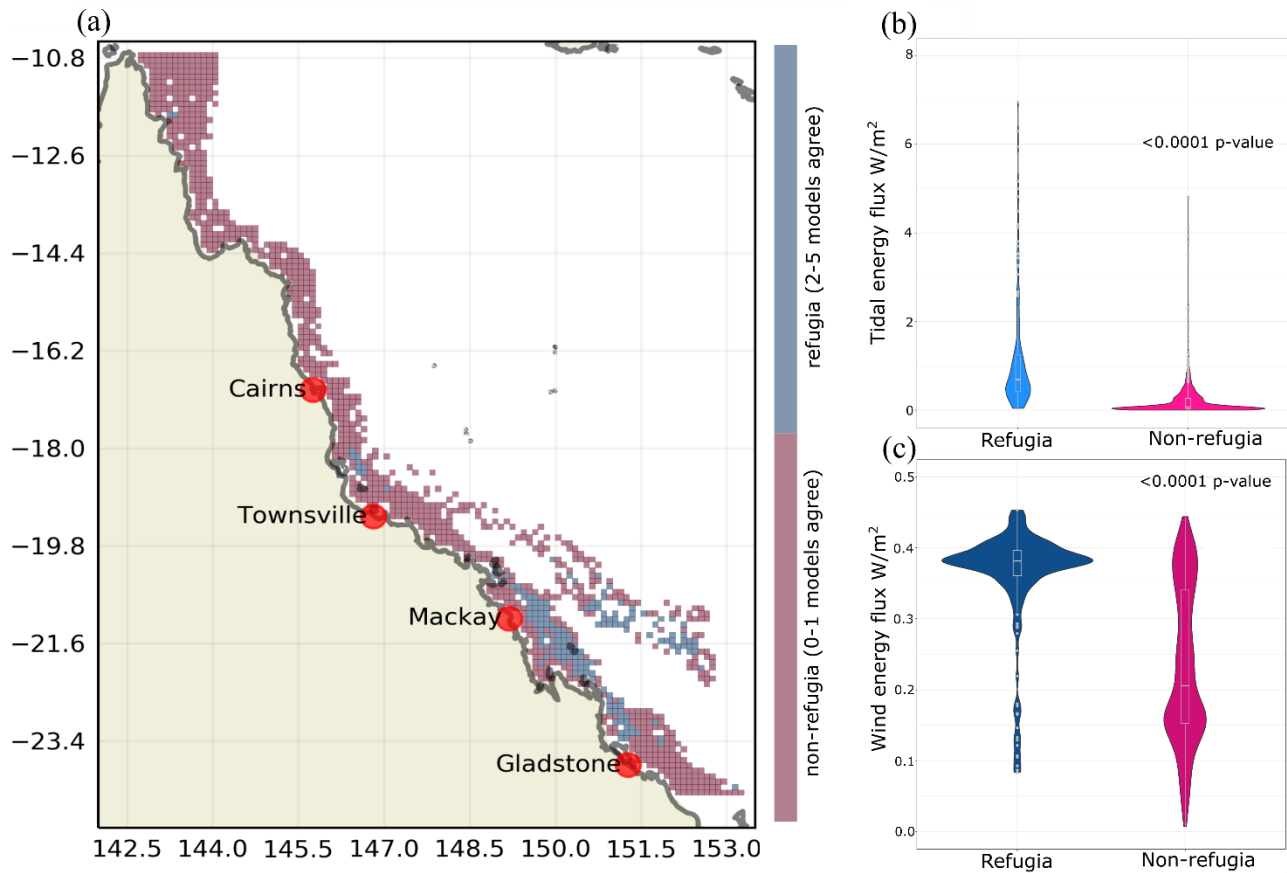


Figure 4.2: The downscaled outputs of the atmospheric reanalysis product ERA5 were used to further validate climate model agreement of refugia and non-refugia locations and test for tidal and wind energy in refugia and non-refugia locations. (a) The map shows where the climate refugia from two or more downscaled climate models agree with the downscaled ERA5 refugia locations from 1999-2019. (b) Wind and (c) tidal energy flux is shown for refugia and non-refugia locations as violin plots to display the probability density and significance testing using the emmeans package in R. Wind energy flux calculations are based on the mean of these austral summer bleaching years, 2002, 2016, 2017, and summer months, December, January, February, March. (c) *Not included are outliers reaching up to 18 in the tidal energy flux, the y-axis was limited between 0,8 to better display most data.

4.4.4 LOSS OF CLIMATE REFUGIA

Under low emissions equating to $<1.5^{\circ}\text{C}$ or $<2.0^{\circ}\text{C}$ of warming by 2100 (SSP1-1.9 and SSP1-2.6), climatologically identified refugia typically persist in experiencing the lowest 20% of annual mean DHW values within any particular year, until at least the end of this century (i.e., ensemble mean refugia locations maintain lower DHW than non-refugia, Figure 4.3a). In contrast, most refugia are lost (i.e., do not stay below the 20th percentile of annual DHWs) after the mid-century under the two high emissions scenarios, SSP3-7.0 and SSP5-8.5 (Figure 4.3a). Irrespective of emissions scenario we find that refugia are typically lost after ~ 3 degrees of globally averaged warming above preindustrial (1860-1880) levels (Figure 4.3b).

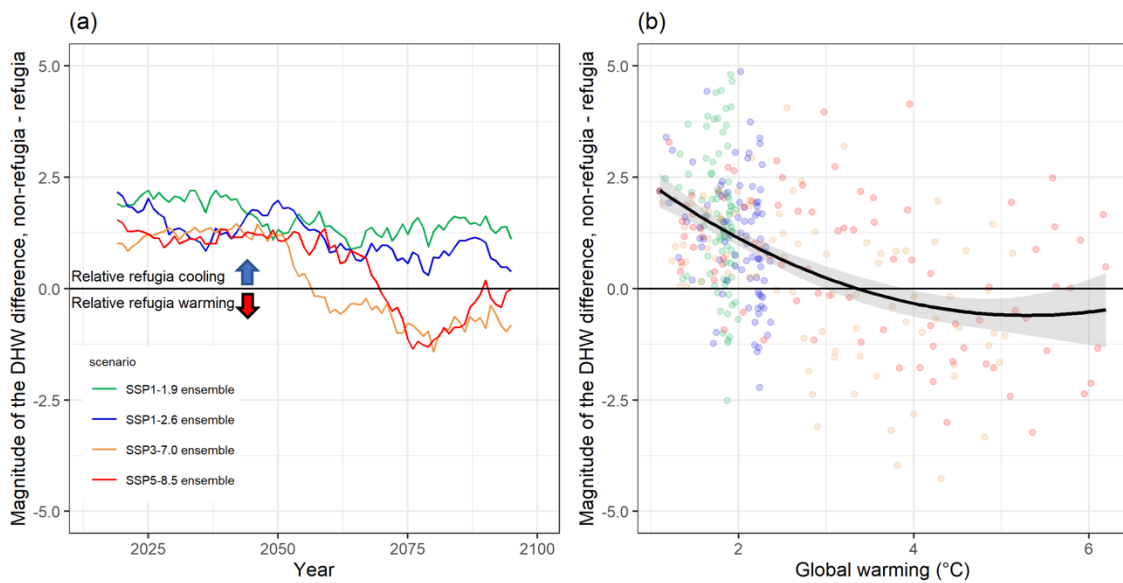


Figure 4.3: Refugia outlook under climate change scenarios. (a) Following a rolling mean of 11 years, Degree Heating Weeks (DHW) values in refugia locations were subtracted from the non-refugia locations per model and then calculated as an ensemble mean difference per scenario, displaying the difference per year in DHW. (b) Differences prior to the rolling window were then plotted against global average temperatures relative to pre-industrial time (1860-1880) from the corresponding climate model. A second-degree polynomial was applied to all scenarios with shaded areas denoting the standard error.

Refugia locations among all scenarios exceed the 8 DHW threshold much later than non-refugia locations (Figure 4.3). It is useful to see the climate projections for each scenario, refugia and non-refugia, before they are subtracted in Figure 4.3a (Figure 4.4) as it enables a perspective similar to chapter 3 on the magnitude of warming (Section 3.4.1). The dashed lines represent the refugia locations and importantly, following mid-century these trends are above the non-refugia trends for the high emissions scenarios (Figure 4.4). This is indicating the warming of the refugia, as demonstrated in Figure 4.3a and Figure 4.3b. The solid black line indicates the 8 DHW threshold, and the higher scenarios far exceed this threshold in the second half of the century (Figure 4.4). The lower scenarios' refugia locations clearly maintain a less impacted status, showing that trends are often below the 8 DHW threshold, notably in the lowest scenario (Figure 4.4).

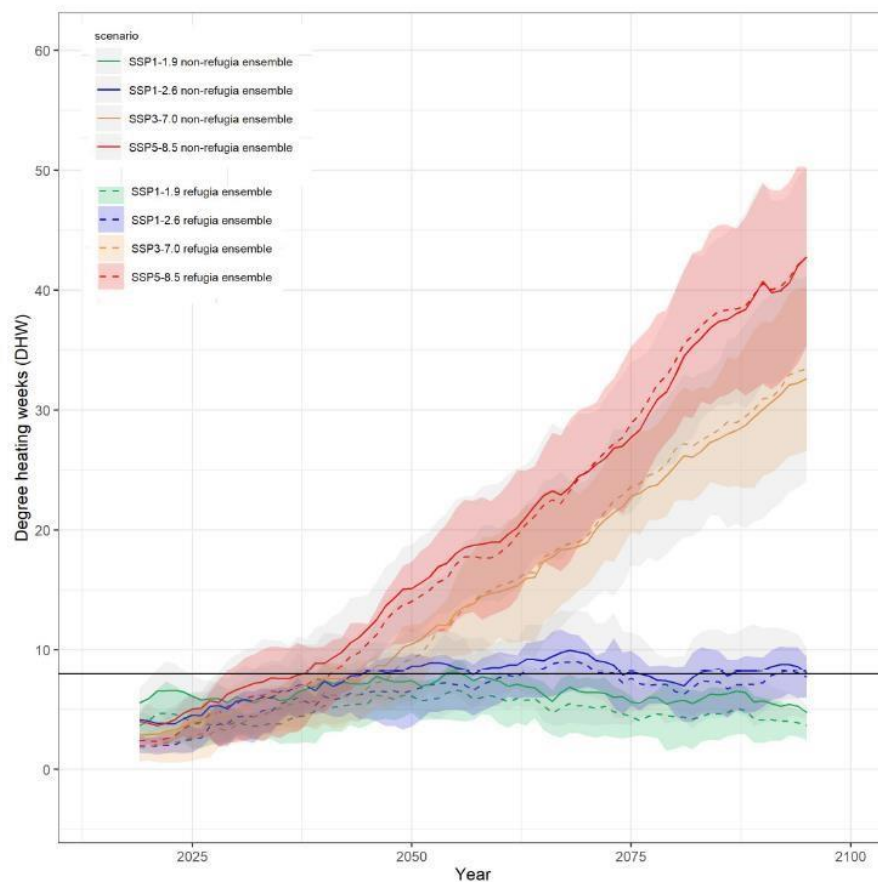


Figure 4.4: Metrics of coral stress were extracted across the Great Barrier Reef for four socioeconomic pathways as an ensemble of five climate models for non-refugia and refugia locations. Coral stress metrics disaggregate magnitude as Degree Heating Weeks (DHW) shown using a rolling window of 11 years. The multi-model mean is made up of MRI-ESM2-0, EC-Earth3-Veg, UKESM1-0-LL, CNRM-ESM2-1, and IPSLES2-0. Shaded areas denote the standard deviation for each scenario averaged across models. The horizontal black line in 1A marks 8 DHW, a metric of coral stress that often leads to mortality.

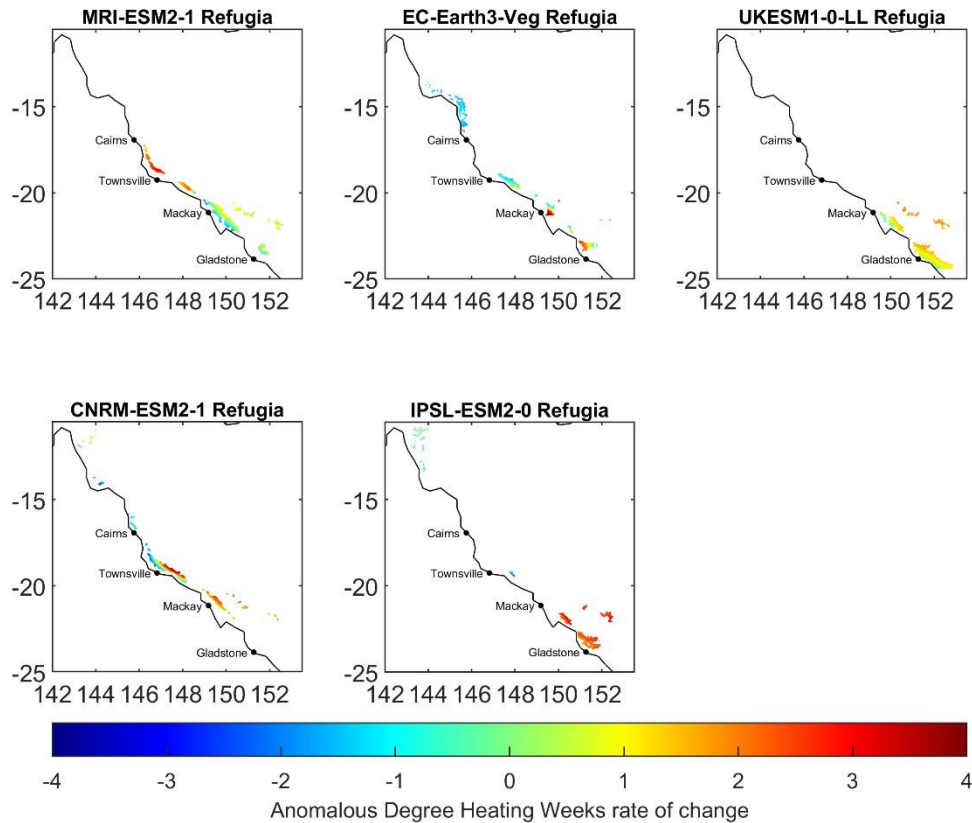
4.4.5 RATE OF DEGREE HEATING WEEKS WARMING

The rate of refugia loss varies across the reef with northern regions retaining their status longer than central and southern regions (Figure 4.5). Refugia locations and wind strength can be overwhelmed by the general patterns of warming, which is occurring dominantly in the southern GBR and nearshore (Figure 4.5a). Warming is occurring in higher climate-change scenarios at a faster rate in the areas that have been deemed as climate refugia than the rest of the GBR (non-refugia) except in the model EC-Earth3-Veg (Döscher et al., 2021) (Figure 4.5a, Figure 4.5b). The negative values represent a slower rate of warming that is not representative of the magnitude of warming.

The rate of warming using SSP5-8.5 DHW values per model also reveals a latitudinal and nearshore warming signal in all models except EC-Earth3-Veg (Döscher et al., 2021) (Figure 4.5a). Rates of warming were similarly calculated for surface air temperature but, the DHW values were focused on just refugia locations per model (Figure 4.5a, Figure 4.6). The expected tripling and quadrupling of the magnitude of warming projected under SSP5-8.5 and SSP3-7.0 compared to lower emissions scenarios from chapter 3 is reinforced in this general pattern of warming with the loss of refugia (Figure 4.3a, Figure 4.5a, Figure 4.6). The warming of refugia per model in Figure 4.5b is further explained by the rate of warming over refugia pixels on the map in Figure 4.5a. The simple visual analysis demonstrates that more refugia pixels are warming in all other models more than EC-Earth3-Veg. Complementary to this story is the noticeable difference in EC-Earth3-Veg when showing the difference of warming

between refugia and non-refugia locations in Figure 4.5b. Clearly, the warming pattern in EC-Earth3-Veg is different. Uniquely in EC-Earth3-Veg, the deemed present-day refugia for this model have escaped the warming trend under all emissions scenarios (Figure 4.5a, Figure 4.5b). Also, speaking to model variability is the large warming of refugia in MRI-ESM2-0 under SSP3-7.0 (Figure 4.5b). Under SSP3-7.0 for the model MRI-ESM2-0, this rapid warming of refugia could be driving the more rapid loss of refugia seen in the multi-model ensemble for SSP3-7.0 (Figure 4.3a).

(a)



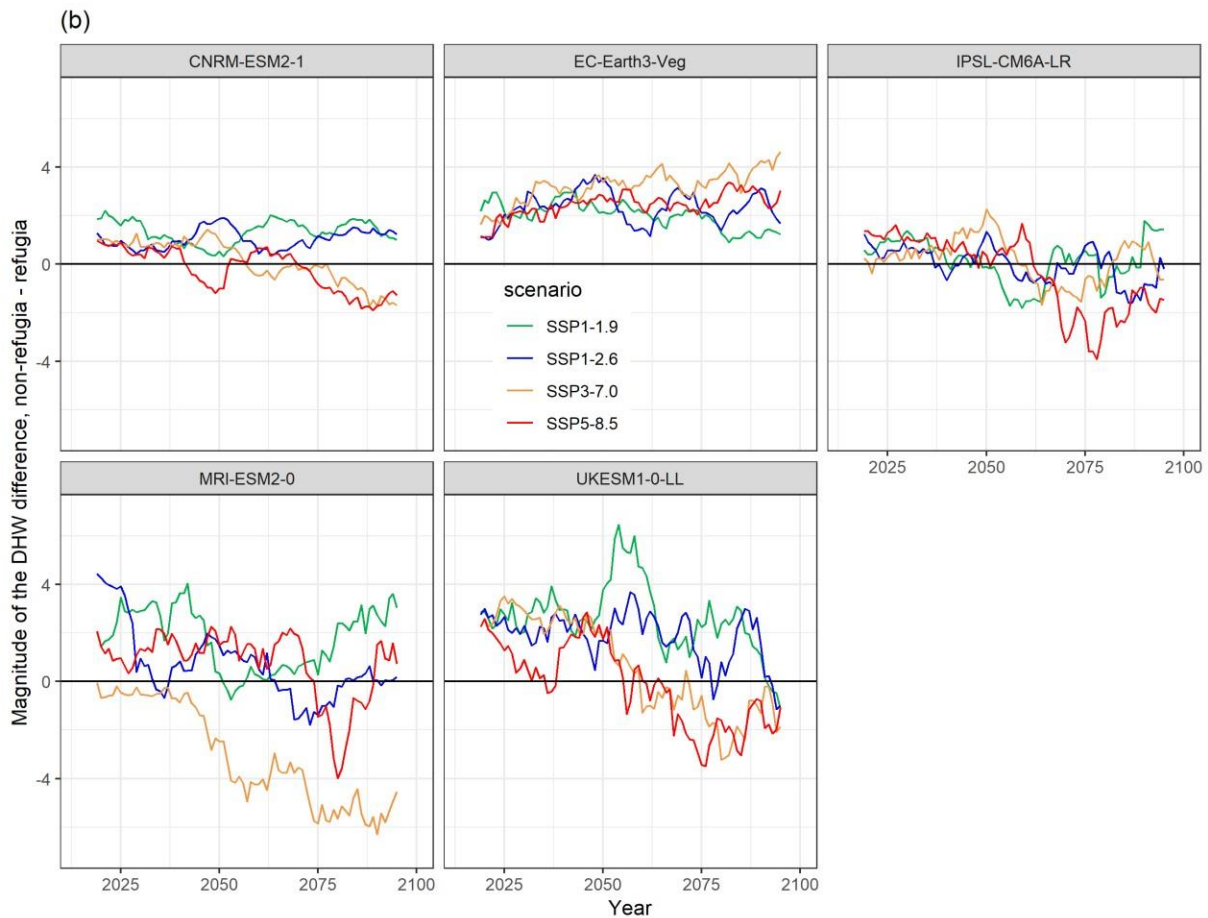


Figure 4.5: (a) The rate of relative warming (slope) for refugia locations was calculated using Degree Heating Weeks (DHW) input values from the highest socioeconomic pathway, SSP5-8.5, per model relative to the median value across the entire spatial grid, 142.0°W, 157.0°E, 30.0°S, 10.0°S at a 10 km horizontal resolution over depths of 4-50 m. The median value per year across the Great Barrier Reef Marine Park Authority (GBRMPA) grid was subtracted from each cell per year, then a least squares linear regression was fitted per cell across the entire time series, 2014-2100. Austral summer was placed in the middle of the calendar year when calculating the annual maximum temperature to avoid double counting. The blue colours indicate less warming relative to the median value across the GBR while red colours indicate the most relative warming. (b) Complementary to Figure 4.3 but displayed per model displaying the difference in DHW between refugia and non-refugia per year in DHW.

4.4.6 RATE OF RELATIVE SURFACE AIR TEMPERATURE WARMING

Refugia locations and wind strength can be overwhelmed by the general patterns of air surface temperature warming which is occurring dominantly in the southern and nearshore GBR under SSP5-8.5 (Figure 4.6). Air surface temperature is used to demonstrate the latitudinal and nearshore warming trends seen in the loss of refugia under high emissions. The air surface temperature variable from SSP5-8.5 per model was calculated as a rate of warming relative to the median value across the entire GBR grid. The warming trends are shown per model to demonstrate model variability in the spatial pattern of warming (Figure 4.6). A nearshore and latitudinal trend is seen in all models except EC-Earth3-Veg. The unique spatial pattern of warming for ECEarth3-Veg is helpful to further understand the mechanisms driving warming in all other models as the EC-Earth3-Veg signal should always be different than the rest of the models.

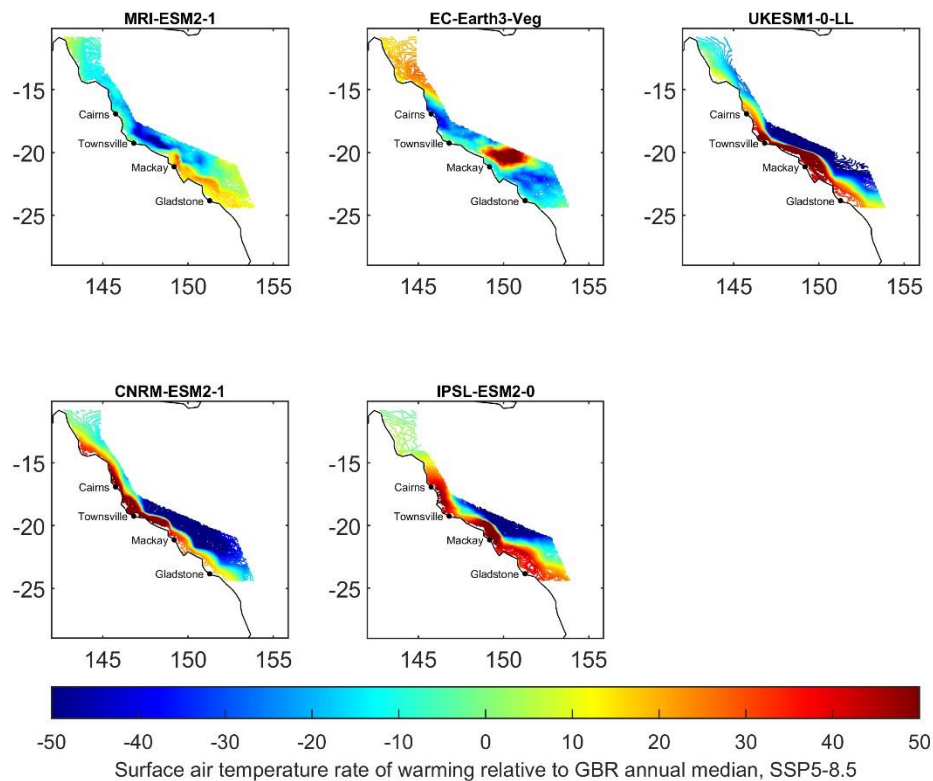


Figure 4.6: The rate of warming (slope) for refugia locations was calculated using air surface temperature, or the tas variable, values from the highest shared socioeconomic pathway, SSP5-8.5, per model. The air surface temperature was calculated relative to the median value across the entire spatial grid per year. The median value per year within the Great Barrier Reef Marine Park Authority boundary was subtracted from each cell per year, then a linear regression was fitted per cell across the entire time series, 2014-2100.

Complementary to the relative rates of warming from air surface temperature and DHW, the timeseries plots of refugia locations per model are similar to the ensemble trend of refugia locations warming under high scenarios (Figure 4.3a) in all models except EC-Earth3-Veg (Figure 4.5b). Further, the timeseries is also plotted as the trends for refugia and non-refugia (Figure 4.7), before the difference calculation in Figure 4.3a. The timeseries before the difference calculation helps reveal the overarching warming trends per model, showing the differences in magnitude, or DHW (Figure 4.7). The separation of warming patterns between models is extremely useful as the atmospheric variables that drive the S2P3-R v2.0 downscaling need to be explored to identify the drivers of these changes under a warmer world.

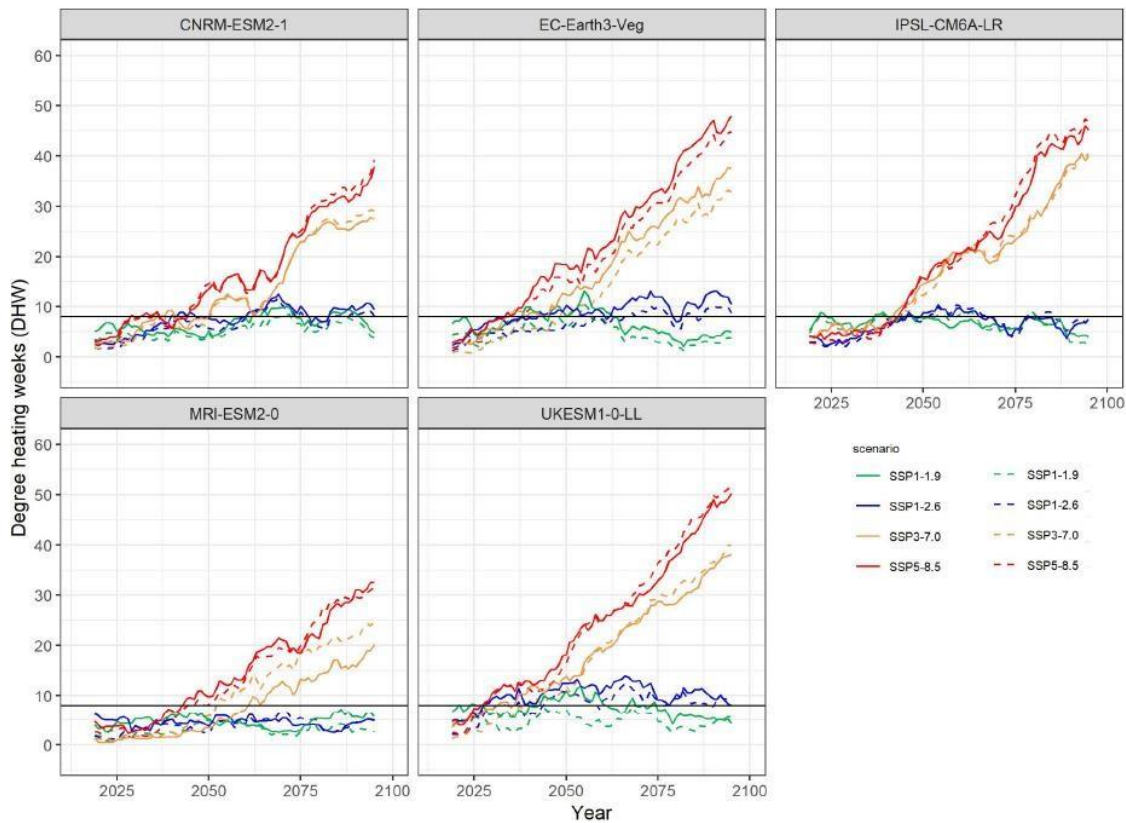


Figure 4.7: Metrics of coral stress were extracted across the Great Barrier Reef for each of the five climate models with four shared socioeconomic pathways for non-refugia and refugia locations. Coral stress metrics disaggregate magnitude as Degree Heating Weeks (DHW) shown using a rolling window of 11 years. The horizontal black line marks 8 DHW, a metric of coral stress that often leads to mortality.

4.4.7 PROJECTED CHANGES IN WIND

CMIP6 projections suggest that a north-south dipole exists in wind-speeds at times when bleaching is occurring (Figure 4.8a), such that wind speeds decline in southern areas, which reduce the mixing – and therefore cooling potential – of the water column (Figure 4.8a). In contrast, wind speeds increase in the north, elevating mixing potential. Ensemble wind speed from SSP5-8.5 over the refugia locations are projected to slightly reduce by 0.24 ms^{-1} SE 0.02 (<0.0001 p-value) from present-day (1999-2019) to after mid-century (2050-2100) during bleaching conditions (Figure 4.9). Present-day wind

speeds in refugia locations are consistently higher than non-refugia locations even though they are expected to slightly reduce (Figure 4.9). These results represent the ensemble average, and it is important to note that projected wind speed in refugia and non-refugia locations are variable on a per model basis (Table 4.1). Importantly, EC-Earth3-Veg does not show a unique signal that would be informative of maintaining a refugia status in higher scenarios when compared to other models (Figure 4.9, Table 4.1, Figure 4.10).

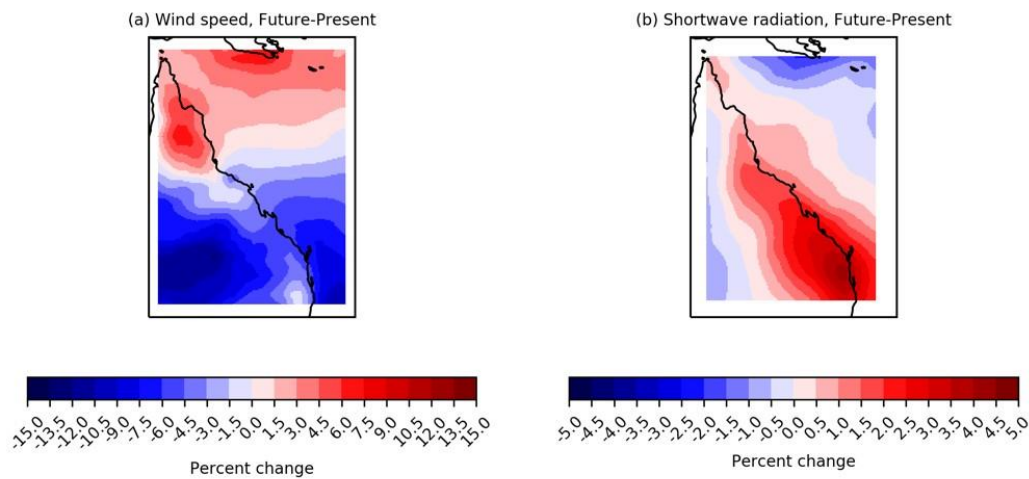


Figure 4.8: 21st Century wind speed and shortwave radiation change. SSP5-8.5 bleaching conditions were isolated within the (a) wind speed and (b) shortwave radiation variables displaying the percentage of change in present-day (1999-2019) to future (2050-2100) conditions under SSP5-8.5. Bleaching conditions are defined as austral summer months, December, January, February, March, calculated as austral summer years (i.e., July 31, 2050 – August 1, 2051) with the median value across the GBR grid having an annual maximum Degree Heating Weeks ≥ 2 .

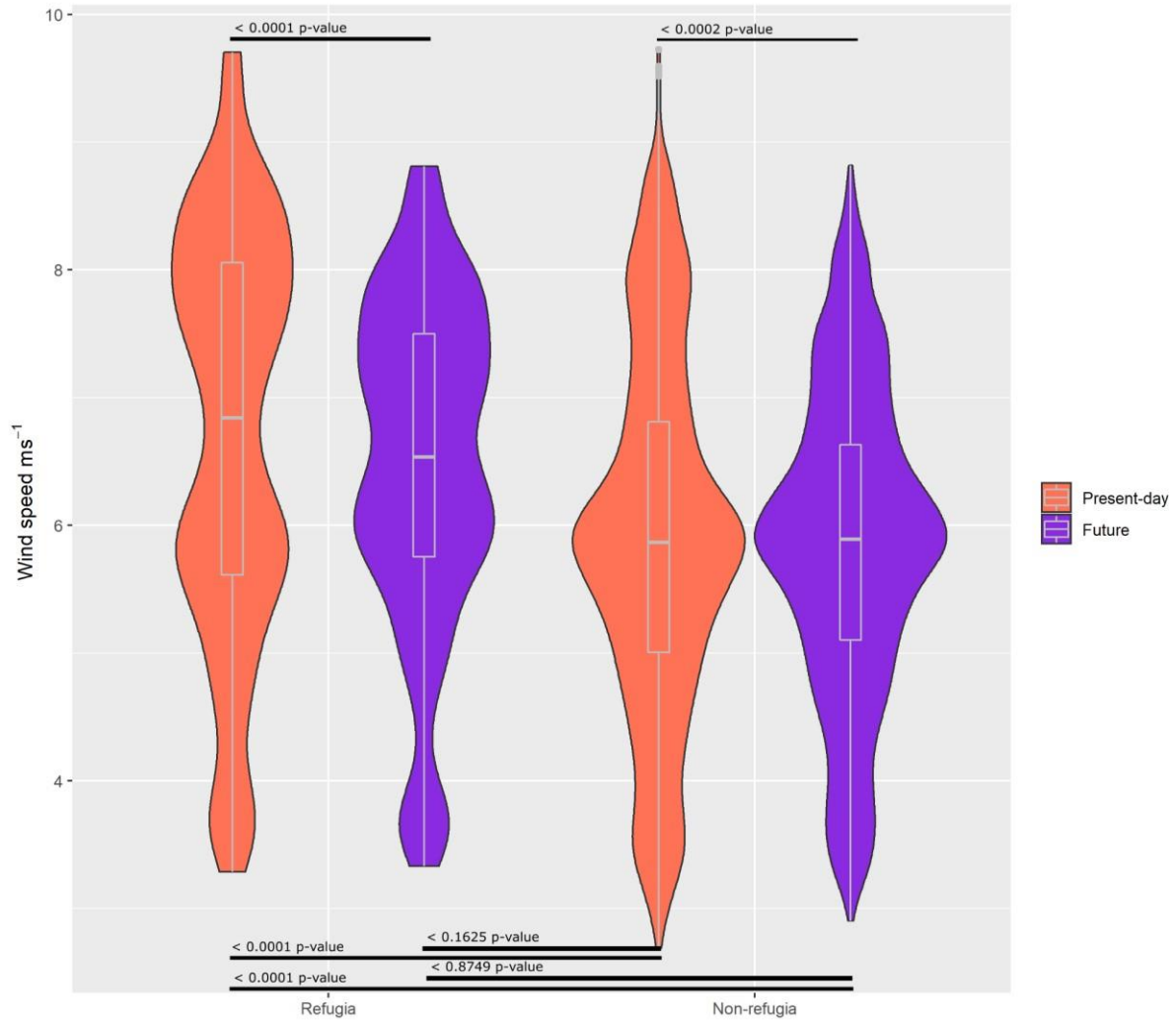
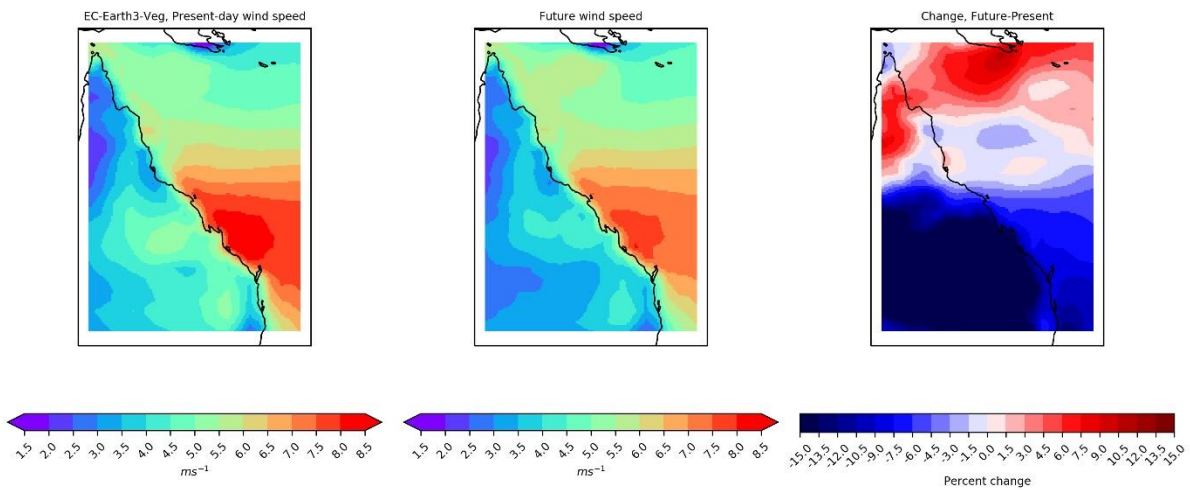


Figure 4.9: Wind speed values from SSP5-8.5 are shown between refugia and non-refugia locations for present-day (1999-2019) and future (2050-2100) bleaching conditions.

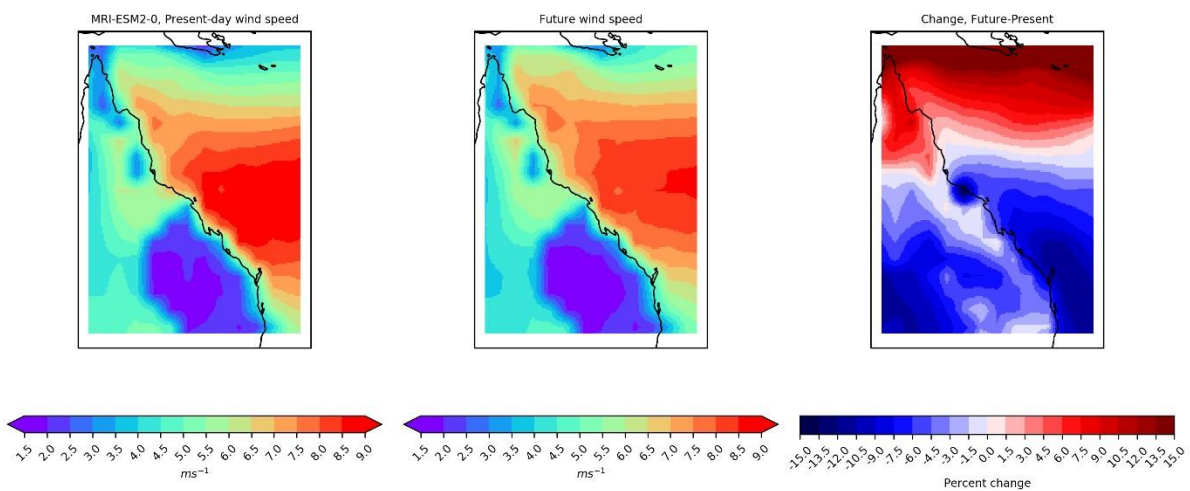
Table 4.1: Wind speed is calculated and compared in refugia and non-refugia locations per model. (R – refugia, N- non-refugia, MRI - MRI-ESM2-0, ECE - EC-Earth3-Veg, UAE - UKESM1-0-LL, CNRM - CNRM-ESM2-1, and IPSL - IPSL-ESM2-0)

model	present wind m/s-1	future wind m/s-1	estimate	SE	df	t-ratio	p-value
R-MRI	6.35 ±0.04	6.16 ±0.04	0.19	0.05	10990	3.56	0.0004
NR-MRI	5.98 ±0.04	5.9 ±0.04	0.08	0.05	10990	1.41	0.1594
R-ECE	6.27 ±0.04	6.02 ±0.04	0.25	0.05	10990	4.78	<0.0001
NR-ECE	6.19 ±0.04	5.94 ±0.04	0.25	0.05	10990	4.27	<0.0001
R-UKE	6.99 ±0.04	6.53 ±0.04	0.46	0.05	10990	8.79	<0.0001
NR-UKE	6.52 ±0.04	6.17 ±0.04	0.35	0.05	10990	6.04	<0.0001
R-CNRM	6.07 ±0.04	6.39 ±0.04	-0.32	0.05	10990	-6.12	<0.0001
NR-CNRM	6.04 ±0.04	6.36 ±0.04	-0.32	0.05	10990	-5.43	<0.0001
R-IPSL	4.84 ±0.04	4.92 ±0.04	-0.08	0.05	10990	-1.54	0.1237
NR-IPSL	4.78 ±0.04	4.88 ±0.04	-0.1	0.05	10990	-1.73	0.0845

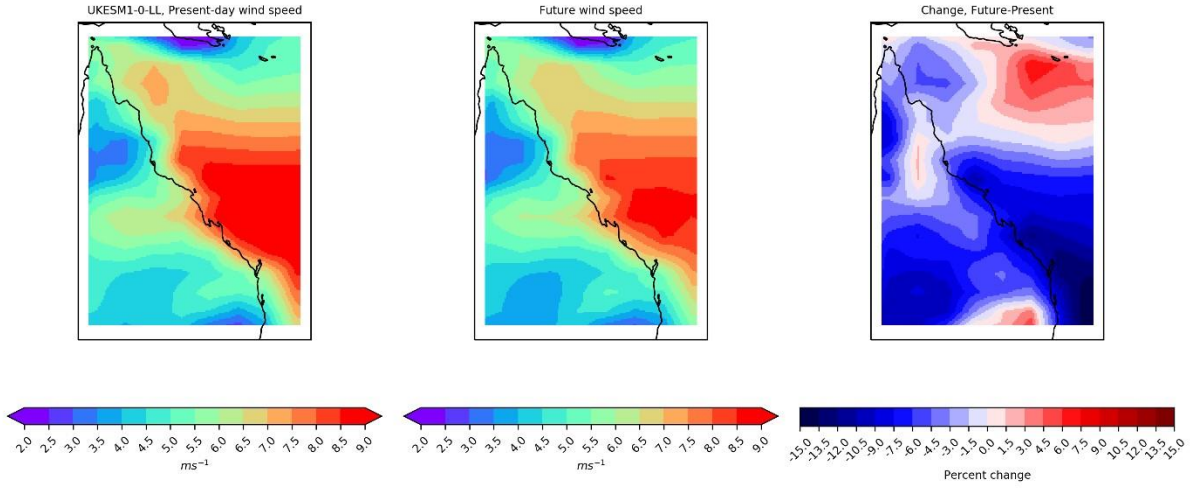
(a)



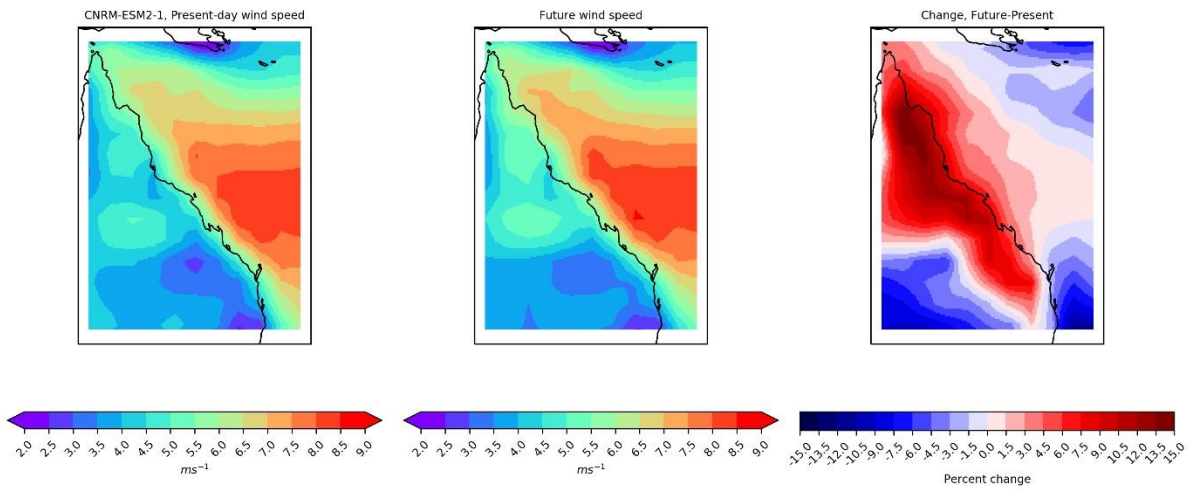
(b)



(c)



(d)



(e)

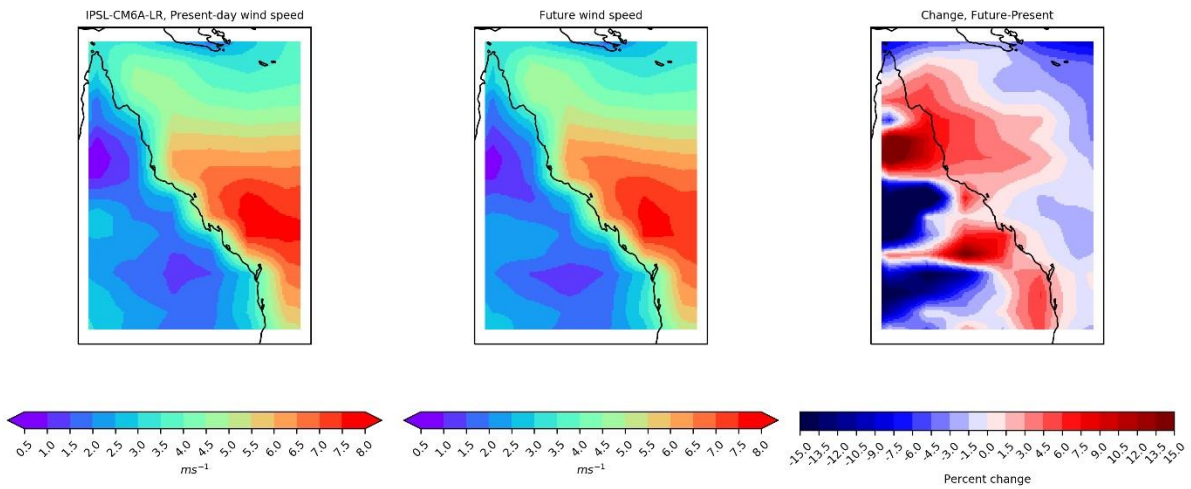


Figure 4.10: Wind speed is shown under SSP5-8.5 for present-day, future, and the difference in shortwave radiation during bleaching conditions per model (a) EC-Earth3Veg, (b) MRI-ESM2-0, (c) UKESM1-0-LL, (d) CNRM-ESM2-1, and (e) IPSL-ESM2-0. Bleaching conditions are defined as austral summer months, December, January, February, March, calculated as austral summer years (i.e., July 31, 2050 – August 1, 2051) with the annual maximum Degree Heating Weeks (DHW) within the Great Barrier Reef Marine Park Authority boundary having a median value of $DHW \geq 2$.

4.4.8 PROJECTED CHANGES IN SHORTWAVE RADIATION

The difference between present-day and future shortwave radiation under SSP5-8.5 is highest in the nearshore and southern GBR with increases spanning the entire GBR (Figure 4.8b). Moreover, the southern GBR will experience a relative increase in shortwave radiation, which can both increase heating and potentially exacerbate the photosynthetic stress that causes bleaching (Enríquez et al., 2005, Figure 4.8b). These conditions are consistent with an increase in frequency or magnitude of high-pressure events. As an ensemble, shortwave radiation over refugia locations is expected to significantly increase by 3.67 W/m^2 SE 0.21 (<0.0001 p-value) during future bleaching conditions (Figure 4.11). Shortwave radiation is also expected to significantly increase in non-refugia locations by 3.15 W/m^2 SE 0.12 (<0.0001 p-value) (Figure 4.11). Our analysis reveals shortwave radiation as the dominant atmospheric variable in the S2P3-R v2.0 downscaling that is driving the loss of climate refugia under high scenarios due to the EC-Earth3-Veg model behaving differently than other models. EC-Earth3-Veg is the only model that does not lose its' refugia status under warming conditions (Table 4.2, Figure 4.12). Therefore, EC-Earth3-Veg uniquely shows a significant decline in shortwave radiation during bleaching conditions into the future of 5.31 W/m^2 SE 0.5 (<0.0001 p-value) over refugia locations and a decline of 5.36 W/m^2 SE 0.6 (<0.0001 p-value) over non-refugia locations (Table 4.2). This model also does not reflect the general spatial pattern of shortwave radiation seen in all other models showing increases over refugia locations (Figure 4.12).

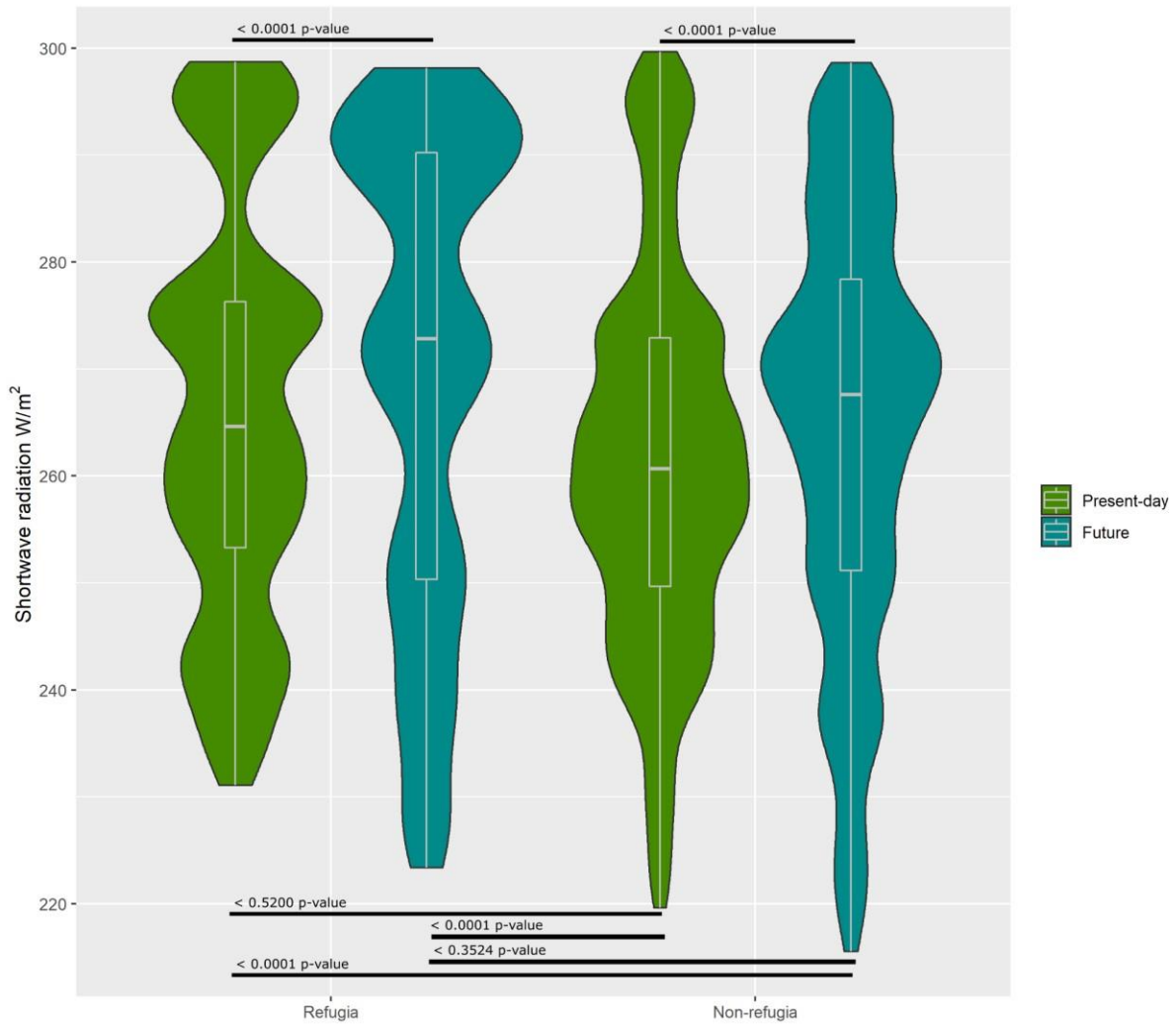
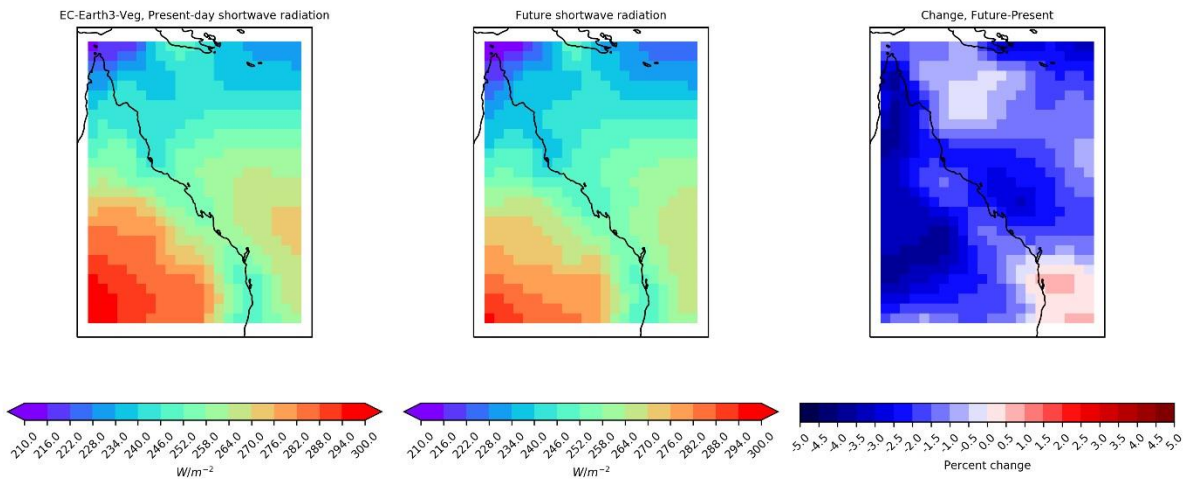


Figure 4.11: Shortwave radiation values are shown from SSP5-8.5 between refugia and non-refugia locations for present-day (1999-2019) and future (2050-2100) bleaching conditions.

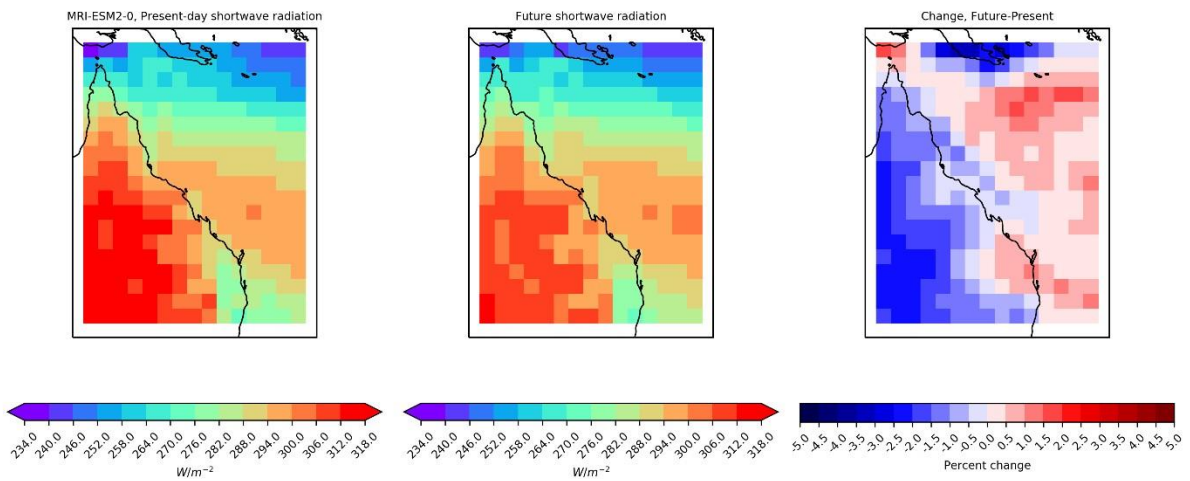
Table 4.2: Shortwave radiation is calculated and compared in refugia locations per model. (R – refugia, N- non-refugia, MRI - MRI-ESM2-0, ECE - EC-Earth3-Veg, UKE - UKESM1-0-LL, CNRM - CNRM-ESM2-1, and IPSL - IPSL-ESM2-0)

model	present shortwave W/m2	future shortwave W/m2	estimate	SE	df	t-ratio	p-value
R-MRI	287.2 ±0.4	286.4 ±0.4	0.77	0.5	10990	1.48	0.1384
NR-MRI	284.6 ±0.4	283.9 ±0.4	0.72	0.6	10990	1.19	0.2333
R-ECE	248.3 ±0.4	243 ±0.4	5.31	0.5	10990	10.24	<0.0001
NR-ECE	247.4 ±0.4	242 ±0.4	5.36	0.6	10990	8.9	<0.0001
R-UKE	267.9 ±0.4	279.9 ±0.4	-12.04	0.5	10990	-23.22	<0.0001
NR-UKE	265.4 ±0.4	276.8 ±0.4	-11.39	0.6	10990	-18.9	<0.0001
R-CNRM	253.9 ±0.4	265.7 ±0.4	-11.78	0.5	10990	-22.73	<0.0001
NR-CNRM	253.3 ±0.4	265.3 ±0.4	-11.98	0.6	10990	-19.87	<0.0001
R-IPSL	256.1 ±0.4	254.8 ±0.4	1.35	0.5	10990	2.61	0.009
NR-IPSL	256.8 ±0.4	255.3 ±0.4	1.56	0.6	10990	2.59	0.0096

(a)

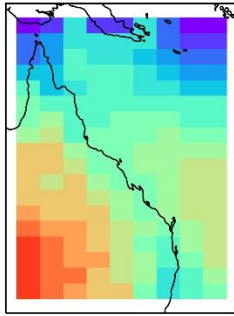


(b)

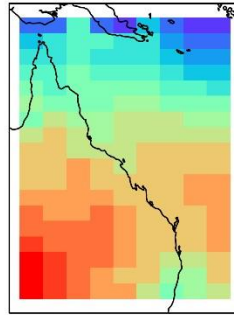


(c)

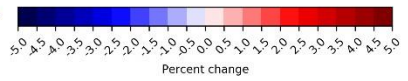
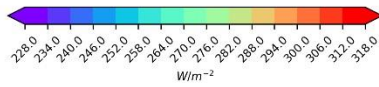
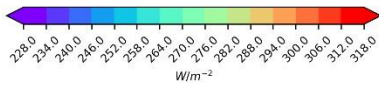
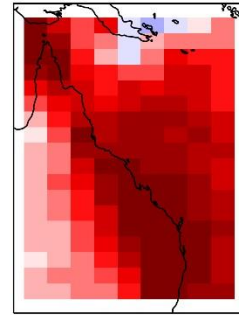
UKESM1-0-LL, Present-day shortwave radiation



Future shortwave radiation

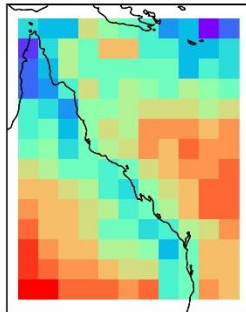


Change, Future-Present

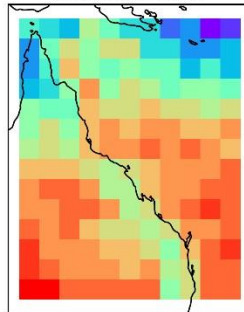


(d)

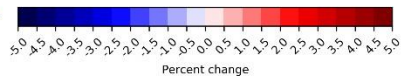
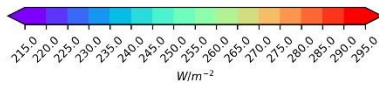
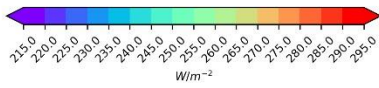
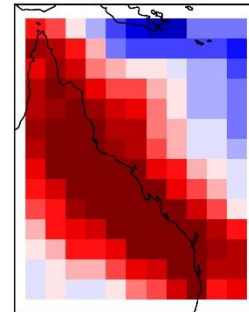
CNRM-ESM2-1, Present-day shortwave radiation



Future shortwave radiation

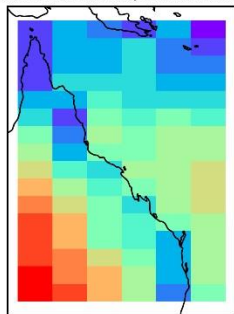


Change, Future-Present

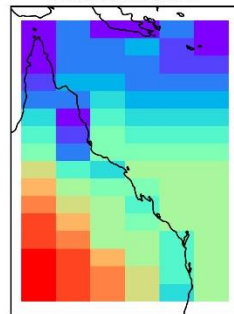


(e)

IPSL-CM6A-LR, Present-day shortwave radiation



Future shortwave radiation



Change, Future-Present

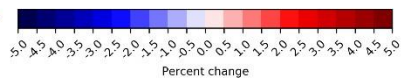
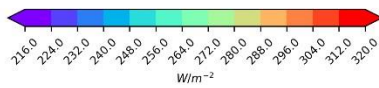
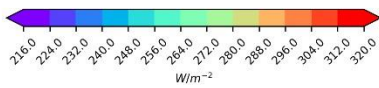
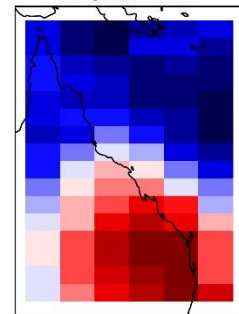


Figure 4.12: Shortwave radiation is shown under SSP5-8.5 for present-day, future, and the difference in shortwave radiation during bleaching conditions per model (a) ECEarth3-Veg, (b) CNRM-ESM2-1, (c) IPSL-ESM2-0, (d) MRI-ESM2-0, and (e) UKESM10-LL. Bleaching conditions are defined as austral summer months, December, January, February, March, calculated as austral summer years (i.e. July 31 2050 – August 1, 2051) with the annual maximum Degree Heating Weeks (DHW) within the Great Barrier Reef Marine Park Authority boundary having a median value of $DHW \geq 2$.

The rate of refugia loss varies across the reef with refugia in northern regions persisting longer than those in central and southern regions (Figure 4.5). CMIP6 projections suggest that a north-south dipole exists in wind-speeds at times when bleaching is occurring (Figure 4.8a), such that wind speeds decline in southern areas, which reduce the mixing – and therefore cooling potential – of the water column. In contrast, wind speeds increase in the north (Figure 4.8a), elevating mixing potential. Moreover, the southern GBR is projected to experience a relative increase in shortwave radiation, which can both increase heating and potentially exacerbate the photosynthetic stress that causes bleaching (Enríquez et al., 2005; Skirving et al., 2017) (Figure 4.8b).

4.5 DISCUSSION

Global-scale coral bleaching events are expected to occur more regularly as global average temperatures increase (Dixon et al., 2022; Frieler et al., 2013; Van Hooidonk et al., 2016). A recent SST based study using statistical downscaling by Dixon et al (2022) projects a loss of nearly all (84.1% globally and 86% on the GBR) refugia under 1.5°C and a complete loss of the remaining refugia under 2°C. Differences in the locations of refugia in the Dixon study were hypothesized to be due to interannual and seasonal SST variability (Dixon et al., 2022).

The semi-dynamic downscaling processes in this study enable a more sophisticated spatiotemporal analysis of climate projections over coral reefs. Accounting for tides and

winds prove to be important variables when quantifying areas of climate refugia in the context of thermal exposure.

4.5.1 ATMOSPHERIC CIRCULATION DRIVING CHANGES TO WIND AND SHORTWAVE RADIATION

The modelled change in shortwave radiation (Figure 4.8b), linked to increased bleaching in the Southern GBR, is potentially driven by a projected weakening in the Hadley circulation influencing the descending branch over the GBR known as the Subtropical Ridge (Timbal & Drosowsky, 2013). As the planet warms, climate models project an expansion of the Hadley circulation poleward (Dey et al., 2019; Frierson et al., 2007; Hu et al., 2013; Lu & Vecchi, 2007.; Seidel et al., 2008) causing an intensification and poleward shift of the Subtropical Ridge (Dey et al., 2019; Grose et al., 2015; Kent et al., 2013). The latitudinal dipole in changing wind speeds projected into the future (Figure 4.8a) can potentially be explained by an increase in the summer monsoon intensity during bleaching conditions (Brown et al., 2016; Dey et al., 2019).

4.5.2 CLIMATE MODEL VARIABILITY

The use of an ensemble of climate models, rather than a single model, allows us to explore the most likely outcome, i.e., the multi-model mean (IPCC, 2021), but also alternative potential outcomes. Downscaling of one of the five models - EC-Earth (Döscher et al., 2021) – gave more optimistic projections than the others. Using this model, relative thermal refugia persist under all four climate scenarios (Figure 4.5b). Our analysis using EC-Earth predicts more refugia in the north than we see with other models (Figure 4.5a). This climatological distribution of refugia, combined with the northerly bias seen in refugia persistence, contributes to the anomalous refugia persistence identified from EC-Earth.

4.5.3 DOWNSCALING LIMITATIONS

Large mesoscale processes will result in lateral advection not simulated within the downscaling presented here. Lateral advection could occur through eddies, western boundary currents, the Hiri and the East Australian currents. Glynn (1996) hypothesized that vigorous circulation (for example in upwelling centres, oceanic banks, island shores) may provide corals with a refuge from warming ocean temperatures (Baird et al., 2018; Glynn, 1996). The South Equatorial Current reaches the Australian continent between latitude 14°S and 18°S (Andrews & Clegg, 1989; Burrage, 1993; Church, 1987) when the East Australian Current then flows southward and the Hiri Current flows northward. The location of bifurcation varies seasonally and inter-annually and these currents mostly influence waters on the outer shelf (Burrage, 1993; Wolanski & Spagnol, 2000). This location of bifurcation marks the division of the warm tropical and cool subtropical gyres. The impact of these processes on the downscaling presented here will only be felt through the imposed atmospheric forcing. Despite these limitations, the dominance of atmospheric forcing in driving shallow water extreme events, and importance of tidal mixing in moderating these events (Halloran et al., 2021), combined with the potential offered by a simplified, and therefore computationally efficient, shelf sea model to undertake multi-model and model-scenario downscaling, make such an approach very valuable.

4.5.4 CLIMATE TRAJECTORY UNCERTAINTY FOR CORALS

Even under the lowest emissions trajectories we still face a committed warming. The frequency of severe coral bleaching events (when DHW >8) is expected to be 5 events per decade under SSP1-2.6 and 3 events per decade under SSP1-1.9 surrounding 2060 (McWhorter et al., 2021). The increasing frequency and magnitude of warming events into the future make corals extremely vulnerable to mortality from climate change (Bozec et al., 2020; Frieler et al., 2013; Hoegh-Guldberg, 1999; Hughes, Anderson, et al., 2018; Hughes et al., 2017; King et al., 2017; Van Hooidonk et al., 2016). One widespread warming event, or a succession of warming events could have severe and

irreversible consequences eliminating any concept of a refugia. Under low emissions trajectories, the locations of refugia show an average trend of less DHW than the rest of the GBR, which means these locations are slightly less vulnerable in terms of magnitude, yet not necessarily in terms of frequency. Even during more frequent events, if these refugia contain a lower magnitude of stress than the rest of the GBR, such locations could become increasingly valuable to the entire reef system as sustained refugia or areas to facilitate recovery (Bozec et al., 2020; Hock et al., 2017).

Global policy decisions that would result in high emissions trajectories will likely be at the cost of the identified refugia in this study. Low emissions trajectories offer a less impacted future with a greater opportunity for recovery and survival. If these refugia maintain their less impacted status, they could potentially provide larvae to hydrodynamically connected reefs, facilitating the recovery process after bleaching events (Bode et al., 2018; Cheung et al., 2021; Hock et al., 2017). The identified persistent refugia could be targets for management interventions, i.e., further protection such as limitations on overfishing of herbivores (Bozec et al., 2020; Doropoulos et al., 2016; Graham et al., 2015; Hughes et al., 2007; Mumby et al., 2016), the management of nutrient pollution and invasive species control (Brodie et al., 2012). Indeed, the incorporation of 'climate refugia' into management does not preclude the importance of managing other processes that can impact reef trajectories, including water quality and fisheries impacts. Rather, there may be significant benefits in directing some of those standard management practices towards refugia, particularly where they help the robustness of coral populations over time.

4.5.5 CORAL ADAPTATION AND RECOVERY

Climate refugia are likely to support a high abundance of coral colonies relative to non-refugia and may act as important sources for larval export (Cheung et al., 2021). However, the role of such areas for coral adaptation are now the subject of intensive research (McManus et al., 2021; Walsworth et al., 2019) and the outcome remains unclear. On the one-hand, they may have a positive role in bolstering population size

and turnover in other sections of the reef. The maintenance of higher population size will contribute to ecosystem functioning, such as calcification and reef building (Wolfe et al., 2020) and possibly to larger effective (genetic) population size. However, a lower selection pressure on thermal tolerance traits in stress refugia may lead to an accumulation of corals which are maladapted to non-refugia conditions which would potentially slow the rate of adaptation in stressed areas downstream (McManus et al., 2021). Nonetheless, both climate refugia and areas of intense heat stress have roles to play in designing future conservation strategies for the GBR. Our results suggest that such investments in planning are worthwhile because refugia can continue to exist for at least 30 years and potentially longer if global emissions can be contained.

CHAPTER 5

UNDER PRESSURE; CLIMATE CHANGE AT DEPTH

5.1 ABSTRACT

Coral reef heat stress projections have exclusively been made using sea surface temperatures. While sea surface temperature projections are useful for shallower areas of the reef-scape, deeper reef communities (30-150 m) are more likely to have different bottom temperature environments due to various mixing regimes (permanently stratified, permanently unstratified, and periodically stratified (typically seasonal) water). Density stratification creates a buoyancy barrier that effectively partitions the upper and lower parts of the water column. In this study, bottom temperatures from downscaled climate projections are used to classify areas where stratification is 'insulating' bottom temperatures from surface heatwaves during austral summer months. The results suggest that over large areas of the Great Barrier Reef (GBR) (0-50 m) stratification allows for the persistence of anomalously cool bottom waters despite sea surface temperatures warming until global average temperatures reach $\sim 3^{\circ}\text{C}$. At this point, bottom temperatures surpass a recognized thermal threshold of 30°C for bleaching at depth on the GBR. The upper mesophotic zone (30-50 m) is also threatened under a warming planet. This study demonstrates the application of a simple, observationally tractable metric of where seabed temperatures can avoid heatwaves under lower climate emissions. The metric proves to be a valuable tool for the identification of mesophotic refugia in guiding reef management decisions.

5.2 INTRODUCTION

Mesophotic coral ecosystems are defined as reef communities in the mid to lower photic zone (30-150 m) that contain phototrophic taxa (Kahng et al., 2010). Glynn (1996) first

hypothesized that mesophotic coral reefs could potentially be less affected by thermal stress events than shallow coral reefs (< 30 m) and may act as a climate refugia. Aiding in the ability of these mesophotic communities to act as a potential climate refugia are their physical oceanographic circumstances. Mesophotic reef locations are generally located on forereef environments which have more exposure to open ocean physical mixing processes such as upwelling, surface downwelling, and internal waves (Williams et al., 2018, Gove et al., 2006, Lichter et al., 1996). These processes may also provide forms of thermal relief from warming events and aid in the supply of food/nutrients as light becomes more limited at depth (Williams et al., 2018).

In contrast to mixing providing a form of thermal relief, stratification caused by thermal density gradients in the water column could allow for a cooler layer of water near the seabed while the surface is warm. The latest Intergovernmental Panel on Climate Change (IPCC) report reflects the high confidence in the literature demonstrating that the upper 200 m of the ocean will continue to become more stratified due to global warming (Bopp et al., 2013; Capotondi et al., 2012; Helm et al., 2011; IPCC, 2021; Talley et al., 2016; Zika et al., 2018). Increases in stratification across all ocean basins are due to the combined magnitude of warming and near-surface freshening of high latitudes (IPCC, 2021). More fresh, warm water is less dense than more saline cold water further amplifying the stratification process (Pawlowicz et al., 2011). Summer conditions are typically more stratified than winter conditions due to a weakening in winds (Wolanski & Pickard, 2018).

Certain studies are only beginning to explore mesophotic reef communities and the possibility of coral bleaching at depth (Bongaerts et al., 2010) as most coral reef research occurs < 15 m due to certain depth limitations of SCUBA (Bridge et al., 2012). Recent technologies have allowed for further studies on mesophotic coral ecosystems using rebreathers, autonomous underwater vehicles, and remotely operated vehicles (Bridge et al., 2012). Depth has been identified as a strong predictor of coral community composition (Polónia et al., 2015) as mixotrophic corals can shift their energy from autotrophic to heterotrophic pathways as depth increases (Williams et al., 2018).

Although, this is not always the case as spatiotemporal variations in physical processes can influence light and heterotrophic subsidies (Williams et al., 2018).

Coral bleaching was quantified at depth in Frade et al (2018) on the GBR during the 2016 event. Anomalously warm temperatures at depth (40 m) resulted in the bleaching of 40% of surveyed reefs in comparison to 60% bleaching in the shallower locations (10 m) (Frade et al., 2018). Thermal relief was initially provided by upwelling as this bleaching occurred during late February and March (Frade et al., 2018). Frade et al (2018) showed slightly less bleaching during the 2016 event at certain upper mesophotic reef locations in comparison to shallow reef sites. Differences in the abundance distribution of bleaching-susceptible coral taxa (i.e., *Stylophora*, *Isopora*, and *Montipora*) versus bleaching-tolerant coral taxa (i.e., *Porites*, *Leptoseris*, *Acropora* and *Pocillopora*) may indicate relief from bleaching on deeper reefs (Frade et al., 2018). Similarly, Baird et al (2018) observed bleaching during the 2016 event that reflected the attenuation of light across a depth gradient (more bleaching in shallower depths). Higher effects of bleaching were also correlated to higher levels of thermal stress (Baird et al., 2018). Other studies from earlier bleaching events explain depth-related coral bleaching and mortality patterns as potentially attributed to solar radiation increases at depth and discuss possible gradients of thermal relief or biological tolerance (Brown et al., 1999, 2000; Harriott, 1985; Mumby et al., 2011; Rowan et al., 1997).

Deeper reefs can also potentially provide larvae to reefs that have been exposed to disturbances from bleaching, storms, sedimentation, land-based floods, and other impacts (Bongaerts et al., 2010; Bridge et al., 2012; IPCC, 2021; Lindfield et al., 2016; Smith et al., 2016; Thomas et al., 2015). For a coral to provide larvae across depths, it would have to be a depth-generalist coral species or a species that lives across a range of depths. Bongaerts et al (2017) found that depth-generalist coral species represent only a quarter of total coral biodiversity. There is no direct evidence that larval exchange occurs between shallow and mesophotic depths (Rocha et al., 2018). The Rocha et al (2018) study demonstrates that mesophotic reef communities are distinct from shallow communities in assemblage composition and species turnover. In contrast, previous

studies demonstrated high overlap of species across depths showing an overlap of approximately 77% for corals of shallow and upper mesophotic zones, 30-50 m, in the Caribbean (Bridge et al., 2013; Semmler et al., 2017).

Regardless of the highly debated question of whether mesophotic reefs can be a suitable refugia for shallow reef systems or not, mesophotic reefs are understudied and therefore perhaps undervalued. While mesophotic reefs may be more at risk than previous studies indicate for a multitude of reasons, thermal stress continues to be the most immediate threat to coral reefs (Frade et al., 2018; Hughes, Anderson, et al., 2018; Hughes et al., 2017; Hughes Kerry, et al., 2018). The scale of coral thermal stress over the mesophotic zone has yet to be explored using climate projections. Coarse resolution Global Climate Models do not capture the bathymetry or processes that influence the behaviour of the water column such as the influence of tidal and wind mixing processes (McWhorter et al., 2022, Chapter 4).

5.3 METHODS

The S2P3-R v2.0 downscaling approach discussed throughout previous chapters enables the study of bottom temperature climate projections. Depth was parameterized between 0-50 m in these simulations. This study considers 30-50 m to be classified as the upper mesophotic reef community. A metric was developed to locate areas of stratification during austral summer. These stratified locations are hypothesized to provide thermal relief at the seabed when warming conditions are occurring at the surface. This metric calculates a given location that contains a positive surface temperature anomaly on top of a negative bottom temperature anomaly during austral summer. The anomalies are calculated using a present-day summer climatology (1999-2019). Areas of thermal protection due to stratification are identified under four climate emission scenarios using five climate models. Within this chapter, 1.) the locations of stratification are identified demonstrating consistency between downscaled observations and climate models, 2.) bottom temperature projections are analysed, 3.)

future stratification patterns are shown temporally under various climate emission scenarios, and 4.) low wind and low tidal energy are discussed as potential drivers of stratification.

5.3.1 DOWNSCALING

This study uniquely involves the analysis of bottom temperature output, or the temperature at the seabed derived from the 1-D, semi-dynamic S2P3-R v2.0 downscaling (Chapters 2-4). Similar to previous chapters, CMIP6 models MRI-ESM2-0, EC-Earth3-Veg, UKESM1-0-LL, CNRM-ESM2-1, and IPSL-CM6A-LR were used with climate-change scenarios SSP1-1.9, SSP1-2.6, SSP3-7.0 and SSP5-8.5. Downscaled bottom temperature outputs using atmospheric reanalysis product, ERA5, were compared to Australia's Integrated Marine Observing System (IMOS) mooring system observational bottom temperature data for validation (Halloran et al., 2021). The nearest locations from the downscaled output were compared to the mooring system and the results indicate a cool bias at lower latitudes in the modelled data. The cool bias could be due to the model data having a resolution of 10 km² (Halloran et al., 2021). Regardless of a slight cool bias, the relationship of bottom temperature between observations and the model output is linear (Halloran et al., 2021).

5.3.2 SUMMER METRICS APPLIED TO SURFACE AND BOTTOM TEMPERATURE OUTPUTS

Bleaching metrics, such as Degree Heating Weeks (DHW) (Section's 1.7.4, 1.7.5, 1.7.6) and the number of severe bleaching events (Section 3.3.2), used in earlier chapters, could not be calculated because the temperature at which corals undergo bleaching at deeper depths (>15 m) is largely unknown. Importantly, the DHW metric is based on sea surface temperatures (SST), not bottom temperatures. Schramek et al (2018) attempted to quantify DHW at depth accounting for temperature variability. Similarly, this study could not correlate the bleaching thresholds to the bleaching observations

due to the lack of observations and suggests further studies to confirm the application of their DHW algorithm at depth (Schramek et al., 2018).

The bottom and surface temperature anomaly data were used to locate areas that contain a positive surface temperature anomaly on top of a negative bottom temperature anomaly. Since bleaching on the GBR typically occurs during austral summer months (Skirving et al., 2019), surface and bottom temperature anomalies were calculated during December, January, February, and March. The anomalies were calculated in relation to the average summer conditions from 1999-2019. For each cell per year, the positive surface temperature anomalies (> 0) were given a value of 1, similarly the negative bottom temperature anomalies (< 0) were given a value of 1. The two variables then separately contain values of 0 and 1. The bottom and surface temperature anomaly data were then added. The values that summed to 2 were then kept as locations of stratification, or locations with a positive surface temperature anomaly while having a negative bottom temperature anomaly during summer months.

Bottom and surface temperature output variables were analysed per model per scenario using the following steps:

- 1) The first step of the analysis was to recalculate the calendar year placing the austral summer in the middle of the year, this has been described in earlier chapters (i.e., July 31, 1999 – August 1, 2000). (Section 3.3.2)
- 2) Secondly, the summer months, December, January, February, and March, were selected to represent the time when bleaching is most likely to occur (Skirving et al., 2019).
- 3) A climatology was created from 1999-2019 using the average value from the summer months.
- 4) The climatology was then used to create an annual summer mean anomaly for the surface and bottom temperature variables.
- 5) The Great Barrier Reef Marine Park Authority (GBRMPA) boundary was used to mask the values within the GBRMPA boundary for consistency.

5.3.4 DOWNSCALED ERA5 VALIDATION

ERA5 atmospheric reanalysis product was downscaled using S2P3-R v2.0 to relate the observational data to the climate model data. We found in earlier chapters that downscaled ERA5 outputs prove useful for explaining why spatial patterns are non-random (Section 4.4.2). The bottom and surface temperature output used a similar method between the downscaled observations and climate models to isolate the locations of stratification (Figure 5.1). Austral summer months were used (December, January, February, March). The climatology for the downscaled ERA5 outputs, surface, and bottom temperature, was different than the climatology used for the climate model data. The climatology for the downscaled ERA5 outputs was created from years 1980-1998 and the anomalies were created from years 1998-2019. The downscaled climate model climatology was from 1999-2019 and the projections were to the end of the century. The annual summer mean anomaly was further used to calculate the stratified locations.

5.3.5 DOWNSCALED ERA5 BASED WIND AND TIDAL ENERGY FLUX CALCULATIONS

Wind and tidal energy prove to be important influences for thermal relief (McWhorter et al., 2022, Chapter 4). The method in this study uses the opposite approach, exploring areas of low wind and low tidal energy to explore the cause of stratified locations. Wind and tidal energy outputs were extracted from the S2P3R v2.0 downscaled ERA5 simulation to compare the differences between stratified and unstratified locations. The energy flux calculations, including the statistical methods used for comparison, are described in the methods section in chapter 4 (Section 4.3.5). Similar statistics were used from the refugia and non-refugia comparison in chapter 4 (Section 4.3.5). Additive mixed effect models were used to explore differences in wind and tidal energy between stratified and unstratified locations using the ‘bam’ function (Wood, 2004) in R version 4.1.1 (Pinheiro et al., 2021) where longitude and latitude were included as a smooth

function to account for the spatial correlation of the data. Pairwise comparisons were determined using the 'pairs' function (Lenth, 2021) in R version 4.1.1 (Pinheiro et al., 2021).

5.4 RESULTS

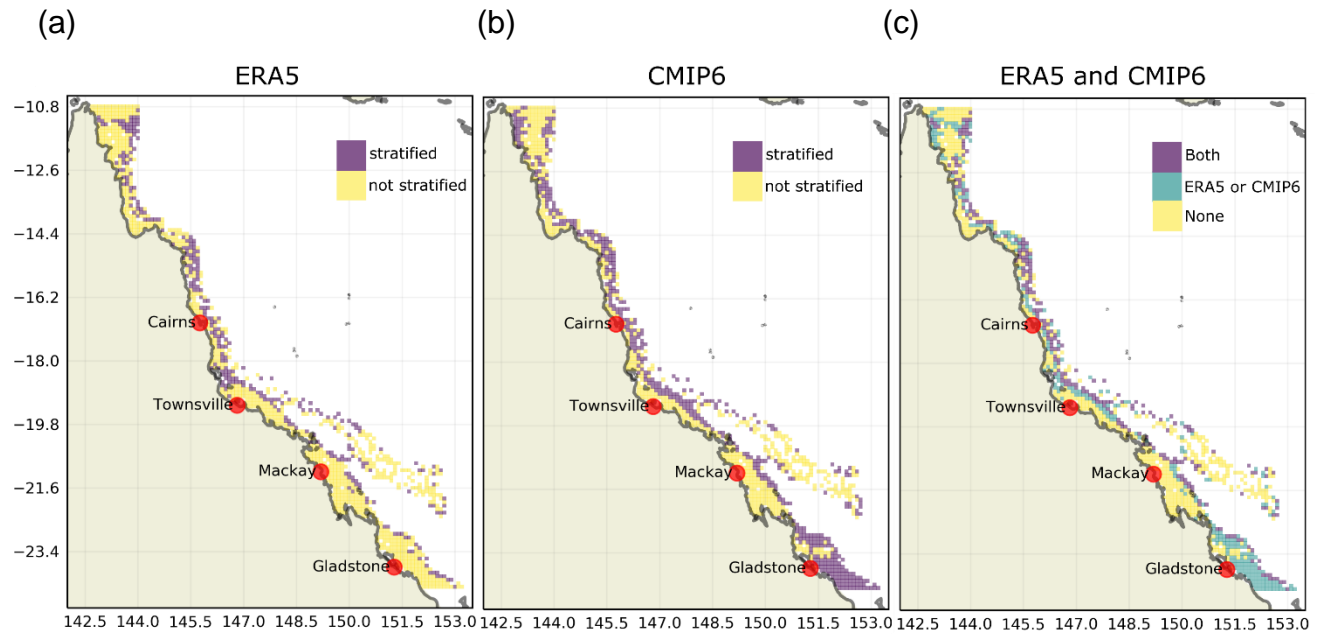
5.4.1 LOCATIONS OF STRATIFICATION DURING AUSTRAL SUMMER

There are stratified locations most dominantly clustered in the north, central, and part of the southern GBR that show agreement between the downscaled observations and the downscaled climate models (Figure 5.1 (a, b, c)). This validation gives confidence to the results demonstrating that the spatial pattern is not just a random artifact of the climate model variability. The identified locations could provide thermal protection to coral ecosystems during future warming events if the stratification persists and warming is limited at depth into the future. The warmer than normal surface anomaly in combination with a cooler than normal bottom temperature anomaly is informative of the surface mixed layer. The surface mixed layer refers to a layer of common density and often changes seasonally. The location of the surface mixed layer depth is useful in identifying the thermal buffer for the upper mesophotic community or corals that are below the thermocline.

Most of the stratified locations are from depths 30-50 m, but the stratification is distributed across all depths meaning that depth is not the only variable driving these conditions (Figure 5.1 d). There are two spikes of the stratified locations in depths of 15 m and 25 m (Figure 5.1d) that may be attributed to plateau or basin like bathymetry with a low tidal range (Figure 5.1d).

There is a clear spatial pattern in the north, central, and part of the southern GBR that can be potentially attributed to the depth and a lack of mixing from tidal and wind energy (Figure 5.1 (a, b, c)). Importantly, the unstratified areas also show agreement between the observations and climate models, for example, in the shallow nearshore, the area

that branches off in the central and southern GBR, and parts of the far north and southern GBR. The unstratified locations are likely to be shallow, well mixed and more reflective of locations identified in chapter 4.



(d)

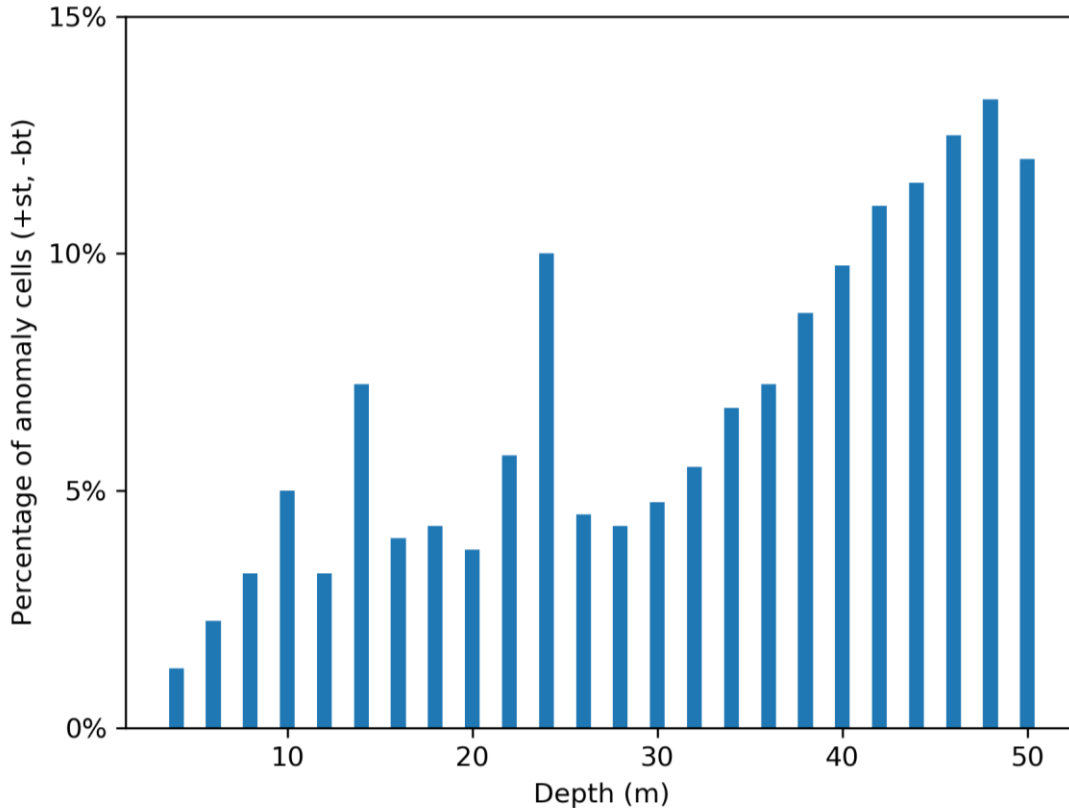


Figure 5.1: (a) Downscaled ERA5 surface and bottom temperatures were calculated as the percentage of years with the identified stratification pattern (positive surface temperature on top of a negative bottom temperature anomaly) during summer months based on a climatology from 1980-1999, anomalies are calculated from 1999-2019 during summer months (December, January, February, March). (b) Areas with identified stratification are shown as a percentage of years using four scenarios (SSP1-1.9, SSP1-2.6, SSP3-7.0, SSP5-8.5) and five downscaled climate models from 2020-2040 summer months relative to summer conditions from 1999-2019. (c) A map showing the agreement between (a) and (b), and (d) the distribution of the range of depths for the anomalously stratified locations based on climate models is shown as a percentage of cells per depth bin.

5.4.2 DOWNSCALED ERA5 TIDAL AND WIND MECHANISMS

There is less tidal energy flux and slightly less wind energy flux in the identified stratified locations of the GBR (tidal energy flux p-value 0.0076, wind energy flux p-value 0.7703)

(Figure 5.2 (a, b)). Tidal energy is assumed to be stable into the future under this simulation, not accounting for sea-level rise; therefore, a loss of stratification would likely be driven by the general increases in temperature and potentially future changes in wind mixing patterns.

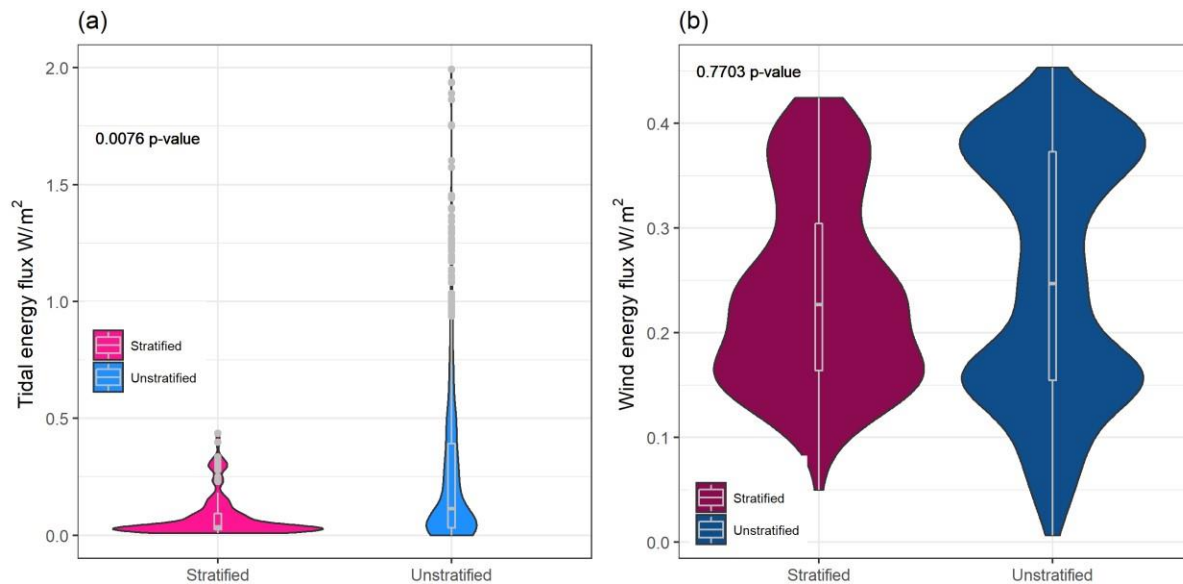


Figure 5.2: The downscaled ERA5 simulation shows (a) tidal energy flux and (b) wind energy flux from 1999-2019 in stratified and unstratified locations. Additive mixed effect models were used to explore differences between stratified and unstratified locations using the ‘bam’ function in R version 4.1.1 where longitude and latitude were included as a smoothed function to account for the spatial correlation of the data. Pairwise comparisons were determined using the ‘pairs’ function in R version 4.1.1.

5.4.3 FURTHER VALIDATION OF STRATIFICATION CONDITIONS

The stratification conditions are not dominated by a single month or a single climate model (Figure 5.3, Figure 5.4). The identified locations between months and climate models are very consistent providing more confidence to this phenomenon and demonstrating that the spatial pattern is not random. The month of March is showing the

lowest number of stratified locations which is sensible as the seasonal changes are beginning to occur with an expected increase in winds in the fall (Figure 5.3). The downscaled climate models show generally consistent patterns of agreement (Figure 5.4), although, model variability is expected to some degree as models are best used as ensembles (IPCC, 2021).

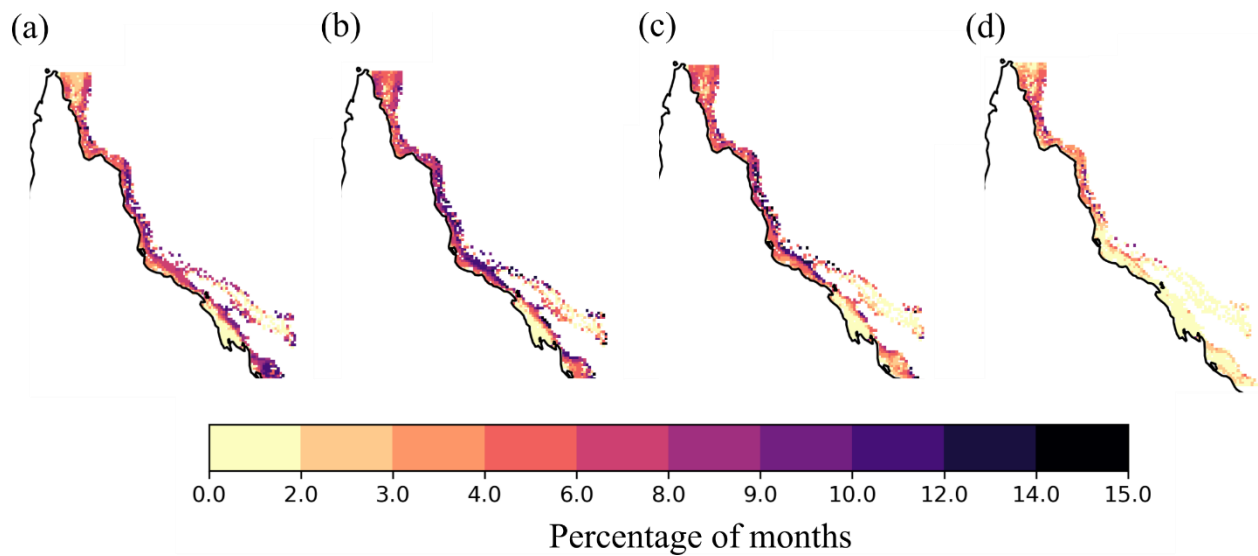


Figure 5.3: Stratification for each summer month as a percentage of years from 2020-2040, (a) December, (b) January, (c) February, and (d) March.

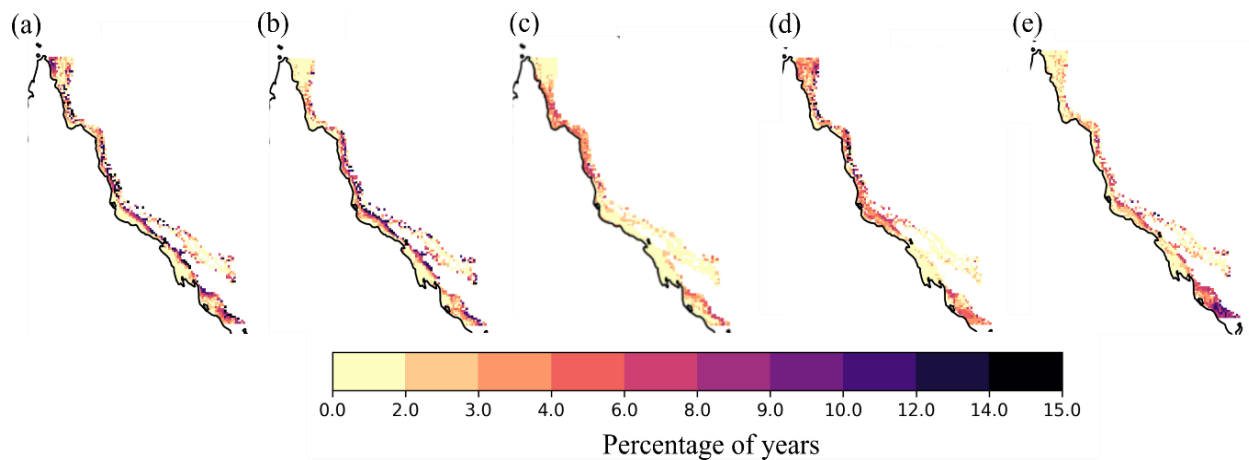


Figure 5.4: The summer stratification as a percentage of years from 2020-2040 per model, (a) MRI-ESM2-0, (b) EC-Earth3-Veg, (c) UKESM1-0-LL, (d) CNRM-ESM2-1 and (e) IPSL-CM6ALR.

5.4.4 FUTURE STRATIFICATION

Under high climate emissions there is an increase in the difference between surface and bottom temperatures over the identified stratified locations after mid-century (Figure 5.5). These results suggest a confirmation of the literature in that stratification is expected to increase under warming due to increases in surface water temperatures (IPCC, 2021). These findings also demonstrate that increases of $\sim 0.25^{\circ}\text{C}$ in the difference between surface and bottom temperatures are expected to occur under high emissions scenarios throughout the GBR and with larger increases of $\sim 0.5^{\circ}\text{C}$ in the areas identified as stratified (Figure 5.5). The entire GBR grid has less of a difference between surface and bottom temperatures than the stratified areas identified in this study by approximately 1°C (Figure 5.5).

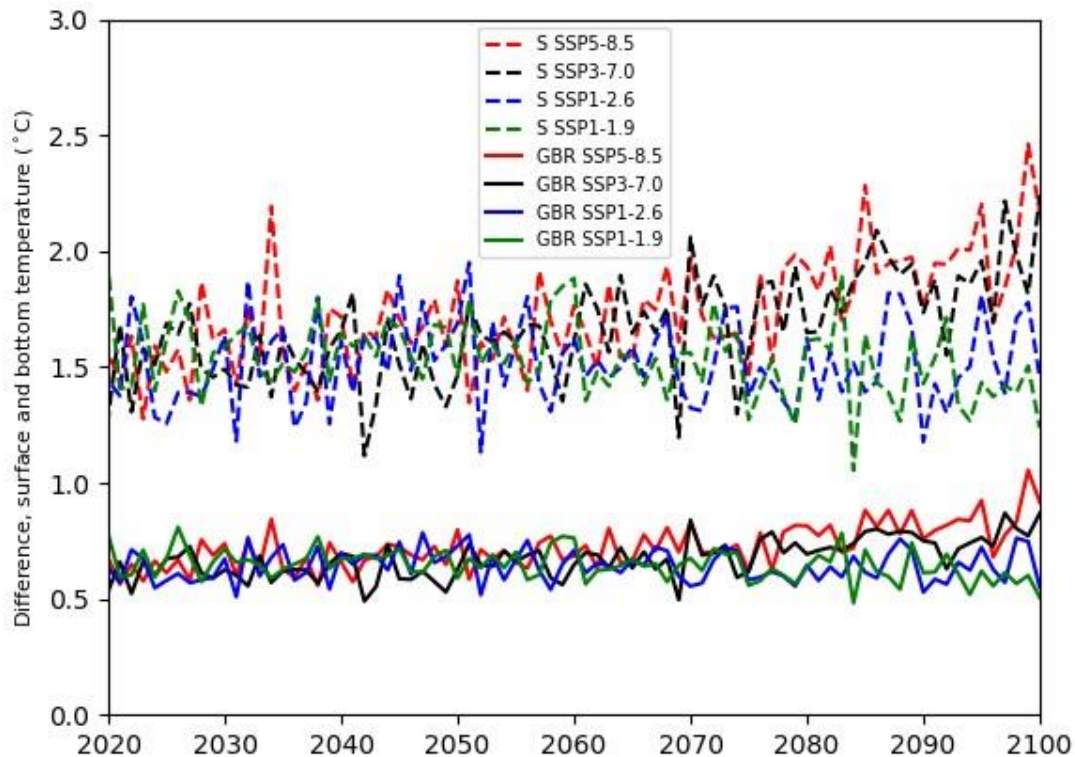


Figure 5.5: The difference between surface and bottom temperature was taken per model as a summer average and then calculated as an ensemble mean per year per scenario (SSP1-1.9, SSP1-2.6, SSP3-7.0, SSP5-8.5) for stratified locations (S), dashed lines, and the entire Great Barrier Reef (GBR), solid lines.

5.4.5 PROJECTIONS OF THE AUSTRAL SUMMER STRATIFICATION

The locations of stratification no longer keep waters periodically below climatological levels from mid-century onwards under higher emissions scenarios (Figure 5.6). Declines in the stratification locations correlate to the general pattern of warming expected in each climate scenario. For example, even the warming in SSP1-1.9 is expected to increase and exceed 1.5°C of global warming before it returns to 1.5°C by the end of the century and this is shown in the stratified locations (Figure 5.6). Lower emissions scenarios, SSP1-1.9 and SSP1-2.6, show a slight decline in the stratified locations after mid-century retaining ~10% of cells on the GBR (Figure 5.6). Rapid

increases in warming after mid-century in SSP3-7.0 and SSP5-8.5 are warming bottom temperature waters driving the loss of the anomalous stratification entirely and threatening the upper mesophotic reef ecosystem (Figure 5.7b).

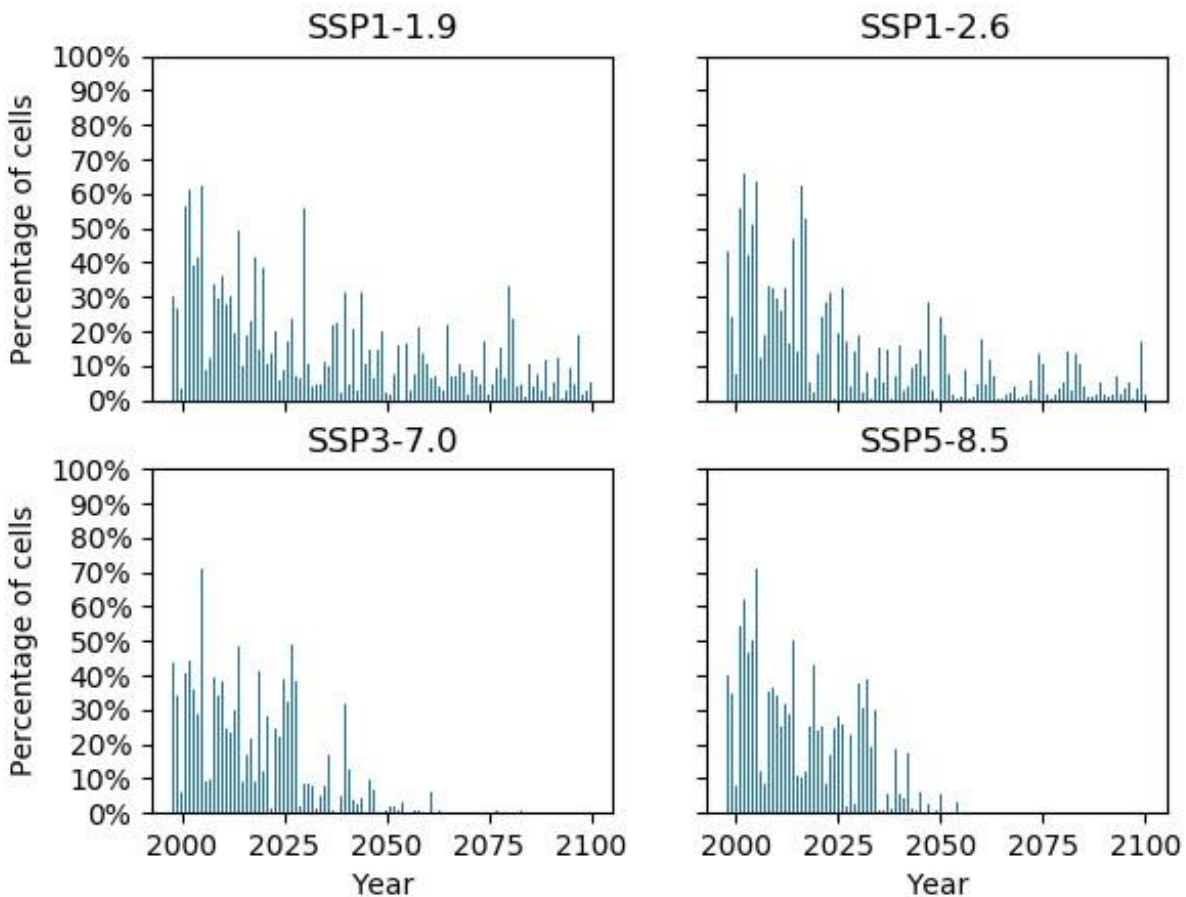


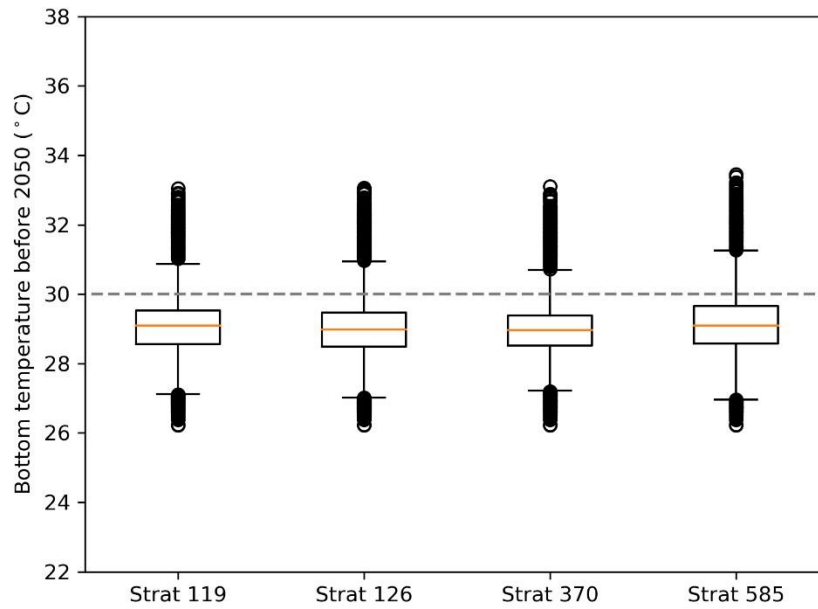
Figure 5.6: Stratified locations shown annually for SSP1-1.9, SSP1-2.6, SSP3-7.0, and SSP5-8.5.

5.4.6 BOTTOM TEMPERATURE PROJECTIONS

Bottom temperatures are increasing in the identified locations of stratification under high emissions (Figure 5.7 (a, b)). The loss of a cool bottom temperature anomaly can be attributed to the warming shown in Figure 5.7 under SSP3-7.0 and SSP5-8.5. Bottom temperature median values increase by $\sim 2^{\circ}\text{C}$ in high emissions scenarios after mid-

century (Figure 5.7 (a, b)). After mid-century, SSP1-2.6 shows a slight rise in median bottom temperature by $\sim 1^{\circ}\text{C}$ while SSP1-1.9 shows even less of a rise in median bottom temperatures for stratified locations.

(a)



(b)

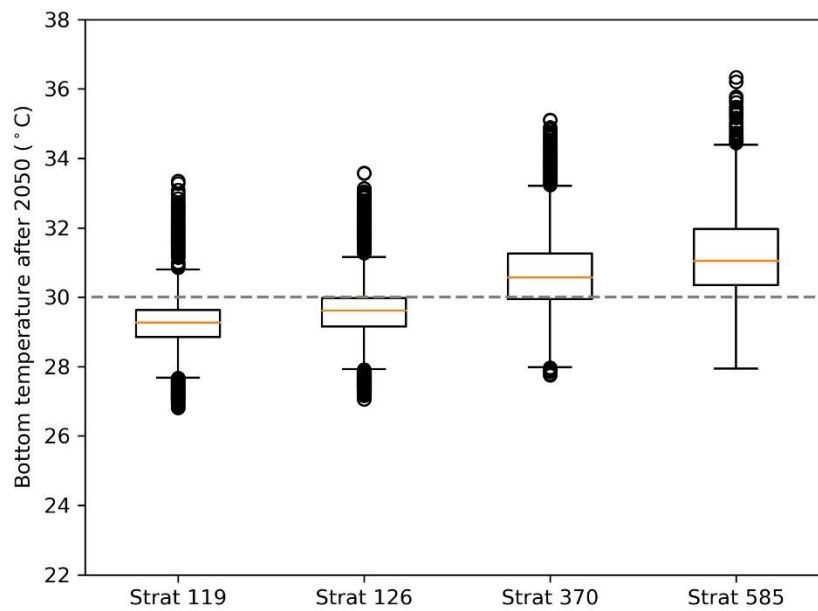


Figure 5.7: Ensemble bottom temperature values per scenario in areas with summer stratification (Strat) (a) before 2050 and (b) after 2050. Bottom temperatures were calculated as ensemble means from summer months within each scenario, SSP1-1.9, SSP1-2.6, SSP3-7.0,

and SSP5-8.5. The orange line represents the median value. The box boundaries are the first quartile and the third quartile. The whiskers show the range of data. A thermal threshold of 30°C was also placed on top of these figures to show when bleaching typically occurs at depth based on Frade et al. (2018). (119 – SSP1-1.9, 126 - SSP1-2.6, 370 – SSP3-7.0, 585 – SSP5-8.5)

Frade et al (2018) studied mesophotic reefs during the 2016 event on the GBR and broadly associates bleaching with bottom temperatures around 30°C (Frade et al., 2018). In this study, median bottom temperature values remain near 28°C, consistent with non-bleaching conditions in Frade et al (2016), until warming increases in higher scenarios after mid-century (Figure 5.7 (a, b)). After mid-century, median bottom temperature values exceed 30°C for stratified locations under higher emission climate-change scenarios SSP3-7.0 and SSP5-8.5 (Figure 5.7b). Given the magnitude of projected increases in global average temperatures under high emissions scenarios it is likely that bleaching and mortality can be expected down to the upper mesophotic zone (30-50 m).

5.5 DISCUSSION

Rises in SSTs are expected to increase stratification under a warming planet (IPCC, 2021). In theory, the increases in stratification could allow for thermal protection of mesophotic reefs, however evidence to confirm this hypothesis was not found in the model simulations. The findings in this chapter do however demonstrate that SST warming in stratified locations of GBR will also warm bottom temperatures from 0-50 m. Since tidal energy flux is assumed constant in this study, not accounting for sea level rise, the drivers of the loss of stratification, or the anomalously cool bottom temperature waters could be due to increases in warming in combination with changes to mixing processes.

5.5.1 CAVEATS FROM THE S2P3-R V2.0 DOWNSCALING

The stratification pattern demonstrated in this study could be exacerbated in certain locations due to the lack of horizontal mixing processes simulated in the S2P3-R v2.0 downscaling. Therefore, it will be important to account for open ocean influences, especially boundary currents, or ocean currents along a continental margin (west or eastern boundary currents), in future studies. Frade et al (2018) discusses that the bifurcation of the South Equatorial Current is critical to determining the location of the thermocline and cool relief from deeper waters during times of upwelling. The boundary conditions brought to mesophotic reefs by the branches of the South Equatorial Current, northward Hiri Current and the southward Eastern Australian Current would benefit fringing reefs along this boundary more than reefs embedded in the complex reef matrix. Although, some boundary conditions bring warm water so the cooling influence from these waters should be further explored. Validation using 3D hydrodynamic modelling could provide useful information verifying the locations of stratified reefs in this study while accounting for the influence of boundary currents on the thermal regime. Ocean observations such as gliders, Argo floats, moorings, and other ocean sensors could also provide valuable information recognizing various thermal influences on the reef environment.

5.5.2 SEASONAL PROPERTIES, THERMAL REGIME OF WINTER MIXING

Summer stratification was tested as a theory of thermal refugia for coral reefs across depths 0-50 m on the GBR. This study does not explore the projected influence of warming at depth during winter, a time of more mixing conditions in the water column (Wolanski & Pickard, 2018). In the future under additional warming, winter mixing could further transport the warm surface waters down to reefs that may have been protected by the thermocline. The winter thermal regime could then become more threatening for ecosystems at certain depths into the future. During the 2017 mass bleaching event on the GBR, Frade et al (2018) speculates that the warming event could have occurred due to the lack of seasonal thermal relief from the previous mass bleaching event in 2016. The seasonal variability between temperatures at depth could be a critical

component to their resilience, this is demonstrated in high latitude reef ecosystems such as in Bermuda (Courtney et al., 2017; Jackson et al., 2014; Smith et al., 2013).

5.5.3 WIND PROJECTIONS

Projected changes in large scale wind conditions could alter the locations of stratification identified in this study. Stronger winds could mix warmer waters downwards or weaker winds could allow for additional stratification across depths. As mentioned in chapter 4, there is a great deal of uncertainty surrounding changes to the Walker circulation (DiNezio et al., 2009; Vecchi et al., 2006; Vecchi & Soden, 2007). There is more certainty in the literature surrounding future changes to the Hadley circulation (Frierson et al., 2007; Lu et al., 2007). The wind patterns associated with the projected changes to the Hadley circulation could be driving increases in the wind mixing over the far north and northern GBR and less mixing in the central and southern GBR (Chapter 4, Figure 4.8). Regardless of projected wind conditions, warming of bottom temperature water occurs under higher emissions scenarios and is evident within this study (Figure 5.6). Changes in future winds could be driving warm surface water down to bottom waters that were previously stratified.

5.5.4 SEA LEVEL RISE

Sea Level Rise (SLR) is one additional consideration for the evaluation of stratified locations that may be providing thermal relief to mesophotic coral reefs. The S2P3-R v2.0 simulations do not account for SLR which could alter the tidal energy and water column depth. It is estimated that under RCP8.5 by the end of 2100 there will be ~1 m of SLR (IPCC, 2021). It is unlikely that ~1 m on SLR will have a large impact on the downscaling simulations and therefore, computing resources were not given towards this calculation.

5.6 CONCLUSION

The warming trends demonstrated in this chapter provide an initial step towards understanding climate impacts at depth (0-50 m) and a potential signal of thermal relief for the upper mesophotic reef community under lower emissions trajectories. Under SSP3-7.0 and SSP5-8.5 the increase in bottom temperatures in stratified locations is informative of the loss of anomalously cool bottom temperatures and a potential refuge for corals (Figure 5.6 (a, b), Figure 5.7). Under high emissions, little support is offered for mesophotic reef climate refugia as warming influences bottom temperatures regardless of stratification. The resilience of coral reefs across a range of depths should not solely be dependent on finding areas of refuge to reduce additional stressors such as invasive species, overfishing, and pollution, but on keeping carbon emissions as low as possible.

CHAPTER 6

CONCLUSION AND FUTURE RESEARCH DIRECTIONS

6.1 CONCLUSION

6.1.1 THESIS OVERVIEW

The spatial extent of anomalously warm sea surface temperatures causing the 2016, 2017, and 2020 mass coral bleaching and mortality events impacted the Great Barrier Reef (GBR) on many different levels. Estimated mortality of ~30% of the reef has altered certain locations in community composition and ecosystem function (Bozec et al., 2020; Hughes, Anderson, et al., 2018; Hughes, Kerry, et al., 2018, Stuart-Smith et al., 2018). The ability of corals to recover is now being tested and observed following the warming events. The recent Australia Institute of Marine Science Long-Term Monitoring Report has shown regrowth of faster growing species such as *Acroporids*, but other slow-growing species are less able to recover and remain the most vulnerable species to bleaching (Hughes, Kerry, et al., 2018). Coral tissue loss can further drive outbreaks of coral disease (Miller et al., 2009). For example, following the 2005 Caribbean warming event, an outbreak of five coral diseases impacted 19 *scleractinian* species resulting in an average loss of 51.5% coral cover in the northeast Caribbean (Miller et al., 2009). The mortality of corals further drives the erosion of reef structures that support functional reef ecosystems (Roff et al., 2015) and overgrowth from fleshy algae (McCook et al., 2001). It is imperative to develop an understanding of how the remaining corals on the GBR have persisted under thermal stress. The recent events create opportunities for scientific investigations on the existence of thermal refugia. The information surrounding the reasoning for thermal refugia can be explored through modelling dimensions of time, space, and depth. The timing of shallow water coral bleaching events can be generally informed by the Degree Heating Weeks (DHW) algorithm (Donner et al., 2005; Hughes et al., 2018a; Skirving et al., 2020), or the duration of an anomalous warming event. The DHW algorithm also provides useful

information on the spatial dimension of warming. The onset of 8 DHW has proven to be informative of the spatial patterns influencing mass coral mortality (Donner et al., 2005; Hughes et al., 2018a; Skirving et al., 2020).

Alternatively, areas with the lowest DHWs during recent events signal thermal refugia and can potentially enable the recovery of the reefs that have experienced mortality (Cheung et al., 2021). The locations of thermal refugia from present-day conditions are tested using the S2P3-R v2.0 downscaling method, driven with observations, leading to the discovery of early onset relief from anomalous warming provided by tidal and wind energy flux. These locations prove to be well mixed due to tidal and wind energy in the water column, contributing to thermal relief during bleaching events. Downscaling climate models in this study has enabled our ability to refine projections for areas of previous relief and test the ability of these locations to provide thermal relief into the future. The areas of refugia demonstrate increased warming relative to other areas of the GBR as the planet reaches $\sim 3^{\circ}\text{C}$ of global warming but remain less impacted under lower emissions scenarios (SSP1-1.9 and SSP1-2.6). The changes to the atmospheric patterns at this critical time of warming suggest that increases in wind speed in the northern GBR and decreases in wind speed in the southern GBR are driving these changes under increased warming. Additionally, increases in shortwave radiation are also magnifying the warming of refugia, most dominantly in the nearshore and southern regions of the GBR. The physical processes, atmospheric and oceanic, show important changes to the heat budget over the GBR at this critical time in warming, potentially damaging the remaining areas of the reef with high species richness and diversity.

Further highlighted is the need for bottom temperature coral stress metrics as DHW metrics are surface temperature based and should therefore be used for shallow reefs that are more reflective of surface temperatures. While areas with increases in stratification provide early onset thermal relief to the upper mesophotic zone (30-50 m) with warming below $\sim 1.5^{\circ}\text{C}$, increases in global warming proves to warm bottom temperatures (0-50 m) threatening deeper reefs.

6.1.2 SUMMARY FOR THE BROADER CORAL REEF COMMUNITY

Coral reef studies in different parts of the world can now utilize the S2P3-R v2.0 downscaling method to run relatively simple computing of climate projections on local to regional reefs. The scale used for these studies (10 km) can be adjusted as needed using the resolution of local bathymetry. The methods outlined in each of these chapters can also be used in different parts of the world as physical processes, tidal, wind, or stratification, could be contributing to areas of thermal relief, or climate refugia across a range of depths. These results potentially offer a silver lining to communities that have been deemed as 'losers' of climate change offering hope in finding areas of thermal relief for conservation.

6.1.3 CLIMATE ACTION

Society needs to adhere to SSP1-1.9 which means technology needs to advance to extract CO₂ in combination with becoming less dependent on fossil fuels. The applications of green energy need to outpace the rate of climate emissions. Arguably everything we, as a global society, need to do to adhere to the Paris Agreement has been identified in the most recent IPCC report. The largest push to act upon these changes falls in the hands of major policy makers and the wealthiest people in the world. According to the Paris Agreement, capitalistic markets need to focus more on equality and the global well-being to further reduce emissions. These aspirations for capitalistic markets directly conflict with the nature of capitalism, in that the main motivation is profit. I would suggest a global climate tax upon all goods and services, like a carbon tax but covering all harmful greenhouse gases. The tax can then go towards making green energy more cost-effective and towards progressing other forms of sustainable change. The price of the climate tax could be raised to account for the scale of damages due to climate change. The tax could also be used to be relocate and aid those that are impacted the greatest from climate change, for example, island nations that are displaced due to sea level rise. It is my opinion that economic shifts will

hold the greatest power in driving change, and this may only occur as a result of natural disasters increasing in frequency and intensity.

6.1.4 CORAL REEF MANAGEMENT STRATEGIES

The information in this thesis can be used by managers in a practical sense such as informing zoning plans and aiding in the knowledge of restoration practices. The temporal dimension provides a timeline for increasing threatens to the GBR and potentially coral reefs at large. The best-case emissions scenario, SSP1-1.9 reflects a committed warming from present-day conditions of an additional severe mass coral bleaching event per decade (Chapter 3). The committed warming is expected to occur just after mid-century when the temperatures surpass 1.5°C under SSP1-1.9. For management and policy, this important threshold in time reflects the need for urgent action to protect and conserve the areas that remain less impacted from thermal stress within the next ~10 years. Resilience in this sense can be defined as reducing all possible additional stressors to the reef to aid in the survivability of the reef during warming events. The spatial component of the thesis can broadly inform locations of climate refugia, or areas worth protecting.

Climate vulnerability is just one aspect on top of multiple factors that can influence reef resiliency. Local impacts to the biology of the reef can make the reef more vulnerable and more susceptible to increased degradation. Reducing human impacts to the reef through creating 'no take' zones have proven to be effective strategies (GBRMPA, 2021). In this thesis, thresholds have been established temporally, spatially, and across depths to advise in the timing and spatial protection of less impacted reefs.

In combination with climate action to meet the 1.5°C target in the Paris Agreement, management decisions can be made to reduce additional stress on the reef. For example, crown-of-thorns sea stars (COTS) predate on corals. COTS outbreaks occur on certain reefs throughout the GBR and are culled to aid in the survival of corals (GBRMPA, 2021). Sedimentation and excess nutrients can drive coral mortality in a few

different ways; 1.) reduce light, 2.) drive increases in fleshy algae, and 3.) drive increased predation from COTS (MacNeil et al., 2019). CSIRO's water quality model (eReefs, <https://ereefs.org.au/ereefs>) has successfully informed management of run-off from farms in the watersheds surrounding the GBR (Baird et al., 2021). The improvement in water quality can further aid in easing coral stress.

In addition to limiting threats on the reef from human stressors, more direct forms of management are being taken to aid in the restoration of reefs. Coral larvae studies are increasing in the need to find innovative ways to restore reefs such as assisted gene flow. There are many aspects to coral larvae studies that can aid in restoration activities such as the ability of larvae to settle on different substrates, to spatial and temporal variation in dispersal. Assisted gene flow could aid in the migration of genotypes with heritable traits, or traits that are more resilient to warming (Anthoney et al., 2017). Coral rubble can bind and form coral reefs, recent management interventions are exploring substrate stabilisation strategies to aid in coral recovery (Ceccarelli et al., 2020; Wolfe et al., 2021; Kenyon et al., 2020). Geoengineering solutions are also being explored experimentally on the GBR which test the manipulation of oceanic or atmospheric conditions to reduce temperatures, marine cloud brightening is one example. Geoengineering solutions are often high risk and therefore require careful examination from government and research combined (MacDonald et al., 2019).

Management decisions to restore and conserve the remaining reefs cannot be effective without climate action even under the lowest emission target. The consequences of thermal stress to the GBR under high emissions scenarios, SSP3-7.0 and SSP5-8.5, will have devastating consequences for corals and the biodiversity these reefs currently support. The areas of refugia will become smaller and face greater risk as warming continues. As the refugia locations diminish, the need for protection and conservation will continue to grow in importance.

6.2 FUTURE RESEARCH DIRECTIONS

6.2.1 REGIONAL PROJECTIONS USING 3-D MODELLING

The application of using a regional 3-D model that accounts for vertical and horizontal processes for climate projections will greatly depend on computing costs. While the S2P3-R v2.0 downscaling method does not simulate horizontal advection processes or resolve regions with large freshwater inputs, it is very efficient computationally.

Therefore, the regions where S2P3-R v2.0 fails could be run with eReefs (<https://ereefs.org.au/ereefs>) to optimize computing time. The downscaled outputs from S2P3-R v2.0 and eReefs can then be combined to one product. Following the simulations, more models and scenarios can continue to be added.

Photosynthetically Active Radiation (PAR) is a valuable measurement of the light spectrum reaching corals of various species across a range of depths and can aid in measuring coral bleaching (Edmunds et al., 2018). The biological component of the S2P3-R v2.0 downscaling which outputs PAR, can be improved by replacing the nitrate data from World Ocean Atlas with the nitrate data used in eReefs. Currently, World Ocean Atlas data is limited to ship-based observations and is not fully capturing the influence of land-based nitrate, especially from river inputs. The land-based influences of nitrate are important when simulating biogeochemical coastal processes and these data can be provided by eReefs. One of the main applications of the eReefs model is to simulate excess nutrient run-off on the GBR to better manage agricultural chemicals within certain watersheds (Baird et al., 2021). Therefore, the nutrient data in eReefs is considered extremely sophisticated. The improvements to the biological component of the downscaling through eReefs can contribute to the quality of the PAR output variable which may provide a more realistic depiction of coral bleaching.

The future of downscaling climate models is heading in the 3-D modelling direction and will become more feasible as our computing infrastructure develops. Although, the application of models will be most critical in the next decade to influence climate action and resources such as S2P3-R v2.0 might be more feasible than 3-D models to run more efficient and frequent simulations.

6.2.2 EXPLORATION OF LARGER ATMOSPHERIC CHANGES UNDER WARMING

Thermal relief due to shading from clouds and/or winds will be important for the GBR. This study, among others, has presented reasoning for further exploring climatic patterns such as the summer monsoon, the subtropical ridge and ENSO. The atmospheric patterns surrounding the GBR can influence the spatial patterns of future warming. While there is great uncertainty surrounding the changes expected in larger circulation drivers that influence bleaching conditions, Walker and Hadley circulation are arguably two of the strongest drivers of future change to the GBR. Additionally, oceanographic changes to the location of the bifurcation of the South Equatorial Current as well as the changes to the strength of the Hiri and Eastern Australian Current will be extremely important for future studies.

6.2.3 IMPORTANCE OF DOWNSCALING CLIMATE PROJECTIONS

Most ecological studies do not even explore downscaled data for climate projections and many downscaled products are not accounting for coastal physics such as the interaction of tides and winds with the complex features of the seafloor. The scientific community has yet to master quantifying coastal processes, as they are extremely complex. Given that these are the locations where most ecosystems of relevance and necessity exist for humans, improving upon our ability to measure climate exposure to vulnerable ecosystems such as coral reefs are extremely important. Modelling techniques are growing in their sophistication and their computing time as the window to understand these ecosystems shortens. In an ideal world, computers could perfectly replicate the biogeochemistry and physical processes surrounding an ecosystem such as coral reefs to better inform conservation. In the event of time, the best resources available need to be utilized and compared to make practical decisions on spatiotemporal patterns of not just coral reef vulnerability, but coastal ecosystems at large.

ACKNOWLEDGEMENTS

Thank you to my reviewers for their time and expertise finalising this document and critiquing my research.

Thank you to my principal supervisor, Paul Halloran, for his expertise, patience, and guidance. You always believed in me and our work. It has been an honour and a privilege to be your student. You have inspired and motivated me and for that I will be eternally grateful.

I owe a debt of gratitude to my second supervisor, Peter Mumby, for providing me with additional supervision during the COVID19 pandemic as my QUEX 12- month commitment grew into two and a half years. I had the privilege and the honour of being supervised by an expert scientist. The knowledge and support you provided brought relevance to my research on the Great Barrier Reef.

George Roff (Jez), I value and admire your genuine desire to help students. Your work ethic, humility, and ability to solve complex, statistical problems was extremely uplifting and helpful.

William Skirving, your knowledge, and expertise in applying metrics for coral bleaching was foundational to my research. Ben Marsh, your validation checks on the Degree Heating Weeks code were very helpful.

The field work opportunities I have had have taught me invaluable lessons on corals while reigniting my passion and purpose. Chris Perry, Ines Lange, and Kristen Brown, thank you for the adventures and the opportunities to expand my knowledge beyond my direct research.

The research community in both of my labs provided unconditional support and much needed caffeine breaks. I admire their intelligence, endurance, and their ability to

produce incredible research. Tania Kenyon, you are a natural leader and teacher, you were always there for me. Sarah Holmes, Aimme Coggins, George Manville, Gen Hinde, Neill MacKay, Robert Mason, Andrea Rochner, Fikri Sjahrudin, Amelia Desbiens, Yves-Marie Bozec, Carolina Castro, Morane Le Nohaic, Laura Puk, Karlo Hock, Mandy Cheung, Taison Chang, Hannah Allan, Devin Rowell, Liz Buccheri and Kenny Wolf, each of you added value and reassurance.

My dedicated QUEX cohort gave me strength and friendship. Harriet Goodrick, Steve Burrows, Rebecca Millington, Carolina Chong Montenegro, Leah Clarke, Jodie Koep, Jonathan Birch, Jimmy Wangdi, Francisca Ribeiro, Marta Nabais; your kindness, intelligence, and genuine support will never be forgotten.

I am very grateful to Rosanna Griffith Mumby for the countless chats and your kindness. David Hein-Griggs, for all your rapid computing help. Thank you to Ute Schluster, Emma Kennedy, Simone Blomberg, Peter Cox, and Andrew Watson for your guidance.

I owe special gratitude to my parents, Dan and Barbara McWhorter, for providing me with the opportunity to pursue my passion, giving me an education and teaching me to be resilient and brave. Thank you to my grandparents, Rose, Jim, and Jane for their unconditional love and support. Kevin, Kaitlin, and Kelliann McWhorter, my siblings, you inspire me and rejuvenated me during the many long-distance calls. James Lang-Stevenson thank you for your kindness, care, and comfort.

Doug Stoltz thank you for guiding me to this opportunity, you always want the best for people, and you carry intelligence and a zest for life. Meredith Epp, you inspire me to keep working towards my dreams as I watch you do the same. Kelly Tiece and Kelly Kelleher, thank you for your constant honesty and enthusiasm. Hayley Williamson, EJ Holden, Alysia Fischer, Ryan Beecroft, and Katey Stanely for your friendship and guidance. Dan Hoy, thank you for your last-minute edits and interest in my research.

Special thanks to all the excellent teachers and advisors along the way that have nurtured my passion that led me to this point.

To the QUEX Institute, thank you for funding my PhD between the Universities of Exeter and Queensland. I also want to thank the Great Barrier Reef Marine Park Authority for providing me with a Reef Guardian Research Award and the ARC Centre of Excellence for Coral Reef Studies for providing financial support for excellent information exchange and networking conferences.

REFERENCES

- Abbs, D. (2012). The impact of climate change on the climatology of tropical cyclones in the Australian region.
- Abram, N. J., Gagan, M. K., Cole, J. E., Hantoro, W. S., & Mudelsee, M. (2008). Recent intensification of tropical climate variability in the Indian Ocean. *Nature Geoscience*, 1, 849–853.
- Adachi, Y., Yukimoto, S., Deushi, M., Obata, A., Nakano, H., Tanaka, T. Y., Hosaka, M., Sakami, T., Yoshimura, H., & Hirabara, M. (2013). Basic performance of a new earth system model of the Meteorological Research Institute (MRI-ESM1). *Pap. Meteorol. Geophys*, 64, 1–19.
- Andrews, J. C., & Clegg, S. (1989). Coral Sea circulation and transport deduced from modal information models. *Deep Sea Research Part A. Oceanographic Research Papers*, 36(6), 957–974.
- Baird, A. H., Madin, J. S., Álvarez-Noriega, M., Fontoura, L., Kerry, J. T., Kuo, C.-Y., Precoda, K., Torres-Pulliza, D., Woods, R. M., & Zawada, K. J. (2018). A decline in bleaching suggests that depth can provide a refuge from global warming in most coral taxa. *Marine Ecology Progress Series*, 603, 257–264.
- Baker, A. C., Glynn, P. W., & Riegl, B. (2008). Climate change and coral reef bleaching: An ecological assessment of long-term impacts, recovery trends and future outlook. *Estuarine, Coastal and Shelf Science*, 80(4), 435–471.
- Bakun, A. (2006). Fronts and eddies as key structures in the habitat of marine fish larvae: Opportunity, adaptive response and competitive advantage. *Scientia Marina*, 70(S2), 105–122.
- Barker, S., & Ridgwell, A. (2012). Ocean acidification. *Nature Education Knowledge*, 3(10), 21.
- Beaman, R. J. (2010). 3DGBR: A high-resolution depth model for the Great Barrier Reef and Coral Sea. *Marine and Tropical Sciences Facility (MTSRF) Project*, 2, 13.
- Berkelmans, R., Weeks, S. J., & Steinberga, C. R. (2010). Upwelling linked to warm summers and bleaching on the Great Barrier Reef. *Limnology and Oceanography*, 55(6), 2634–2644.
- Berkelmans, R., & Willis, B. L. (1999). Seasonal and local spatial patterns in the upper thermal limits of corals on the inshore Central Great Barrier Reef. *Coral Reefs*, 18(3), 219–228.
- Berry, G., Jakob, C., & Reeder, M. (2011). Recent global trends in atmospheric fronts. *Geophysical Research Letters*, 38, L21812, <https://doi.org/10.1029/2011GL049481>
- Beyer, H. L., Kennedy, E. V., Beger, M., Chen, C. A., Cinner, J. E., Darling, E. S., Eakin, C. M., Gates, R. D., Heron, S. F., & Knowlton, N. (2018). Risk-sensitive planning for conserving coral reefs under rapid climate change. *Conservation Letters*, 11(6), e12587.
- Bindoff, N. L., Stott, P. A., AchutaRao, K. M., Allen, M. R., Gillett, N., Gutzler, D., Hansingo, K., Hegerl, G., Hu, Y., & Jain, S. (2013). *Detection and attribution of climate change: From global to regional*.
- Bode, M., Bode, L., Choukroun, S., James, M. K., & Mason, L. B. (2018). Resilient reefs may exist, but can larval dispersal models find them? *PLoS Biology*, 16(8), e2005964.
- Bongaerts, P., Ridgway, T., Sampayo, E. M., & Hoegh-Guldberg, O. (2010). Assessing the 'deep reef refugia' hypothesis: Focus on Caribbean reefs. *Coral Reefs*, 29(2), 309–327.

- Bongaerts, P., Riginos, C., Brunner, R., Englebert, N., Smith, S. R., & Hoegh-Guldberg, O. (2017). Deep reefs are not universal refuges: Reseeding potential varies among coral species. *Science Advances*, 3(2), e1602373.
- Bopp, L., Resplandy, L., Orr, J. C., Doney, S. C., Dunne, J. P., Gehlen, M., Halloran, P., Heinze, C., Ilyina, T., & Seferian, R. (2013). Multiple stressors of ocean ecosystems in the 21st century: Projections with CMIP5 models. *Biogeosciences*, 10(10), 6225–6245.
- Boucher, O., Denvil, S., Levavasseur, G., Cozic, A., Caubel, A., Foujols, M.-A., Meurdesoif, Y., Cadule, P., Devilliers, M., Dupont, E., & Lurton, T. (2019). *IPSL IPSL-CM6A-LR model output prepared for CMIP6 ScenarioMIP ssp126*. Earth System Grid Federation. <https://doi.org/10.22033/ESGF/CMIP6.5262>
- Bozec, Y.-M., Hock, K., Mason, R. A., Baird, M. E., Castro-Sanguino, C., Condie, S. A., Puotinen, M., Thompson, A., & Mumby, P. J. (2020). Cumulative impacts across Australia's Great Barrier Reef: A mechanistic evaluation. *BioRxiv*.
- Bricker, S. B., Longstaff, B., Dennison, W., Jones, A., Boicourt, K., Wicks, C., & Woerner, J. (2008). Effects of nutrient enrichment in the nation's estuaries: A decade of change. *Harmful Algae*, 8(1), 21–32.
- Bridge, T. C., Hughes, T. P., Guinotte, J. M., & Bongaerts, P. (2013). Call to protect all coral reefs. *Nature Climate Change*, 3(6), 528–530.
- Bridge, T. C. L., Fabricius, K. E., Bongaerts, P., Wallace, C. C., Muir, P. R., Done, T. J., & Webster, J. M. (2012). Diversity of Scleractinia and Octocorallia in the mesophotic zone of the Great Barrier Reef, Australia. *Coral Reefs*, 31(1), 179–189.
- Brinkman, R., Wolanski, E., Deleersnijder, E., McAllister, F., & Skirving, W. (2002). Oceanic inflow from the coral sea into the Great Barrier Reef. *Estuarine, Coastal and Shelf Science*, 54(4), 655–668.
- Brodie, J. E., Kroon, F. J., Schaffelke, B., Wolanski, E. C., Lewis, S. E., Devlin, M. J., Bohnet, I. C., Bainbridge, Z. T., Waterhouse, J., & Davis, A. M. (2012). Terrestrial pollutant runoff to the Great Barrier Reef: An update of issues, priorities and management responses. *Marine Pollution Bulletin*, 65(4–9), 81–100.
- Brown, B. E., Ambarsari, I., Warner, M. E., Fitt, W. K., Dunne, R. P., Gibb, S. W., & Cummings, D. G. (1999). Diurnal changes in photochemical efficiency and xanthophyll concentrations in shallow water reef corals: Evidence for photoinhibition and photoprotection. *Coral Reefs*, 18(2), 99–105.
- Brown, B. E., Dunne, R. P., Warner, M. E., Ambarsari, I., Fitt, W. K., Gibb, S. W., & Cummings, D. G. (2000). Damage and recovery of Photosystem II during a manipulative field experiment on solar bleaching in the coral *Goniastrea aspera*. *Marine Ecology Progress Series*, 195, 117–124.
- Brown, J. R., Moise, A. F., Colman, R., & Zhang, H. (2016). Will a warmer world mean a wetter or drier Australian monsoon? *Journal of Climate*, 29(12), 4577–4596.
- Bruyère, C. L., Done, J. M., Holland, G. J., & Fredrick, S. (2014). Bias corrections of global models for regional climate simulations of high-impact weather. *Climate Dynamics*, 43(7), 1847–1856.
- Buddemeier, R. W., & Hopley, D. (1988). *Turn-ons and turn-offs: Causes and mechanisms of the initiation and termination of coral reef growth*. Lawrence Livermore National Lab., CA (USA).
- Burrage, D. D. (1993). Coral Sea currents.(The seas around us-number 3). *Corella-Pages: 17: 135-145*.

- Burrage, D. M., Church, J. A., & Steinberg, C. R. (1991). Linear systems analysis of momentum on the continental shelf and slope of the central Great Barrier Reef. *Journal of Geophysical Research: Oceans*, 96(C12), 22169–22190.
- Burrage, D. M., Steinberg, C. R., Skirving, W. J., & Kleypast, J. A. (1996). Mesoscale circulation features of the Great Barrier Reef region inferred from NOAA satellite imagery. *Remote Sensing of Environment*, 56(1), 21–41.
- Byrne, M. P., & O'gorman, P. A. (2013). Land–ocean warming contrast over a wide range of climates: Convective quasi-equilibrium theory and idealized simulations. *Journal of Climate*, 26(12), 4000–4016.
- Cacciapaglia, C., & van Woesik, R. (2016). Climate-change refugia: Shading reef corals by turbidity. *Global Change Biology*, 22(3), 1145–1154.
- Cai, W., Santoso, A., Wang, G., Yeh, S.-W., An, S.-I., Cobb, K. M., Collins, M., Guilyardi, E., Jin, F.-F., & Kug, J.-S. (2015). ENSO and greenhouse warming. *Nature Climate Change*, 5(9), 849–859.
- Cai, W. J., Shi, G., Cowan, T., Bi, D., & Ribbe, J. (2005). The response of the Southern Annular Mode, the East Australian Current, and the southern mid-latitude ocean circulation to global warming. *Geophysical Research Letters - GEOPHYS RES LETT*, 32. <https://doi.org/10.1029/2005GL024701>
- Cai, W., Sullivan, A., & Cowan, T. (2009). Climate change contributes to more frequent consecutive positive Indian Ocean dipole events. *Geophysical Research Letters*, 36, L23704. <https://doi.org/10.1029/2009GL040163>
- Cai, W., Zheng, X.-T., Weller, E., Collins, M., Cowan, T., Lengaigne, M., ... Yamagata, T. (2013). Projected response of the Indian Ocean dipole to greenhouse warming. *Nature Geoscience*, 6, 999–1007.
- Cane, M. A. (1983). Oceanographic events during el nino. *Science*, 222(4629), 1189–1195.
- Canuto, V. M., Howard, A., Cheng, Y., & Dubovikov, M. S. (2001). Ocean turbulence. Part I: One point closure model—Momentum and heat vertical diffusivities. *Journal of Physical Oceanography*, 31(6), 1413–1426.
- Capotondi, A., Alexander, M. A., Bond, N. A., Curchitser, E. N., & Scott, J. D. (2012). Enhanced upper ocean stratification with climate change in the CMIP3 models. *Journal of Geophysical Research: Oceans*, 117(C4).
- Cappo, M., Stowar, M., & MacNeil, A. (2010). The influence of zoning (closure to fishing) on fish communities of the shoals and reef bases of the Great Barrier Reef Marine Park. *Results of Repeated Surveys of the Southern Banks and Cardwell Shoals, and an Overview with Regional Comparisons. Report to the Australian Government's Marine and Tropical Sciences Research Facility (MTSRF). Australian Institute of Marine Science (AIMS), Townsville (73 Pp.)*.
- Catto, J., Nicholls, N., Jakob, C., & Shelton, K. (2014). Atmospheric fronts in current and future climates. *Geophysical Research Letters*, 41, 7642–7650.
- Chang, C. W. J., Tseng, W. L., Hsu, H. H., Keenlyside, N., & Tsuang, B. J. (2015). The Madden-Julian oscillation in a warmer world. *Geophysical Research Letters*, 42, 6034–6042.
- Chelton, D. B., & Schlax, M. G. (1996). Global observations of oceanic Rossby waves. *Science*, 272(5259), 234–238.
- Cheung, M. W., Hock, K., Skirving, W., & Mumby, P. J. (2021). Cumulative bleaching undermines systemic resilience of the Great Barrier Reef. *Current Biology*.

- Church, J. A. (1987). East Australian Current adjacent to the Great Barrier Reef. *Marine and Freshwater Research*, 38(6), 671–683.
- Chollett, I., & Mumby, P. J. (2013). Reefs of last resort: Locating and assessing thermal refugia in the wider Caribbean. *Biological Conservation*, 167, 179–186.
- Church, J. A., Godfrey, J. S., Jackett, D. R., & McDougall, T. J. (1991). A model of sea level rise caused by ocean thermal expansion. *Journal of Climate*, 4(4), 438–456.
- Christensen, J. H., Kanikicharla, K. K., Marshall, G., & Turner, J. (2013). Climate phenomena and their relevance for future regional climate change.
- Coles, R. G., Rasheed, M. A., McKenzie, L. J., Grech, A., York, P. H., Sheaves, M., McKenna, S., & Bryant, C. (2015). The Great Barrier Reef World Heritage Area seagrasses: Managing this iconic Australian ecosystem resource for the future. *Estuarine, Coastal and Shelf Science*, 153, A1–A12.
- Collins, M., An, S.-I., Cai, W., Ganachaud, A., Guilyardi, E., Jin, F.-F., ... Wittenberg, A. (2010). The impact of global warming on the tropical Pacific Ocean and El Niño. *Nature Geoscience*, 3, 391–397.
- Cohen, J., Screen, J. A., Furtado, J. C., Barlow, M., Whittleston, D., Coumou, D., Francis, J., Dethloff, K., Entekhabi, D., & Overland, J. (2014). Recent Arctic amplification and extreme mid-latitude weather. *Nature Geoscience*, 7(9), 627–637.
- Courtney, T. A., Lebrato, M., Bates, N. R., Collins, A., De Putron, S. J., Garley, R., Johnson, R., Molinero, J.-C., Noyes, T. J., & Sabine, C. L. (2017). Environmental controls on modern scleractinian coral and reef-scale calcification. *Science Advances*, 3(11), e1701356.
- Darling, E. S., McClanahan, T. R., Maina, J., Gurney, G. G., Graham, N. A., Januchowski-Hartley, F., Cinner, J. E., Mora, C., Hicks, C. C., & Maire, E. (2019). Social–environmental drivers inform strategic management of coral reefs in the Anthropocene. *Nature Ecology & Evolution*, 3(9), 1341–1350.
- Deliang, C., & Inger, H. (2008). *Empirical-statistical downscaling. Danvers, MA*. USA: World Scientific Publishing Company.
- Deser, C., Phillips, A. S., & Alexander, M. A. (2010). Twentieth century tropical sea surface temperature trends revisited. *Geophysical Research Letters*, 37, L10701, <https://doi.org/10.1029/2010GL043321>
- Dey, R., Lewis, S. C., Arblaster, J. M., & Abram, N. J. (2019). A review of past and projected changes in Australia's rainfall. *Wiley Interdisciplinary Reviews: Climate Change*, 10(3), e577.
- Diaz, H. F., & Bradley, R. S. (2004). The Hadley circulation: Present, past, and future. In *The Hadley circulation: Present, past and future* (pp. 1–5). Springer.
- Dietzel, A., Bode, M., Connolly, S. R., & Hughes, T. P. (2020). Long-term shifts in the colony size structure of coral populations along the Great Barrier Reef. *Proceedings of the Royal Society B*, 287(1936), 20201432.
- DiNezio, P. N., Clement, A. C., Vecchi, G. A., Soden, B. J., Kirtman, B. P., & Lee, S.-K. (2009). Climate response of the equatorial Pacific to global warming. *Journal of Climate*, 22(18), 4873–4892.
- Dixon, A. M., Forster, P. M., Heron, S. F., Stoner, A. M., & Beger, M. (2022). Future loss of local-scale thermal refugia in coral reef ecosystems. *Plos Climate*, 1(2), e0000004.

- Done, T., Whetton, P., Jones, R., Berkemans, R., Lough, J., Skirving, W., & Wooldridge, S. (2003). Global climate change and coral bleaching on the Great Barrier Reef. *Final Report to the State of Queensland Greenhouse Taskforce through the Department of Natural Resources and Mines*, 49.
- Donner, S. D. (2009). Coping with commitment: Projected thermal stress on coral reefs under different future scenarios. *PLoS One*, 4(6), e5712.
- Donner, S. D., Skirving, W. J., Little, C. M., Oppenheimer, M., & Hoegh-Guldberg, O. V. E. (2005). Global assessment of coral bleaching and required rates of adaptation under climate change. *Global Change Biology*, 11(12), 2251–2265.
- Doropoulos, C., Roff, G., Bozec, Y.-M., Zupan, M., Werminghausen, J., & Mumby, P. J. (2016). Characterizing the ecological trade-offs throughout the early ontogeny of coral recruitment. *Ecological Monographs*, 86(1), 20–44.
- Döscher, R., Acosta, M., Alessandri, A., Anthoni, P., Arneth, A., Arsouze, T., Bergmann, T., Bernadello, R., Bousetta, S., Caron, L.-P., Carver, G., Castrillo, M., Catalano, F., Cvijanovic, I., Davini, P., Dekker, E., Doblas-Reyes, F. J., Docquier, D., Echevarria, P., ... Zhang, Q. (2021). The EC-Earth3 Earth System Model for the Climate Model Intercomparison Project 6. *Geosci. Model Dev. Discuss.*, 2021, 1–90. <https://doi.org/10.5194/gmd-2020-446>
- Drenkard, E. J., Stock, C., Ross, A. C., Dixon, K. W., Adcroft, A., Alexander, M., Balaji, V., Bograd, S. J., Butenschön, M., & Cheng, W. (2021). Next-generation regional ocean projections for living marine resource management in a changing climate. *ICES Journal of Marine Science*.
- Dunn, J. G., Sammarco, P. W., & LaFleur Jr, G. (2012). Effects of phosphate on growth and skeletal density in the scleractinian coral *Acropora muricata*: A controlled experimental approach. *Journal of Experimental Marine Biology and Ecology*, 411, 34–44.
- Eakin, C. M., Morgan, J. A., Heron, S. F., Smith, T. B., Liu, G., Alvarez-Filip, L., Baca, B., Bartels, E., Bastidas, C., & Bouchon, C. (2010). Caribbean corals in crisis: Record thermal stress, bleaching, and mortality in 2005. *PloS One*, 5(11), e13969.
- Egbert, G. D., Bennett, A. F., & Foreman, M. G. (1994). TOPEX/POSEIDON tides estimated using a global inverse model. *Journal of Geophysical Research: Oceans*, 99(C12), 24821– 24852.
- Egbert, G. D., & Erofeeva, S. Y. (2002). Efficient inverse modeling of barotropic ocean tides. *Journal of Atmospheric and Oceanic Technology*, 19(2), 183–204.
- Ekman, V. W. (1905). *On the influence of the earth's rotation on ocean-currents*.
- Enríquez, S., Méndez, E. R., & -Prieto, R. I. (2005). Multiple scattering on coral skeletons enhances light absorption by symbiotic algae. *Limnology and Oceanography*, 50(4), 1025–1032.
- Fischer, H., Wahlen, M., Smith, J., Mastoianni, D., & Deck, B. (1999). Ice core records of atmospheric CO₂ around the last three glacial terminations. *Science*, 283(5408), 1712– 1714.
- Fitt, W. K., Gates, R. D., Hoegh-Guldberg, O., Bythell, J. C., Jatkar, A., Grottooli, A. G., Gomez, M., Fisher, P., Lajuenesse, T. C., & Pantos, O. (2009). Response of two species of Indo-Pacific corals, *Porites cylindrica*

- and *Stylophora pistillata*, to short-term thermal stress: The host does matter in determining the tolerance of corals to bleaching. *Journal of Experimental Marine Biology and Ecology*, 373(2).
- Frade, P. R., Bongaerts, P., Englebert, N., Rogers, A., Gonzalez-Rivero, M., & Hoegh-Guldberg, O. (2018). Deep reefs of the Great Barrier Reef offer limited thermal refuge during mass coral bleaching. *Nature Communications*, 9(1), 1–8.
- Frieler, K., Meinshausen, M., Golly, A., Mengel, M., Lebek, K., Donner, S. D., & Hoegh-Guldberg, O. (2013). Limiting global warming to 2 C is unlikely to save most coral reefs. *Nature Climate Change*, 3(2), 165–170.
- Frierson, D. M., Lu, J., & Chen, G. (2007). Width of the Hadley cell in simple and comprehensive general circulation models. *Geophysical Research Letters*, 34(18).
- Gattuso, J.-P., Magnan, A., Billé, R., Cheung, W. W., Howes, E. L., Joos, F., Allemand, D., Bopp, L., Cooley, S. R., & Eakin, C. M. (2015). Contrasting futures for ocean and society from different anthropogenic CO₂ emissions scenarios. *Science*, 349(6243).
- Gillett, N. P., & Fyfe, J. C. (2013). Annular mode changes in the CMIP5 simulations. *Geophysical Research Letters*, 40(6), 1189–1193.
- Gleeson, M. W., & Strong, A. E. (1995). Applying MCSST to coral reef bleaching. *Advances in Space Research*, 16(10), 151–154.
- Glynn, P. W. (1984). Widespread coral mortality and the 1982–83 El Niño warming event. *Environmental Conservation*, 11(2), 133–146.
- Glynn, P. W. (1988). El Niño—Southern oscillation 1982–1983: Nearshore population, community, and ecosystem responses. *Annual Review of Ecology and Systematics*, 19(1), 309–346.
- Glynn, P. W. (1996). Coral reef bleaching: Facts, hypotheses and implications. *Global Change Biology*, 2(6), 495–509.
- Glynn, P. W., & D'croz, L. (1990). Experimental evidence for high temperature stress as the cause of El Niño-coincident coral mortality. *Coral Reefs*, 8(4), 181–191.
- Glynn, P. W., Maté, J. L., Baker, A. C., & Calderón, M. O. (2001). Coral bleaching and mortality in Panama and Ecuador during the 1997–1998 El Niño–Southern Oscillation event: Spatial/temporal patterns and comparisons with the 1982–1983 event. *Bulletin of Marine Science*, 69(1), 79–109.
- Gonzalez-Espinosa, P. C., & Donner, S. D. (2021). Cloudiness reduces the bleaching response of coral reefs exposed to heat stress. *Global Change Biology*, 27(15), 3474–3486.
- Gove, J. M., McManus, M. A., Neuheimer, A. B., Polovina, J. J., Drazen, J. C., Smith, C. R., Merrifield, M. A., Friedlander, A. M., Ehses, J. S., & Young, C. W. (2016). Near-island biological hotspots in barren ocean basins. *Nature Communications*, 7(1), 1–8.
- Graham, N. A., Jennings, S., MacNeil, M. A., Mouillot, D., & Wilson, S. K. (2015). Predicting climate-driven regime shifts versus rebound potential in coral reefs. *Nature*, 518(7537), 94–97.
- Graham, N. A., Wilson, S. K., Carr, P., Hoey, A. S., Jennings, S., & MacNeil, M. A. (2018). Seabirds enhance coral reef productivity and functioning in the absence of invasive rats. *Nature*, 559(7713), 250–253.

- Great Barrier Reef Marine Park Authority (GBRMPA). (2004). *Great Barrier Reef Marine Park Boundary (Version 2)*. Great Barrier Reef Marine Park Authority 2004, Great Barrier Reef Marine [Dataset] 1A604884-6982-4B05-93E3-F025623CB1E3. Retrieved from <http://www.gbrmpa.gov.au/geoportal>.
- Great Barrier Reef Marine Park Authority (GBRMPA). (2009). *Great barrier reef outlook report 2009: In brief*. Great Barrier Reef Marine Park Authority.
- Great Barrier Reef Marine Park Authority (GBRMPA). (2012). *Informing the outlook for Great Barrier Reef coastal ecosystems*.
- Great Barrier Reef Marine Park Authority (GBRMPA). (2013). *Great Barrier Reef Region strategic assessment: Strategic assessment report. Draft for public comment*.
- Great Barrier Reef Marine Park Authority (GBRMPA). (2019). *Great Barrier Reef Outlook Report 2019*. Great Barrier Reef Marine Park Authority.
- Green, E. P., & Bruckner, A. W. (2000). The significance of coral disease epizootiology for coral reef conservation. *Biological Conservation*, 96(3), 347–361.
- Griffies, S. M., Harrison, M. J., Pacanowski, R. C., & Rosati, A. (2004). A technical guide to MOM4. *GFDL Ocean Group Tech. Rep*, 5, 342.
- Griffin, D. A., & Middleton, J. H. (1986). Coastal-trapped waves behind a large continental shelf island, southern Great Barrier Reef. *Journal of Physical Oceanography*, 16(10), 1651–1664.
- Griffin, D. A., Middleton, J. H., & Bode, L. (1987). The tidal and longer-period circulation of Capricornia, Southern Great Barrier Reef. *Marine and Freshwater Research*, 38(4), 461–474.
- Grose, M. R., Risbey, J. S., Moise, A. F., Osbrough, S., Heady, C., Wilson, L., & Erwin, T. (2017). Constraints on southern Australian rainfall change based on atmospheric circulation in CMIP5 simulations. *Journal of Climate*, 30(1), 225–242.
- Grose, M., Timbal, B., Wilson, L., Bathols, J., & Kent, D. (2015). The subtropical ridge in CMIP5 models, and implications for projections of rainfall in southeast Australia. *Australian Meteorological and Oceanographic Journal*, 65(1), 90–106.
- Grottoli, A. G., Rodrigues, L. J., & Palardy, J. E. (2006). Heterotrophic plasticity and resilience in bleached corals. *Nature*, 440(7088), 1186–1189.
- Grottoli, A. G., Warner, M. E., Levas, S. J., Aschaffenburg, M. D., Schoepf, V., McGinley, M., Baumann, J., & Matsui, Y. (2014). The cumulative impact of annual coral bleaching can turn some coral species winners into losers. *Global Change Biology*, 20(12), 3823–3833.
- Halloran, P. R., McWhorter, J. K., Arellano Nava, B., Marsh, R., & Skirving, W. (2021). S2P3-R v2. 0: Computationally efficient modelling of shelf seas on regional to global scales. *Geoscientific Model Development Discussions*, 1–30.
- Harborne, A. R., Nagelkerken, I., Wolff, N. H., Bozec, Y.-M., Dorenbosch, M., Grol, M. G., & Mumby, P. J. (2016). Direct and indirect effects of nursery habitats on coral-reef fish assemblages, grazing pressure and benthic dynamics. *Oikos*, 125(7), 957–967.

- Harriott, V. J. (1985). Mortality rates of scleractinian corals before and during a mass bleaching event. *Marine Ecology Progress Series. Oldendorf*, 21(1), 81–88.
- Harris, P. T., Bridge, T. C., Beaman, R. J., Webster, J. M., Nichol, S. L., & Brooke, B. P. (2013). Submerged banks in the Great Barrier Reef, Australia, greatly increase available coral reef habitat. *ICES Journal of Marine Science*, 70(2), 284–293.
- Helm, K. P., Bindoff, N. L., & Church, J. A. (2011). Observed decreases in oxygen content of the global ocean. *Geophysical Research Letters*, 38(23).
- Heron, S. F., Liu, G., Eakin, C. M., Skirving, W. J., Muller-Karger, F. E., Vega-Rodriguez, M., De La Cour, J. L., Burgess, T. F., Strong, A. E., & Geiger, E. F. (2014). *Climatology development for NOAA Coral Reef Watch's 5-km product suite*.
- Heron, S. F., Maynard, J. A., Van Hooidek, R., & Eakin, C. M. (2016). Warming trends and bleaching stress of the world's coral reefs 1985–2012. *Scientific Reports*, 6(1), 1–14.
- Hock, K., Wolff, N. H., Ortiz, J. C., Condie, S. A., Anthony, K. R., Blackwell, P. G., & Mumby, P. J. (2017). Connectivity and systemic resilience of the Great Barrier Reef. *PLoS Biology*, 15(11), e2003355.
- Hoegh-Guldberg, O. (1999). Climate change, coral bleaching and the future of the world's coral reefs. *Marine and Freshwater Research*, 50(8), 839–866.
- Hoegh-Guldberg, O., Berkelmans, R., & Oliver, J. (1997). Coral bleaching: Implications for the Great Barrier Reef Marine Park. *Proceedings of The Great Barrier Reef Science, Use and Management Conference, 25–29 November, 1996, Townsville, Australia*, 210–224.
- Hoegh-Guldberg, O., Cai, R., Poloczanska, E. S., Brewer, P. G., Sundby, S., Hilmi, K., Fabry, V. J., Jung, S., Skirving, W., & Stone, D. A. (2014). *The ocean*.
- Hoegh-Guldberg, O., Jacob, D., Bindi, M., Brown, S., Camilloni, I., Diedhiou, A., Djalante, R., Ebi, K., Engelbrecht, F., & Guiot, J. (2018). Impacts of 1.5 C global warming on natural and human systems. *Global Warming of 1.5 C. An IPCC Special Report*.
- Hoegh-Guldberg, O., Mumby, P. J., Hooten, A. J., Steneck, R. S., Greenfield, P., Gomez, E., Harvell, C. D., Sale, P. F., Edwards, A. J., & Caldeira, K. (2007). Coral reefs under rapid climate change and ocean acidification. *Science*, 318(5857), 1737–1742.
- Holland, M. M., & Bitz, C. M. (2003). Polar amplification of climate change in coupled models. *Climate Dynamics*, 21(3), 221–232.
- Hopley, D., Smithers, S. G., & Parnell, K. (2007). *The geomorphology of the Great Barrier Reef: Development, diversity and change*. Cambridge University Press.
- Hu, Y., Tao, L., & Liu, J. (2013). Poleward expansion of the Hadley circulation in CMIP5 simulations. *Advances in Atmospheric Sciences*, 30(3), 790–795.
- Hughes, R. N., Hughes, D. J., & Smith, I. P. (2014). Limits to understanding and managing outbreaks of crown-of-thorns starfish (*Acanthaster* spp.). *Oceanography and Marine Biology: An Annual Review*, 52, 133–200.

- Hughes, T. P., Anderson, K. D., Connolly, S. R., Heron, S. F., Kerry, J. T., Lough, J. M., Baird, A. H., Baum, J. K., Berumen, M. L., & Bridge, T. C. (2018). Spatial and temporal patterns of mass bleaching of corals in the Anthropocene. *Science*, *359*(6371), 80–83.
- Hughes, T. P., Baird, A. H., Bellwood, D. R., Card, M., Connolly, S. R., Folke, C., Grosberg, R., Hoegh-Guldberg, O., Jackson, J. B., & Kleypas, J. (2003). Climate change, human impacts, and the resilience of coral reefs. *Science*, *301*(5635), 929–933.
- Hughes, T. P., Kerry, J. T., Álvarez-Noriega, M., Álvarez-Romero, J. G., Anderson, K. D., Baird, A. H., Babcock, R. C., Beger, M., Bellwood, D. R., & Berkelmans, R. (2017). Global warming and recurrent mass bleaching of corals. *Nature*, *543*(7645), 373–377.
- Hughes, T. P., Kerry, J. T., Baird, A. H., Connolly, S. R., Dietzel, A., Eakin, C. M., Heron, S. F., Hoey, A. S., Hoogenboom, M. O., & Liu, G. (2018). Global warming transforms coral reef assemblages. *Nature*, *556*(7702), 492–496.
- Hughes, T. P., Rodrigues, M. J., Bellwood, D. R., Ceccarelli, D., Hoegh-Guldberg, O., McCook, L., Moltschanivskyj, N., Pratchett, M. S., Steneck, R. S., & Willis, B. (2007). Phase shifts, herbivory, and the resilience of coral reefs to climate change. *Current Biology*, *17*(4), 360–365.
- Hurrell, J. W., Kushnir, Y., Ottersen, G., & Visbeck, M. (2003). An overview of the North Atlantic oscillation. *Geophysical Monograph-American Geophysical Union*, *134*, 1–36.
- IPCC, 2018: Global warming of 1.5°C. An IPCC Special Report on the impacts of global warming of 1.5°C, above pre-industrial levels and related global greenhouse gas emission pathways, in the context of, strengthening the global response to the threat of climate change, sustainable development, and efforts to, & eradicate poverty. (n.d.). [V. Masson-Delmotte, P. Zhai, H. O. Pörtner, D. Roberts, J. Skea, P.R. Shukla, A. Pirani, W. Moufouma-Okia, C. Péan, R. Pidcock, S. Connors, J. B. R. Matthews, Y. Chen, X. Zhou, M. I. Gomis, E. Lonnoy, T. Maycock, M. Tignor, T. Waterfield (eds.)]. *In Press*.
- IPCC, 2019: IPCC Special Report on the Ocean and Cryosphere in a Changing Climate. (n.d.). [H.-O. Pörtner, D.C. Roberts, V. Masson-Delmotte, P. Zhai, M. Tignor, E. Poloczanska, K. Mintenbeck, A. Alegría, M. Nicolai, A. Okem, J. Petzold, B. Rama, N.M. Weyer (eds.)]. *In press*.
- IPCC, 2021: Climate Change 2021: The Physical Science Basis. Contribution of Working Group I to the Sixth & Assessment Report of the Intergovernmental Panel on Climate Change. (n.d.). [Masson-Delmotte, V., P. Zhai, A. Pirani, S. L. Connors, C. Péan, S. Berger, N. Caud, Y. Chen, L. Goldfarb, M. I. Gomis, M. Huang, K. Leitzell, E. Lonnoy, J. B. R. Matthews, T. K. Maycock, T. Waterfield, O. Yelekçi, R. Yu and B. Zhou (eds.)]. *Cambridge University Press. In Press*.
- Jackson, J. B. C., Donovan, M. K., Cramer, K. L., & Lam, V. V. (2014). Status and trends of Caribbean coral reefs. *Global Coral Reef Monitoring Network, IUCN, Gland, Switzerland*, 1970–2012.
- Ji, F., Evans, J. P., Argueso, D., Fita, L., & Di Luca, A. (2015). Using large-scale diagnostic quantities to investigate change in East Coast lows. *Climate Dynamics*, *45*, 2443–2453.
- Jokiel, P. L., & Coles, S. L. (1990). Response of Hawaiian and other Indo-Pacific reef corals to elevated temperature. *Coral Reefs*, *8*(4), 155–162.

- Jones, C., & Carvalho, L. M. (2006). Changes in the activity of the madden–Julian oscillation during 1958–2004. *Journal of Climate*, 19, 6353–6370.
- Jones, P. D., & Mann, M. E. (2004). Climate over past millennia. *Reviews of Geophysics*, 42(2).
- Julian, P. R., & Chervin, R. M. (1978). A study of the Southern Oscillation and Walker Circulation phenomenon. *Monthly Weather Review*, 106(10), 1433–1451.
- Kahng, S. E., Garcia-Sais, J. R., Spalding, H. L., Brokovich, E., Wagner, D., Weil, E., Hinderstein, L., & Toonen, R.J. (2010). Community ecology of mesophotic coral reef ecosystems. *Coral Reefs*, 29(2), 255–275.
- Kajikawa, Y., Wang, B., & Yang, J. (2009). A multi-time scale Australian monsoon index. *International Journal of Climatology*, 30, 1114–1120. <https://doi.org/10.1002/joc.1955>
- Kavousi, J., & Keppel, G. (2018). Clarifying the concept of climate change refugia for coral reefs. *ICES Journal of Marine Science*, 75(1), 43–49.
- Kelly, E. L., Eynaud, Y., Williams, I. D., Sparks, R. T., Dailer, M. L., Sandin, S. A., & Smith, J. E. (2017). A budget of algal production and consumption by herbivorous fish in an herbivore fisheries management area, Maui, Hawaii. *Ecosphere*, 8(8), e01899.
- Kent, D. M., Kirono, D. G., Timbal, B., & Chiew, F. H. (2013). Representation of the Australian sub-tropical ridge in the CMIP3 models. *International Journal of Climatology*, 33(1), 48–57.
- Kenyon, T. M., Doropoulos, C., Dove, S., Webb, G. E., Newman, S. P., Sim, C. W., Arzan, M., & Mumby, P. J. (2020). The effects of rubble mobilisation on coral fragment survival, partial mortality and growth. *Journal of Experimental Marine Biology and Ecology*, 533, 151467.
- Kerry, J. T., & Bellwood, D. R. (2015). Do tabular corals constitute keystone structures for fishes on coral reefs? *Coral Reefs*, 34(1), 41–50.
- King, A. D., Karoly, D. J., & Henley, B. J. (2017). Australian climate extremes at 1.5 C and 2 C of global warming. *Nature Climate Change*, 7(6), 412–416.
- Kitahara, M. V., Fukami, H., Benzoni, F., & Huang, D. (2016). The new systematics of Scleractinia: Integrating molecular and morphological evidence. In *The Cnidaria, past, present and future* (pp. 41–59). Springer.
- Kleypas, J. A., & Burrage, D. M. (1994). Satellite observations of circulation in the southern Great Barrier Reef, Australia. *International Journal of Remote Sensing*, 15(10), 2051–2063.
- Kleypas, J. A., Castruccio, F. S., Curchitser, E. N., & Mcleod, E. (2015). The impact of ENSO on coral heat stress in the western equatorial Pacific. *Global Change Biology*, 21(7), 2525–2539.
- Kleypas, J. A., & Yates, K. K. (2009). Coral reefs and ocean acidification. *Oceanography*, 22(4), 108–117.
- Knutson, T. R., McBride, J. L., Chan, J., Emanuel, K., Holland, G., Landsea, C., Held, I., Kossin, J. P., Srivastava, A. K., & Sugi, M. (2010). Tropical cyclones and climate change. *Nature Geoscience*, 3(3), 157–163.
- Knutson, T. R., Sirutis, J. J., Garner, S. T., Vecchi, G. A., & Held, I. M. (2008). Simulated reduction in Atlantic hurricane frequency under twenty-first-century warming conditions. *Nature Geoscience*, 1(6), 359–364.
- Kwiatkowski, L., Cox, P. M., Economou, T., Halloran, P. R., Mumby, P. J., Booth, B. B., Carilli, J., & Guzman, H. M. (2013). Caribbean coral growth influenced by anthropogenic aerosol emissions. *Nature Geoscience*, 6(5), 362–366.

- Kwiatkowski, L., Halloran, P. R., Mumby, P. J., & Stephenson, D. B. (2014). What spatial scales are believable for climate model projections of sea surface temperature? *Climate Dynamics*, 43(5–6), 1483–1496.
- Lamb, J. B., Van De Water, J. A., Bourne, D. G., Altier, C., Hein, M. Y., Fiorenza, E. A., Abu, N., Jompa, J., & Harvell, C. D. (2017). Seagrass ecosystems reduce exposure to bacterial pathogens of humans, fishes, and invertebrates. *Science*, 355(6326), 731–733.
- Lange, I. D., Perry, C. T., & Alvarez-Filip, L. (2020). Carbonate budgets as indicators of functional reef “health”: A critical review of data underpinning census-based methods and current knowledge gaps. *Ecological Indicators*, 110, 105857.
- Lavender, S. L., & Walsh, K. J. E. (2011). Dynamically downscaled simulations of Australian region tropical cyclones in current and future climates. *Geophysical Research Letters*, 38(10).
- Lee, S.-H., & Seo, K.-H. (2011). A multi-scale analysis of the interdecadal change in the Madden-Julian oscillation. *Atmosphere*, 21, 143–149.
- Lemos, M. C., & Rood, R. B. (2010). Climate projections and their impact on policy and practice. *Wiley Interdisciplinary Reviews: Climate Change*, 1(5), 670–682.
- Lenth, R., Singmann, H., Love, J., Buerkner, P., & Herve, M. (2018). Emmeans: Estimated marginal means, aka least-squares means. *R Package Version*, 1(1), 3.
- Lenth, R. V. (2021). *Emmeans: Estimated marginal means, aka least-squares means. R package version 1.6. 1.*
- Liao, E., Lu, W., Yan, X.-H., Jiang, Y., & Kidwell, A. (2015). The coastal ocean response to the global warming acceleration and hiatus. *Scientific Reports*, 5(1), 1–10.
- Lindfield, S. J., Harvey, E. S., Halford, A. R., & McIlwain, J. L. (2016). Mesophotic depths as refuge areas for fishery-targeted species on coral reefs. *Coral Reefs*, 35(1), 125–137.
- Liu, G., Strong, A. E., Skirving, W., & Arzayus, L. F. (2006). Overview of NOAA coral reef watch program’s near-real time satellite global coral bleaching monitoring activities. *Proceedings of the 10th International Coral Reef Symposium*, 1793, 1783–1793.
- Logan, C. A., Dunne, J. P., Ryan, J. S., Baskett, M. L., & Donner, S. D. (2021). Quantifying global potential for coral evolutionary response to climate change. *Nature Climate Change*.
- Lough, J. M. (2007). *Climate and climate change on the Great Barrier Reef*.
- Lough, J. M., Anderson, K. D., & Hughes, T. P. (2018). Increasing thermal stress for tropical coral reefs: 1871–2017. *Scientific Reports*, 8(1), 1–8.
- Lough, J. M., & Barnes, D. J. (2000). Environmental controls on growth of the massive coral *Porites*. *Journal of Experimental Marine Biology and Ecology*, 245(2), 225–243.
- Loya, Y., Eyal, G., Treibitz, T., Lesser, M. P., & Appeldoorn, R. (2016). *Theme section on mesophotic coral ecosystems: Advances in knowledge and future perspectives*. Springer.
- Loya, Y., Sakai, K., Yamazato, K., Nakano, Y., Sambali, H., & Van Woesik, R. (2001). Coral bleaching: The winners and the losers. *Ecology Letters*, 4(2), 122–131.
- Lu, J., Vecchi, G. A., & Reichler, T. (2007). Expansion of the Hadley cell under global warming. *Geophysical Research Letters*, 34(6).

- Luckhurst, B. E., & Luckhurst, K. (1978). Analysis of the influence of substrate variables on coral reef fish communities. *Marine Biology*, 49(4), 317–323.
- Luo, J.-J., Sasaki, W., & Masumoto, Y. (2012). Indian Ocean warming modulates Pacific climate change. *Proceedings of the National Academy of Sciences*, 109, 18701–18706.
- Machu, E., Goubanova, K., Le Vu, B., Gutknecht, E., & Garçon, V. (2015). Downscaling biogeochemistry in the Benguela eastern boundary current. *Ocean Modelling*, 90, 57–71.
- MacMartin, D. G., Ricke, K. L., & Keith, D. W. (2018). Solar geoengineering as part of an overall strategy for meeting the 1.5 C Paris target. *Philosophical Transactions of the Royal Society A: Mathematical, Physical and Engineering Sciences*, 376(2119), 20160454.
- Madden, R. A., & Julian, P. R. (1971). Detection of a 40–50 day oscillation in the zonal wind in the tropical Pacific. *Journal of Atmospheric Sciences*, 28(5), 702–708.
- Madden, R. A., & Julian, P. R. (1972). Description of global-scale circulation cells in the tropics with a 40–50 day period. *Journal of Atmospheric Sciences*, 29(6), 1109–1123.
- Madden, R. A., & Julian, P. R. (1994). Observations of the 40–50-day tropical oscillation—A review. *Monthly Weather Review*, 122(5), 814–837.
- Madin, J. S., Baird, A. H., Bridge, T. C., Connolly, S. R., Zawada, K. J., & Dornelas, M. (2018). Cumulative effects of cyclones and bleaching on coral cover and species richness at Lizard Island. *Marine Ecology Progress Series*, 604, 263–268.
- Mann, K. H., & Lazier, J. R. (2013). *Dynamics of marine ecosystems: Biological-physical interactions in the oceans*. John Wiley & Sons.
- Marsh, H., O'Shea, T. J., & Reynolds III, J. E. (2012). *Ecology and conservation of the Sirenia: Dugongs and manatees* (Issue 18). Cambridge University Press.
- Marsh, R., Hickman, A. E., & Sharples, J. (2015). S2P3-R (v1. 0): A framework for efficient regional modelling of physical and biological structures and processes in shelf seas. *Geoscientific Model Development*, 8(10), 3163–3178.
- Marshall, D. (1995). Influence of topography on the large-scale ocean circulation. *Journal of Physical Oceanography*, 25(7), 1622–1635.
- Marshall, G. J. (2003). Trends in the Southern Annular Mode from observations and reanalyses. *Journal of Climate*, 16(24), 4134–4143.
- Marshall, P. A., & Baird, A. H. (2000). Bleaching of corals on the Great Barrier Reef: Differential susceptibilities among taxa. *Coral Reefs*, 19(2), 155–163.
- Marshall, J. F., & Davies, P. J. (1988). Halimeda bioherms of the northern Great Barrier Reef. *Coral Reefs*, 6(3), 139–148.
- Mather, P., & Bennett, I. (1984). *A coral reef handbook: A guide to the fauna, flora and geology of Heron Island and adjacent reefs and cays*.

- Maynard, J. A., Beeden, R., Puotinen, M., Johnson, J. E., Marshall, P., Van Hooidonk, R., Heron, S. F., Devlin, M., Lawrey, E., & Dryden, J. (2016). Great Barrier Reef no-take areas include a range of disturbance regimes. *Conservation Letters*, 9(3), 191–199.
- McCook, L., Jompa, J., & Diaz-Pulido, G. (2001). Competition between corals and algae on coral reefs: A review of evidence and mechanisms. *Coral Reefs*, 19(4), 400–417.
- McGowan, H., & Theobald, A. (2017). ENSO weather and coral bleaching on the Great Barrier Reef, Australia. *Geophysical Research Letters*, 44(20), 10,601–10,607.
- McKenzie, L. J., Collier, C. J., Langlois, L. A., Yoshida, R. L., Smith, N., & Waycott, M. (2017). *Marine Monitoring Program: Annual report for inshore seagrass monitoring 2015-2016*.
- McLeod, E., Salm, R., Green, A., & Almany, J. (2009). Designing marine protected area networks to address the impacts of climate change. *Frontiers in Ecology and the Environment*, 7(7), 362–370.
- McManus, L. C., Forrest, D. L., Tekwa, E. W., Schindler, D. E., Colton, M. A., Webster, M. M., Essington, T. E., Palumbi, S. R., Mumby, P. J., & Pinsky, M. L. (2021). Evolution and connectivity influence the persistence and recovery of coral reefs under climate change in the Caribbean, Southwest Pacific, and Coral Triangle. *Global Change Biology*.
- McPhaden, M. J. (2004). Evolution of the 2002/03 El Niño. *Bulletin of the American Meteorological Society*, 85(5), 677–696.
- McWhorter, J. K., Halloran, P. R., Roff, G., Skirving, W. J., Perry, C. T., & Mumby, P. J. (2021). The importance of 1.5° C warming for the Great Barrier Reef. *Global Change Biology*.
- McWhorter, J. K., Halloran, P. R., Roff, G., Skirving, W. J., & Mumby, P. J. (2022). Climate refugia on the Great Barrier Reef fail when global warming exceeds 3°C. *Global Change Biology*.
- Merchant, C. J., Embury, O., Bulgin, C. E., Block, T., Corlett, G. K., Fiedler, E., Good, S. A., Mittaz, J., Rayner, N. A., & Berry, D. (2019). Satellite-based time-series of sea-surface temperature since 1981 for climate applications. *Scientific Data*, 6(1), 1–18.
- Merrifield, M. A., & Maltrud, M. E. (2011). Regional sea level trends due to a Pacific trade wind intensification. *Geophysical Research Letters*, 38(21).
- Messmer, V., Jones, G. P., Munday, P. L., Holbrook, S. J., Schmitt, R. J., & Brooks, A. J. (2011). Habitat biodiversity as a determinant of fish community structure on coral reefs. *Ecology*, 92(12), 2285–2298.
- Middleton, J. H., Coutis, P., Griffin, D. A., Macks, A., McTaggart, A., Merrifield, M. A., & Nippard, G. J. (1994). Circulation and water mass characteristics of the southern Great Barrier Reef. *Marine and Freshwater Research*, 45(1), 1–18.
- Miller, J., Muller, E., Rogers, C., Waara, R., Atkinson, A., Whelan, K. R. T., Patterson, M., & Witcher, B. (2009). Coral disease following massive bleaching in 2005 causes 60% decline in coral cover on reefs in the US Virgin Islands. *Coral Reefs*, 28(4), 925.
- Morelli, T. L., Daly, C., Dobrowski, S. Z., Dulen, D. M., Ebersole, J. L., Jackson, S. T., Lundquist, J. D., Millar, C. I., Maher, S. P., & Monahan, W. B. (2016). Managing climate change refugia for climate adaptation. *PLoS One*, 11(8), e0159909.

- Morita, T., Nakićenović, N., & Robinson, J. (2000). Overview of mitigation scenarios for global climate stabilization based on new IPCC emission scenarios (SRES). *Environmental Economics and Policy Studies*, 3(2), 65–88.
- Moum, J. N., & Nash, J. D. (2000). Topographically induced drag and mixing at a small bank on the continental shelf. *Journal of Physical Oceanography*, 30(8), 2049–2054.
- Mumby, P., Chisholm, J., Edwards, A., Clark, C., Roark, E., Andrefouet, S., & Jaubert, J. (2001). Unprecedented bleaching-induced mortality in *Porites* spp. At Rangiroa Atoll, French Polynesia. *Marine Biology*, 139(1), 183–189.
- Mumby, P. J., Elliott, I. A., Eakin, C. M., Skirving, W., Paris, C. B., Edwards, H. J., Enríquez, S., Iglesias-Prieto, R., Cherubin, L. M., & Stevens, J. R. (2011). Reserve design for uncertain responses of coral reefs to climate change. *Ecology Letters*, 14(2), 132–140.
- Mumby, P. J., Steneck, R. S., Adjeroud, M., & Arnold, S. N. (2016). High resilience masks underlying sensitivity to algal phase shifts of Pacific coral reefs. *Oikos*, 125(5), 644–655.
- Nicholls, N., Landsea, C., & Gill, J. (1998). Recent trends in Australian region tropical cyclone activity. *Meteorology and Atmospheric Physics*, 65, 197–205.
- Nugues, M. M., & Roberts, C. M. (2003). Coral mortality and interaction with algae in relation to sedimentation. *Coral Reefs*, 22(4), 507–516.
- Oliver, E. C., Donat, M. G., Burrows, M. T., Moore, P. J., Smale, D. A., Alexander, L. V., Benthuisen, J. A., Feng, M., Gupta, A. S., & Hobday, A. J. (2018). Longer and more frequent marine heatwaves over the past century. *Nature Communications*, 9(1), 1–12.
- O'Neill, B. C., Tebaldi, C., Vuuren, D. P. van, Eyring, V., Friedlingstein, P., Hurtt, G., Knutti, R., Kriegler, E., Lamarque, J.-F., & Lowe, J. (2016). The scenario model intercomparison project (ScenarioMIP) for CMIP6. *Geoscientific Model Development*, 9(9), 3461–3482.
- Palumbi, S. R. (2004). Marine reserves and ocean neighborhoods: The spatial scale of marine populations and their management. *Annu. Rev. Environ. Resour.*, 29, 31–68.
- Pankhurst, N. W., & Munday, P. L. (2011). Effects of climate change on fish reproduction and early life history stages. *Marine and Freshwater Research*, 62(9), 1015–1026.
- Pawlowicz, R., Wright, D. G., & Millero, F. J. (2011). The effects of biogeochemical processes on oceanic conductivity/salinity/density relationships and the characterization of real seawater. *Ocean Science*, 7(3), 363–387.
- Pepler, A. S., Di Luca, A., Ji, F., Alexander, L. V., Evans, J. P., & Sherwood, S. C. (2016). Projected changes in east Australian midlatitude cyclones during the 21st century. *Geophysical Research Letters*, 43, 334–340.
- Pickard, G. L., Donguy, J.-R., Hénin, C., & Rougerie, F. (1977). *A review of the physical oceanography of the Great Barrier Reef and western Coral Sea*.
- Pierson, D. C., Kratzer, S., Strömbeck, N., & Håkansson, B. (2008). Relationship between the attenuation of downwelling irradiance at 490 nm with the attenuation of PAR (400 nm–700 nm) in the Baltic Sea. *Remote Sensing of Environment*, 112(3), 668–680.

- Pinheiro, J., Bates, D., DebRoy, S., & Sarkar, D. (2021). *R Core Team (2021). Nlme: Linear and Nonlinear Mixed Effects Models. R package version 3.1-152.*
- Pitcher, R., Doherty, P., Arnold, P., Hooper, J., Gribble, N., Chalmers, S., Coles, R., Ehrke, B., Good, N., & Kistler, S. (2007). *Seabed biodiversity on the continental shelf of the Great Barrier Reef World Heritage Area.*
- Polónia, A. R. M., Cleary, D. F. R., de Voogd, N. J., Renema, W., Hoeksema, B. W., Martins, A., & Gomes, N. C. M. (2015). Habitat and water quality variables as predictors of community composition in an Indonesian coral reef: A multi-taxon study in the Spermonde Archipelago. *Science of the Total Environment*, 537, 139–151.
- Polzin, K. L., Toole, J. M., Ledwell, J. R., & Schmitt, R. W. (1997). Spatial variability of turbulent mixing in the abyssal ocean. *Science*, 276(5309), 93–96.
- Pomeroy, L. R. (1974). The ocean's food web, a changing paradigm. *Bioscience*, 24(9), 499–504.
- Ponder, W., Hutchings, P., & Chapman, R. (2002). Overview of the conservation of Australian marine invertebrates. *Report for Environment Australia, Australian Museum, Sydney.*
- Power, S., Delage, F., Chung, C., Kociuba, G., & Keay, K. (2013). Robust twenty-first-century projections of El Niño and related precipitation variability. *Nature*, 502(7472), 541–545.
- Pozo Buil, M., Jacox, M. G., Fiechter, J., Alexander, M. A., Bograd, S. J., Curchitser, E. N., Edwards, C. A., Rykaczewski, R. R., & Stock, C. A. (2021). A dynamically downscaled ensemble of future projections for the California Current System. *Frontiers in Marine Science*, 8, 324.
- Pratchett, M. S., Munday, P. L., Wilson, S. K., Graham, N. A., Cinner, J. E., Bellwood, D. R., Jones, G. P., Polunin, N. V., & McClanahan, T. R. (2008). Effects of climate-induced coral bleaching on coral-reef fishes—Ecological and economic consequences. In *Oceanography and marine biology* (pp. 257–302). CRC Press.
- Read, M. A., & Limpus, C. J. (2002). The green turtle, *Chelonia mydas*, in Queensland: Feeding ecology of immature turtles in Moreton Bay, southeastern Queensland. *MEMOIRS QUEENSLAND MUSEUM*, 48(1), 207–214.
- Read, M., Hemson, G., & Olds, J. (2018). Value of islands for the marine environment. *Australian Island Arks: Conservation, Management and Opportunities*, 193–205.
- Reaser, J. K., Pomerance, R., & Thomas, P. O. (2000). Coral bleaching and global climate change: Scientific findings and policy recommendations. *Conservation Biology*, 14(5), 1500–1511.
- Riahi, K., Vuuren, D. P. van, Kriegler, E., Edmonds, J., O'Neill, B. C., Fujimori, S., Bauer, N., Calvin, K., Dellink, R., Fricko, O., Lutz, W., Popp, A., Cuaresma, J. C., KC, S., Leimbach, M., Jiang, L., Kram, T., Rao, S., Emmerling, J., ... Tavoni, M. (2017). The Shared Socioeconomic Pathways and their energy, land use, and greenhouse gas emissions implications: An overview. *Global Environmental Change*, 42, 153–168.
<https://doi.org/10.1016/j.gloenvcha.2016.05.009>
- Ridgway, K. R., Benthuisen, J. A., & Steinberg, C. (2018). Closing the gap between the Coral Sea and the equator: Direct observations of the north Australian western boundary currents. *Journal of Geophysical Research: Oceans*, 123(12), 9212–9231.
- Riegl, B., & Piller, W. E. (2003). Possible refugia for reefs in times of environmental stress. *International Journal of Earth Sciences*, 92(4), 520–531.

- Riley, G. A. (1957). Phytoplankton of the north central sargasso sea, 1950–52 1. *Limnology and Oceanography*, 2(3), 252–270.
- Risbey, J. S., Pook, M. J., McIntosh, P. C., Wheeler, M. C., & Hendon, H. H. (2009). On the remote drivers of rainfall variability in Australia. *Monthly Weather Review*, 137(10), 3233–3253.
- Robinson, G. (1982). Influence of the 1982–83 El Niño on Galápagos marine life. *El Niño in the Galápagos Islands: The, 1983*, 153–190.
- Rocha, L. A., Pinheiro, H. T., Shepherd, B., Papastamatiou, Y. P., Luiz, O. J., Pyle, R. L., & Bongaerts, P. (2018). Mesophotic coral ecosystems are threatened and ecologically distinct from shallow water reefs. *Science*, 361(6399), 281–284.
- Rodrigues, L. J., & Grottoli, A. G. (2007). Energy reserves and metabolism as indicators of coral recovery from bleaching. *Limnology and Oceanography*, 52(5), 1874–1882.
- Roff, G., Zhao, J., & Mumby, P. J. (2015). Decadal-scale rates of reef erosion following El Niño related mass coral mortality. *Global Change Biology*, 21(12), 4415–4424.
- Rogelj, J., Luderer, G., Pietzcker, R. C., Kriegler, E., Schaeffer, M., Krey, V., & Riahi, K. (2015). Energy system transformations for limiting end-of-century warming to below 1.5 C. *Nature Climate Change*, 5(6), 519–527.
- Rowan, R., Knowlton, N., Baker, A., & Jara, J. (1997). Landscape ecology of algal symbionts creates variation in episodes of coral bleaching. *Nature*, 388(6639), 265–269.
- Safaie, A., Silbiger, N. J., McClanahan, T. R., Pawlak, G., Barshis, D. J., Hench, J. L., Rogers, J. S., Williams, G. J., & Davis, K. A. (2018). High frequency temperature variability reduces the risk of coral bleaching. *Nature Communications*, 9(1), 1–12.
- Sanderson, B. M., O'Neill, B. C., & Tebaldi, C. (2016). What would it take to achieve the Paris temperature targets? *Geophysical Research Letters*, 43(13), 7133–7142.
- Santoso, A., McGregor, S., Jin, F.-F., Cai, W., England, M. H., An, S.-I., McPhaden, M. J., & Guilyardi, E. (2013). Late-twentieth-century emergence of the El Niño propagation asymmetry and future projections. *Nature*, 504(7478), 126–130.
- Schleussner, C.-F., Lissner, T. K., Fischer, E. M., Wohland, J., Perrette, M., Golly, A., Rogelj, J., Childers, K., Schewe, J., & Frieler, K. (2016). Differential climate impacts for policy relevant limits to global warming: The case of 1.5 C and 2 C. *Earth System Dynamics*, 7(2), 327–351.
- Schramek, T. A., Colin, P. L., Merrifield, M. A., & Terrill, E. J. (2018). Depth-dependent thermal stress around corals in the tropical Pacific Ocean. *Geophysical Research Letters*, 45(18), 9739–9747.
- Seferian, R. (2018). *CNRM-CERFACS CNRM-ESM2-1 model output prepared for CMIP6 CMIP*. Earth System Grid Federation. <https://doi.org/10.22033/ESGF/CMIP6.1391>
- Séférian, R., Nabat, P., Michou, M., Saint-Martin, D., Voldoire, A., Colin, J., Decharme, B., Delire, C., Berthet, S., & Chevallier, M. (2019). Evaluation of CNRM Earth System Model, CNRM-ESM2-1: Role of Earth System Processes in Present-Day and Future Climate. *Journal of Advances in Modeling Earth Systems*, 11(12), 4182–4227.

- Seidel, D. J., Fu, Q., Randel, W. J., & Reichler, T. J. (2008). Widening of the tropical belt in a changing climate. *Nature Geoscience*, 1(1), 21–24.
- Sellar, A. A., Jones, C. G., Mulcahy, J. P., Tang, Y., Yool, A., Wiltshire, A., O’connor, F. M., Stringer, M., Hill, R., & Palmieri, J. (2019). UKESM1: Description and evaluation of the UK Earth System Model. *Journal of Advances in Modeling Earth Systems*, 11(12), 4513–4558.
- Semmler, R. F., Hoot, W. C., & Reaka, M. L. (2017). Are mesophotic coral ecosystems distinct communities and can they serve as refugia for shallow reefs? *Coral Reefs*, 36(2), 433–444.
- Sharples, J. (1999). Investigating the seasonal vertical structure of phytoplankton in shelf seas. *Marine Models*, 1(1–4), 3–38.
- Sharples, J., Ross, O. N., Scott, B. E., Greenstreet, S. P., & Fraser, H. (2006). Inter-annual variability in the timing of stratification and the spring bloom in the North-western North Sea. *Continental Shelf Research*, 26(6), 733–751.
- Sheppard, C. R. (2003). Predicted recurrences of mass coral mortality in the Indian Ocean. *Nature*, 425(6955), 294–297.
- Simpson, J. H., & Sharples, J. (2012). *Introduction to the physical and biological oceanography of shelf seas*. Cambridge University Press.
- Skirving, W., Enríquez, S., Hedley, J. D., Dove, S., Eakin, C. M., Mason, R. A., De La Cour, J. L., Liu, G., Hoegh-Guldberg, O., & Strong, A. E. (2017). Remote sensing of coral bleaching using temperature and light: Progress towards an operational algorithm. *Remote Sensing*, 10(1), 18.
- Skirving, W., & Guinotte, J. (2000). The sea surface temperature story on the Great Barrier Reef during the coral bleaching event of 1998. In *Oceanographic Processes of Coral Reefs* (pp. 321–334). CRC Press.
- Skirving, W., Heron, M., & Heron, S. (2006). The hydrodynamics of a bleaching event: Implications for management and monitoring. *Coral Reefs and Climate Change: Science and Management*, 61, 145–161.
- Skirving, W., Heron, S. F., Marsh, B. L., Liu, G., De La Cour, J. L., Geiger, E. F., & Eakin, C. M. (2019). The relentless march of mass coral bleaching: A global perspective of changing heat stress. *Coral Reefs*, 38(4), 547–557.
- Skirving, W., Marsh, B., De La Cour, J., Liu, G., Harris, A., Maturi, E., Geiger, E., & Eakin, C. M. (2020). CoralTemp and the Coral Reef Watch Coral Bleaching Heat Stress Product Suite Version 3.1. *Remote Sensing*, 12(23), 3856.
- Smith, S. D., & Banke, E. G. (1975). Variation of the sea surface drag coefficient with wind speed. *Quarterly Journal of the Royal Meteorological Society*, 101(429), 665–673.
- Smith, S. R., Sarkis, S., Murdoch, T. J., Weil, E., Croquer, A., Bates, N. R., Johnson, R. J., de Putron, S., & Andersson, A. J. (2013). Threats to coral reefs of Bermuda. In *Coral reefs of the United Kingdom overseas territories* (pp. 173–188). Springer.
- Smith, T. B., Brandtneris, V. W., Canals, M., Brandt, M. E., Martens, J., Brewer, R. S., Kadison, E., Kammann, M., Keller, J., & Holstein, D. M. (2016). Potential structuring forces on a shelf edge upper mesophotic coral ecosystem in the US Virgin Islands. *Frontiers in Marine Science*, 3, 115.

- Solomon, S., Manning, M., Marquis, M., & Qin, D. (2007). *Climate change 2007-the physical science basis: Working group I contribution to the fourth assessment report of the IPCC* (Vol. 4). Cambridge university press.
- Speare, P., & Stowar, M. (2007). Preliminary findings from the first baseline survey of the Magnetic Shoals. *Project Progress Report. Reef and Rainforest Research Centre*.
- Steinberg, C. (2007). *Impacts of climate change on the physical oceanography of the Great Barrier Reef*.
- Stella, J. S., Pratchett, M. S., Hutchings, P. A., & Jones, G. P. (2011). Diversity, importance and vulnerability of coral-associated invertebrates. *Oceanography and Marine Biology: An Annual Review*, 49, 43–116.
- Stimson, J., Sakai, K., & Sembali, H. (2002). Interspecific comparison of the symbiotic relationship in corals with high and low rates of bleaching-induced mortality. *Coral Reefs*, 21(4), 409–421.
- Stocker, T. (2014). *Climate change 2013: The physical science basis: Working Group I contribution to the Fifth assessment report of the Intergovernmental Panel on Climate Change*. Cambridge university press.
- Talley, L. D., Feely, R. A., Sloyan, B. M., Wanninkhof, R., Baringer, M. O., Bullister, J. L., Carlson, C. A., Doney, S. C., Fine, R. A., & Firing, E. (2016). Changes in ocean heat, carbon content, and ventilation: A review of the first decade of GO-SHIP global repeat hydrography. *Annual Review of Marine Science*, 8, 185–215.
- Teh, L. S., Teh, L. C., & Sumaila, U. R. (2013). A global estimate of the number of coral reef fishers. *PLoS One*, 8(6), e65397.
- Thomas, C. J., Bridge, T. C., Figueiredo, J., Deleersnijder, E., & Hanert, E. (2015). Connectivity between submerged and near-sea-surface coral reefs: Can submerged reef populations act as refuges? *Diversity and Distributions*, 21(10), 1254–1266.
- Thompson, D. W., Solomon, S., Kushner, P. J., England, M. H., Grise, K. M., & Karoly, D. J. (2011). Signatures of the Antarctic ozone hole in Southern Hemisphere surface climate change. *Nature Geoscience*, 4, 741–749.
- Timbal, B., & Drosowsky, W. (2013). The relationship between the decline of Southeastern Australian rainfall and the strengthening of the subtropical ridge. *International Journal of Climatology*, 33(4), 1021–1034.
- Trenberth, K. E. (1997). The definition of el nino. *Bulletin of the American Meteorological Society*, 78(12), 2771–2778.
- Vallis, G. K. (2011). *Climate and the Oceans*. Princeton University Press.
- Van Hoodonk, R., Maynard, J. A., Liu, Y., & Lee, S.-K. (2015). Downscaled projections of Caribbean coral bleaching that can inform conservation planning. *Global Change Biology*, 21(9), 3389–3401.
- Van Hoodonk, R., Maynard, J. A., & Planes, S. (2013). Temporary refugia for coral reefs in a warming world. *Nature Climate Change*, 3(5), 508–511.
- Van Hoodonk, R., Maynard, J., Tاملander, J., Gove, J., Ahmadi, G., Raymundo, L., Williams, G., Heron, S. F., & Planes, S. (2016). Local-scale projections of coral reef futures and implications of the Paris Agreement. *Scientific Reports*, 6(1), 1–8.
- Van Oppen, M. J., & Medina, M. (2020). Coral evolutionary responses to microbial symbioses. *Philosophical Transactions of the Royal Society B*, 375(1808), 20190591.

- Van Vuuren, D. P., Edmonds, J., Kainuma, M., Riahi, K., Thomson, A., Hibbard, K., Hurtt, G. C., Kram, T., Krey, V., & Lamarque, J.-F. (2011). The representative concentration pathways: An overview. *Climatic Change*, 109(1), 5–31.
- Van Zanten, B. T., Van Beukering, P. J., & Wagtendonk, A. J. (2014). Coastal protection by coral reefs: A framework for spatial assessment and economic valuation. *Ocean & Coastal Management*, 96, 94–103.
- Vecchi, G. A., & Soden, B. J. (2007). Global warming and the weakening of the tropical circulation. *Journal of Climate*, 20(17), 4316–4340.
- Vecchi, G. A., Soden, B. J., Wittenberg, A. T., Held, I. M., Leetmaa, A., & Harrison, M. J. (2006). Weakening of tropical Pacific atmospheric circulation due to anthropogenic forcing. *Nature*, 441(7089), 73–76.
- Veron, J. E. (2011). Corals: Biology, skeletal deposition, and reef-building. *Encyclopedia of Modern Coral Reefs: Structure, Form and Process*, 275–281.
- Veron, J. E. N. (2000). *Corals of the World* (Issue C/593.6 V4).
- Walsworth, T. E., Schindler, D. E., Colton, M. A., Webster, M. S., Palumbi, S. R., Mumby, P. J., Essington, T. E., & Pinsky, M. L. (2019). Management for network diversity speeds evolutionary adaptation to climate change. *Nature Climate Change*, 9(8), 632–636.
- Wang, G., & Cai, W. (2013). Climate-change impact on the 20th-century relationship between the Southern Annular Mode and global mean temperature. *Scientific Reports*, 3(1), 1–6.
- Webster, J. M., Beaman, R. J., Bridge, T., Davies, P. J., Byrne, M., Williams, S., Manning, P., Pizarro, O., Thornborough, K., & Woolsey, E. (2008). From corals to canyons: The Great Barrier Reef margin. *EOS, Transactions American Geophysical Union*, 89(24), 217–218.
- Weeks, S. J., Bakun, A., Steinberg, C. R., Brinkman, R., & Hoegh-Guldberg, O. (2010). The Capricorn Eddy: A prominent driver of the ecology and future of the southern Great Barrier Reef. *Coral Reefs*, 29(4), 975–985.
- Wheeler, M. C., Hendon, H. H., Cleland, S., Meinke, H., & Donald, A. (2009). Impacts of the Madden-Julian oscillation on Australian rainfall and circulation. *Journal of Climate*, 22(6), 1482–1498.
- Whetton, P. H., Grose, M. R., & Hennessy, K. J. (2016). A short history of the future: Australian climate projections 1987–2015. *Climate Services*, 2, 1–14.
- Wiedenmann, J., D'Angelo, C., Smith, E. G., Hunt, A. N., Legiret, F.-E., Postle, A. D., & Achterberg, E. P. (2013). Nutrient enrichment can increase the susceptibility of reef corals to bleaching. *Nature Climate Change*, 3(2), 160–164.
- Wilby, R. L., Charles, S. P., Zorita, E., Timbal, B., Whetton, P., & Mearns, L. O. (2004). Guidelines for use of climate scenarios developed from statistical downscaling methods. *Supporting Material of the Intergovernmental Panel on Climate Change, Available from the DDC of IPCC TGCI A*, 27.
- Wilkinson, C., & Hodgson, G. (1999). Coral reefs and the 1997-1998 mass bleaching and mortality. *Nature & Resources*, 35(2), 16–25.
- Wilkinson, C. R., & Souter, D. (2008). *Status of Caribbean coral reefs after bleaching and hurricanes in 2005*.

- Williams, G. J., Sandin, S. A., Zgliczynski, B. J., Fox, M. D., Gove, J. M., Rogers, J. S., Furby, K. A., Hartmann, A. C., Caldwell, Z. R., & Price, N. N. (2018). Biophysical drivers of coral trophic depth zonation. *Marine Biology*, 165(4), 1–15.
- Willis, B. L., Page, C. A., & Dinsdale, E. A. (2004). Coral disease on the great barrier reef. In *Coral health and disease* (pp. 69–104). Springer.
- Wolanski, E. (1993). Water circulation in the Gulf of Carpentaria. *Journal of Marine Systems*, 4(5), 401–420.
- Wolanski, E., Drew, E., Abel, K. M., & O'Brien, J. (1988). Tidal jets, nutrient upwelling and their influence on the productivity of the alga *Halimeda* in the Ribbon Reefs, Great Barrier Reef. *Estuarine, Coastal and Shelf Science*, 26(2), 169–201.
- Wolanski, E., & Pickard, G. L. (2018). *Physical oceanographic processes of the Great Barrier Reef*. CRC Press.
- Wolanski, E., & Spagnol, S. (2000). Sticky waters in the Great Barrier reef. *Estuarine, Coastal and Shelf Science*, 50(1), 27–32.
- Wolanski, E., & Thomson, R. E. (1984). Wind-driven circulation on the northern Great Barrier Reef continental shelf in summer. *Estuarine, Coastal and Shelf Science*, 18(3), 271–289.
- Wolfe, K., Anthony, K., Babcock, R. C., Bay, L., Bourne, D. G., Burrows, D., Byrne, M., Deaker, D. J., Diaz-Pulido, G., & Frade, P. R. (2020). Priority species to support the functional integrity of coral reefs. *Oceanography and Marine Biology*.
- Wood, S. (2018). Mixed GAM computation vehicle with GCV/AIC/REML smoothness estimation and GAMMs by REML/PQL. *R Package Version*, 1.8-23.
- Wood, S. N. (2004). mgcv: GAMs with GCV smoothness estimation and GAMMs by REML/PQL. R package version 1.1-8. *R Foundation for Statistical Computing, Vienna, Austria, Available on the Web at [Http://Www. R-Project. Org](http://www.R-Project.Org)*.
- Wood, S. N. (2011). Fast stable restricted maximum likelihood and marginal likelihood estimation of semiparametric generalized linear models. *Journal of the Royal Statistical Society: Series B (Statistical Methodology)*, 73(1), 3–36.
- Wood, S. N. (2017). *Generalized additive models: An introduction with R*. CRC press.
- Woodhead, P. M. J. (1970). Sea-surface circulation in the southern region of the Great Barrier Reef, spring 1966. *Marine and Freshwater Research*, 21(2), 89–102.
- World Meteorological Organization. (2007). *Scientific assessment of ozone depletion: 2006. Global Ozone Research and Monitoring Project–Report No. 50*. Geneva Switzerland.
- Xu, Z., Han, Y., & Yang, Z. (2019). Dynamical downscaling of regional climate: A review of methods and limitations. *Science China Earth Sciences*, 62(2), 365–375.
- York, P. H., Carter, A. B., Chartrand, K., Sankey, T., Wells, L., & Rasheed, M. A. (2015). Dynamics of a deep-water seagrass population on the Great Barrier Reef: Annual occurrence and response to a major dredging program. *Scientific Reports*, 5(1), 1–9.
- York, P. H., Macreadie, P. I., & Rasheed, M. A. (2018). Blue Carbon stocks of Great Barrier Reef deep-water seagrasses. *Biology Letters*, 14(12), 20180529.

- Zhang, X., Oke, P. R., Feng, M., Chamberlain, M. A., Church, J. A., Monselesan, D., Sun, C., Matear, R. J., Schiller, A., & Fiedler, R. (2016). A near-global eddy-resolving OGCM for climate studies. *Geoscientific Model Development Discussions*, 1–52.
- Zika, J. D., Skliris, N., Blaker, A. T., Marsh, R., Nurser, A. G., & Josey, S. A. (2018). Improved estimates of water cycle change from ocean salinity: The key role of ocean warming. *Environmental Research Letters*, 13(7), 074036.